THE BELT AND ROAD OF ANIMAL DISEASES

EDITED BY: Shao-Lun Zhai and Feng Li
PUBLISHED IN: Frontiers in Veterinary Science

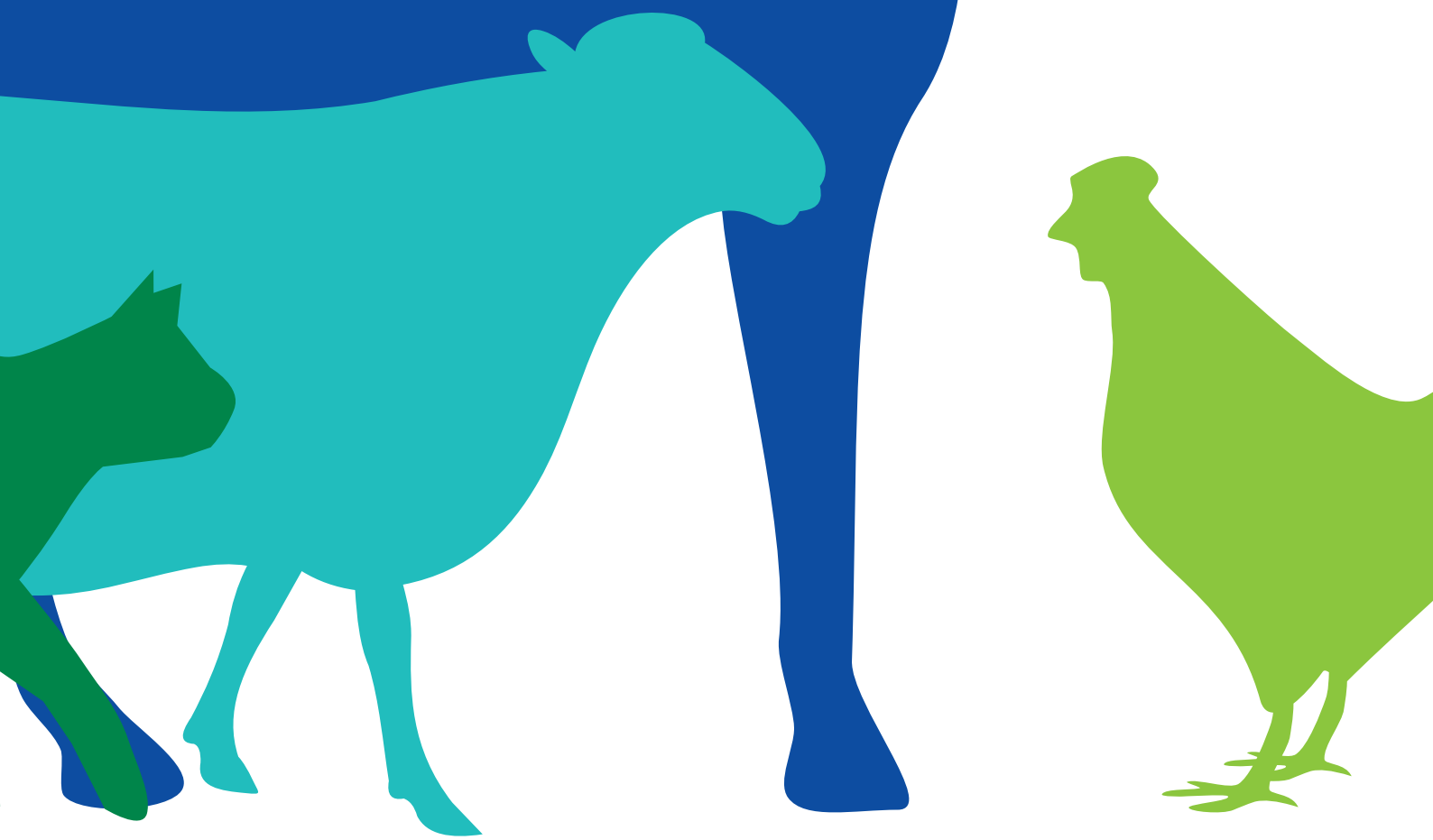

frontiers Research Topics

ISSN 1664-8714
ISBN 978-2-88971-952-5
DOI 10.3389/978-2-88971-952-5

About Frontiers

Frontiers is more than just an open-access publisher of scholarly articles: it is a pioneering approach to the world of academia, radically improving the way scholarly research is managed. The grand vision of Frontiers is a world where all people have an equal opportunity to seek, share and generate knowledge. Frontiers provides immediate and permanent online open access to all its publications, but this alone is not enough to realize our grand goals.

Frontiers Journal Series

The Frontiers Journal Series is a multi-tier and interdisciplinary set of open-access, online journals, promising a paradigm shift from the current review, selection and dissemination processes in academic publishing. All Frontiers journals are driven by researchers for researchers; therefore, they constitute a service to the scholarly community. At the same time, the Frontiers Journal Series operates on a revolutionary invention, the tiered publishing system, initially addressing specific communities of scholars, and gradually climbing up to broader public understanding, thus serving the interests of the lay society, too.

Dedication to Quality

Each Frontiers article is a landmark of the highest quality, thanks to genuinely collaborative interactions between authors and review editors, who include some of the world's best academicians. Research must be certified by peers before entering a stream of knowledge that may eventually reach the public - and shape society; therefore, Frontiers only applies the most rigorous and unbiased reviews.
Frontiers revolutionizes research publishing by freely delivering the most outstanding research, evaluated with no bias from both the academic and social point of view. By applying the most advanced information technologies, Frontiers is catapulting scholarly publishing into a new generation.

What are Frontiers Research Topics?

Frontiers Research Topics are very popular trademarks of the Frontiers Journals Series: they are collections of at least ten articles, all centered on a particular subject. With their unique mix of varied contributions from Original Research to Review Articles, Frontiers Research Topics unify the most influential researchers, the latest key findings and historical advances in a hot research area! Find out more on how to host your own Frontiers Research Topic or contribute to one as an author by contacting the Frontiers Editorial Office: frontiersin.org/about/contact

THE BELT AND ROAD OF ANIMAL DISEASES

Topic Editors:
Shao-Lun Zhai, Guangdong Academy of Agricultural Sciences, China
Feng Li, South Dakota State University, United States

Citation: Zhai, S.-L., Li, F., eds. (2021). The Belt and Road of Animal Diseases. Lausanne: Frontiers Media SA. doi: 10.3389/978-2-88971-952-5

Table of Contents

frontiers in Veterinary Science

EDITORIAL
published: 08 November 2021
doi: 10.3389/fvets.2021.795556

Editorial: The Belt and Road of Animal Diseases

Shao-Lun Zhai [1,2,3,4]*

[1] Institute of Animal Health, Guangdong Academy of Agricultural Sciences, Guangzhou, China, [2] Scientific Observation and Experiment Station of Veterinary Drugs and Diagnostic Techniques of Guangdong, Ministry of Agriculture of Rural Affairs, Guangzhou, China, [3] Key Laboratory of Animal Disease Prevention of Guangdong, Guangzhou, China, [4] Guangdong Laboratory for Lingnan Modern Agriculture, Maoming Branch, Maoming, China

Keywords: the belt and road, transboundary animal infectious diseases, exotic animal, spread, transmission

Editorial on the Research Topic

The Belt and Road of Animal Diseases

INTRODUCTION

The Belt and Road Initiative (BRI) is a global development strategy adopted by the Chinese government in 2013. This investment and infrastructure development strategy drives the world's economic development. However, this initiative has resulted in an increase in the transnational spread of animal diseases, which caused a significant economic loss to the global animal industry. For example, in 2013, Peste des petits ruminant virus entered China (1); in 2015, Senecavirus A outbreak occurred in China (2); since 2018, African swine fever virus swept into east Asia and Southeast Asia (3); in 2019; lumpy skin disease virus emerged in China (4); in 2013, Porcine Epidemic Diarrhea was found in the United States (5). Strategies to avoid or reduce transnational spread of animal infectious diseases is an important issue, which can be addressed by a multidisciplinary approach including rapid virus detection, metagenomic sequencing, and epidemiology. Other measures such as scientific popularization of disease knowledge, combating smuggling activities, border trade control, and wildlife management should facilitate the control and prevention of these rapidly evolving infectious diseases of animals in a timely and effective manner.

The aim of this Research Topic is to offer an opportunity to collect the newest research and development in the field of "The Belt and Road" of Animal Diseases. Early warning, virus detection, genetic evolution, disseminating disease knowledge, combating smuggling activities, border trade control (among others) are topics that we aim to explore.

ORGANIZATION OF THE RESEARCH TOPIC

In this Research Topic, we received 16 manuscripts, 11 (1 review, 9 original research, 1 brief research report) were accepted for publication. Among them, 9 papers involved virus research, and two papers involved bacterial research. In 9 viral topic-related papers, 5 papers involved nidovirus research; 2 papers involved circovirus research; one paper involved herpesvirus research; one paper focused on picornavirus research. The first nidovirus paper reported the genetic diversity (Genotype 1, 2, 3) of ORF3 gene of porcine epidemic diarrhea virus (PEDV) in Guangxi, China, more specifically, the continuous deletions from 172 to 554 bp of ORF3 gene occurred in some PEDV strains (Lu et al.). The second nidovirus research paper described a re-outbreak of PEDV

OPEN ACCESS

Edited and reviewed by:
Michael Kogut, Agricultural Research Service, United States Department of Agriculture (USDA), United States

***Correspondence:**
Shao-Lun Zhai
zhaishaolun@163.com
orcid.org/0000-0003-3217-2256

Specialty section:
This article was submitted to Veterinary Infectious Diseases, a section of the journal Frontiers in Veterinary Science

Received: *15 October 2021*
Accepted: *19 October 2021*
Published: *08 November 2021*

Citation:
Zhai S-L (2021) Editorial: The Belt and Road of Animal Diseases. Front. Vet. Sci. 8:795556. doi: 10.3389/fvets.2021.795556

with 97.8% similarity with the vaccine strain CV777 in one vaccinated farm, indicating that current commercial PEDV vaccine could not fully protect pigs against the epidemic strains (Gao et al.). The two papers all emphasized the research and development of an effective and broad-spectrum PEDV vaccine. The third nidovirus study showed that porcine enteric alphacoronavirus (PEAV) could inhibit IFN-α, IFN-β, OAS, Mx1, and PKR mRNA expression in infected peyer's patches *in vivo* (Xu, Gong, et al.). The forth nidovirus paper, a review article, mainly summarized the apoptosis roles in swine response to viral infection and pathogenesis of four swine coronaviruses including PEDV, PEAV, transmissible gastroenteritis virus (TGEV), and porcine deltacoronavirus (PDCoV) (Xu, Zhang, et al.). The two papers revealed the pathogenesis of viral infections and laid the foundation to develop an appropriate strategy for the prevention and control of swine diarrhea diseases. The fifth nidovirus paper described a monoclonal antibody against porcine CD163 SRCR5 domain, which partially could block the infection of porcine reproductive and respiratory syndrome virus (PRRSV) (Zhang et al.). It may provide a foundation of antiviral therapy for PRRSV. In two circovirus studies, the authors established two different methods to detect porcine circovirus 3 (PCV3). One was colorimetric isothermal multiple-self-matching-initiated amplification assay, which might be a good practical choice for epidemiological investigation and point-of-care testing of PCV3 (Gou et al.). Another was single multiple cross displacement amplification assay, which could be widely applied in PCV3 detection in laboratories or in rural areas (Bian et al.). During eighth virus theme-related study, Xu, Gao, Wu, et al. identified that UL46 gene of pseudorabies virus (PRV) could encode the nucleocytoplasmic shuttling protein. In the final paper, Zhou et al. first reported seneca valley virus (SVV) in buffalos in China, and sequence analysis showed the SVV strain was close to one wild boar-origin strain, which revealed potential cross-species transmission of SVV.

In two bacterial studies, Liu et al. collected genotype data of Brucella strains from 11 countries along the Silk Road, the combination of whole-genome sequencing and single-nucleotide polymorphism (WGS-SNP) phylogenetic analysis showed that some genotypes spread within the national borders and other genotypes continuously expanded and spread in countries along with Silk Road. The authors strengthen that there is an urgent need for the control (especially entry-exit quarantine of animal brucellosis) of transfer and trade of infected sheep/goats in countries along the Silk Road. Li et al. reported the host cytokine response differences in piglets infected with toxigenic and non-toxigenic staphylococcus hyicus (S. hyicus) It was helpful to understand the pathogenic mechanisms of S. hyicus.

CONCLUSION

Since the beginning of 2020, The Research Topic began to receive the manuscript submission, and invited more than 60 research team from the world to submit the manuscript. But we finally received 16 manuscripts that might be caused on on-going COVID-19 pandemic, which clearly affects our research and work progress. Although the Topic provides overviews of some pathogen cross-region threats and discusses current and novel strategies for the detection and control, the manuscripts associated with transboundary infectious diseases and foreign diseases (especially Peste des petits ruminant, African swine fever and lumpy skin disease) were lacking. In the following work, we hope that more scientists pay more attention to these diseases in order to reduce or prevent the spread of transboundary infectious diseases and foreign diseases in animals.

AUTHOR CONTRIBUTIONS

S-LZ wrote the editorial and approved it for publication.

FUNDING

This work was supported by the two grants (Nos. 2019B020211005 and 2019B020217002) from the Guangdong Science and Technology Department, the Jinying's Star Talent Program (Grant No. R2018PY-JX003) and Disciplinary Team Construction Program (Grant No. 202122TD) from Guangdong Academy of Agricultural Sciences, the grant (No. 201906040005) from Guangzhou Science and Technology Bureau, and the two grants (Nos. 2021KJ114 and 2021KJ119) from the Department of Agriculture and Rural Affairs of Guangdong Province.

REFERENCES

1. Bao J, Wang Q, Zhang Y, Liu C, Li L, Wang Z. Complete genome sequence of a novel variant strain of peste des petits ruminants virus, China/XJYL/2013. *Genome Announc*. (2014) 2:E00762–14. doi: 10.1128/GenomeA.00762-14
2. Wu Q, Zhao X, Bai Y, Sun B, Xie Q, Ma J. The first identification and complete genome of senecavirus a affecting pig with idiopathic vesicular disease in China. *Transbound Emerg Dis.* (2017) 64:1633–40. doi: 10.1111/Tbed.12557
3. Mighell E, Ward MP. African swine fever spread across Asia, 2018-2019. *Transbound Emerg Dis.* (2021) 68:2722–32. doi: 10.1111/tbed.14039
4. Lv DH, Zhai SL, Wei WK, Zhai Q, Wen XH, Chen QL. Threat of lumpy skin disease to the Chinese cattle industry. *Vet Rec.* (2021) 188:315–6. doi: 10.1002/vetr.434
5. Williamson S, Strugnell B, Thomson J, Webster G, McOrist S, Clarke H. Emergence of severe porcine epidemic diarrhoea in pigs in the USA. *Vet Rec.* (2013) 173:146–8. doi: 10.1136/vr.f4947

Conflict of Interest: The author declares that the research was conducted in the absence of any commercial or financial relationships that could be construed as a potential conflict of interest.

frontiers in Veterinary Science

ORIGINAL RESEARCH
published: 03 July 2020
doi: 10.3389/fvets.2020.00449

Porcine enteric alphacoronavirus Inhibits *IFN-α*, *IFN-β*, *OAS*, *Mx1*, and *PKR* mRNA Expression in Infected Peyer's Patches *in vivo*

Zhichao Xu[1], *Lang Gong*[2], *Peng Peng*[1], *Yufang Liu*[1], *Chunyi Xue*[1] *and Yongchang Cao*[1]*

[1] State Key Laboratory of Biocontrol, School of Life Science, Sun Yat-Sen University, Guangzhou, China, [2] College of Veterinary Medicine, South China Agricultural University, Guangzhou, China

Porcine enteric alphacoronavirus (PEAV) is a newly identified swine enteropathogenic coronavirus that causes watery diarrhea in neonatal piglets. The pathogenesis and host immune responses of PEAV infection are not fully characterized. The reason lies in the stomach environment, which would degrade cell-cultured live viruses *via* oral infection, making it difficult to establish an effective infection model to study the pathogenesis and host immune responses in pigs with a mature immune system. To solve this problem, in this study, coated PEAV-loaded microspheres were developed by centrifugal granulation-fluidized bed coating and demonstrated as an effective oral delivery system/animal infection model to protect PEAV virion against the complex gastrointestinal environment *in vitro* and to cause infection in weaned piglets *in vivo*. Weaned piglets orally inoculated with coated PEAV-loaded microspheres developed diarrhea and virus RNA was detected in rectal swabs from one to seven days post inoculation. In addition, microscopic lesions in the small intestine were observed, and viral antigens were also detected in the small intestines with PEAV immunohistochemical staining. Importantly, PEAV significantly inhibited mRNA expression of *IFN-α*, *IFN-β*, *OAS*, *Mx1*, and *PKR*, the genes involved in modulation of the host immune responses, in infected Peyer's patches, indicating that PEAV can overcome the antiviral response to cause damage when infection occurs. Collectively, our research successfully established a PEAV animal infection model in weaned piglets and suggested that the observed gene expression profile might help explain immunological changes associated with PEAV infection.

Keywords: coated *Porcine enteric alphacoronavirus* (PEAV)-loaded microspheres, pathogenesis, antiviral response, Peyer's patches, weaned piglets

OPEN ACCESS

Edited by:
Shao-Lun Zhai,
Guangdong Academy of Agricultural Sciences, China

Reviewed by:
Pascale Quéré,
Institut National de la Recherche Agronomique (INRA), France
Rahul K. Nelli,
Iowa State University, United States

***Correspondence:**
Yongchang Cao
caoych@mail.sysu.edu.cn

Specialty section:
This article was submitted to Veterinary Infectious Diseases, a section of the journal Frontiers in Veterinary Science

Received: *10 April 2020*
Accepted: *19 June 2020*
Published: *03 July 2020*

Citation:
Xu Z, Gong L, Peng P, Liu Y, Xue C and Cao Y (2020) Porcine enteric alphacoronavirus Inhibits IFN-α, IFN-β, OAS, Mx1, and PKR mRNA Expression in Infected Peyer's Patches in vivo. Front. Vet. Sci. 7:449. doi: 10.3389/fvets.2020.00449

INTRODUCTION

PEAV, as the newest strain of porcine CoVs, was first detected by our team via genomic analysis of samples collected from a diarrhea-outbreak in swine herds in Guangdong, China in 2017 (1), and this novel swine enteric CoV was subsequently confirmed to have existed in China since at least August 2016 by a retrospective detection study (2). In addition, the retrospective investigation of 236 samples from 45 swine farms showed that the prevalence of PEAV in pigs was reported to be

43.53% in Guangdong, China in August 2016 to May 2017 (2). Apart from Guangdong, a PEAV-like strain, CN/FJWT/2018, was recently discovered in Fujian, China (3), indicating a continuing threat to pig farms.

The complete genome of the PEAV strain GDS04 was reported after it was first identified (1). The full-length genome of PEAV is about 27 kb (1), arranged in the order of: 5′ UTR-ORF1a/1b-S-NS3-E-M-N-NS7a-3′ UTR (4). It is known that the S protein has many important characteristics in CoVs, such as virus attachment and entry, and induction of neutralizing antibodies *in vivo* (5). Of note, compare to other reported CoVs, PEAV has the smallest S protein of only 1129 amino acids (1).

PEAV caused clinical symptoms similar to other porcine enteric pathogens, such as PEDV and TGEV, characterized by vomiting, diarrhea, dehydration, and a mortality rate as high as 90% in piglets (1, 6). Since PEAV was reported in pigs (1), other groups have identified another two swine enteric HKU2-related CoVs, SADS-CoV, and SeACoV, in the same region. The newborn piglets were subsequently inoculated with isolated SADS-CoV and SeACoV strains which caused PEAV-like diarrheal disease (6–8).

PEAV is an important enteropathogen in pigs, but currently no report is involved in modulation of the host immune responses against PEAV infection. Oral infection of pigs with a mature immune system, like weaned piglets, can truly reflect the effect of the virus on the host immune responses. Moreover, according to our pre-experiment, cell-cultured PEAV doesn't cause infection in weaned piglets by orally feeding. In order to solve the problem, we successfully established an animal infection model of coated PEAV-loaded microspheres. In brief, we initially generated coated PEAV-loaded microspheres and evaluated the acid-resistance and enteric solubility *in vitro* and *in vivo* and further challenged microspheres to investigate the pathogenicity of PEAV in 33-day-old conventionally weaned piglets. Subsequent to the establishment of the animal infection model, we assessed the effect of PEAV on the antiviral molecules in Peyer's patches in inoculated piglets by real-time PCR.

MATERIALS AND METHODS

Virus Propagation in Vero Cells

Vero cells were obtained from ATCC (ATCC number: CCL-81) (USA) and cultured in Dulbecco's modified eagle medium (DMEM) (Hyclone, USA), supplemented with 10% fetal bovine serum (FBS) (BOVOGEN, Australia), 100 U/mL penicillin, and 100 U/mL streptomycin in 37°C with 5% CO_2 incubator. The maintenance medium for PEAV propagation was DMEM supplemented with 10 μg/mL trypsin (Gibco, USA) and cultured under the conditions described above. The PEAV GDS04 strain was isolated from piglets with severe diarrhea in our laboratory (8).

Virus propagation was performed as previously described (8). Briefly, Vero cells were seeded into T175 flasks and cultured for 90% confluence. One mL of PEAV GDS04 strain together with 50 mL of maintenance medium were added to flasks after the cell monolayers were washed three times with sterile pH 7.4 1 × phosphate buffered saline (PBS). The virus-inoculated cells were cultured continuously at 37°C in 5% CO_2 to observe the cytopathic effect (CPE). Around one day post-infection (d.p.i.), >80% CPE was evidently observed in the inoculated cell monolayers; the flasks were then twice frozen at −80°C and thawed. The cells and supernatants were harvested together and stored at −80°C until subsequent viral titers' determination. Virus titers were calculated using the Reed-Muench method (9) and expressed as $TCID_{50}$ per milliliter.

Pigs

The animal study was approved by the Institutional Animal Care and Use Committee of the Sun Yat-sen University (Guangdong, China) and animals were treated in accordance with the regulations and guidelines of this committee. Thirty-three-day-old healthy conventional weaned piglets, crossbred of Duroc × Landrace × Native pigs of Guangdong of China, were procured from Wen' s Foodstuffs Group Co., Ltd. (Guangdong, China). All pigs were housed in the vivarium under standard environmental conditions and maintained in our animal facility with food and water *ad libitum* for a minimum of 7 days before the experimentation.

Production of Coated PEAV-Loaded Microspheres (PEAV-Coated)

PEAV-Coated were prepared using centrifugal granulation-fluidized bed coating technology as described previously, with some modifications (10). Briefly, we added the commercial sucrose microspheres (450 g) (Anhui Sunhere Pharmaceutical Excipients Co., Ltd, China) into a centrifugal granulator (Shenzhen Xinyite Science and Technology Co., Ltd, China), and adjusted the solid rotation disc' s speed to 27 × *g* to keep the vorticity of the microspheres. We also adjusted the supply air velocity and the exhaust air velocity to 326 × *g* and 666 × *g*, respectively. We subsequently set the machine to spray pure water (80–100 mL) to blend the powders into the microspheres at 0.02 × *g* for 30 min by a tangential spray nozzle. About 136 g new powders were constantly added into the microspheres. Then the final product was dried at 37°C for 1 h under the same air quantity. Subsequently, the dried PEAV-loaded microspheres smaller than 0.7 mm were screened by sieving, and then filled into a fluidized bed apparatus with a bottom spray configuration (Shenzhen Xinyite Science and Technology Co., Ltd., China). We used the magnetic stirrer to mix enteric coating suspensions (Weight gain 25%) with 6% Hydroxypropyl methyl cellulose phthalate (HPMCP) (Shanghai Yunhong Chemical Co., Ltd., China), and then PEAV-loaded microspheres were continuously sprayed with the enteric coating suspensions at 0.25 mL/min through a spray nozzle at the bottom of the fluidized bed apparatus. Of note, the relative bed temperature needed to be kept at 29°C to avoid an agglomeration of the microspheres during the coating process. After all the enteric coating suspensions were sprayed out, the products needed to dry for an additional 30 min.

Characterization of PEAV-Coated

According to the method described by Kashappa-Goud H. Desai and Steven P. Schwendeman (11), we used a Hitachi S-3400N scanning electron microscope (Hitachi, Japan) to examine the surface morphology of microspheres by taking SEM images.

Briefly, we fixed the microspheres on a brass stub with a double-sided adhesive tape and then coated them with ∼3–5 nm electrically conductive gold for 100 s at 40 W in a vacuum. Then, the excitation voltage was set as 8–10 kV to take the images of the microsphere surface. One hundred randomly selected samples of PEAV-Coated were selected to measure the diameter with a Vernier caliper (Guangzhou Heyue Biotechnology Co., Ltd., China) to determine the size distribution of the PEAV-Coated. In addition, 100 samples of PEAV-Coated or sucrose microspheres were randomly selected and measured with Electronic scales (Sartorius Group, Germany) to calculate the weight gain of the single microsphere and to analyze the weight gain of the single PEAV-Coated.

In vitro and *in vivo* Acid Resistance and Enteric Solubility Study of PEAV-Coated

In line with previous studies (12), we used simulated gastric fluid and simulated intestinal fluid to determine the acid resistance and enteric solubility of PEAV-Coated *in vitro*. Briefly, PEAV-Coated were successively incubated in pH 1.2 simulated gastric fluid prepared with 2 g/L NaCl, 3.2 g/L porcine pepsin, 0.7% HCl, and pH 6.8 simulated intestinal fluid prepared with 6.8 g/L NaH_2PO_4, 7.7% 0.2 N NaOH, and 10 g/L pancreatin at 37°C for 2 h, and freeze-dried powders containing the PEAV GDS04 strain were treated under the same conditions. The $TCID_{50}$ assay as described above was used to analyze the acid resistance of PEAV-Coated after the simulated gastric fluid treatment.

To analyze the acid resistance and enteric solubility of PEAV-Coated *in vivo*, weaned piglets were orally inoculated with these microspheres to assess virus shedding according to previous studies with some modifications (10). Briefly, 18 conventionally weaned piglets were randomly divided into three groups with six piglets in each, and were housed in three separate rooms. On day 0, weaned piglets in group one were orally challenged with 20 g of PEAV-Coated containing a total of 2×10^5 $TCID_{50}$ of the PEAV GDS04 strain (1 gram of microspheres contained 1×10^4 $TCID_{50}$ of PEAV GDS04 strain). Weaned piglets in groups two and three as controls were orally inoculated with 20 mL of maintenance medium or 20 mL of maintenance medium containing a total of 2×10^5 $TCID_{50}$ of the PEAV GDS04 strain (1 milliliter of medium contained 1×10^4 $TCID_{50}$ of PEAV GDS04 strain), respectively. After challenge, rectal swabs were collected from each piglet on day 0, 2, 4, 6, and 8 after the challenge to assess PEAV virus shedding with real-time PCR as described below.

Experimental Infection With PEAV-Coated in Conventional Weaned Piglets

Twenty-four conventionally weaned piglets, negative of the major porcine enteric viruses including PDCoV, PEDV, TGEV, PRoV, and PEAV by testing the rectal swabs on day −1 as previously described (13), were randomly divided into two groups with 12 piglets in each and were housed in two separate rooms. On day 0, weaned piglets in one group were orally challenged with 100 g/head of PEAV-Coated containing a total of 1×10^6 $TCID_{50}$ of the PEAV GDS04 strain (1 gram of microspheres contained 1×10^4 $TCID_{50}$ of PEAV GDS04 strain) for 3 days and weaned piglets in another group were orally inoculated with 100 g/head sucrose microspheres for 3 days and served as uninfected controls. After infection, clinical signs of vomiting, diarrhea, and lethargy were observed daily in each piglet. In addition, the diarrhea severity of each piglet was scored daily according to the previous criteria (14): 0 = normal, 1 = soft (cowpie), 2 = liquid with some solid content, 3 = watery with no solid content.

Rectal swabs were collected from each piglet before inoculation and then every day until 7 d.p.i. and were homogenized in 1 mL sterile pH 7.4 1 × PBS immediately after collection. Six of the challenged piglets and six of the negative control piglets were randomly selected from each group and humanely sacrificed for necropsy at 3 d.p.i., and the remaining weaned piglets were necropsied at 7 d.p.i. At necropsy, the fresh Peyer's patches from ileum were collected for analysis of the antiviral molecules with real-time RT-PCR and the fresh jejunum were also analyzed with histopathology and immunohistochemistry.

RNA Isolation and Real-Time PCR Analysis

RNA extraction and RT were performed as previously described with some modifications (8). Briefly, viral RNA was extracted from the rectal swab fluids from each piglet by using an RNeasy kit (Magen, China) according to the manufacturer' instruction. Two μg of viral RNA was converted to cDNA by using an RT-PCR kit (TaKaRa, Dalian). Primers for the nucleocapsid (*n*) gene of PEAV (sense: 5′-CTGACTGTTGTT GAGGTTAC-3′; antisense: 5′-TCTGCCAAAGCTTGTTTAAC-3′), and probe (5′-FAM-TCACAGTCTCGTTCTCGCAATCA-TARMA-3′) were designed as previously described (15) and synthesized by Invitrogen Company (Shanghai, China). The real-time PCR assay was performed on an Applied Biosystem 7500 instrument (Life Technologies, USA) with a 20-μL volume containing 1 μL of cDNA, 10 μL of Thunderbird Probe qPCR Mix, 0.04 μL 50 × Rox reference dye (TOYOBO, Shanghai), 0.2 μmol/L of probe, and a 0.3 μmol/L of each gene-specific primer. The PCR program was as follows: 95°C for 30 s; 45 cycles of 95°C for 5 s, 62°C for 30 s. The *n* gene was amplified by using the specific primers (sense: 5′-CCGCTCGAGATGG CAACTGTTAATTGG-3′; antisense: 5′-CGCGGATCCCGATTA ATAATCTCATCCAC-3′) that were designed according to the sequence of PEAV strain GDS04 (GenBank, Accession no: MF167434.1), and the PCR products were ligated with the pEGFP-N1 vector (Clontech, USA) by using a PCR cloning kit (NEB, USA), and then the 10-fold serially diluted known plasmid concentration was used as the template to construct a real-time PCR standard curve in each plate. The quantity of PEAV viral RNA in rectal swabs was calculated based on the cycle threshold (Ct) values for the standard curve.

To analyze antiviral molecular changes in the piglets with PEAV infection, equal quantities (1 g) of Peyer's patches were homogenized in sterile pH 7.4 1 × PBS, and 200 μL of the supernatant was used for RNA extraction by using an RNeasy kit (Magen, China) following the manufacturer's instruction. Two μg of total RNA was converted to cDNA by using an RT-PCR kit (TaKaRa, Dalian). The specific primers for porcine

IFN-α (sense: 5′-TCTCATGCACCAGAGCCA-3′; antisense: 5′-CCTGGACCACAGAAGGGA-3′), *IFN-β* (sense: 5′-AGTG CATCCTCCAAATCGCT-3′; antisense: 5′-GCTCATGGA AAGAGCTGTGGT-3′), *PKR* (sense: 5′-AAAGCGGACAAG TCGAAAGG-3′; antisense: 5′-TCCACTTCATTTCCATAGTCT TCTGA-3′), *OAS* (sense: 5′-GAGCTGCAGCGAGACTTCCT-3′; antisense: 5′-TGCTTGACAAGGCGGATGA-3′), *Mx1* (sense: 5′-GGCGTGGGAATCAGTCATG-3′; antisense: 5′-AGGA AGGTCTATGAGGGTCAGATCT-3′), and glyceraldehydes-3-phosphate dehydrogenase (*GAPDH*; sense: 5′-CCTTCCGT GTCCCTACTGCCAAC-3′; antisense: 5′-GACGCCTGCTTCAC CACCTTCT-3′) were designed as previously described (16, 17) and synthesized by Sangon Company (Shanghai, China). The real-time PCR assay was performed on an Applied Biosystem 7500 instrument (Life Technologies, USA) with a 20-μL volume containing 1 μL of cDNA, 10 μL of 2 × SYBR green Premix *Ex Taq* (TaKaRa, Dalian), and 0.4 μM of each gene-specific primer. The amplification conditions were referring to previous publications (16) and were as follows: 95°C for 30 s; then 40 cycles of 95°C for 3 s, 60°C for 30 s; and 1 cycle of 95°C for 15 s, 60°C for 1 min, and 95°C for 15 s, 60°C for 15 s. A melt curve for the PCR products was obtained to determine the specificity of the amplification at the final step. The antiviral molecules expressions were calculated relative to the expression of the reference gene *GAPDH* and presented as the change (*n*-fold) relative to the control samples.

Histological and Immunohistochemical Staining

Histological and Immunohistochemical staining were performed as previously described with some modifications (8). Briefly, at necropsy, the jejunum tissue samples of the piglets from the challenged and control groups were separated, routinely fixed in 10% formalin, embedded, sectioned, and stained with hematoxylin and eosin (H&E); the slides were then examined and analyzed with conventional light microscopy. Five-μm sections of formalin-fixed paraffin-embedded tissues were mounted onto positively charged glass slides. Slides were air dried at 60 °C for 120 min prior to deparaffinization. Slides were then rinsed and incubated with target retrieval solution (Servicebio, China). The sections were incubated with PEAV (GenBank, Accession no: MF167434.1) specific mouse antisera (Wen's Foodstuffs Group Co., Ltd, China) (1:400) as the primary antibody for 12 h at 4 °C after to block with 1% BSA (Solarbio, China). They were then incubated with peroxidase-labeled goat anti-mouse IgG secondary antibody (Dako, Denmark) (1:200) for 50 min at room temperature prior to visualization with a 3, 3′-diaminobenzidine (DAB) chromogen kit (Dako, Denmark). In addition, hematoxylin was used for counterstaining. Jejunum tissue samples from uninfected piglets were used as a negative control.

Statistical Analysis

Statistical comparisons were performed using GraphPad Prism software. The significance of the differences between the treatment group and controls in the mRNA expressions [$TCID_{50}$, antiviral molecules (*IFN-α/β*, *OAS*, *PKR*, and *Mx1*)] was determined by the ANOVA and Mann-Whitney accordingly.

RESULTS

Centrifugal Granulation-Fluidized Bed Coating Manufactures the PEAV-Coated

Viruses by oral feeding failed to infect the body due to the labile components that were degraded by the acid pH of the stomach (18). To successfully infect the animals, we used centrifugal granulation technology to load the freeze-dried powders containing the PEAV GDS04 strain onto sucrose microspheres (**Figure 1A**). To protect PEAV from low pH while facilitating controlled virion release in the intestine, pH-resistant enteric coating (HPMCP) was loaded on the PEAV-loaded microspheres using a fluidized bed coating apparatus after a drying process (**Figure 1B**). The final products of the manufacturing process yielded the coated mini-spheres, with a faint-yellow surface (**Figure 1C**).

PEAV-Coated Structural Characterization

To observe the encapsulation effect of PEAV in the microspheres, we used a scanning electron microscope to examine the morphology of the microspheres. As shown in **Figure 2B**, a scanning electron micrograph revealed the microparticles containing PEAV characterized by their pill shape, rough surface, lack of porosity, and relatively uniformed size. In addition, compared to sucrose microspheres, PEAV-Coated were around 1.3 times larger (**Figure 2A**). Further, we found that more than 95% of microspheres were in the size range of 700–800 μm in diameter (**Figure 2C**). In addition, single PEAV-Coated weight gained 60% more than single sucrose microspheres (**Figure 2D**).

PEAV-Coated Have Acid Resistance and Enteric Solubility *in vitro* and *in vivo*

Considering that viruses by oral feeding overcoming the acid pH of the stomach is the key to infection, we examined the acid resistance and enteric solubility of PEAV-Coated *in vitro* and *in vivo*. As shown in **Figures 3A,B**, we found that the shape of PEAV-Coated was unaffected after simulated gastric fluid treatment, but it could dissolve in simulated intestinal fluid. In addition, compared to the microspheres before treatment, virus titers in microspheres after the simulated gastric fluid treatment dropped slightly (**Figure 3C**). To further determine whether PEAV-Coated could resist gastric acid *in vivo*, we fed weaned piglets with PEAV-Coated and the control groups with DMEM without mixing with sucrose microspheres or PEAV without mixing with sucrose microspheres. As shown in **Figure 3D**, in half of the weaned piglets orally inoculated with PEAV-Coated PEAV RNA could be detected in fecal swabs at the sixth day after the challenge. In contrast, no PEAV RNA were detected in DMEM and PEAV-inoculated weaned piglets.

PEAV-Coated Caused Diarrhea in Weaned Piglets

In order to determine whether PEAV-Coated could infect weaned piglets, 33-day old conventionally weaned piglets

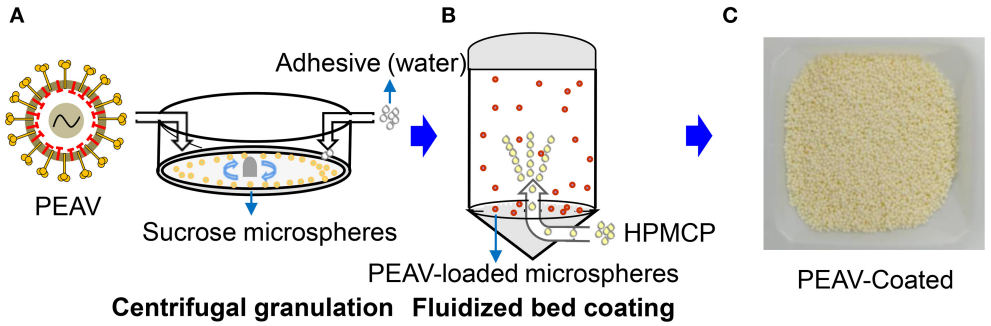

FIGURE 1 | Generation of PEAV-Coated by Centrifugal granulation-fluidized bed coating. **(A)** The freeze-dried powders containing the PEAV GDS04 strain were loaded onto sucrose microspheres with pure water as an adhesive by using centrifugal granulation technology. The enteric coating (HPMCP) **(B)** was successively sprayed onto the PEAV-loaded microspheres by using a fluidized bed apparatus. **(C)** The final product was the PEAV-Coated.

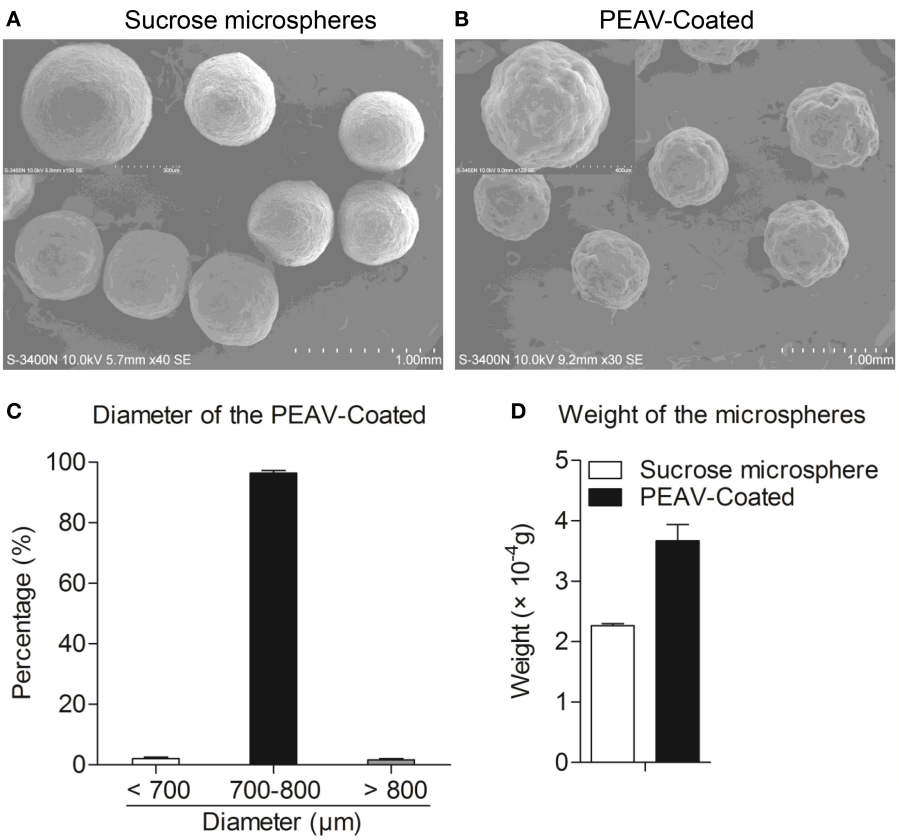

FIGURE 2 | Appearance, size distribution, and weight gain of PEAV-Coated. Scanning electron micrographs of sucrose microspheres **(A)** and PEAV-Coated **(B)** (scale bar 1.0 mm, 300 μm or 400 μm in **A,B**). **(C)** Size distribution of freshly prepared PEAV-Coated was measured using a Vernier caliper and data were plotted as the percentage of different diameters. **(D)** One hundred freshly prepared PEAV-Coated or sucrose microspheres were randomly selected and measured with Electronic scales to calculate the weight gain of the single microsphere. Results are representative of three independent experiments. Data are represented as mean ± SD, $n = 3$.

were orally infected with PEAV-Coated at a dose of 1×10^6 $TCID_{50}$/100 g/head. Compared to the negative control, watery diarrhea was observed in all weaned piglets inoculated with PEAV-Coated from 1 d.p.i. to 7 d.p.i. (**Figure 4A**). We further examined the viral shedding by real-time PCR in fecal swabs collected from inoculated-piglets from 1 d.p.i. to 7 d.p.i.. As shown in **Figure 4B**, PEAV RNA was detected in PEAV-Coated-challenged piglets, while no PEAV RNA was detected in sucrose microspheres-challenged piglets during the study. Taken together, these results suggest that PEAV-Coated could infect weaned piglets to cause diarrhea *in vivo*.

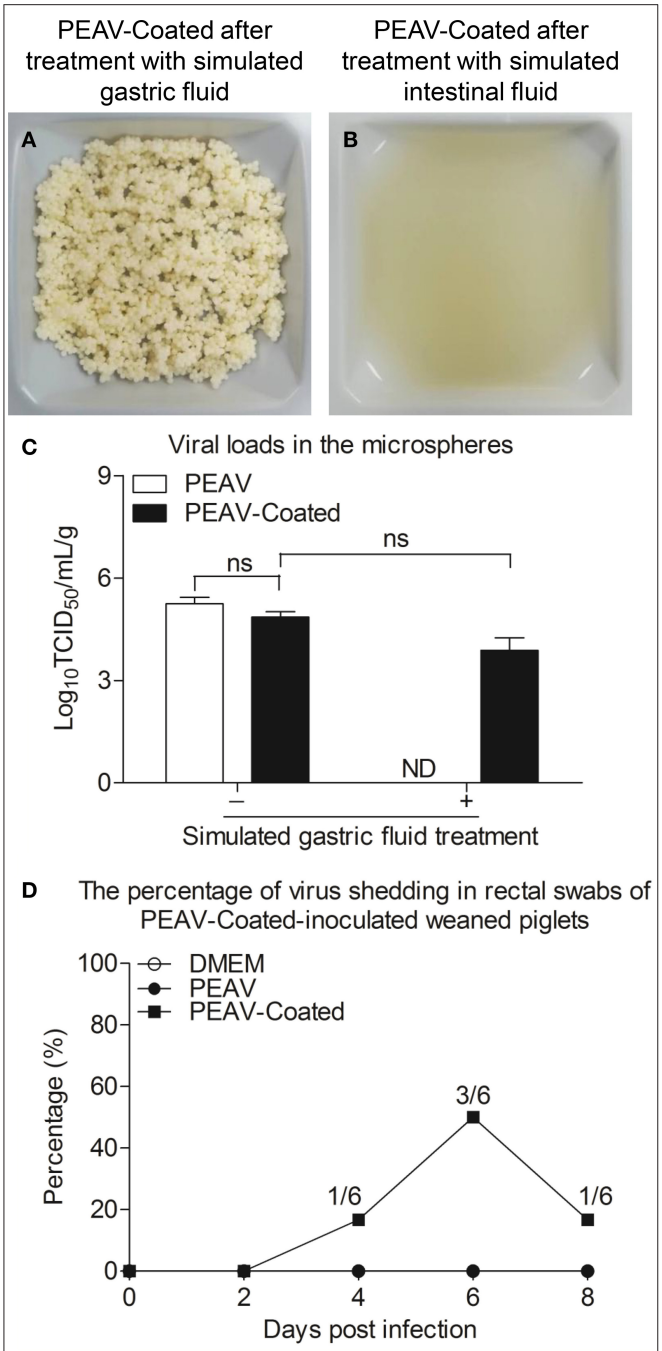

FIGURE 3 | Acid resistance and dissolvability of the PEAV-Coated in intestinal fluid *in vitro* and *in vivo*. PEAV-Coated were treated with the simulated gastric fluid **(A)** and the simulated intestinal fluid **(B)**. The acid resistance of the PEAV-Coated was analyzed before and after the simulated gastric fluid treatment by a $TCID_{50}$ assay, and PEAV was treated and analyzed equally as the control **(C)**. Weaned piglets were orally inoculated with PEAV-Coated, PEAV, and maintenance medium. Rectal swabs were collected from the piglets on days 0, 2, 4, 6, and 8 post inoculation and the virus shedding of PEAV were examined through real-time PCR using specific primers. The percentage of PEAV infection was calculated in **(D)**. Results of $TCID_{50}$ are representative of three independent experiments. Data are represented as mean ± SD, $n = 3$. ND means non-detectable.

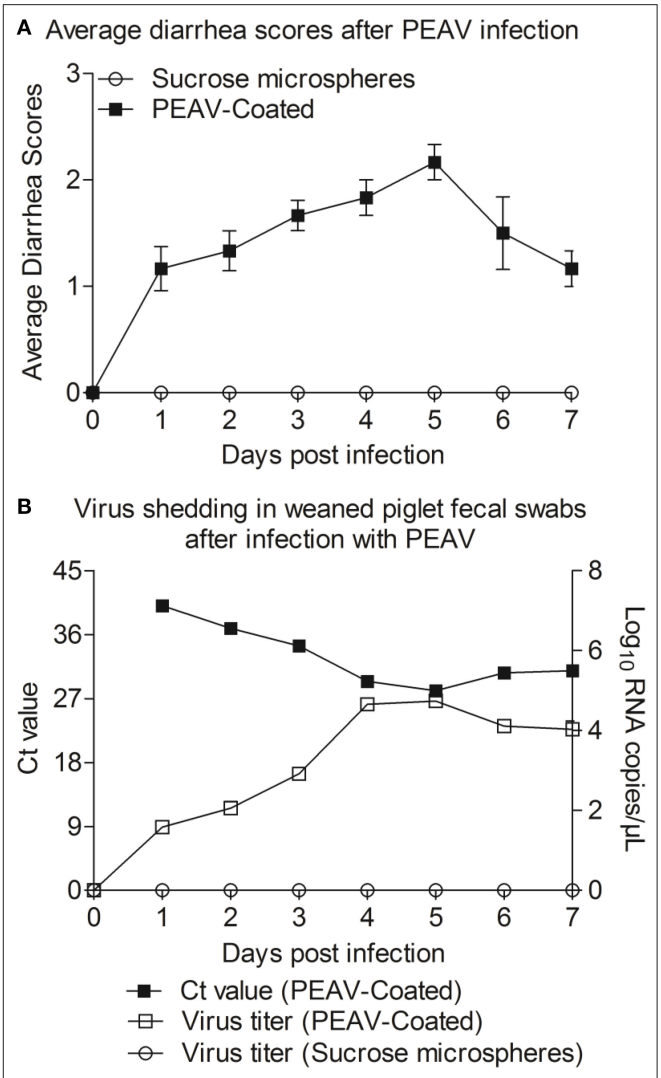

FIGURE 4 | Reproduction of watery diarrhea and fecal viral shedding in weaned piglets inoculated with PEAV-Coated *via* oral feeding. **(A)** Average diarrhea scores after PEAV-Coated infection. **(B)** Ct values of group PEAV-Coated inoculated weaned piglet fecal swabs and viral RNA shedding in fecal swabs after PEAV-Coated inoculation or sucrose microspheres inoculation.

PEAV-Coated Inhibits an Antiviral Response in Peyer's Patches

Type I interferon (IFN-α/β) plays an important role in innate immune response, which prompted us to examine the effect of PEAV on IFN-α and IFN-β. We found that PEAV could inhibit the mRNA expressions of *IFN-α* ($p < 0.05$) and *IFN-β* ($p < 0.05$) in Peyer's patches from PEAV-Coated-challenged weaned piglets at 7 d.p.i. (**Figure 5**). It was reported that IFN-stimulated genes (ISGs) could be induced after IFNs production (19). We further examined the mRNA expressions of ISGs in Peyer's patches from weaned piglets infected with PEAV-Coated at 3 d.p.i. and 7 d.p.i.. As shown in **Figure 6**, we found that PEAV

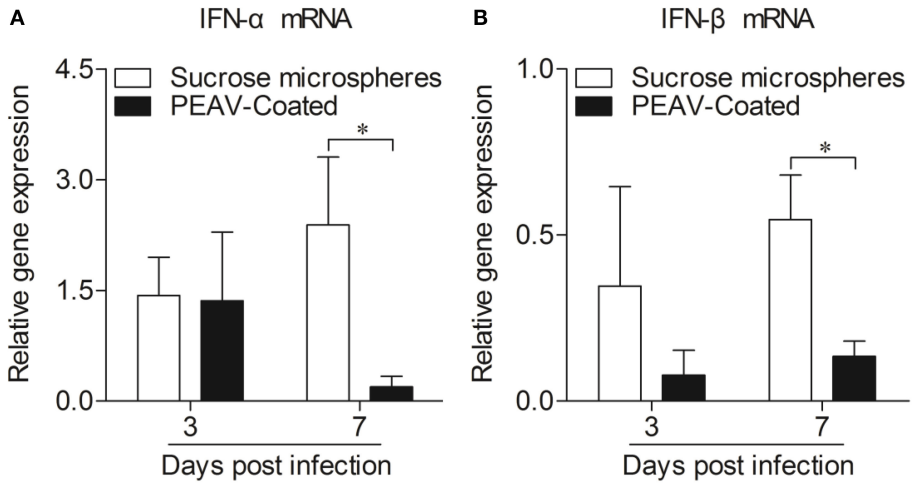

FIGURE 5 | Expressions of mRNA of type I interferon in Peyer's patches from weaned piglets after infection with PEAV-Coated at 3 d.p.i. and 7 d.p.i. The mRNA expressions of *IFN-α* **(A)** and *IFN-β* **(B)** in Peyer's patches from weaned piglets after infection with PEAV-Coated were examined with real-time PCR using specific primers at 3 d.p.i. and 7 d.p.i. The mRNA expression levels of these cytokines were calculated relative to the expression level of *GAPDH*. Data are represented as mean ±SD, $n = 6$. *$p < 0.05$.

could inhibit the mRNA expressions of *OAS* ($p < 0.05$), *Mx1* ($p < 0.05$), and *PKR* ($p < 0.01$ or $p < 0.05$) in Peyer's patches, indicating that PEAV could overcome an antiviral response to infect pigs.

PEAV-Coated Caused Histopathological Lesions and had Viral Antigen Distribution in Small Intestine

Pathology tests were conducted to determine the histological changes in the jejunum of weaned piglets infected with the PEAV-Coated. Compare to the negative control (**Supplemental Figures 1A,C**), the typical histological lesions characterized by intestinal villus detachment due to injury of intestinal epithelial cells were observed in intestinal villus from piglets that were necropsied at 3 d.p.i. and 7 d.p.i. (**Supplemental Figures 1B,D**). Consistent with the histopathological results, PEAV antigens were detected in the villous enterocytes of jejunum collected from PEAV-Coated-challenged piglets that were necropsied at 3 d.p.i. and 7 d.p.i. (**Supplemental Figures 1F,H**), but no PEAV antigen in the negative control was detected by immunohistochemical analysis (**Supplemental Figures 1E,G**), indicating that PEAV-Coated could cause intestinal lesions in weaned piglets.

DISCUSSION

Since PEAV was first reported in pigs in early February 2017 in Guangdong, China (1), this novel swine enteric CoV has been widely detected in areas of southern China, including Guangdong and Fujian (2, 3). Although a few studies have demonstrated that PEAV was highly pathogenic to newborn piglets (6–8), there are no published papers reporting the pathogenicity of PEAV in weaned piglets and the effect of PEAV infection on antiviral responses *in vivo* is still unclear. In the present study, PEAV-Coated were developed by the centrifugal granulation-fluidized bed coating apparatus and were used on orally inoculated weaned piglets to evaluate the pathogenicity to weaned piglets and to set up a model to explore antiviral response *in vivo*.

Oral infection of pigs with mature immune systems, like weaned piglets, can truly reflect the effect of the enterovirus on the host's immune responses. In another of our studies, we found that weaned piglets inoculated with cell-cultured PEAV GDS04 strain at a medium dose (2×10^5 $TCID_{50}$) could not develop diarrhea and that no PEAV was detected in the rectal swabs (data not shown), which was possibly due to the fact that the viruses could not overcome the acid pH level of the stomach by oral feeding, which can degrade labile components (18). This contradicts the idea that PEAV is transmitted through the fecal-oral route (20). We speculated that on farms, weaned piglets with mature immune systems might be infected by feeding on PEAV-infected pigs' feces, which may protect the virus from stomach acid damage. This has been confirmed by the protective effect of feed-back in sows with intestinal contents containing PEDV (21). Since it has been reported that the PEDV oral vaccine prepared by centrifugal granulation-fluidized bed coating technology could protect PEDV antigens against the complex gastrointestinal environment *in vitro* and *in vivo* and induced obvious immune responses in weaned piglets (10), we proposed that oral pellets containing the virus prepared by centrifugal granulation-fluidized bed coating technology might overcome the low pH and enzymes of the stomach to infect the body. To test our hypothesis, freeze-dried powders containing the PEAV GDS04 strain were loaded onto sucrose microspheres using centrifugal granulation technology. It was reported that HPMCP can improve the digestive stability and intestinal transport of green tea catechins (22). To further facilitate PEAV release in the gut, HPMCP was selected as an enteric polymer by fluidized

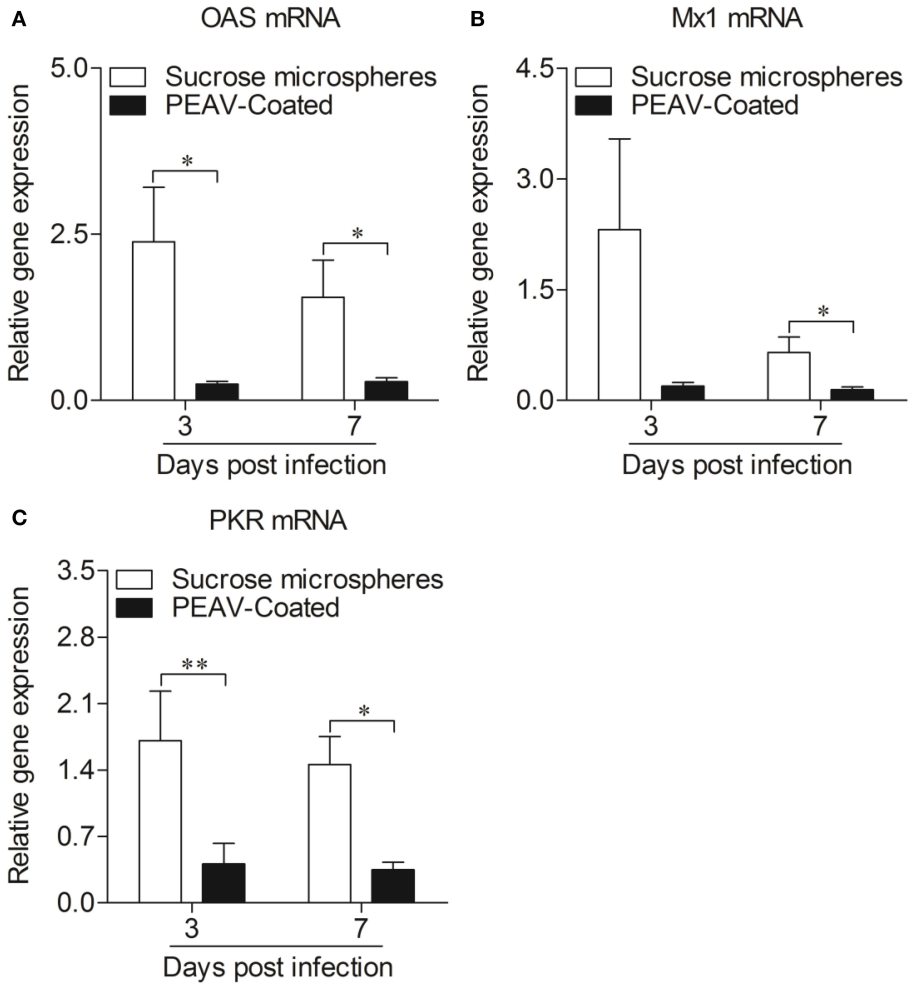

FIGURE 6 | Expressions of antiviral molecules mRNA in Peyer's patches from weaned piglets after infection with PEAV-Coated at 3 d.p.i. and 7 d.p.i. The mRNA expressions of *OAS* **(A)**, *Mx1* **(B)**, and *PKR* **(C)** in Peyer's patches from weaned piglets after infection with PEAV-Coated were examined with real-time PCR using specific primers at 3 d.p.i. and 7 d.p.i. The mRNA expression levels of these molecules were calculated relative to the expression level of *GAPDH*. Data are represented as mean ± SD, $n = 6$. $^{**}p < 0.01$, $^{*}p < 0.05$.

bed coating technology. As we discussed above, for infection in weaned piglets, gastric acid resisted by PEAV-Coated is the key. As shown in **Figure 3**, PEAV-Coated was verified to be able to resist acid in *in vitro* and *in vivo* experiments, while PEAV were to a large extent reduced by the simulated gastric acid treatment or no PEAV was detected in the rectal swabs from PEAV-inoculated weaned piglets. In addition, we found that there were no significant differences in virus titers between PEAV freeze-dried powders and PEAV-Coated, indicating that the virus survival was unaffected by the sucrose microspheres, the HPMCP, and the preparation process. This information suggests coated microspheres prepared by centrifugal granulation-coating technology might be a common and effective oral delivery system to protect the virus against the complex gastrointestinal environment to achieve infection *in vivo*. This is of great importance because it can be used to study the effect of enteroviruses on the host immune system *in vivo*. In addition, in order to control intestinal CoV infection in piglets, it requires viable virus particles to reach the intestine to generate mucosal immunity in sows, which is passed on to piglets *via* milk (23). Our research in PEAV prepared a candidate tool for the effective control of PEAV.

As a newly identified swine pathogen, the pathogenicity of PEAV in weaned piglets is still unknown. We infected the 33-day-old weaned piglets with the PEAV-Coated *via* oral feeding. While PEAV normally leads to severe watery diarrhea in newborn piglets (8), PEAV only caused mild diarrhea in weaned piglets, which suggests that the pathogenicity of PEAV varies among pigs of different ages, but it still poses a huge threat to weaned piglets and newborn piglets in pig farms. Interestingly, unlike in newborn piglets (6, 8), there was no vomiting and death in weaned piglets infected by PEAV-Coated (data not shown), which was found in other porcine enteric CoVs infection, such as PDCoV, PEDV, and TGEV (24–26), indicating that

these CoVs are more harmful to newborn piglets than weaned piglets. However, compared to PEAV-Coated, cell-cultured PEAV without coated didn't cause any diarrhea in weaned piglets (data not shown). Taken together, all these results speculate that age-dependent pathogenicity in PEAV as well as in other entero-CoVs is related ti stomach acid degradation.

Neonatal suckling piglets are not appropriate targets to study immune responses by virus infection due to their fragile and immature immune systems (26). Weaned piglets were used to successfully reveal the innate immune responses with PDCoV infection (26) and indicated that weaned piglets might be useful in studying the effect of PEAV on the immune system. However, as we discovered (data not shown), oral delivery of cell-cultured PEAV without a coating didn't cause diseases in weaned piglets. The successful establishment of the infection model in weaned piglets by PEAV-Coated system removed the obstacle. The infection model allows us to control the type and quantity of virus, and to simulate the fecal-oral route, which will help us to better study the pathogenic mechanism of porcine intestinal CoVs and lay a foundation for the preparation of a PEAV oral vaccine.

Innate immunity is thought to be the first line of host defense against a wide variety of pathogenic infections (27). Of note, type I interferon (IFN-α/β), as important cytokines of innate immunity induced by virus invasion, could establish an anti-viral state in infected sites, and also regulate the development of an adaptive immune response (19). The small intestinal mucosa, which contains immune tissues, is thought to be the primary site for defense against enteropathogens (28). Microscopic lesions and viral antigens were also found in the small intestines of PEAV-Coated-challenged piglets (**Supplemental Figure 1**), indicating that PEAV could destroy mucosal tissue localized in the gut. Peyer's patches, occupied in the jejunum and ileum, serve as the primary inductive sites for intestinal immunity (29–31). It was reported that SADS-CoV antagonizes IFN-β production *via* blocking IPS-1 and RIG-I in IPEC-J2 cells (32). Interestingly, we also found that PEAV could inhibit the mRNA expressions of *IFN-α* and *IFN-β* in Peyer's patches at 7 d.p.i., consistent with the results *in vitro* (**Supplemental Figure 2**), indicating that PEAV infection could inhibit the body's anti-viral state. It is known that ISGs, such as dsRNA activated protein kinase R (PKR) (33), 2′-5′-oligoadenylate synthetase (OAS) (34), and Mx proteins (35), induced by IFNs can directly act against virus infection (36). Consistent with the type I interferon results, PEAV could inhibit the mRNA expressions of *OAS*, *Mx1*, and *PKR* in Peyer's patches. All these results suggest that this virus could overcome the antiviral response to infect the body. Interestingly, the antiviral response was not detected *in vivo*, possibly due to the timing of the test. Since PEAV inhibited an antiviral response *in vivo*, several important questions are raised. For example, what's the viral protein of PEAV inhibiting the expressions of these cytokines *in vivo*? And what is the exact underlying mechanism? What's the immune cell dynamics after PEAV infection in pigs? Further efforts will be required to elucidate the molecular mechanisms underlying the pathogenesis of PEAV infection.

In summary, our research successfully established a PEAV animal infection model in weaned piglets. Remarkably, inoculation of weaned piglets with PEAV obviously inhibited *IFN-α*, *IFN-β*, *OAS*, *Mx1,* and *PKR* mRNA expression in infected Peyer's patches *in vivo*. These findings have provided insights for further studies of the molecular mechanism underlying PEAV infection resistant host immune responses.

DATA AVAILABILITY STATEMENT

All datasets presented in this study are included in the article/**Supplementary Material**.

ETHICS STATEMENT

The animal study was supervised by the Institutional Animal Care and Use Committee of Sun Yat-sen University (IACUC DD-17-1003) and used in accordance with regulation and guidelines of this committee.

AUTHOR CONTRIBUTIONS

YC and ZX conceived and designed the experiments. ZX and PP performed the experiments. ZX analyzed the data. LG, YL, CX, and YC contributed reagents, materials, analysis tools. ZX wrote the paper. YC checked and finalized the manuscript. All authors read and approved the final manuscript.

FUNDING

This work was supported by the National Natural Science Foundation, China (31902248 and 31741118), National Key Research and Development Program, China (2016YFD0500101), Guangdong Natural Science Foundation (2018B030314003), and the Fundamental Research Funds for the Central University (19lgpy188).

SUPPLEMENTARY MATERIAL

The Supplementary Material for this article can be found online at: https://www.frontiersin.org/articles/10.3389/fvets.2020.00449/full#supplementary-material

Supplemental Figure 1 | Intestinal changes in weaned piglets inoculated with PEAV-Coated. **(A,C)** H&E-stained jejunum tissue sections of sucrose microspheres-challenged piglets at 3 d.p.i. and 7 d.p.i. **(B,D)** H&E-stained jejunum tissue sections of PEAV-Coated-challenged piglets at 3 d.p.i. and 7 d.p.i. (Blunt intestinal villus was indicated by arrows). **(E,G)** Immunohistochemically stained jejunum tissue sections of sucrose microspheres-challenged piglets at 3 d.p.i. and 7 d.p.i. **(F,H)** Immunohistochemically stained jejunum tissue sections of PEAV-Coated-challenged piglets at 3 d.p.i. and 7 d.p.i.

Supplemental Figure 2 | Infection of IPEC-J2 cells with PEAV strain GDS04 inhibits Sendai virus (SeV)-induced expression of *IFN-β in vitro*. IPEC-J2 cells (2×10^5) were mock infected or infected with PEAV at an MOI of 0.5. Twelve hours after PEAV infection, cells were treated with SeV at an MOI of 1. Twelve hours after SeV treatment, mRNA expressions of *IFN-α* **(A)** and *IFN-β* **(B)** were measured by real-time PCR using specific primers. The mRNA expression levels of these molecules were calculated relative to the expression level of *GAPDH*. Data are represented as mean ±SD, $n = 9$. $^*p < 0.05$, $^{***}p < 0.001$. (SeV is able to induce a good IFN-β response, but not IFN-α in IPEC-J2 cells).

REFERENCES

1. Gong LLJ, Zhou Q, Xu Z, Chen L, Zhang Y, Xue Y, et al. A New Bat-HKU2-like coronavirus in Swine, China, 2017. *Emerging Infect Dis.* (2017) 23:1607–9. doi: 10.3201/eid2309.170915
2. Zhou L, Sun Y, Lan T, Wu R, Chen J, Wu Z, et al. Retrospective detection and phylogenetic analysis of swine acute diarrhoea syndrome coronavirus in pigs in southern China. *Transbound Emerg Dis.* (2018) 66:687–95. doi: 10.1111/tbed.13008
3. Li KL, Bi H, Gu Z, Gong J, Luo W, Zhang S, et al. Complete genome sequence of a novel swine acute diarrhea syndrome coronavirus, CH/FJWT/2018, isolated in fujian, China, in 2018. *Microbiol Resour Announc.* (2018) 7:e01259–18. doi: 10.1128/MRA.01259-18
4. Lau SK, Woo PC, Li KS, Huang Y, Wang M, Lam CS, et al. Complete genome sequence of bat coronavirus HKU2 from Chinese horseshoe bats revealed a much smaller spike gene with a different evolutionary lineage from the rest of the genome. *Virology.* (2007) 367:428–39. doi: 10.1016/j.virol.2007.06.009
5. Cruz DJ, Kim CJ, Shin HJ. The GPRLQPY motif located at the carboxy-terminal of the spike protein induces antibodies that neutralize Porcine epidemic diarrhea virus. *Virus Res.* (2008) 132:192–6. doi: 10.1016/j.virusres.2007.10.015
6. Zhou P, Fan H, Lan T, Yang XL, Shi WF, Zhang W, et al. Fatal swine acute diarrhoea syndrome caused by an HKU2-related coronavirus of bat origin. *Nature.* (2018) 556:255–8. doi: 10.1038/s41586-018-0010-9
7. Pan Y, Tian X, Qin P, Wang B, Zhao P, Yang YL, et al. Discovery of a novel swine enteric alphacoronavirus (SeACoV) in southern China. *Vet Microbiol.* (2017) 211:15–21. doi: 10.1016/j.vetmic.2017.09.020
8. Xu Z, Zhang Y, Gong L, Huang L, Lin Y, Qin J, et al. Isolation and characterization of a highly pathogenic strain of Porcine enteric alphacoronavirus causing watery diarrhoea and high mortality in newborn piglets. *Transbound Emerg Dis.* (2019) 66:119–30. doi: 10.1111/tbed.12992
9. Reed LJMH. A simple method of estimating fifty per cent endpoints. *Am J Epidemiol.* (1938) 27:3. doi: 10.1093/oxfordjournals.aje.a118408
10. Wen Z, Xu Z, Zhou Q, Li W, Wu Y, Du Y, et al. Oral administration of coated PEDV-loaded microspheres elicited PEDV-specific immunity in weaned piglets. *Vaccine.* (2018) 36:6803–9. doi: 10.1016/j.vaccine.2018.09.014
11. Desai KG, Schwendeman SP. Active self-healing encapsulation of vaccine antigens in PLGA microspheres. *J Control Release.* (2013) 165:62–74. doi: 10.1016/j.jconrel.2012.10.012
12. Davitt CJ, Mcneela EA, Longet S, Tobias J, Aversa V, Mcentee CP, et al. A novel adjuvanted capsule based strategy for oral vaccination against infectious diarrhoeal pathogens. *J Control Release.* (2016) 233:162–73. doi: 10.1016/j.jconrel.2016.05.001
13. Xu Z, Zhong H, Zhou Q, Du Y, Chen L, Zhang Y, et al. A highly pathogenic strain of porcine deltacoronavirus caused watery diarrhea in newborn piglets. *Virol Sin.* (2018) 33:131–41. doi: 10.1007/s12250-018-0003-8
14. Chen Q, Gauger P, Stafne M, Thomas J, Arruda P, Burrough E, et al. Pathogenicity and pathogenesis of a United States porcine deltacoronavirus cell culture isolate in 5-day-old neonatal piglets. *Virology.* (2015) 482:51–9. doi: 10.1016/j.virol.2015.03.024
15. Zhou L, Sun Y, Wu JL, Mai KJ, Chen GH, Wu ZX, et al. Development of a TaqMan-based real-time RT-PCR assay for the detection of SADS-CoV associated with severe diarrhea disease in pigs. *J Virol Methods.* (2018) 255:66–70. doi: 10.1016/j.jviromet.2018.02.002
16. Borca MV, Gudmundsdottir I, Fernandez-Sainz IJ, Holinka LG, Risatti GR. Patterns of cellular gene expression in swine macrophages infected with highly virulent classical swine fever virus strain Brescia. *Virus Res.* (2008) 138:89–96. doi: 10.1016/j.virusres.2008.08.009
17. Huang C, Zhang Q, Guo XK, Yu ZB, Xu AT, Tang J, et al. Porcine reproductive and respiratory syndrome virus nonstructural protein 4 antagonizes beta interferon expression by targeting the NF-kappaB essential modulator. *J Virol.* (2014) 88:10934–45. doi: 10.1128/JVI.01396-14
18. Davitt CJ, Lavelle EC. Delivery strategies to enhance oral vaccination against enteric infections. *Adv Drug Deliv Rev.* (2015) 91:52–69. doi: 10.1016/j.addr.2015.03.007
19. Xie S, Chen XX, Qiao S, Li R, Sun Y, Xia S, et al. Identification of the RNA pseudoknot within the 3′ end of the porcine reproductive and respiratory syndrome virus genome as a pathogen-associated molecular pattern to activate antiviral signaling via RIG-I and toll-like receptor 3. *J Virol.* (2018) 92:e00097-18. doi: 10.1128/JVI.00097-18
20. Yang Y-L, Yu J-Q, Huang Y-W. Swine enteric alphacoronavirus (swine acute diarrhea syndrome coronavirus): an update three years after its discovery. *Virus Res.* (2020) 285:198024. doi: 10.1016/j.virusres.2020.198024
21. Goede D, Morrison RB. Production impact & time to stability in sow herds infected with porcine epidemic diarrhea virus (PEDV). *Prev Vet Med.* (2016) 123:202–7. doi: 10.1016/j.prevetmed.2015.11.010
22. Chung JH, Lee SJ, Chung JO, Oh YJ, Hwang JA, Kim YK, et al. Effect of hydroxypropyl methyl cellulose phthalate coating on digestive stability and intestinal transport of green tea catechins. *Integr Med Res.* (2014) 3:34–7. doi: 10.1016/j.imr.2013.11.001
23. Wen Z, Xu Z, Zhou Q, Li W, Wu Y, Du Y, et al. A heterologous 'prime-boost' anti-PEDV immunization for pregnant sows protects neonatal piglets through lactogenic immunity against PEDV. *Lett Appl Microbiol.* (2019) 69:258–63. doi: 10.1111/lam.13197
24. Moon HWK, Lambert LJ, Stark G, Booth SL. Age-dependent resistance to transmissible gastroenteritis of swine. III Effects of epithelial cell kinetics on coronavirus production and on atrophy of intestinal villi. *Vet Pathol.* (1975) 12:434–45. doi: 10.1177/030098587501200500610
25. Shibata ITT, Mori M, Ono M, Sueyoshi M, Uruno K. Isolation of porcine epidemic diarrhea virus in porcine cell cultures and experimental infection of pigs of different ages *Vet Microbiol.* (2000) 15:173–82. doi: 10.1016/S0378-1135(99)00199-6
26. Xu Z, Zhong H, Huang S, Zhou Q, Du Y, Chen L, et al. Porcine deltacoronavirus induces TLR3, IL-12, IFN-alpha, IFN-beta and PKR mRNA expression in infected Peyer's patches in vivo. *Vet Microbiol.* (2019) 228:226–33. doi: 10.1016/j.vetmic.2018.12.012
27. Li Z, Wang Y, Li X, Li X, Cao H, Zheng SJ. Critical roles of glucocorticoid-induced leucine zipper in infectious bursal disease virus (IBDV)-induced suppression of type I Interferon expression and enhancement of IBDV growth in host cells via interaction with VP4. *J Virol.* (2013) 87:1221–31. doi: 10.1128/JVI.02421-12
28. Yuan C, Zhang E, Huang L, Wang J, Yang Q. Oral administration of inactivated porcine epidemic diarrhea virus activate DCs in porcine Peyer's patches. *BMC Vet Res.* (2018) 14:239. doi: 10.1186/s12917-018-1568-z
29. Vazquez-Torres AF, Fang FC. Cellular routes of invasion by enteropathogens. *Curr Opin Microbiol.* (2000) 3:54–9. doi: 10.1016/S1369-5274(99)00051-X
30. Van Kruiningen HJW, Freda BJ, Holmes KA. Distribution of peyer's patches in the distal ileum. *Inflamm Bowel Dis.* (2002) 8:180–5. doi: 10.1097/00054725-200205000-00004
31. Kapoor K, Opinder S. Ileal and jejunal Peyer's patches in buffalo calves: histomorphological comparison. *Vet World.* (2015) 8:1273–8.doi: 10.14202/vetworld.2015.1273-1278
32. Zhou Z, Sun Y, Yan X, Tang X, Li Q, Tan Y, et al. Swine acute diarrhea syndrome coronavirus (SADS-CoV) antagonizes interferon-beta production via blocking IPS-1 and RIG-I. *Virus Res.* (2020) 278:197843. doi: 10.1016/j.virusres.2019.197843
33. Williams BR. PKR; a sentinel kinase for cellular stress. *Oncogene.* (1999) 18:6112–20. doi: 10.1038/sj.onc.1203127

34. Sanfilippo C, Pinzone MR, Cambria D, Longo A, Palumbo M, Di Marco R, et al. OAS gene family expression is associated with HIV-related neurocognitive disorders. *Mol Neurobiol.* (2018) 55:1905–14. doi: 10.1007/s12035-017-0460-3
35. Zhou J, Chen J, Zhang XM, Gao ZC, Liu CC, Zhang YN, et al. Porcine Mx1 protein inhibits classical swine fever virus replication by targeting nonstructural protein NS5B. *J Virol.* (2018) 92. doi: 10.1128/JVI.02147-17
36. Lenschow DJ, Lai C, Frias-Staheli N, Giannakopoulos NV, Lutz A, Wolff T, et al. IFN-stimulated gene 15 functions as a critical antiviral molecule against influenza, herpes, and Sindbis viruses. *Proc Natl Acad Sci USA.* (2007) 104:1371–6. doi: 10.1073/pnas.0607038104

Conflict of Interest: The authors declare that the research was conducted in the absence of any commercial or financial relationships that could be construed as a potential conflict of interest.

frontiers in Veterinary Science

ORIGINAL RESEARCH
published: 24 July 2020
doi: 10.3389/fvets.2020.00435

Genetic Diversity of Porcine Epidemic Diarrhea Virus With a Naturally Occurring Truncated ORF3 Gene Found in Guangxi, China

Ying Lu[1], Xueli Su[1], Chen Du[1], Liyuan Mo[1], Purui Ke[1], Ruomu Wang[1], Lian Zhong[1], Cui Yang[2], Ying Chen[1], Zuzhang Wei[1], Weijian Huang[1], Yuying Liao[2]* and Kang Ouyang[1]**

[1] Laboratory of Animal Infectious Disease and Molecular Immunology, College of Animal Science and Technology, Guangxi University, Nanning, China, [2] Laboratory of Poultry, Guangxi Institute of Animal Science, Nanning, China

OPEN ACCESS

Edited by:
Shao-Lun Zhai, Guangdong Academy of Agricultural Sciences, China

Reviewed by:
Faten Abdelaal Okda, St. Jude Children's Research Hospital, United States
Jean-Pierre Frossard, Animal and Plant Health Agency, United Kingdom

***Correspondence:**
Weijian Huang
huangweijian-1@163.com
Yuying Liao
315951610@qq.com
Kang Ouyang
ouyangkang@gxu.edu.cn

Specialty section:
This article was submitted to Veterinary Infectious Diseases, a section of the journal Frontiers in Veterinary Science

Received: *29 February 2020*
Accepted: *16 June 2020*
Published: *24 July 2020*

Citation:
Lu Y, Su X, Du C, Mo L, Ke P, Wang R, Zhong L, Yang C, Chen Y, Wei Z, Huang W, Liao Y and Ouyang K (2020) Genetic Diversity of Porcine Epidemic Diarrhea Virus With a Naturally Occurring Truncated ORF3 Gene Found in Guangxi, China. Front. Vet. Sci. 7:435. doi: 10.3389/fvets.2020.00435

Porcine epidemic diarrhea virus (PEDV) is one of the major enteric pathogens, causing severe enteric disease, resulting in enormous economic losses. The ORF3 gene encodes an accessory protein which is related to the infectivity and virulence of PEDV. In this study, 33 PEDV positive field samples were collected from Guangxi, from 2017 to 2019, and the genetic diversity of ORF3 was investigated. Thirty-eight strains of ORF3 were obtained, and these were composed of five strains of ORF3 named Guangxi naturally truncated strains that were 293 bp in length, with continuous deletions from 172 to 554 bp. The Guangxi naturally truncated strains encoded a truncated protein of 89 amino acids, which had clustered into a new group referred to as Group 3, and these might be involved in the variations of virulence. Three genotypes (G1-1 subgroup, G1-3 subgroup, and Group 3) existed simultaneously in Guangxi based on the genetic and evolutionary analysis of the ORF3 gene. The sequence information in the current study will hopefully facilitate the establishment of a diagnostic method that can differentiate the PEDV field stains. Continued surveillance will be useful for monitoring PEDV transmission. Differentiation of the ORF3 genes in PEDV field strains can help us to choose an appropriate PEDV vaccine candidate in the future and prevent outbreaks of PED more effectively.

Keywords: pigs, PEDV, ORF3, genetic diversity, naturally truncated gene

INTRODUCTION

Porcine epidemic diarrhea virus (PEDV) is one of the major enteric pathogens currently threatening the swine population worldwide (1). Clinically, pigs infected with PEDV cause severe enteric diseases with a high mortality rate in suckling piglets, resulting in tremendous economic losses (2–6). The disease is mainly transmitted through feces (7), air (8), and contaminated feeds (9).

PEDV first emerged in Europe in the 1970s and then spread across Europe and into Asia (10). In China, outbreaks of PEDV have been observed on most swine breeding farms since late 2010 (6, 8, 11). PEDV has rapidly spread across 34 states of America, Canada, and has returned to devastate the swine industry in Asia after being diagnosed in the USA in April 2013 (12, 13).

PEDV is an enveloped, positive-stranded RNA virus in the genus *Alphacoronavirus*, family *Coronaviridae*, order *Nidovirales* (14, 15). The genome of a PEDV is ∼28 kb in length and is composed of seven open reading frames (ORFs) arranged in the order

5′-ORF1a/1b-S-ORF3-E-M-N-3′, which encodes four structural proteins and 17 non-structural proteins (nsp1-nsp16, and ORF3) (16, 17).

The full length of the ORF3 gene is 675 bp, encoding 224 amino acids. The PEDV ORF3 gene has been found to have a low sequence conservation through analysis of the amino acid sequences and their homologs across the alpha-coronavirus genus (18, 19). The ORF3 encodes an ion channel protein and regulates virus production (20), and its naturally truncated form might cause attenuation of the virus to the natural host. The differentiation of ORF3 could be a marker of adaptation to cell cultures and attenuation of virus, and this could be a valuable tool for studying the molecular epidemiology of PEDV (5, 21). To investigate the genetic diversity of PEDV in Guangxi, we sequenced the full-length ORF3 gene of 33 PEDV positive field samples collected from 2017 to 2019.

MATERIALS AND METHODS

Thirty-three intestinal samples were taken from piglets with clinical diarrhea from different pig farms in Guangxi between 2017 and 2019. Thirty-eight strains of PEDV ORF3 were obtained. Five strains were clustered into a new group referred to as Group 3, while there were 24 and nine strains which were clustered into the G1-1 and G1-3 subgroups, respectively.

Samples were homogenized with a 20% glycerin and PBS stock preservation solution (GPSs). The suspensions were then vortexed and centrifuged for 5 min at 3,000 × g. The supernatants were collected and stored at −80°C before utilization. The vaccine strains CV777 (Harbin Weike Biological Co. Ltd, Harbin, China), AJ1102-R (Wuhan Keqian Biological Co., Ltd, Wuhan, China) and Zhejiang-08 (China Animal Husbandry Industry Co., Ltd, Beijing, China) were purchased as controls.

Total RNA was extracted using a humoral virus DNA/RNA kit (Axygen Scientific, Union City, CA, USA), and transcribed into cDNA by Oligo dTs, dNTP mix, and M-MLV Reverse Transcriptase reagent (TaKaRa, Dalian, China). The primers, ORF3F: 5′-GTCCTAGACTTCAACCTTACGAAG-3′ and ORF3R: 5′-AACTACTAGACCATTATCATTCAC-3′ were used for PCR at 95°C for 5 min followed by 30 cycles of denaturation at 95 °C for 15 s, annealing at 55°C for 30 s and extension at 72°C for 1 min (22). The expected size of PCR products is 740 bp, which contained the full ORF3 gene with a length of 675 bp.

The RT-PCR products were analyzed using 1.5% agarose gel electrophoresis and visualized by ultraviolet illumination. The expected DNA band was purified using a Gel Extraction Kit (OMEGA biotech, Doraville, GA, USA), and cloned into a pMD-18T vector (TaKaRa, Dalian, China). The sequences of the positive clones were determined by Beijing Genomics Institute (Guangzhou, China). The validated genome sequences of ORF3 were submitted to GenBank under the accession numbers MK895557∼MK895560 and MN518432∼MN518465.

One-hundred and thirteen reference strains of PEDV ORF3 from different countries collected on different dates were selected for the genetic analysis (**Supplementary Table 1**). Sequences were analyzed by using software packages, DNAstar, MEGA5.2, and iTOL v.5. Multiple nucleotide and amino acid sequence alignments were analyzed by applying the ClustalV method with the MegAlign program and the ClustalW alignment tool in the MEGA5.2 software, respectively. The MEGA 5.2 program was applied to construct phylogenetic trees by using the neighbor-joining method, the tree topology was constructed using the Poisson model and the robustness of the phylogenetic tree was evaluated by bootstrapping using 1,000 replicates (23). The

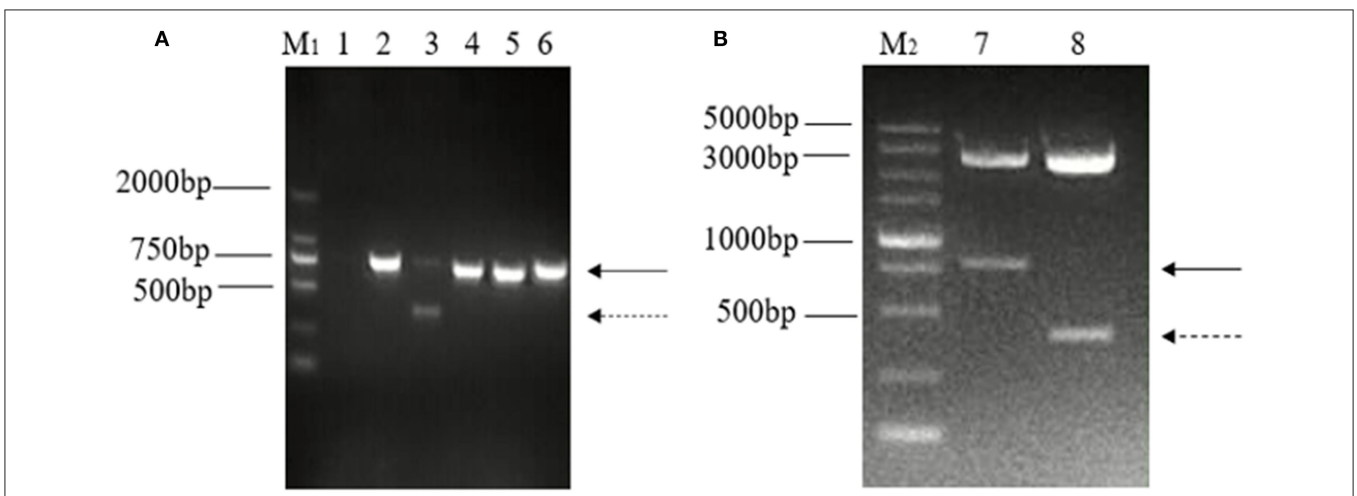

FIGURE 1 | Detection and identification of two distinct bands of the ORF3 gene of PEDV in Guangxi. **(A)** Amplification of ORF3 gene in PEDV positive samples. M_1: DL 2000 marker; Lane 1: negative control; Lane 2: predicted product (740 bp); Lane 3: predicted product (740 bp) and large genomic deletion (∼358 bp); Lane 4: CV777 strain; Lane 5: Zhejiang-08 strain; Lane 6: AJ1102 strain. **(B)** Identification of the plasmid, pMD-18T-ORF3, by enzyme digestion using PstI and BamHI. M_2: DL 5000 marker; Lane 1: The solid arrows indicate the predicted products (740 bp); Lane 2: The dashed arrows indicate products of PEDV variants with a large genomic deletion (∼358 bp).

resulting tree was visualized by using iTOL v.5 (Interactive Tree of Life, http://itol.embl.de/).

RESULTS

Amplification and Identification of the PEDV ORF3 Gene

The ORF3 gene was amplified using the primer pair for ORF3 from generated cDNA, and one distinct band of unexpected shorter sizes was observed in five PCR products in addition to the predicted band. Both bands of nucleotide were cloned into a pMD-18T vector and were identified by enzyme digestion using *PstI* and *BamHI* (**Figure 1**).

Nucleotide Alignment of the ORF3 Gene Sequence

In this study, thirty-eight strains of PEDV ORF3 were obtained from 33 samples in Guangxi between 2017 and 2019 (**Table 1**). There were five strains (CHN/GXNN-4-2/2018, CHN/GXQZ-3-2/2018, CHN/GXQZ-6-2/2018, CHN/GXLB-1-2/2019 and CHN/GXQZ-1-2/2019) of ORF3 which were only 293bp in length, and the rest of the 33 strains had a complete ORF3 gene sequence, with a length of 675 bp. When these five Guangxi naturally truncated strains were compared with the main reference strains for nucleotide alignment (**Supplementary Table 1**), we found that the five strains all had continuous deletions from 172 to 554 bp, and exhibited 98.0–99.3% nucleotide identity with them. In addition, the Guangxi naturally truncated strains had the highest homology of up to 95.9–96.6%, when compared with AJ1102, and exhibited 94.2–95.6% nucleotide identity when compared with the CV777, truncated CV777 strain, Zhejiang-08 and attenuated DR13. Interestingly, one unique substitution at C78T was found to be present in the Guangxi naturally truncated strains in the present study (**Figure 2**), as well as two unique substitutions at T99C and T636C in the AJ1102 strain.

A sketch map of the ORF3 comparisons of the strains, including CV777, AJ1102, truncated CV777, Zhejiang-08, attenuated DR13, and the Guangxi naturally truncated strains is shown in **Figure 3**. The results show that the ORF3 gene of CV777 and AJ1102 were complete, and the truncated CV777, Zhejiang-08 strain and attenuated DR13 strain had 49 nucleotide deletions at 245–294 bp. Importantly, the Guangxi naturally truncated strains contained all the missing regions of these reference strains.

TABLE 1 | Origins and information regarding the Guangxi strains from 2017 to 2019.

Name	Collection area	Collection date	ORF3 gene size	Accession number
CHN/GXWZ-1/2017	Wuzhou	2017.08	675 bp	MN518432
CHN/GXWZ-2/2017	Wuzhou	2017.08	675 bp	MN518433
CHN/GXNN-1/2017	Nanning	2017.11	675 bp	MK895557
CHN/GXQZ-1/2017	Qinzhou	2017.11	675 bp	MN518434
CHN/GXGG-1/2018	Guigang	2018.03	675 bp	MN518435
CHN/GXYL-1/2018	Yulin	2018.03	675 bp	MN518452
CHN/GXNN-5/2018	Nanning	2018.03	675 bp	MN518461
CHN/GXLZ-1/2018	Liuzhou	2018.04	675 bp	MN518449
CHN/GXBH-1/2018	Beihai	2018.05	675 bp	MN518442
CHN/GXNN-1/2018	Nanning	2018.06	675 bp	MK895558
CHN/GXQZ-1/2018	Qinzhou	2018.07	675 bp	MN518453
CHN/GXQZ-2/2018	Qinzhou	2018.08	675 bp	MN518454
CHN/GXQZ-3-1/2018	Qinzhou	2018.08	675 bp	MN518455
CHN/GXQZ-3-2/2018	Qinzhou	2018.08	293 bp	MN518456
CHN/GXQZ-4/2018	Qinzhou	2018.08	675 bp	MN518457
CHN/GXQZ-6-1/2018	Qinzhou	2018.08	675 bp	MN518459
CHN/GXQZ-6-2/2018	Qinzhou	2018.08	293 bp	MN518460
CHN/GXGG-2/2018	Guigang	2018.10	675 bp	MN518436
CHN/GXNN-2/2018	Nanning	2018.10	675 bp	MK895559
CHN/GXBH-2/2018	Beihai	2018.10	675 bp	MN518443
CHN/GXBH-6/2018	Beihai	2018.10	675 bp	MN518447
CHN/GXBH-7/2018	Beihai	2018.10	675 bp	MN518448
CHN/GXQZ-5/2018	Qinzhou	2018.10	675 bp	MN518458
CHN/GXNN-4-1/2018	Nanning	2018.11	675 bp	MN518440
CHN/GXNN-4-2/2018	Nanning	2018.11	293 bp	MN518441
CHN/GXBH-3/2018	Beihai	2018.11	675 bp	MN518444
CHN/GXBH-4/2018	Beihai	2018.11	675 bp	MN518445
CHN/GXBH-5/2018	Beihai	2018.11	675 bp	MN518446
CHN/GXLB-1/2018	Laibin	2018.11	675 bp	MN518450
CHN/GXLB-2/2018	Laibin	2018.11	675 bp	MN518451
CHN/GXGG-3/2018	Guigang	2018.12	675 bp	MN518437
CHN/GXNN-3/2018	Nanning	2018.12	675 bp	MK895560
CHN/GXLB-1-1/2019	Laibin	2019.01	675 bp	MN518462
CHN/GXLB-1-2/2019	Laibin	2019.01	293 bp	MN518463
CHN/GXQZ-1-1/2019	Qinzhou	2019.01	675 bp	MN518464
CHN/GXQZ-1-2/2019	Qinzhou	2019.01	293 bp	MN518465
CHN/GXNN-1/2019	Nanning	2019.04	675 bp	MN518438
CHN/CXNN-2/2019	Nanning	2019.04	675 bp	MN518439

Alignment of Amino Acid Sequences

The results of amino acid sequence analysis indicated that all the strains were separated into three groups (**Figure 4**). Among the Guangxi strains in this study, 33 strains were 675 bp in length and encoded a protein of 224 amino acids, and these belong to Group 1. The Guangxi naturally truncated strains were 293 bp in length and encoded a truncated protein of 89 amino acids, and these formed a new group referred to as Group 3. The ORF3 genes of the Guangxi naturally truncated strains exhibited 94.4–97.8% amino acids identity, whereas they had 69.3–72.7% identity to the truncated CV777, Zhejiang-08 and attenuated DR13 strains, and 65.2–71.9% identity to the CV777 and AJ1102. Within Group 2, there are 11 reference strains (including truncated CV777, Zhejiang-08, and attenuated DR13 strain) and translation in these strains was terminated early because of specific deletions, which were located at amino acids 86L−102L and 104G−121F, respectively.

In terms of predicted amino acid sequence, strains in G1-1 and G1-3 subgroups all had an ORF3 of 224 amino acids, but their genotypes were different because of the amino acid

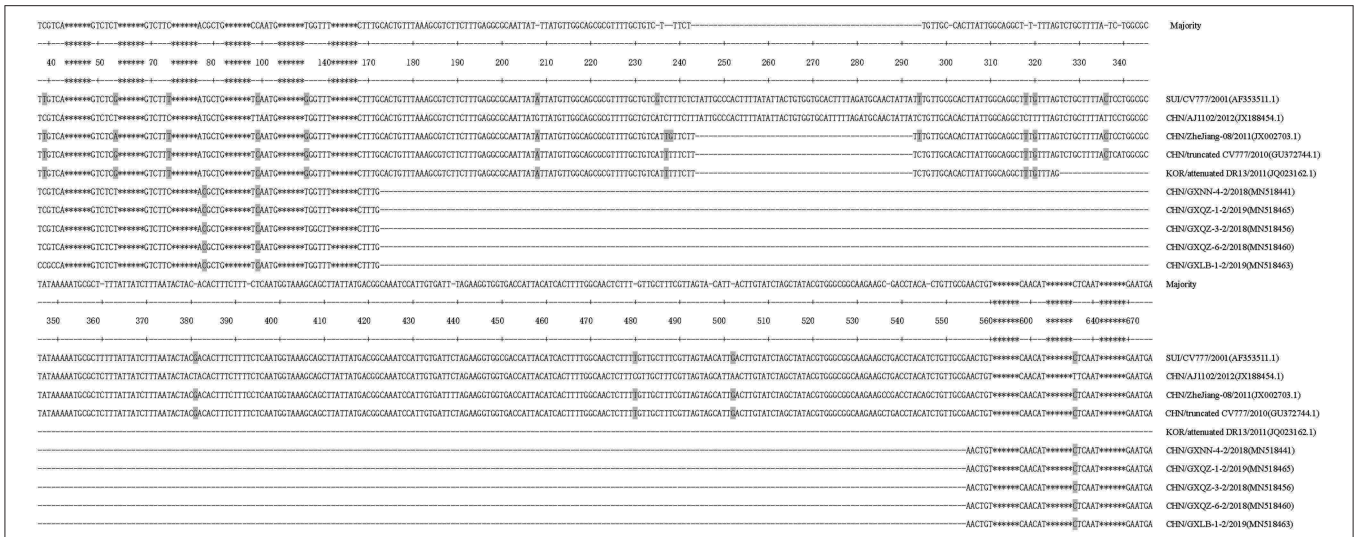

FIGURE 2 | Alignment of nucleotide sequences of ORF3 genes of the Guangxi naturally truncated strains and reference strains. Multiple nucleotide sequence alignments were analyzed by applying the Clustal V method with the MegAlign program. The asterisks indicate the genes with no differences found and those not shown in the figure, whereas the dashed lines represent the deleted nucleotides, and the shadows indicate the unique substitutions of the Guangxi naturally truncated strains.

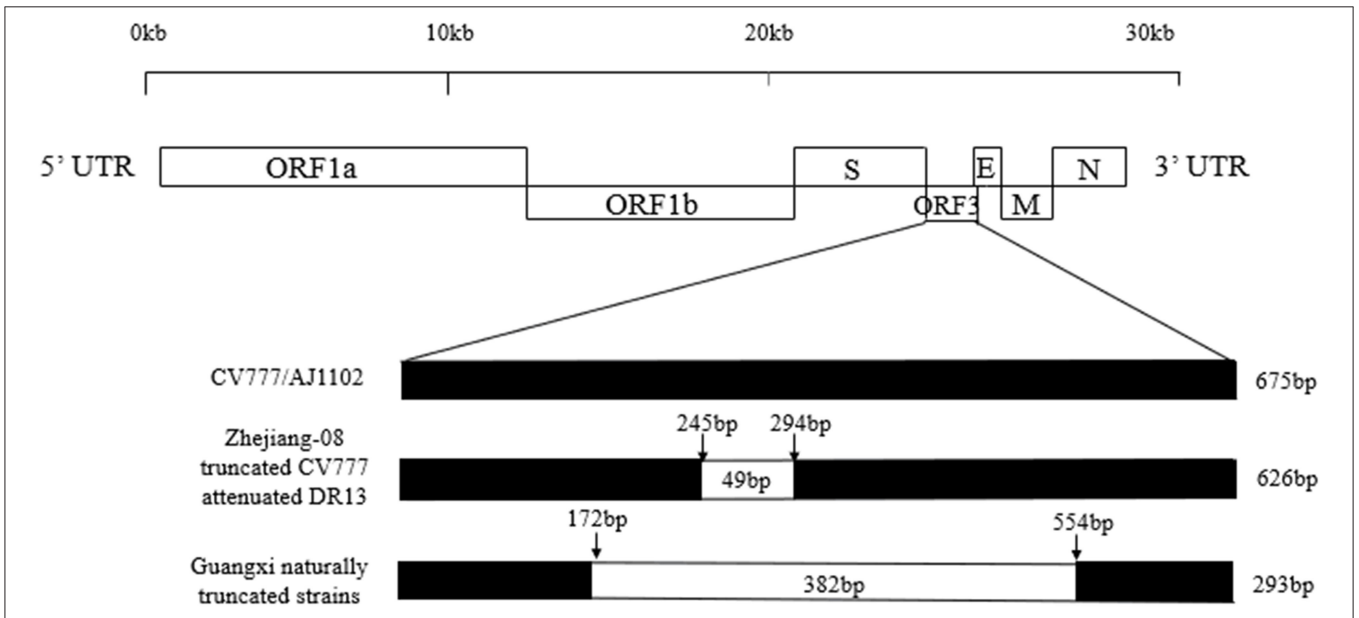

FIGURE 3 | Comparison map of the ORF3 gene deletion in the Guangxi naturally truncated and reference strains. The ORF3 nucleotide sequences of the vaccine strains, CV777 and AJ1102, were 675bp, while the strains of truncated CV777, Zhejiang-08 and attenuated DR13 were 626 bp. The ORF3 of the Guangxi naturally truncated strains were all 293 bp, which contained the deletion area of the reference vaccine strain described above.

mutations (5, 24); six specific amino acids (L24S, I70V, V80F, C107F, D168N, and Q182H) were present the G1-3 subgroups (**Figure 4**). Two strains (CV777 and LZC) were classified as G1-2 subgroups since there were only four substitutions, without V80F and Q182H. The Guangxi naturally truncated strains with 89aa in Group 3 were found to have a long length deletion, which were located at amino acids 61S−71F, 86L−119A, and 124H−129L, respectively. In addition, the L81 is located immediately before the truncation site in Group 2, while Group 2 consisted mostly of the cell-adapted strains.

Phylogenetic Tree of the Amino Acid Sequences

To analyze the phylogenetic relationships of the 38 strains (**Table 1**) and the 113 reference strains from various parts of

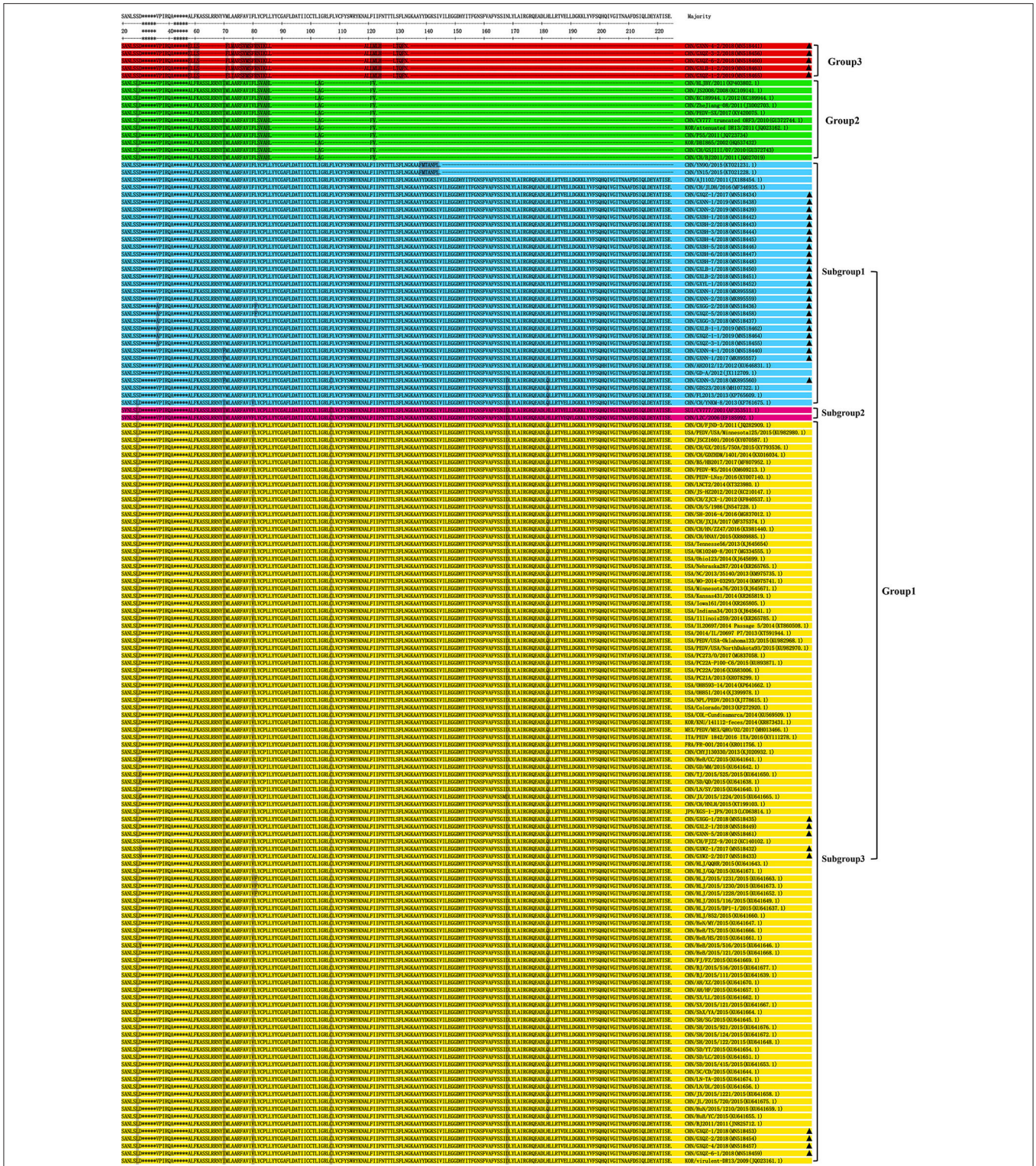

FIGURE 4 | Alignment of amino acid sequences of ORF3 proteins of the Guangxi PEDV and reference strains. The asterisks indicate the segments with no differences and not shown in the figure, whereas the dashed lines indicate deleted amino acids, and the shadows represent the unique substitutions of the chosen strains. Each PEDV strain is indicated in the following format: Country origin (three letter code: CHN, China; FRA, France; ITA, Italy; JPN, Japan; KOR, Korea; MEX, Mexico; SUI, Switzerland; USA, the United States)/strain name/year of sample collection (Genbank accession number). The Group 3 consisted of Guangxi naturally truncated strains which were coded in red. G1-1 subgroup, G1-2 subgroup, G1-3 subgroup and Group 2 were coded in blue, pink, yellow, and green, respectively. The triangle symbols represent the Guangxi field strains obtained in this study.

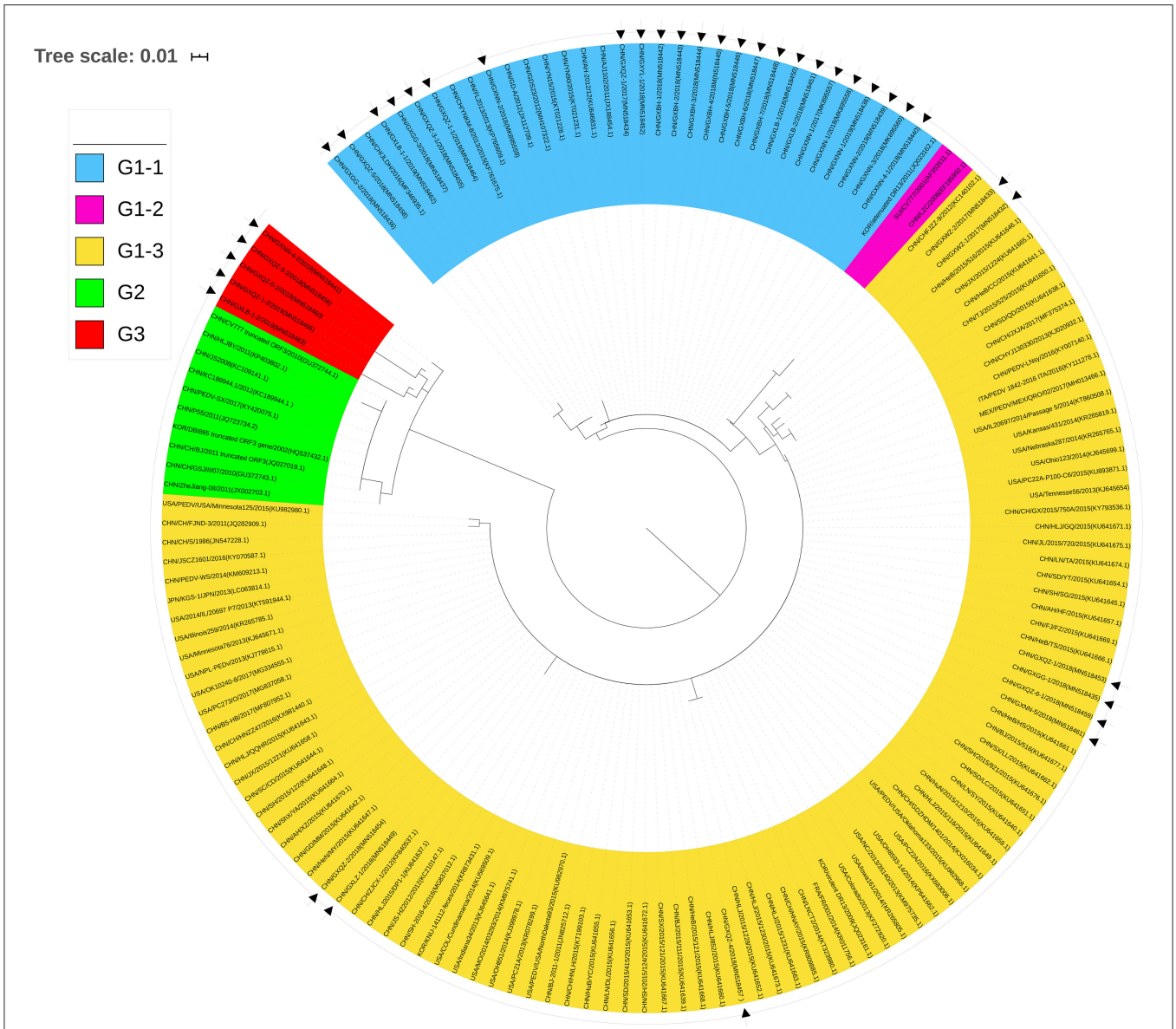

FIGURE 5 | Phylogenetic tree of ORF3 of PEDV samples based on the amino acid sequences. Sequences of reference and vaccine strains were obtained from GeneBank, the accession numbers are shown in **Supplementary Table 1**. Tree topology was constructed using the Poisson model and bootstrap re-sampling (1,000 data sets) of the multiple alignments was used to test the statistical robustness of the trees obtained by the neighbor-joining method from MEGA 5.2. Each PEDV strain is indicated in the following format: Country origin (three letter code: CHN, China; FRA, France; ITA, Italy; JPN, Japan; KOR, Korea; MEX, Mexico; SUI, Switzerland; USA, the United States)/strain name/year of sample collection (Genbank accession number). The Group 3 consisted of Guangxi naturally truncated strains which were coded in red. G1-1 subgroup, G1-2 subgroup, G1-3 subgroup, and Group 2 were coded in blue, pink, yellow, and green, respectively. The triangle symbols represent the Guangxi field strains obtained in this study.

the world (**Supplementary Table 1**), we constructed a neighbor-joining phylogenetic tree using their ORF3 amino acid sequences (**Figure 5**).

Twenty-four strains were clustered into the G1-1 subgroup together with the major domestic strains such as YN15 and vaccine strains AJ1102 and GD-A, while nine strains were clustered to the G1-3 subgroup with major foreign strains such as PC22A and OH851. CV777 and LZC strains were clustered into the G1-2 subgroup. The deletions of the ORF3 gene such as the truncated CV777, Zhejiang-08 and other strains were clustered into Group 2. More importantly, the Guangxi naturally truncated strains were clustered into a new group referred to as Group 3.

DISCUSSION

PED is a highly contagious intestinal infectious disease in pigs caused by PEDV, which has seriously affected the development of the pig breeding industry and caused significant economic losses.

Since 2010, there has been a new round of PED epidemic in China (11, 21, 25, 26). In addition, most pig production countries in Europe, America, and Southeast Asia also have a large-scale epidemic of PED (27–29). It has recently been proposed that PEDV ORF3 plays a role in regulating PEDV replication and pathogenesis (1, 20, 30). Moreover, it has been demonstrated, by using reverse genetics systems, that the ORF3 is dispensable for viral growth *in vitro* (31–33). The 49 nucleotide deletion at 245–294 bp is thought to be a marker of cellular adaptation, because most cell-adapted strains contain these deletions, but the evaluation of ORF3 slightly changed strains on cell culture need to be further investigated. It can also be used to distinguish the cell adaptive strains from the wild strains (34). This suggests that ORF3 may be a multifunctional protein involved in cellular processes, but the exact biological function of PEDV ORF3 needs to be further defined (35). Therefore, understanding the genetic variations of the ORF3 gene is crucial for further studies on the biological functions of PEDV.

In this study, 38 PEDV strains from Guangxi were obtained from 33 field samples collected on pig farms. Among them, 24 strains were clustered into the G1-1 subgroup, and these were in the same branch as the reference strains, such as vaccine strain AJ1102, and 9 strains were in a branch of the G1-3 subgroup with reference strains such as foreign strains PC22A and OH851. Importantly, there were 5 strains with naturally truncated ORF3 genes and these formed a new gene group in a separate branch, and these were different when compared to the highly adapted cell strains such as the Chinese HLJBY and JS2008. We showed that the length of the deduced amino acid sequences of the ORF3 had only 89aa which was unique among the tested strains. Based on the genetic and evolutionary analysis of the ORF3 gene, we found that the endemic PEDV strains in Guangxi were complicated with three genotypes (G1-1 subgroup, G1-3 subgroup, and Group 3) co-existing simultaneously. The S protein is known to be an appropriate viral gene for determining the genetic relatedness among PEDV isolates, and the non-S INDEL and classical genogroups can be clearly differentiated in an S protein phylogenetic tree (7, 36). The variants in the S protein may change the virulence and tissue tropism of PEDV. However, the ORF3 and S gene are under different evolutionary pressures, and the correlation between the mutation rate of ORF3 gene and the pressure of selection of the host's immune response need to be further investigated.

There has been at least one type of ORF3 gene deletion reported. It is the type of deletion which mostly occurs during extensive passaging of the virus in cell cultures and this has been correlated with viral attenuation (19). With the deletion, the ORF3 gene of an attenuated-type virus has 49 nucleotide deletions, and this leads to a reading frame-shift and an early termination of translation (20). It is mainly represented by the strains of truncated CV777, Zhejiang-08, JS2008, HLJBY, and attenuated DR13, which only has a 91aa truncated protein (18, 24, 37–39). It is noteworthy that the ORF3 protein of the Guangxi naturally truncated strains contain only residues of 89aa, since the 382-nucleotide deletion in the ORF3 results in a frameshift mutation and an early termination of translation. Like the L81 which is critical for PEDV rescue in reverse genetics and could possibly play an important role in the inhibitory activity of the ORF3 (30), the amino acid site of the E58 is located immediately before the truncation site in the five Guangxi natural truncated strains, and this specific region is due to the mutation of the amino acids, but the function of this is unknown. The effect of the Guangxi naturally truncated strains on ORF3 functions and viral pathogenicity remains to be investigated. It is worth considering whether the truncated part of the ORF3 gene should be used as a genetic marker for establishing methods to distinguish between different strains.

PEDV strains with naturally occurring truncated ORF3 genes were found from different parts of Guangxi, originating from Qinzhou, Nanning, and Laibin, which suggested that this type of PEDV is present in only certain areas. Interestingly, the Guangxi naturally truncated strains all co-exist with strains of the G1-1 subgroup which contain complete ORF3 genes, which means that this type of PEDV may not infect pigs independently. The presence of different subtypes of PEDV in pigs may accelerate the mutation of the virus, and this can also increase the difficulty for the clinical prevention and control of PEDV. We have purified these two types of viruses by using the plaque assay and pathogenicity studies are currently in progress with these. The effect of the deletion of ORF3 associated with viral replication or virulence would be important for the understanding the gene function. Previously, JS2008 was considered to be a recombination of a vaccine strain and a PEDV variant strain (38). It is not possible to speculate whether these five strains with naturally truncated ORF3 genes is a recombination of the vaccine strain and a PEDV variant strain, and this needs further confirmation.

This study identified 38 strains of PEDV ORF3 in the Guangxi province of China from 2017 to 2019. There were five naturally truncated strains which were clustered into a new group and these had longer length deletions in both nucleotides and amino acids sequences. This will hopefully facilitate the establishment of a diagnostic method that can differentiate the PEDV field stains. Further studies are needed to clarify the effects of the naturally truncated ORF3 gene on the virulence of these PEDV strains. Phylogenetic analysis revealed that three types PEDV strains, G1-1 subgroup, G1-3 subgroup and Group 3, co-circulated in the swine population in the Guangxi province of China. Continued surveillance will be useful for monitoring PEDV transmission. Differentiation of ORF3 genes in PEDV field strains can also help us to choose an appropriate PEDV vaccine candidate in the future and prevent outbreaks of PED more effectively.

DATA AVAILABILITY STATEMENT

The datasets generated for this study can be found in the GenBank MK895557∼MK895560 and MN518432∼MN518465.

ETHICS STATEMENT

The animal study was reviewed and approved by the Animal Care & Welfare Committee of Guangxi University.

AUTHOR CONTRIBUTIONS

WH, YLi, and KO: conceptualization and project administration. YLu, LM, PK, RW, LZ, CY, YC, and ZW: data curation. YLu, XS, CD, and YC: formal analysis. WH and KO: funding acquisition, supervision, and writing—review and editing. CY and YLi: resources. YLu, XS, and CD: writing—original draft.

FUNDING

This work was supported by Guangxi Science and Technology Bureau (grant number AA17204057-1); Natural Science Foundation of Guangxi province (grant number 2017GXNSFAA198138); Guangxi Institute of animal Science Research Project (2019-12); Scientific Research Foundation of Guangxi University (grant number XGZ170239); and the One-Hundred Talent Program of Guangxi.

ACKNOWLEDGMENTS

We are grateful to Dr. Dev Sooranna, Imperial College London, for English language editing of the manuscript.

SUPPLEMENTARY MATERIAL

The Supplementary Material for this article can be found online at: https://www.frontiersin.org/articles/10.3389/fvets.2020.00435/full#supplementary-material

REFERENCES

1. Kaewborisuth C, Yingchutrakul Y, Roytrakul S, Jongkaewwattana A. Porcine epidemic diarrhea virus (PEDV) ORF3 interactome reveals inhibition of virus replication by cellular VPS36 protein. *Viruses.* (2019) 11:382. doi: 10.3390/v11040382
2. Jung K, Annamalai T, Lu Z, Saif LJ. Comparative pathogenesis of US porcine epidemic diarrhea virus (PEDV) strain PC21A in conventional 9-day-old nursing piglets vs. 26-day-old weaned pigs. *Vet Microbiol.* (2015) 178:31–40. doi: 10.1016/j.vetmic.2015.04.022
3. Stevenson GW, Hoang H, Schwartz KJ, Burrough ER, Sun D, Madson D, et al. Emergence of porcine epidemic diarrhea virus in the United States: clinical signs, lesions, and viral genomic sequences. *J Vet Diag Invest.* (2013) 25:649–54. doi: 10.1177/1040638713501675
4. Oka T, Saif LJ, Marthaler D, Esseili MA, Meulia T, Lin CM, et al. Cell culture isolation and sequence analysis of genetically diverse US porcine epidemic diarrhea virus strains including a novel strain with a large deletion in the spike gene. *Vet Microbiol.* (2014) 173:258–69. doi: 10.1016/j.vetmic.2014.08.012
5. Su Y, Liu Y, Chen Y, Zhao B, Ji P, Xing G, et al. Detection and phylogenetic analysis of porcine epidemic diarrhea virus in central China based on the ORF3 gene and the S1 gene. *Virol J.* (2016) 13:192. doi: 10.1186/s12985-016-0646-8
6. Sun RQ, Cai RJ, Chen YQ, Liang PS, Chen DK, Song CX. Outbreak of porcine epidemic diarrhea in suckling piglets, China. *Emerg Infect Dis.* (2012) 18:161–3. doi: 10.3201/eid1801.111259
7. Lin CM, Saif LJ, Marthaler D, Wang QH. Evolution, antigenicity and pathogenicity of global porcine epidemic diarrhea virus strains. *Virus Res.* (2016) 226:20–39. doi: 10.1016/j.virusres.2016.05.023
8. Li Y, Wu Q, Huang L, Yuan C, Wang J, Yang Q. An alternative pathway of enteric PEDV dissemination from nasal cavity to intestinal mucosa in swine. *Nat Commun.* (2018) 9:3811. doi: 10.1038/s41467-018-06056-w
9. Dee S, Neill C, Singrey A, Clement T, Cochrane R, Jones C, et al. Modeling the transboundary risk of feed ingredients contaminated with porcine epidemic diarrhea virus. *BMC Vet Res.* (2016) 12:51. doi: 10.1186/s12917-016-0674-z
10. Song D, Park B. Porcine epidemic diarrhoea virus: a comprehensive review of molecular epidemiology, diagnosis, and vaccines. *Virus Genes.* (2012) 44:167–75. doi: 10.1007/s11262-012-0713-1
11. Li W, Li H, Liu Y, Pan Y, Deng F, Song Y, et al. New variants of porcine epidemic diarrhea virus, China, 2011. *Emerg Infect Dis.* (2012) 18:1350–3. doi: 10.3201/eid1803.120002
12. Lin CN, Chung WB, Chang SW, Wen CC, Liu H, Chien CH, et al. US-like strain of porcine epidemic diarrhea virus outbreaks in Taiwan, 2013-2014. *J Vet Med Sci.* (2014) 76:1297–9. doi: 10.1292/jvms.14-0098
13. Song D, Moon H, Kang B. Porcine epidemic diarrhea: a review of current epidemiology and available vaccines. *Clin Exp Vaccine Res.* (2015) 4:166–76. doi: 10.7774/cevr.2015.4.2.166
14. Sato T, Oroku K, Ohshima Y, Furuya Y, Sasakawa C. Efficacy of genogroup 1 based porcine epidemic diarrhea live vaccine against genogroup 2 field strain in Japan. *Virol J.* (2018) 15:28. doi: 10.1186/s12985-018-0940-8
15. Yu J, Chai X, Cheng Y, Xing G, Liao A, Du L, et al. Molecular characteristics of the spike gene of porcine epidemic diarrhoea virus strains in Eastern China in 2016. *Virus Res.* (2018) 247:47–54. doi: 10.1016/j.virusres.2018.01.013
16. Cheun-Arom T, Temeeyasen G, Tripipat T, Kaewprommal P, Piriyapongsa J, Sukrong S, et al. Full-length genome analysis of two genetically distinct variants of porcine epidemic diarrhea virus in Thailand. *Infect Genet Evol.* (2016) 44:114–21. doi: 10.1016/j.meegid.2016.06.046
17. Ye S, Li Z, Chen F, Li W, Guo X, Hu H, et al. Porcine epidemic diarrhea virus ORF3 gene prolongs S-phase, facilitates formation of vesicles and promotes the proliferation of attenuated PEDV. *Virus Genes.* (2015) 51:385–92. doi: 10.1007/s11262-015-1257-y
18. Park SJ, Moon HJ, Luo Y, Kim HK, Kim EM, Yang JS, et al. Cloning and further sequence analysis of the ORF3 gene of wild- and attenuated-type porcine epidemic diarrhea viruses. *Virus Genes.* (2008) 36:95–104. doi: 10.1007/s11262-007-0164-2
19. Teeravechyan S, Frantz PN, Wongthida P, Chailangkarn T, Jaru-Ampornpan P, Koonpaew S, et al. Deciphering the biology of porcine epidemic diarrhea virus in the era of reverse genetics. *Virus Res.* (2016) 226:152–71. doi: 10.1016/j.virusres.2016.05.003
20. Wang K, Lu W, Chen J, Xie S, Shi H, Hsu H, et al. PEDV ORF3 encodes an ion channel protein and regulates virus production. *FEBS Lett.* (2012) 586:384–91. doi: 10.1016/j.febslet.2012.01.005
21. Chen J, Wang C, Shi H, Qiu H, Liu S, Chen X, et al. Molecular epidemiology of porcine epidemic diarrhea virus in China. *Arch Virol.* (2010) 155:1471–6. doi: 10.1007/s00705-010-0720-2
22. Diep NV, Norimine J, Sueyoshi M, Lan NT, Yamaguchi R. Novel porcine epidemic diarrhea virus (PEDV) variants with large deletions in the spike (S) gene coexist with PEDV strains possessing an intact S gene in domestic pigs in Japan: a new disease situation. *PLoS ONE.* (2017) 12:e0170126. doi: 10.1371/journal.pone.0170126
23. Chen N, Li S, Zhou R, Zhu M, He S, Ye M, et al. Two novel porcine epidemic diarrhea virus (PEDV) recombinants from a natural recombinant and distinct subtypes of PEDV variants. *Virus Res.* (2017) 242:90–5. doi: 10.1016/j.virusres.2017.09.013
24. Chen X, Zeng L, Yang J, Yu F, Ge J, Guo Q, et al. Sequence heterogeneity of the ORF3 gene of porcine epidemic diarrhea viruses field samples in Fujian, China, 2010-2012. *Viruses.* (2013) 5:2375–83. doi: 10.3390/v5102375
25. Chen X, Yang J, Yu F, Ge J, Lin T, Song T. Molecular characterization and phylogenetic analysis of porcine epidemic diarrhea virus (PEDV) samples from field cases in Fujian, China. *Virus Genes.* (2012) 45:499–507. doi: 10.1007/s11262-012-0794-x
26. Pan Y, Tian X, Li W, Zhou Q, Wang D, Bi Y, et al. Isolation and characterization of a variant porcine epidemic diarrhea virus in China. *Virol J.* (2012) 9:195. doi: 10.1186/1743-422X-9-195

27. Guo J, Fang L, Ye X, Chen J, Xu S, Zhu X, et al. Evolutionary and genotypic analyses of global porcine epidemic diarrhea virus strains. *Transbound Emerg Dis.* (2019) 66:111–8. doi: 10.1111/tbed.12991
28. Huang YW, Dickerman AW, Pineyro P, Li L, Fang L, Kiehne R, et al. Origin, evolution, and genotyping of emergent porcine epidemic diarrhea virus strains in the United States. *mBio.* (2013) 4:e00737–13. doi: 10.1128/mBio.00737-13
29. Lee S, Lee C. Outbreak-related porcine epidemic diarrhea virus strains similar to US strains, South Korea, 2013. *Emerg Infect Dis.* (2014) 20:1223–6. doi: 10.3201/eid2007.140294
30. Wongthida P, Liwnaree B, Wanasen N, Narkpuk J, Jongkaewwattana A. The role of ORF3 accessory protein in replication of cell-adapted porcine epidemic diarrhea virus (PEDV). *Arch Virol.* (2017) 162:2553–63. doi: 10.1007/s00705-017-3390-5
31. Beall A, Yount B, Lin CM, Hou Y, Wang Q, Saif L, et al. Characterization of a pathogenic full-length cDNA clone and transmission model for porcine epidemic diarrhea virus strain PC22A. *mBio.* (2016) 7:e01451–15. doi: 10.1128/mBio.01451-15
32. Jengarn J, Wongthida P, Wanasen N, Frantz PN, Wanitchang A, Jongkaewwattana A. Genetic manipulation of porcine epidemic diarrhoea virus recovered from a full-length infectious cDNA clone. *J Gen Virol.* (2015) 96:2206–18. doi: 10.1099/vir.0.000184
33. Li C, Li Z, Zou Y, Wicht O, van Kuppeveld FJ, Rottier PJ, et al. Manipulation of the porcine epidemic diarrhea virus genome using targeted RNA recombination. *PLoS ONE.* (2013) 8:e69997. doi: 10.1371/journal.pone.0069997
34. Song DS, Yang JS, Oh JS, Han JH, Park BK. Differentiation of a vero cell adapted porcine epidemic diarrhea virus from Korean field strains by restriction fragment length polymorphism analysis of ORF 3. *Vaccine.* (2003) 21:1833–42. doi: 10.1016/S0264-410X(03)00027-6
35. Zou D, Xu J, Duan X, Xu X, Li P, Cheng L, et al. Porcine epidemic diarrhea virus ORF3 protein causes endoplasmic reticulum stress to facilitate autophagy. *Vet Microbiol.* (2019) 235:209–19. doi: 10.1016/j.vetmic.2019.07.005
36. Lee C. Porcine epidemic diarrhea virus: an emerging and re-emerging epizootic swine virus. *Virol J.* (2015) 12:193. doi: 10.1186/s12985-015-0421-2
37. Chen F, Zhu Y, Wu M, Ku X, Ye S, Li Z, et al. Comparative genomic analysis of classical and variant virulent parental/attenuated strains of porcine epidemic diarrhea virus. *Viruses.* (2015) 7:5525–38. doi: 10.3390/v7102891
38. Li B, Liu H, He K, Guo R, Ni Y, Du L, et al. Complete genome sequence of a recombinant porcine epidemic diarrhea virus strain from Eastern China. *Genome Announc.* (2013) 1:e0010513. doi: 10.1128/genomeA.00105-13
39. Huan C, Pan H, Fu S, Xu W, Gao Q, Wang X, et al. Characterization and evolution of the coronavirus porcine epidemic diarrhoea virus HLJBY isolated in China. *Transbound Emerg Dis.* (2019) 67:65–79. doi: 10.1111/tbed.13321

Conflict of Interest: The authors declare that the research was conducted in the absence of any commercial or financial relationships that could be construed as a potential conflict of interest.

frontiers in Veterinary Science

ORIGINAL RESEARCH
published: 04 August 2020
doi: 10.3389/fvets.2020.00407

The Colorimetric Isothermal Multiple-Self-Matching-Initiated Amplification Using Cresol Red for Rapid and Sensitive Detection of Porcine Circovirus 3

Hongchao Gou[1,2,3,4], *Zhibiao Bian*[1,2,3,4], *Rujian Cai*[1,2,3,4], *Zhiyong Jiang*[1,2,3,4], *Shuai Song*[1,2,3,4], *Yan Li*[1,2,3,4], *Pinpin Chu*[1,2,3,4], *Dongxia Yang*[1,2,3,4], *Ying-An Zang*[5]* and *Chunling Li*[1,2,3,4]*

[1] Institute of Animal Health, Guangdong Academy of Agricultural Sciences, Guangzhou, China, [2] Guangdong Provincial Key Laboratory of Livestock Disease Prevention, Guangzhou, China, [3] Guangdong Open Laboratory of Veterinary Public Health, Guangzhou, China, [4] Scientific Observation and Experiment Station of Veterinary Drugs and Diagnostic Techniques of Guangdong Province, Guangzhou, China, [5] College of Animal Science and Technology, Zhongkai University of Agriculture and Engineering, Guangzhou, China

OPEN ACCESS

Edited by:
Feng Li,
South Dakota State University,
United States

Reviewed by:
Francisco Rivera-Benítez,
Instituto Nacional de Investigaciones Forestales, Agrícolas y Pecuarias (INIFAP), Mexico
Juan Mosqueda,
Universidad Autónoma de Querétaro, Mexico
Yuan Xiao Yuan,
Shandong Academy of Agricultural Sciences, China

***Correspondence:**
Ying-An Zang
1134580900@qq.com
Chunling Li
lclcare@163.com

Specialty section:
This article was submitted to Veterinary Infectious Diseases, a section of the journal Frontiers in Veterinary Science

Received: 20 January 2020
Accepted: 08 June 2020
Published: 04 August 2020

Citation:
Gou H, Bian Z, Cai R, Jiang Z, Song S, Li Y, Chu P, Yang D, Zang Y-A and Li C (2020) The Colorimetric Isothermal Multiple-Self-Matching-Initiated Amplification Using Cresol Red for Rapid and Sensitive Detection of Porcine Circovirus 3. Front. Vet. Sci. 7:407. doi: 10.3389/fvets.2020.00407

In 2016, a novel porcine circovirus (PCV), PCV3, was identified in USA. Subsequently, it was proved to be also epidemic in China, Poland, and Korea. To analyze and control the epidemic situation of PCV3, it is necessary to establish accurate and high-throughput detection methods. In this study, the colorimetric isothermal multiple-self-matching-initiated amplification (IMSA) using cresol red was developed to detect PCV3 for the first time. The reaction can be easily performed by incubating the tube at 63°C for 60 min. By the addition of pH-sensitive indicator dye cresol red, the initial color of the reaction mixture is red. When PCV3 capsid gene DNA was positive in the sample, the color of the reaction mixture changed from red to yellow after the isothermal incubation at 63°C, while the negative control maintained the red color. The colorimetric IMSA displayed good specificity in detecting PCV3, PCV2, and PCV1 and 4 porcine DNA pathogens. Moreover, it has a low and repeatable detection limit of 10 copies, which is consistent with TaqMan-based qPCR, but 10 times more sensitive than PCR. In diagnosing 128 clinical specimens, it not only showed 100% agreement with qPCR but also detected 15 positive results more than PCR. The colorimetric IMSA we offered might be a good choice for PCV3 epidemiological investigation and point-of-care testing.

Keywords: PCV3, isothermal multiple-self-matching-initiated amplification (IMSA), detection, colorimetric assay, cresol red

INTRODUCTION

Porcine circovirus (PCV) is a non-enveloped, circular single-stranded DNA virus, belonging to the genus *Circovirus* within the family *Circoviridae*. PCV1 and PCV2 were reported to be the only two members of PCV for a long time (1). PCV1 was considered non-pathogenic to pigs. However, PCV2 was known to be connected with clinical features including post-weaning multisystemic wasting syndrome (PMWS), porcine dermatitis and nephropathy syndrome (PDNS), porcine respiratory disease complex (PRDC), proliferative and necrotizing pneumonia (PNP), and reproductive disorders (2, 3). PCV2 has caused severe economic losses to the swine industry because of its circulation worldwide (4).

In 2016, a novel porcine circovirus, PCV3, was identified in USA. Similar symptoms with pigs infected by PCV2, such as PDNS and reproductive disorders, also appear in pigs infected by PCV3 (5, 6). Successive studies proved it was epidemic in China, Poland, and Korea (7–10). Considering this, it is necessary to develop a rapid and simple assay for PCV3 detection. Although PCR-based methods have been utilized to detect PCV3, it is not easy to be performed onsite, or laboratories lack expensive thermal cycling equipment and skilled operators (7, 11). Therefore, isothermal amplification methods are suggested to be a suitable choice for point-of-need diagnostics. To meet this demand, recombinase polymerase amplification (RPA) assay for rapid detection of PCV3 has been described (12). However, at least two kinds of enzymes are needed to start the RPA reaction. The expensive reaction reagent may limit its wide application in rural areas.

Compared with RPA, loop-mediated isothermal amplification (LAMP) or isothermal multiple-self-matching-initiated amplification (IMSA) only utilizes strand-displacing DNA polymerase to accomplish robust DNA synthesis (13, 14). This makes them to be good choice for low-cost isothermal methods. What is more, IMSA proved to be more sensitive than LAMP in the previous study (13, 15). Recently, rapid, sensitive, and visual detection assay was achieved by the addition of pH-sensitive indicator dyes. To develop a rapid, convenient, low-cost method suitable for rural areas, the colorimetric IMSA using cresol red was utilized to detect PCV3 in our study. This method showed good potential on rapid examination of clinical samples suspected to be infected by PCV3.

MATERIALS AND METHODS

Ethics Statement

All animal experiments were reviewed and approved by the ethical and ethics commission (Institute of Animal Health, Guangdong Academy of Agricultural Sciences, China). The license number was SYXK (Yue) 2011–0116. Moreover, samples collecting treatment in this study were performed in accordance with national and local laws and guidelines.

Virus, Bacteria, and Cells

PCV2 isolate HN6 (GenBank no: KM035762.1), PCV1, pseudorabies virus (PRV) GD-WH strain (GenBank no: KT936468.1), Haemophilus parasuis (HPS) serotype 5, *Streptococcus suis* (SS) serotype 2, and *Actinobacillus pleuropneumoniae* (APP) Serovar 1 were preserved in our laboratory. They were used to evaluate the specificity of the colorimetric IMSA.

Clinical Samples and Animals

In Guangdong province, a total number of 128 clinical samples were collected from pigs suspected to be infected with PCV3. The tissues include blood, tonsil, lymph gland, lung, kidney, and brain. In addition, 15 blood samples of specific-pathogen-free (SPF) pigs (5 months old), from the Laboratory Animal Center of Southern Medical University, China, were collected. All samples were stored at −80°C until DNA extraction.

DNA Extraction

According to the instructions of the manufacturer, viral DNA in supernatant of cell culture or clinical samples was purified by using the HiPure Viral RNA/DNA Kit (Magen, China). Finally, viral DNA was dissolved in 50 μL nuclease-free water and stored at −80°C. Bacterial DNA was extracted by using the HiPure Bacterial DNA Kit (Magen, China) according to the manufacturer's protocol.

PCR

According to the previously reported methods, PCR was performed in a 25-μL reaction mixture (7). The mixture contained 0.3 μM of each primer, 1× Premix Tag (Takara Biotechnology, China) and 2 μL template DNA. The PCR program was as follows: 94°C for 5 min; 35 cycles at 94°C for 30 s, 55°C for 30 s, and 72°C for 1 min, and a final extension at 72°C for 10 min. The products were analyzed on 2% agarose gel.

TaqMan-Based qPCR

TaqMan-based qPCR for PCV3 genome identification was carried out as is previously reported (6). The 25-μL reaction mixture contained 0.4 μM of each primer and probe, 1× qPCR Probe Master Mix (Vazyme, China), and 2 μL template DNA. The reaction program was set as follows: 95°C for 3 min, followed by 40 cycles at 95°C for 10 s and 60°C for 60 s. FAM fluorescence signals were obtained at the end of each annealing step by the real-time PCR detection system (Roche Light Cycler 480 II, Switzerland). Results with a cycle threshold (Ct) value of <40 were considered positive, while results with no Ct value within 40 cycles were considered negative.

Plasmid Construction

As in the report previously described, partial sequences of capsid gene of PCV3 were amplified by the PCR method from the clinical samples (7). The PCR product was purified by using the Cycle Pure Kit according to the instructions of the manufacturer (Omega, USA). Then, the purified fragment was cloned into pMDTM19-T Vector (TaKaRa Biotechnology, China) and the pMD19T-capsid plasmid was constructed. After the plasmid was transformed into DH5α competent cells, the plasmid DNA was extracted by using the Plasmid Mini Kit I (Omega, USA).

IMSA Primer Design

The conserved region of the capsid gene was determined by alignment of PCV3 strains indexed in the GenBank (accession no: MF589105.1, MF589107.1, MF769811.1, MF769807.1, MF084994.1, KX778720.1, KX898030.1, MG310152.1, MF079254.1, and MG250187.1). According to the principle of IMSA assay, capsid gene sequences of PCV3-US/MO2015 strain (accession no: KX778720.1) were input for IMSA primer design by using the software Primer Premier 5.0 (15). Among multiple sets of primers, the primers targeting to the conserved regions of the capsid gene were selected for subsequent analysis. IMSA primers are listed in **Table 1**.

Colorimetric IMSA

As the previous study described, Tris–HCl and betaine was not included in the colorimetric assay (16). To establish this method,

TABLE 1 | Primers of the colorimetric IMSA assay for PCV3.

Primer name	Sequences 5′-3′	Genome position[a]
DsF	CCCACCCCATGGCTCAACA-CCGGGACATAAATGCTCCAA	SteR: 1465–1483 F3: 1411–1430
DsR	TGGTTTCGGGGTGAAGTAACGG-CCACAAACACTTGGCTCCA	SteF: 1541–1562 R3: 1623–1641
FIT (F1c+F2)	CTCACCCAGGACAAAGCCTCTT-CATTGAACGGTGGGGTCAT	Tc: 1497–1518 F2: 1443–1461
RIT (B1c+B2)	AAGAGGCTTTGTCCTGGGTGAG-AGACGACCCTTATGCGGAA	T: 1497–1518 R2: 1604–1622
SteR	CCCACCCCATGGCTCAACA	1465–1483
SteF	TGGTTTCGGGGTGAAGTAACGG	1541–1562

[a] *The genome of PCV3-US/MO2015 strain (accession no: KX778720.1).*

the reaction mixture containing 10 mM $(NH4)_2SO_4$, 10 mM KCl, 8 mM $MgSO_4$, 0.1% v/v Tween-20, 16 mM cresol red, 0.8 mM dNTPs, and 8 U Bst WarmStart DNA Polymerase (New England Bio-labs, USA) was prepared, and the pH of the mixture was adjusted to 9.0 by using 100 mM KOH. To perform the IMSA reaction, primers' concentration was optimized and determined as 1.6 μM SteF/SteR, 0.8 μM FIT/RIT, and 0.2 μM DsF/DsR. Then, the reaction tube was incubated in a thermostatic device (HB-202, BIOER TECHNOLOGY, China) at 63°C for 60 min. The results can be directly judged with the naked eyes. The yellow color indicated the positive results, while the red color indicated the negative results. In each colorimetric IMSA test, 3 observers were invited to identify colors and read out the results. For each result, every observer read it out 3 times.

Specificity Analysis

DNA extracted from PCV2, PCV1, PRV GD-WH strain, HPS, SS, and APP were used to evaluate the specificity of the colorimetric IMSA.

Sensitivity Analysis

Ten-fold serial dilutions of pMD19T-capsid plasmid DNA (10^5, 10^4, 10^3, 10^2, 10^1, 10^0, and 10^{-1} copies) were used to determine the detection limit of the colorimetric IMSA. The negative control was conducted at the same time. The detection limit of the colorimetric IMSA was compared with qPCR and PCR.

Reproducibility Analysis

To analyze the reproducibility of the colorimetric IMSA, ten-fold serial dilutions of pMD19T-capsid plasmid DNA (10^5, 10^4, 10^3, 10^2, 10^1, 10^0, and 10^{-1} copies) and the negative control were detected for 3 different times.

Evaluation of Clinical Application

A total number of 128 suspected clinical samples and 15 blood samples from SPF pigs were used for DNA extraction and colorimetric IMSA detection. To evaluate the test accuracy of the colorimetric IMSA, its results were identified by TaqMan-based qPCR and PCR.

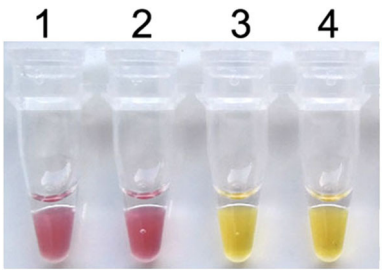

FIGURE 1 | Establishment of the colorimetric IMSA assay for PCV3. Tubes 1–2, negative control. Tubes 3–4, 10^5 copies of PMD19T-capsid plasmid DNA.

RESULTS

Establishment of the Colorimetric IMSA

To establish the colorimetric IMSA assay, Tris–HCl was removed from the reaction mixture but the cresol red was added. After 60 min of incubation at 63°C, the color of the reaction mixture changed to yellow when the plasmid containing partial sequences of the PCV3 capsid gene was used as DNA template, while the negative control keeps the red color (**Figure 1**). So, we judged the positive result of the colorimetric IMSA by observing the yellow color of the reaction tube.

Specificity of the Colorimetric IMSA

To evaluate the specificity of the colorimetric IMSA, pathogens inducing similar clinical syndromes with PCV3, such as PCV2, PCV1, PRV GD-WH strain, HPS, SS, and APP, were used for DNA extraction. For multiple viral or bacterial DNAs, only the plasmid containing partial sequences of the PCV3 capsid gene could start the reaction and the reaction mixture displayed the yellow color (**Figure 2**). This manifested the good specificity of the colorimetric IMSA.

Sensitivity of the Colorimetric IMSA

Ten-fold serial dilutions of plasmid DNA (10^5, 10^4, 10^3, 10^2, 10^1, 10^0, and 10^{-1} copies) were, respectively, used as DNA template to determine the detection limit of the colorimetric

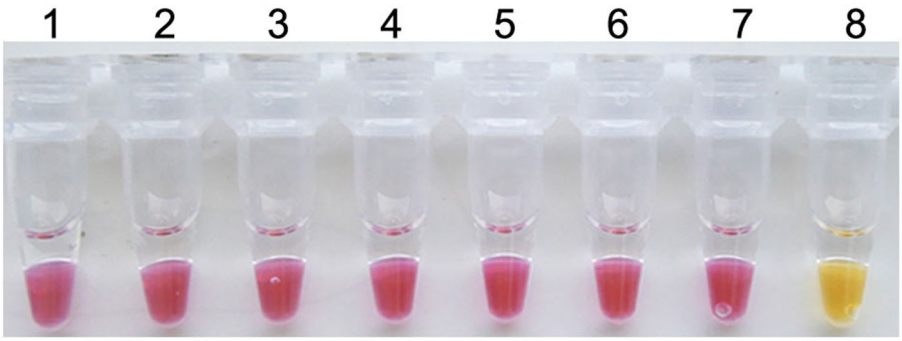

FIGURE 2 | Specificity of the colorimetric IMSA assay for PCV3. Tubes 1–6, DNA of PCV2, PCV1, PRV GD-WH strain, HPS, SS, and APP. Tube 7, negative control. Tube 8, 10^5 copies of PMD19T-capsid plasmid DNA.

IMSA. Moreover, the results were compared with qPCR and PCR. In this study, as low as 10 copies of plasmid DNA can be detected by the colorimetric IMSA and qPCR, while the detection limit of PCR was 100 copies, which was 10 times lower than the colorimetric IMSA and qPCR (**Figure 3**).

Reproducibility of the Colorimetric IMSA

When the colorimetric IMSA was evaluated by detecting ten-fold serial dilutions of pMD19T-capsid plasmid DNA (10^5, 10^4, 10^3, 10^2, 10^1, 10^0, and 10^{-1} copies) and the negative control for 3 different times, the same results were obtained for each dilution sample every time (**Figure 4**). Hence, the colorimetric IMSA showed stable detection reproducibility for samples of different concentrations.

Evaluation of Clinical Application

Among 128 clinical samples, 35 positive results were detected by the PCR method. The positive rate was 27.3% (35/128). In addition to these 35 positive results, the colorimetric IMSA showed 15 positive results more than PCR, which were also positive for TaqMan-based qPCR (**Table 2**). The positive rate was 39.1% (50/128). To analyze the accuracy of IMSA in testing negative animals, 15 blood tissues sampled from SPF pigs were detected by using the colorimetric IMSA, qPCR, and PCR. Fifteen negative results were obtained for these 3 methods (data not shown).

DISCUSSION

PCV2, the main inducer of porcine circovirus-associated diseases (PCAD), severely damaged efficiency of swine production worldwide (1). PCV3, which was firstly identified in PCV2-negative pigs in 2016, causes cardiac pathology and multisystemic inflammation. In addition, PCV2-like syndromes including PDNS and reproductive failure are also associated with PCV3 infection (6). To analyze and control the epidemic situation of PCV3, it is necessary to establish accurate and high-throughput detection methods. Herein, a simple and rapid colorimetric IMSA using cresol red was developed to detect PCV3 for the first time.

In our study, the IMSA primers were designed according to the conserved region of the PCV3 capsid gene, which was the usual detective marker of PCR-based methods (7, 11). The primer design work was not as complicated as those of LAMP, because the IMSA primers consisted of seven basic primers specifically recognizing distinct regions of the target, which can be easily designed by using the software Primer Premier 5.0 (15). The results of colorimetric IMSA can be visually judged within 60 min, which was at least 60 min shorter than qPCR or PCR methods. However, the detection limit of the colorimetric IMSA is as low as 10 copies, which is consistent with qPCR and even 10 times more sensitive than PCR previously reported (7, 11). Moreover, the reproducibility analysis shows that the detection accuracy of the colorimetric IMSA is very stable for samples of different concentrations. In the whole detection process, the colorimetric IMSA only needs simple isothermal equipment to perform the reaction, but results of PCR or qPCR need to be analyzed by agarose gel electrophoresis or sophisticated thermal cycling apparatus. This makes it very suitable for point-of-care tests using the colorimetric IMSA assay. Compared with the LAMP assay using hydroxynaphthol blue for PCV3 detection, the color change from red to yellow of the reaction tube in this study is more easily to be distinguished with the naked eye than that of the color change from purple to sky blue (17). Hence, it is very convenient for the observers to read out and judge the results of the colorimetric IMSA.

When the colorimetric IMSA are used to detect clinical samples, all IMSA-positive samples can be exactly determined by TaqMan-based qPCR, which was proved to be an accurate method for PCV3 DNA detection. Moreover, the colorimetric IMSA displayed no false-positive results for detection of blood samples from SPF pigs. This further manifests its precise test ability. In our results, some IMSA-positive samples were negative for PCR detection. This may be attributed to the more sensitive detection limit of the colorimetric IMSA and qPCR than PCR.

In recent years, PCV3 was continuously identified in China and further surveillance studies showed that PCV3 are epidemic in a number of pig farms in many provinces (7, 10). In our study, the positive detection rate of the suspected clinical samples by colorimetric IMSA and qPCR is 39.1% (50/128), which was

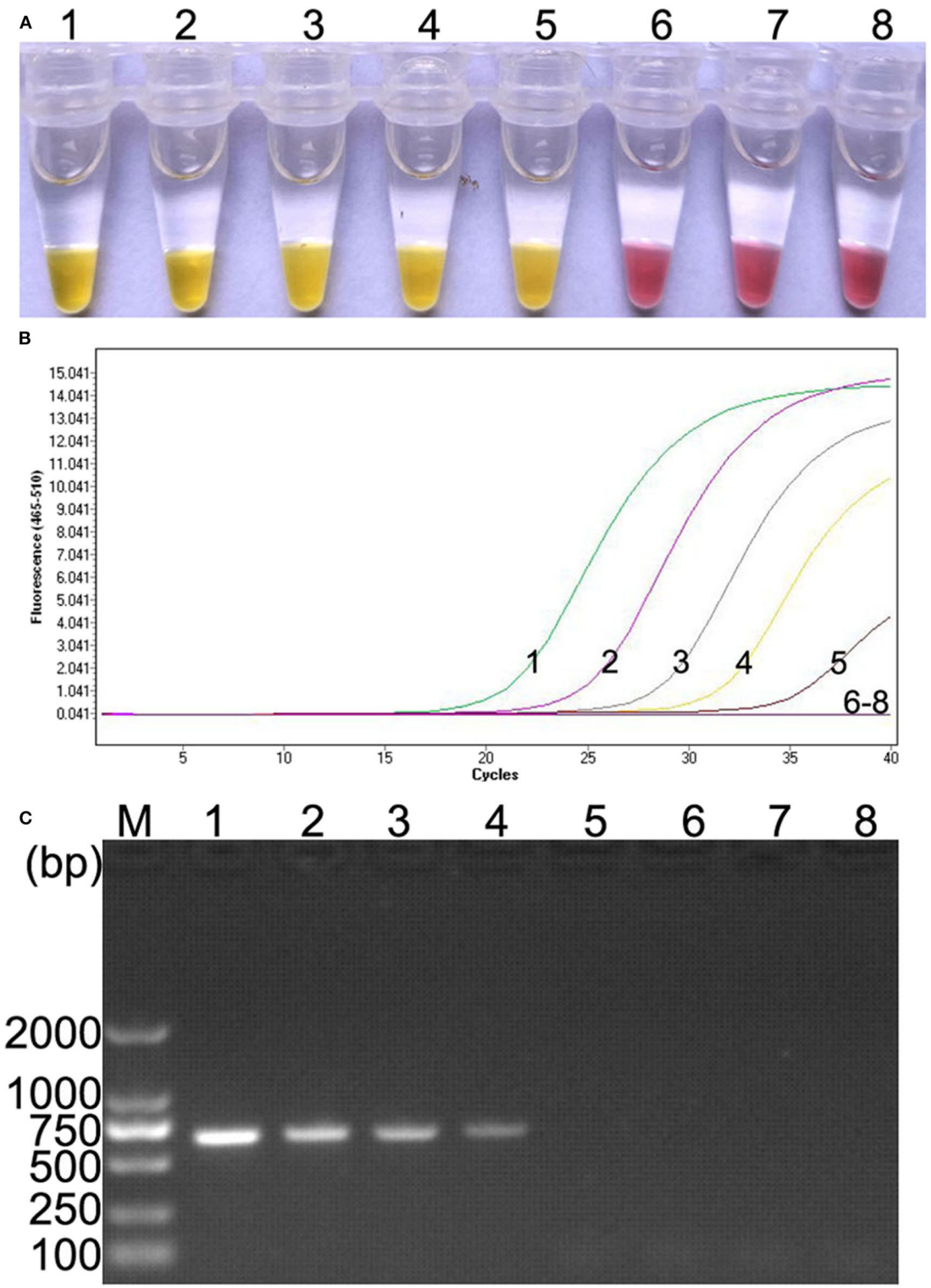

FIGURE 3 | Comparison of sensitivity of the colorimetric IMSA with qPCR and PCR. **(A)** Sensitivity of the colorimetric IMSA. **(B)** Sensitivity of qPCR. **(C)** Sensitivity of PCR analyzed by agarose gel electrophoresis. Tubes or lanes 1–7, ten-fold serially diluted PMD19T-capsid plasmid DNA (10^5, 10^4, 10^3, 10^2, 10^1, 10^0, and 10^{-1} copies). Tube or lane 8: negative control. Lane M, 2,000-bp DNA marker.

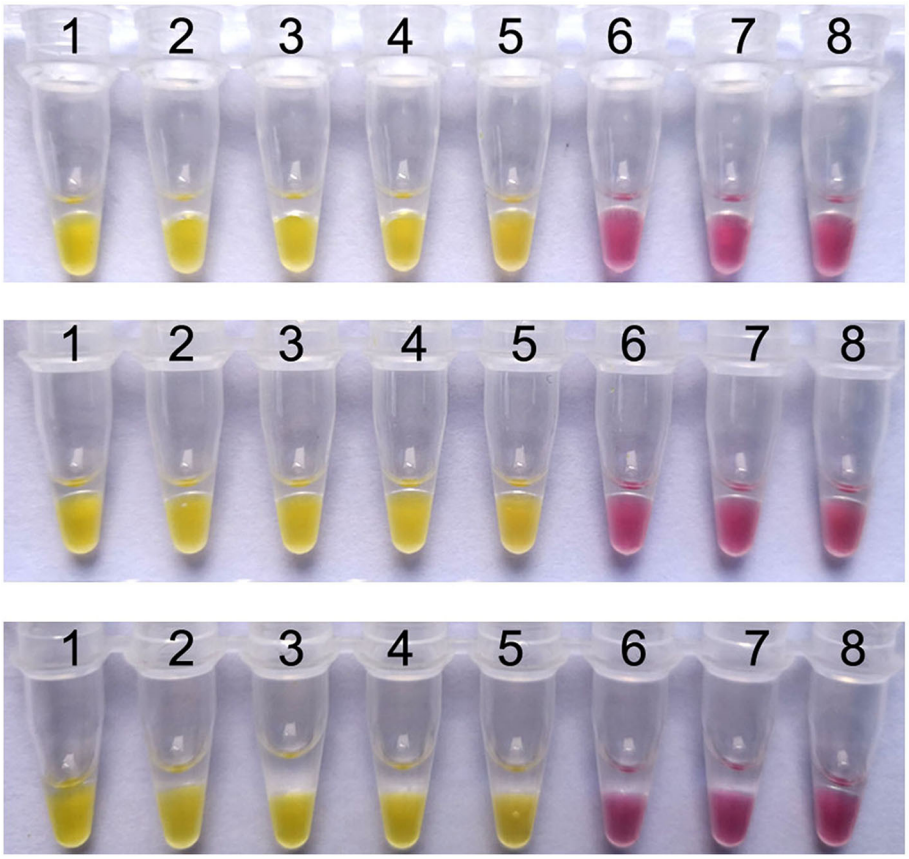

FIGURE 4 | Reproducibility analysis of the colorimetric IMSA. Tubes 1–7, ten-fold serially diluted PMD19T-capsid plasmid DNA (10^5, 10^4, 10^3, 10^2, 10^1, 10^0, and 10^{-1} copies). Tube 8: negative control.

TABLE 2 | Detection of PCV3 in clinical samples by the colorimetric IMSA qPCR and PCR.

Tissues	Number	Positive by qPCR	Positive by PCR	Positive by IMSA
Blood	36	15	8	15
Tonsil	15	8	6	8
Lymph gland	12	5	4	5
Lung	26	6	5	6
Kidney	22	11	9	11
Brain	17	5	3	5
Total	128	50	35	50
Positive rates[a] (%)	/	39.1%	27.3%	39.1%

[a]*Detection rate was defined by no. of positive samples/no. of total samples (%).*

higher than the data in the previous study (11, 12). Our data offers new evidence that PCV3 was epidemic in sick pigs in China. As an emerging virus in 2016, some reports have manifested its connection with PDNS. Pathological lesions and PCV3-specific antigens are detected in various tissues and organs, including the blood, lung, heart, kidney, lymph nodes, and spleen (6, 18). Our results also showed that PCV3 is widely distributed in multiple tissues of the suspected infection pigs. What is more, we find that PCV3 DNA can be detected in the brain tissues of some sick pigs. This is consistent with the findings in some recent reports (19, 20).

In summary, the IMSA assay using cresol red was used for a rapid and sensitive detection of PCV3 for the first time. Not only was this method easy to be performed, but also its results were clearly distinguished with naked eyes. It is likely that the simple method was widely applied in the PCV3 detection in laboratories or rural areas.

DATA AVAILABILITY STATEMENT

The datasets generated for this study are available on request to the corresponding author.

ETHICS STATEMENT

This animal study was reviewed and approved by the ethical and ethics commission (Institute of Animal Health, Guangdong Academy of Agricultural Sciences, China). The license number was SYXK (Yue) 2011–0116. Moreover, sample collecting treatment in this study were performed in accordance with national and local laws and guidelines.

AUTHOR CONTRIBUTIONS

HG carried out the experiment design and drafted the manuscript. PC and DY prepared materials for the experiments. ZB participated in the experiments. SS, ZJ, and YL participated in the analysis of the data. CL, Y-AZ, and RC conceived the study. All authors read and approved the final manuscript.

FUNDING

This work was supported by grants from the Key Projects in the National Research and Development Program during the thirteenth Five-year Plan Period (No. 2018YFD0500804), the Natural Science Foundation of Guangdong, China (Nos. 2019A1515010757, 2017A030310074, and 2020A1515010475), the Science and Technology plan Program of Guangdong, China (Nos. 2017B020202002 and 2014A010107020), the 2018 Rural Revitalization Strategy Project (No. Guangdong Agriculture Planning 2018-54), the Science and Technology Program of Guangzhou, China (Nos. 201804010071 and 201607010380), the Special fund for scientific innovation strategy-construction of high level Academy of Agriculture Science (Nos. R2017YJ-YB2005 and R2018QD-094), and the Social Public Welfare Science and Technology Research Project of Zhongshan, China (No. 2018B1012).

REFERENCES

1. Allan G, Krakowka S, Ellis J, Charreyre C. Discovery and evolving history of two genetically related but phenotypically different viruses, porcine circoviruses 1 and 2. *Virus Res*. (2012) 164:4–9. doi: 10.1016/j.virusres.2011.09.013
2. Tischer I, Gelderblom H, Vettermann W, Koch MA. A very small porcine virus with circular single-stranded DNA. *Nature*. (1982) 295:64–6. doi: 10.1038/295064a0
3. Tischer I, Mields W, Wolff D, Vagt M, Griem W. Studies on epidemiology and pathogenicity of porcine circovirus. *Arch Virol*. (1986) 91:271–6. doi: 10.1007/BF01314286
4. Segales J. Porcine circovirus type 2 (PCV2) infections: clinical signs, pathology and laboratory diagnosis. *Virus Res*. (2012) 164:10–9. doi: 10.1016/j.virusres.2011.10.007
5. Phan TG, Giannitti F, Rossow S, Marthaler D, Knutson TP, Li L, et al. Detection of a novel circovirus PCV3 in pigs with cardiac and multi-systemic inflammation. *Virol J*. (2016) 13:184. doi: 10.1186/s12985-016-0642-z
6. Palinski R, Pineyro P, Shang P, Yuan F, Guo R, Fang Y, et al. A novel porcine circovirus distantly related to known circoviruses is associated with porcine dermatitis and nephropathy syndrome and reproductive failure. *J Virol*. (2017) 91:e01879-16. doi: 10.1128/JVI.01879-16
7. Ku X, Chen F, Li P, Wang Y, Yu X, Fan S, et al. Identification and genetic characterization of porcine circovirus type 3 in China. *Transbound Emerg Dis*. (2017) 64:703–8. doi: 10.1111/tbed.12638
8. Kwon T, Yoo SJ, Park CK, Lyoo YS. Prevalence of novel porcine circovirus 3 in Korean pig populations. *Vet Microbiol*. (2017) 207:178–80. doi: 10.1016/j.vetmic.2017.06.013
9. Stadejek T, Wozniak A, Milek D, Biernacka K. First detection of porcine circovirus type 3 on commercial pig farms in Poland. *Transbound Emerg Dis*. (2017) 64:1350–3. doi: 10.1111/tbed.12672
10. Shen H, Liu X, Zhang P, Wang L, Liu Y, Zhang L, et al. Genome characterization of a porcine circovirus type 3 in South China. *Transbound Emerg Dis*. (2018) 65:264–6. doi: 10.1111/tbed.12639
11. Wang J, Zhang Y, Liu L, Pang X, Yuan W. Development of a TaqMan-based real-time PCR assay for the specific detection of porcine circovirus 3. *J Virol Methods*. (2017) 248:177–80. doi: 10.1016/j.jviromet.2017.07.007
12. Wang J, Zhang Y, Zhang R, Han Q, Liu L, Li R, et al. Recombinase polymerase amplification assay for rapid detection of porcine circovirus 3. *Mol Cell Probes*. (2017) 36:58–61. doi: 10.1016/j.mcp.2017.09.001
13. Ding X, Nie K, Shi L, Zhang Y, Guan L, Zhang D, et al. Improved detection limit in rapid detection of human enterovirus 71 and coxsackievirus A16 by a novel reverse transcription-isothermal multiple-self-matching-initiated amplification assay. *J Clin Microbiol*. (2014) 52:1862–70. doi: 10.1128/JCM.03298-13
14. Notomi T, Mori Y, Tomita N, Kanda H. Loop-mediated isothermal amplification (LAMP): principle, features, and future prospects. *J Microbiol*. (2015) 53:1–5. doi: 10.1007/s12275-015-4656-9
15. Yang Z, Liu W, Liang H, Wen R, Zhang Y. Development and evaluation of LAMP, CPA and IMSA methods for rapid detection of the AML1/ETO fusion gene in acute myeloid leukemia. *Exp Ther Med*. (2018) 16:3353–62. doi: 10.3892/etm.2018.6617
16. Tanner NA, Zhang Y, Evans TC Jr. Visual detection of isothermal nucleic acid amplification using pH-sensitive dyes. *Biotechniques*. (2015) 58:59–68. doi: 10.2144/000114253
17. Park YR, Kim HR, Kim SH, Lee KK, Lyoo YS, Yeo SG, et al. Loop-mediated isothermal amplification assay for the rapid and visual detection of novel porcine circovirus 3. *J Virol Methods*. (2018) 253:26–30. doi: 10.1016/j.jviromet.2017.162.006
18. Jiang H, Wang D, Wang J, Zhu S, She R, Ren X, et al. Induction of porcine dermatitis and nephropathy syndrome in piglets by infection with porcine circovirus type 3. *J Virol*. (2019) 93:e02045-18. doi: 10.1128/JVI.02045-18
19. Chen GH, Mai KJ, Zhou L, Wu RT, Tang XY, Wu JL, et al. Detection and genome sequencing of porcine circovirus 3 in neonatal pigs with congenital tremors in South China. *Transbound Emerg Dis*. (2017) 64:1650–4. doi: 10.1111/tbed.12702
20. Liu C, Chen S, Meng F, Chen R, Zhang Z, Du E, et al. Full-length genome sequences of two Chinese porcine circovirus type 3 strains, NWHEB21 and NWHUN2. *Genome Announc*. (2018) 6:e00062-18. doi: 10.1128/genomeA.00062-18

Conflict of Interest: The authors declare that the research was conducted in the absence of any commercial or financial relationships that could be construed as a potential conflict of interest.

frontiers in Veterinary Science

ORIGINAL RESEARCH
published: 21 August 2020
doi: 10.3389/fvets.2020.00484

Characterization of Nucleocytoplasmic Shuttling of Pseudorabies Virus Protein UL46

Jing-jing Xu[1], Fei Gao[1], Ji-qiang Wu[1], Hao Zheng[1], Wu Tong[1], Xue-fei Cheng[1], Yuting Liu[1], Haojie Zhu[1], Xinling Fu[1], Yifeng Jiang[1], Liwei Li[1], Ning Kong[1], Guoxin Li[1,2] and Guangzhi Tong[1,2]**

[1] Shanghai Veterinary Research Institute, Chinese Academy of Agricultural Sciences, Shanghai, China, [2] Jiangsu Co-innovation Center for the Prevention and Control of Important Animal Infectious Disease and Zoonoses, Yangzhou University, Yangzhou, China

Pseudorabies virus (PRV) is the etiological agent of Aujeszky's disease, which has caused severe economic loss in China since its re-emergence in 2011. UL46, a late gene of herpesvirus, codes for the abundant but non-essential viral phosphoproteins 11 and 12 (VP11/12). In this study, VP11/12 was found to localize inside both the nucleus and cytoplasm. The nuclear localization signal (NLS) of VP11/12 was identified as ^{3}RRARGTRRASWKDASR^{18}. Further research identified α5 and α7 to be the receptors for NLS and the chromosome region maintenance 1 (CRM1) to be the receptor for the nuclear export signal. Moreover, we found that PRV VP11/12 interacts with EP0 and the stimulator of interferon genes protein (STING), whereas the NLS of VP11/12 is the important part for VP11/12 to interact with UL48. To our knowledge, this is the first study to provide reliable evidence verifying the nuclear localization of VP11/12 and its role as an additional shuttling tegument protein for PRV. In addition, this is also the first study to elucidate the interactions between PRV VP11/12 and EP0 as well as between PRV VP11/12 and STING, while identifying the precise interaction sites of PRV VP11/12 and VP16.

Keywords: pseudorabies virus, VP11/12, nucleocytoplasmic shuttling, nuclear localization signal, VP16, EP0, STING

OPEN ACCESS

Edited by:
Shao-Lun Zhai, Institute of Animal Health, Guangdong Academy of Agricultural Sciences, China

Reviewed by:
Xiangdong Li, Yangzhou University, China
Tao Lin, UCONN Health, United States

***Correspondence:**
Guoxin Li
guoxinli@shvri.ac.cn
Guangzhi Tong
gztong@shvri.ac.cn

Specialty section:
This article was submitted to Veterinary Infectious Diseases, a section of the journal Frontiers in Veterinary Science

Received: *01 June 2020*
Accepted: *29 June 2020*
Published: *21 August 2020*

Citation:
Xu J, Gao F, Wu J, Zheng H, Tong W, Cheng X, Liu Y, Zhu H, Fu X, Jiang Y, Li L, Kong N, Li G and Tong G (2020) Characterization of Nucleocytoplasmic Shuttling of Pseudorabies Virus Protein UL46. Front. Vet. Sci. 7:484. doi: 10.3389/fvets.2020.00484

INTRODUCTION

Pseudorabies virus (PRV) is the pathogen for pseudorabies (PR), which is associated with nervous system disorders, respiratory disorders, and reproductive failure, resulting in massive economic loss to the swine industry in China, especially owing to the PRV variant that has emerged since 2011 (1–3).

The taxonomic name for PRV is Suid herpesvirus 1, whereas its original name is Aujeszky's disease virus. PRV is a member of the genus *Varicellovirus* in the subfamily Alphaherpesvirinae, which belongs to the family Herpesviridae. According to a previous study, all PRV genes contain homologs in at least one related alpha herpesvirus. Thus, most genes and certain protein names are derived from their locations within unique regions, in conformity with the prototypical herpes simplex virus type 1 (HSV-1) (4). The structure of the PRV mature virion consists of a linear dsDNA genome, a capsid, a tegument (a protein matrix), and an envelope (4, 5). The PRV genome

is primarily characterized by a unique short (US) region, a unique long (UL) region, internal repeat sequences (IRS), and terminal repeat sequences (6).

The UL46 gene, a late gene of herpesvirus, encoding the abundant but non-essential viral phosphoproteins 11 and 12 (VP11/12) (7–9), is located within the UL regions of the viral genome. VP11/12 is one of the major tegument proteins with a molecular mass of ∼95 kDa (10). The absence of UL46 in the HSV and PRV genomes was reported to have no serious impact on viral titers, one-step growth kinetics, virus replication, or virion morphogenesis in porcine kidney cells (PK-15 cells) and rabbit kidney cells (RK13 cells), only leading to a slight reduction of plaque size (10, 11). Furthermore, Thomas C. Mettenleiter demonstrated that in mice, the neuroinvasion and neurovirulence of PRV-ΔUL46 do not differ significantly from those of the classic PRV strain, Kaplan, via measurement of the mean survival times and viral titers in epithelial cells of nasal mucosa, first-order trigeminal neurons, second-order trigeminal neurons, and pons of infected mice, using immunohistochemistry (12).

However, UL46 is an important gene in herpesviruses and plays an important role in virion assembly and virus growth, especially in the secondary envelopment of viruses and in the inhibition of innate immunity upon viral infection. Moreover, VP11/12 has been reported to serve as the major component of virion tegument, in the form of conserved clusters and functional complexes with pUL47, pUL48, and pUL49 in HSV and PRV (13–15). Additionally, in a study seeking to examine the virus/virus or virus/host interactions, HSV-1 was used to infect human fibroblasts, and VP11/12-related proteins were found as complexes, by immune-affinity purification and mass spectrometry. Further, in this study, at least 23 sites of VP11/12 were shown to be phosphorylated (16). In T cells and primary fibroblasts infected with HSV-1, VP11/12 was shown to function as a substrate of Lck or a Lck-activating kinase and to participate in PI3K-Akt signaling involving virus-induced activation (17–19). In PRV, VP11/12 can induce phosphorylation and expression of ERK1/2; however, it fails to activate the PI3K-Akt signaling pathway.

In previous studies, subcellular localization of VP11/12 was observed in the cytoplasmic or perinuclear regions, in both plasmid-transfected cells and virus-infected cells. In our study, we investigated the intrinsic properties of VP11/12, in the absence of other viral proteins or in PRV JS-2012 infection, and found that VP11/12 localized to the nucleus, as observed by indirect immunofluorescence, and gradually appeared in the cytoplasm as well. Therefore, we sought to elucidate the specific mechanisms and vital functions of the nuclear localization signal (NLS) and nuclear export signal (NES) of VP11/12.

Abbreviations: CRM1, chromosome region maintenance 1; DAPI, 4′,6-diamidino-2-phenylindole; EGFP, enhanced green fluorescent protein; HSV-1, herpes simplex virus type 1; HSV-2, herpes simplex virus type 2; IFA, immunofluorescence assay; LMB, leptomycin B; NES, nuclear export signal; NLS, nuclear localization signal; PRV, pseudorabies virus; STING, stimulator of interferon genes protein; TRS, terminal repeat sequence; UL, unique long regions; US, unique short regions.

MATERIALS AND METHODS

Cell Lines and Viruses

Vero cells, HeLa cells, 293T cells, and PRV variant strain JS-2012 were obtained from the Shanghai Veterinary Research Institute, Chinese Academy of Agricultural Sciences (SHVRI-CAAS, Shanghai, China). Cos-7 cells and NIH/3T3 cells were kindly provided by the Shanghai Stem Cell Bank, Chinese Academy of Sciences (Shanghai, China). All cell lines were grown in Dulbecco's Modified Eagle Medium (DMEM, Gibco, USA) supplemented with 10% fetal bovine serum (FBS, Gibco) at 37°C.

Antibodies and Reagents

Polyclonal antibody anti-UL46 was obtained from SHVRI-CAAS. Anti-FLAG and anti-HA monoclonal antibodies were purchased from Sigma-Aldrich (USA). DAPI and leptomycin B (LMB) were purchased from Beyotime Institute of Biotechnology (Shanghai, China). The monoclonal antibody anti-lamin B2 was purchased from Cell Signaling Technology (CST, USA). Donkey anti-mouse IgG secondary antibodies, Alexa Fluor 594 and Alexa Fluor 488, were purchased from Invitrogen (Thermo Fisher Scientific, USA). Anti-GFP monoclonal antibodies, HRP-conjugated goat anti-mouse IgG, and HRP-conjugated goat anti-rabbit IgG were purchased from ProteinTech (USA). All restriction endonucleases used for cloning procedures were purchased from New England Biolabs (NEB, USA), and homologous recombinases were procured from Vazyme Biotech Co. Ltd. (Nanjing, China). PrimeStar® HS DNA Polymerase was purchased from TaKaRa (Japan).

Plasmid Construction

The full-length UL46 open reading frame, including both the start codon methionine and the stop codon, was PCR-amplified from PRV strain JS-2012 (GenBank accession: KP257591) genomic DNA, using primers that incorporated *Eco*RI sites and homologous sequences in plasmids, p3xFlag-CMV, pEGFP-C3, or pCAGGS. The UL46 fragments were inserted into vectors, p3xFlag-CMV, pEGFP-C3, and pCAGGS, individually, to generate UL46-FLAG, UL46-EGFP, and UL46-HA, respectively. For the positive control, full-length UL47 of PRV JS-2012 genomic DNA was cloned into the *Eco*RI site of p3xFlag-CMV to generate UL47-FLAG. The vector pEGFP-C3 served as the negative control because it could express the enhanced green fluorescent protein (EGFP) protein.

The truncated and mutant UL46 fragments were cloned into the *Eco*RI site of the pEGFP-C3 vector to construct the required plasmids (**Table S1**). To generate plasmids expressing Flag-tagged α1, α3, α4, α5, α6, α7, and α8 were amplified from the cDNA of Vero cells and cloned into *Eco*RI sites of p3xFLAG-CMV. All fragments were inserted into the *Eco*RI site of pEGFP-C3. All primers are listed in **Table S1**. Each construct was confirmed by sequencing performed by the Shanghai Personal Biotechnology Limited Company, and no deletion, insertion, or mutation was detected.

RNA Extraction and Reverse Transcription

Vero cells were collected and frozen at −80°C. Total RNA was extracted by a QIAGEN RNA Extraction Kit (QIAGEN,

Dusseldorf, Germany) according to the manufacturer's instructions. Samples were then digested with DNase I to remove trace amounts of contaminating DNA. The integrity of total RNA was checked for cDNA synthesis using SuperScript™ III reverse transcriptase (Invitrogen, USA).

Transfections and LMB Treatment

To express all proteins *in vitro*, a monolayer of Vero cells, HeLa cells, NIH/3T3 cells, or Cos-7 cells were plated overnight on coverslips in six-well plates (Corning, NY, USA) in DMEM (Gibco, USA) containing 10% FBS, at a density of 2×10^5 cells per well, before transfection. Cells were transfected with mixtures of 1.5–2.0 μg plasmid DNA, Opti-MEM (Gibco, USA), and FuGENE HD Transfection Reagent (Promega, USA), according to the manufacturer's instructions. Indirect immunofluorescence assay (IFA) was then performed. For certain samples, LMB was added into the culture medium at a final concentration of 10 and 20 ng/ml for 4 h.

Immunofluorescence and Confocal Microscopy

After transfection for 24 h, cells were fixed in ice-cold absolute methanol at −20°C for 30 min, washed three times in PBS, and blocked with PBS containing 5% bull serum albumin (Yeasen, Shanghai, China) for 1 h at 28°C. Subsequently, cells were washed three times with PBS and incubated with anti-Flag monoclonal antibody as the primary antibody in six-well plates for 1 h at 37°C. After washing with PBS three times, donkey anti-rabbit IgG secondary antibody, Alexa Fluor 594 (Invitrogen, Shanghai) in PBS, was added to plates for 1 h at 37°C. After each incubation step, cells were washed three times extensively with PBS and stained with DAPI (Beyotime Biotechnology). Samples were analyzed using a Zeiss LSM 880 laser scanning confocal microscope. Images were processed with Adobe Photoshop.

Immunoprecipitation (IP) and Western Blotting Assays

These experiments were carried out as described previously (31); 293T cells were transfected alone or in combination with plasmids UL46-HA, α1-FLAG, α3-FLAG, α4-FLAG, and α6-FLAG using Lipofectamine 3000 (Invitrogen, USA). At 24-h post transfection (hpt), the cells were washed twice with cold PBS and lysed with IP lysis buffer (Thermo Fisher) mixed with inhibitors for protease and phosphatases (BioTool). Except for the inputs of lysates, other cell lysates were incubated with anti-HA agarose (Sigma, cat# A2095) at 4°C overnight. The immunoprecipitates were washed four times with IP lysis buffer and then subjected to western blotting analysis.

Statistical Analysis

Data are presented as mean ± SD. Statistical analysis was performed using GraphPad Prism version 7.0 (San Diego, CA, USA). Differences were considered statistically significant at $P < 0.05$.

RESULTS

VP11/12 Localized in the Nucleus and Cytoplasm in the Presence or Absence of Other Viral Proteins

To study the functions of VP11/12, the NLSs of VP11/12 were predicted via cNLS Mapper (20, 21) and NLStradamus (22). The cNLS Mapper found two potential NLSs in the arginine-rich regions of VP11/12, namely, ^{2}IRRARGTRRASWKDASRRVTEGRTRASC^{29} and ^{662}PRPRTRADDGLYQQPRPVIDLTGHRASRRKSW^{693} (**Figure 1A**). NLStradamus also revealed four potential NLS motifs in VP11/12: ^{4}RARGTRRASWKDASRRV^{20}, ^{482}RRPLRRSRD^{490}, ^{611}RRGVRAAQRFVRRRLSRT^{628}, and ^{685}HRASRRKSWRV^{695} (**Figure 1B**). The NESs of VP11/12 were predicted by NetNES (23), showing that the N-terminal 22nd or 73rd−83rd sequences might have NES (**Figure 1C**). Thus, we hypothesized that VP11/12 might localize in both the nucleus and cytoplasm, even though previous studies reported only a cytoplastic localization of VP11/12.

To identify the subcellular localization of VP11/12 in transfected cells in the absence of other viral proteins, the UL46 gene of the PRV variant JS-2012 was cloned into the C-terminus of EGFP in the eukaryotic expression vector pEGFP-C3 (UL46-EGFP) and in the C-terminus of FLAG in the p3xFlag-CMV vector (UL46-FLAG). The plasmid DNA of UL46-EGFP was transfected into live Vero cells and HeLa cells; 24 h later, cells were fixed with cold methanol. Alternatively, the plasmid of the UL46-FLAG was transfected into NIH/3T3 cells. After 24 h, they were fixed with cold methanol and washed three times with PBS. They were incubated with anti-flag monoclonal antibodies for 1 h at 37°C and then washed three times with PBS. The cells were then incubated with anti-mouse IgG secondary antibody Alexa Fluor 594 for 1 h at 37°C. In order to differentiate between nuclei and cytoplasm, all cells were stained with DAPI and assessed by a Zeiss LSM 880 laser scanning confocal microscope. Consequently, as shown in **Figure 1D**, the transfected UL46-EGFP displayed approximately 84% cytoplasmic and 16% nuclear localization in Vero cells; UL46-FLAG was also shown to be localized to the nuclei and cytoplasm of NIH/3T3 cells. To identify whether GFP in the C-terminus or N-terminus of UL46 could change the subcellular localization of VP11/12, we constructed a plasmid with GFP in the C-terminus of VP11/12, UL46-N-EGFP, and performed IFA analysis. Results of confocal microscopy showed that UL46-N-EGFP localized in both the nucleus and cytoplasm. This indicated that the location of EGFP in either the C-terminus or N-terminus did not influence the subcellular localization of VP11/12; therefore, in subsequent experiments, we chose EGFP in the N-terminus of VP11/12, allowing VP11/12 to translocate to both the nucleus and cytoplasm.

A previous study revealed LMB is an inhibitor of CRM1, one of the major nuclear export receptors for leucine-rich NES-containing proteins (24). We analyzed the amino acid sequence of VP11/12 and concluded it to be a leucine-rich protein, with 53 leucine residues out of 695 amino acids. Based on the prediction for NESs of VP11/12, we hypothesized

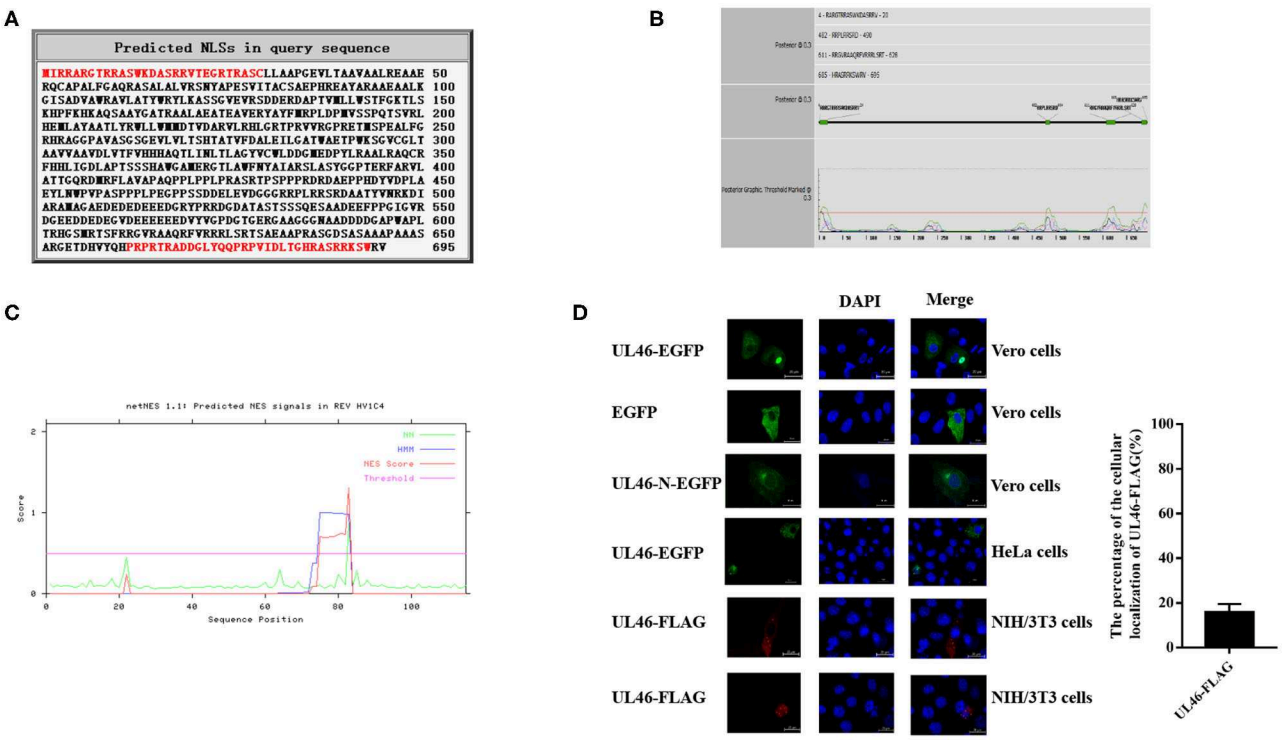

FIGURE 1 | pUL46 as a nucleocytoplasmic shuttling protein. **(A)** cNLS Mapper prediction of the NLSs of pUL46 (in red). **(B)** NLStradamus prediction of the NLSs of pUL46 (in green squares). **(C)** NetNES prediction of the NESs of pUL46 (the peaks of lines). **(D)** Vero cells were transfected with UL46-EGFP, pEGFP-C3, and UL46-N-EGFP; HeLa cells, UL46-EGFP; and NIH/3T3 cells, UL46-FLAG. After 24 h of transfection, Vero, HeLa, and NIH/3T3 cells were subjected to immunofluorescence analysis. Scale bars = 20 μm.

that CRM1 would be the export receptor. To support our hypothesis, Vero cells were transfected with plasmids of UL46-EGFP and treated with 10 or 20 ng/ml of LMB. The positive control, plasmid UL47-FLAG of PRV, was a proven shuttling protein (25), and the negative control, pEGFP-C3, was used in a similar manner as the treatment plasmids, followed by direct immunofluorescence. The results demonstrated that VP11/12 partially localized to the nucleus when cells were treated with 10 ng/ml of LMB and completely localized to the nucleus in the presence of 20 ng/ml, whereas pUL47 alone remained in the nucleus and EGFP localized to the cytoplasm in cells treated with 10 or 20 ng/ml of LMB (**Figure 2**). These results indicated that VP11/12 covalently modifies CRM1 for export to the cytoplasm, depending on the LMB concentration.

VP11/12 has been reported to be localized in the cytoplasm of HSV-1 and HSV-2. Michael Murphy et al. (26) hypothesized that removal of the N-terminal 446 amino acids from the HSV-1 VP11/12 would allow for transport of the protein into the nucleus, although no data were presented to support this hypothesis. In this study, Vero cells were seeded overnight into six-well plates with slides. Cells were infected with PRV variant strain JS-2012 at a multiplicity of infection (MOI) of 0.1 and were examined via IFA using an anti-UL46 polyclonal antibody and DAPI at 0, 3, 6, 9, 12, and 15 h post infection. All samples were observed by Zeiss confocal laser microscopy. IFA results revealed that VP11/12 was present in the nucleus after 6 h of PRV infection, although at a low rate (**Figure 3**).

All the above results demonstrate that VP11/12 translocates into the nucleus from the cytoplasm and is transported into the cytoplasm from the nucleus whether viral proteins were present or not. Moreover, CRM1 was identified as the nuclear export receptor for VP11/12.

Mapping the NLS in VP11/12

Because of UL46 protein, approximately 100 kDa, UL46-EGFP was unable to enter the nucleus without the assistance of additional proteins (26, 27), unless one or more NLSs were present. Considering that some NLSs are short peptides, we constructed truncated fusion plasmids of UL46-EGFP (**Figure 4A**), based on the prediction of NLStradamus, and transfected them into Vero cells. After 24 h, subcellular distribution of the fusion proteins was assessed by indirect fluorescence using a Zeiss LSM 880 confocal microscope [UL46(145–165)-EGFP, UL46(166–300)-EGFP, UL46(301–380)-EGFP, UL46(381–474)-EGFP, UL46(475–500)-EGFP, UL46(501–604)-EGFP, UL46(605–655)-EGFP, and UL46(656–696)-EGFP] and Nikon C1-Si confocal microscope [UL46(1–48)-EGFP and UL46(1–144)-EGFP]. Strikingly, the N-terminal 48 amino

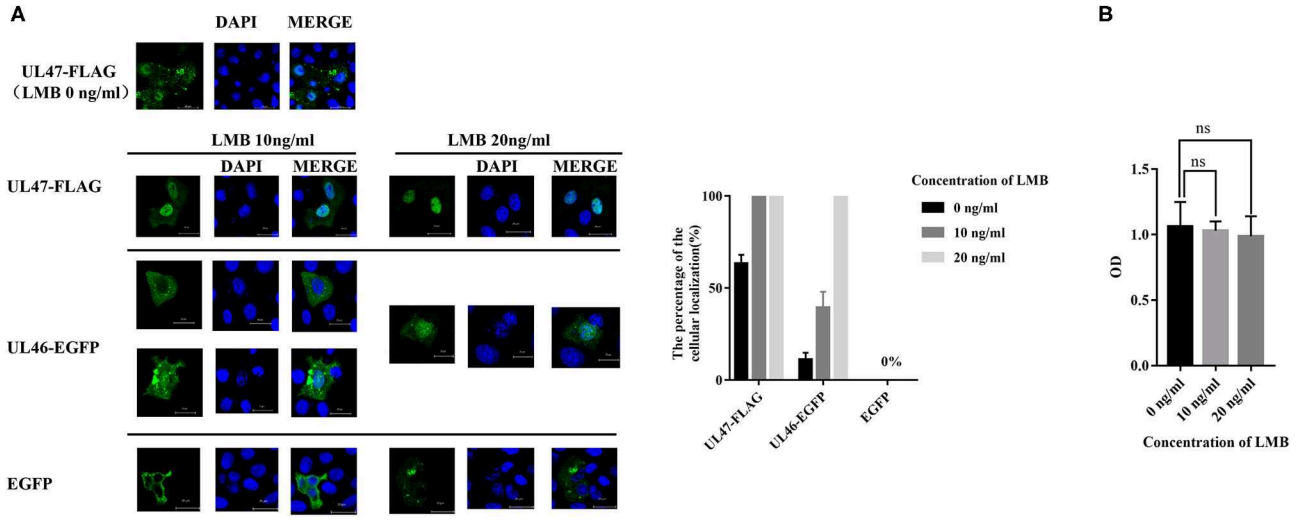

FIGURE 2 | Nuclear localization of UL46-EGFP in cells treated with LMB. **(A)** Vero cells were transfected with UL47-FLAG (positive control), UL46-EGFP, and EGFP-C3 (negative control) and treated with LMB for 24 h. All cell nuclei were stained with DAPI and observed using a laser confocal microscope. Scale bars = 20 μm. **(B)** Cellular toxicity of Vero cells treated with LMB was analyzed using CCK-8 assays.

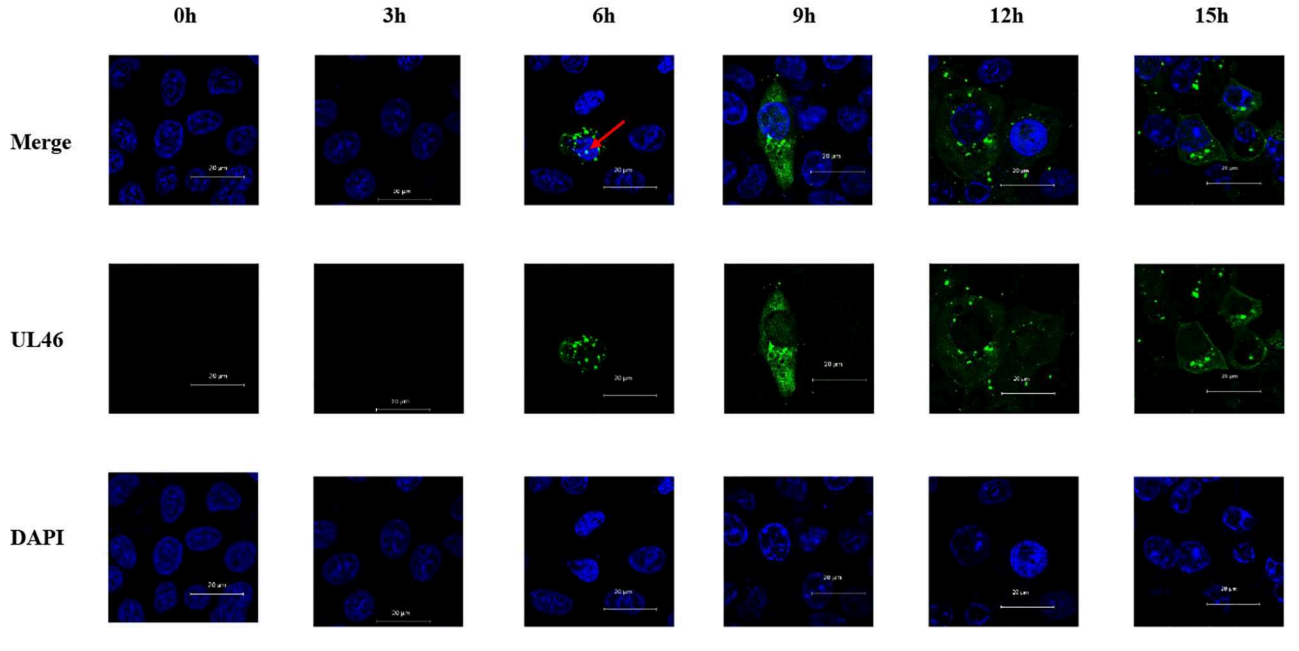

FIGURE 3 | Nuclear localization of VP11/12 during PRV infection. Vero cells were infected with PRV JS-2012 for 0, 3, 6, 9, 12, and 15 h at a multiplicity of infection of 0.01. Infected cells were subjected to immunofluorescence analysis with anti-pUL46 polyclonal antibody, and the nuclei were stained with DAPI. Scale bar = 20 μm.

acid residues from VP11/12 fusion with EGFP revealed nuclear accumulation (**Figure 4B**). Specifically, UL46(1–48)-EGFP and UL46(1–144)-EGFP accumulated not only in the nucleus but also in the cytoplasm. These results suggest the existence of an NLS and potentially an NES within the 48 N-terminal residues of VP11/12, thereby verifying that the NLS is located in the N-terminal amino acids (1–144) of VP11/12.

Identification of the Precise NLS in VP11/12

To identify the NLS, the N-terminal 48-residue peptide was truncated, and the following related plasmids were generated: UL46(1–40)-EGFP, UL46(1–30)-EGFP, UL46(1–25)-EGFP, and UL46(1–20)-EGFP (**Figure 5A**). IFA revealed that all peptides were located in the nucleus (**Figure 5B** and data not shown).

Moreover, to confirm whether VP11/12 contains other NLSs, a plasmid with deletion of the N-terminal 1–20 amino acids,

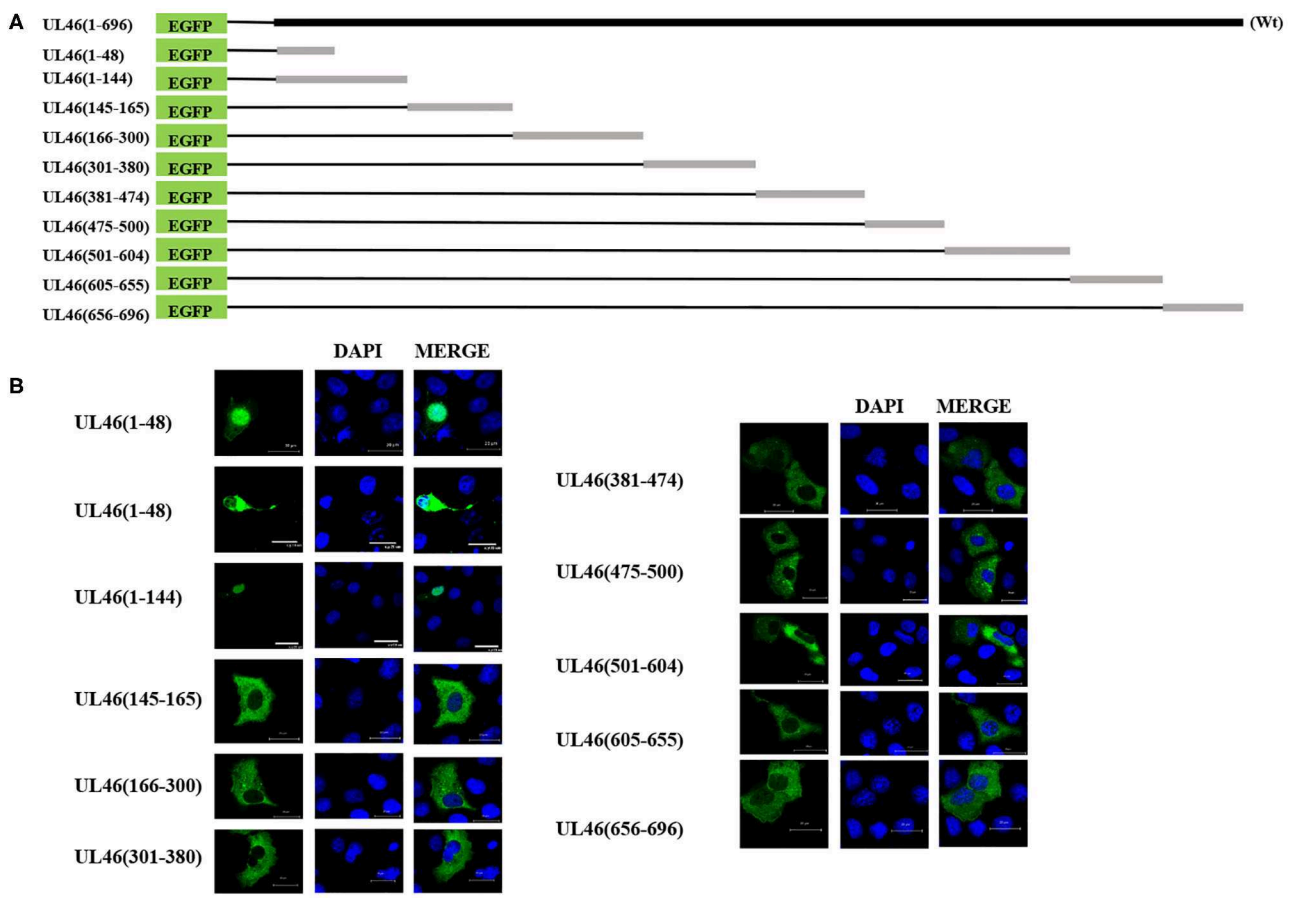

FIGURE 4 | aa1–48 of UL46 as the functional NLS. **(A)** A schematic representation of truncated UL46 predicted by NLStradamus, fused with the C-terminus of EGFP. **(B)** Subcellular localization of the UL46 mutants in **(A)**. Scale bars = 20 μm.

UL46(21–696), was constructed and transfected into Vero cells in six-well plates. UL46(21–696) was not localized in the nucleus but rather was distributed in the cytoplasm (**Figure 5B**). Furthermore, classical NLSs are known to be rich in arginine (28), and this classical characteristic was not observed in UL46(21–696). Hence, these results indicated that no additional classical NLS was present in VP11/12; rather the 20 N-terminal residues formed the only NLS.

To precisely locate the NLS of VP11/12, amino acid residues 18, 17, and 16 of UL46(1–20) were cloned into EGFP-C3, thereby constructing a series of deletions of UL46 (**Figure 5A**). Subcellular localization of these mutants was analyzed, and UL46(3–18)-EGFP was found to display nuclear localization, whereas UL46(3–17)-EGFP, UL46(4–18)-EGFP, and other mutants were only present in the cytoplasm (**Figure 5B** and data not shown). Based on the above evidence, the ^{3}RRARGTRRASWKDASR^{18} peptide was considered to have sufficient residues to guide VP11/12 to the nucleus. To further ensure the effectiveness of the UL46(3–18), we constructed the plasmid NLS-UL35-FLAG fusing with the NLS and PRV UL35 and UL35-FLAG. PRV VP26 encoded by gene UL35 was verified only by cytoplasmic localization without other PRV viral proteins (29, 30). The results showed that all NLS-UL35-FLAG translocated into the nuclei while UL35-FLAG could not. Therefore, it could be concluded that the NLS of UL46 facilitated the transport of NLS-UL35-FLAG into the nuclei. Hence, ^{3}RRARGTRRASWKDASR^{18} was confirmed as the NLS of VP11/12.

Nuclear localization signals consist of many basic amino acids, especially arginine (31). There are 6 arginine residues in UL46(3–18). To identify the critical amino acids in the NLS of VP11/12, glycine replacement mutagenesis was performed with respect to the wide-type UL46(3–18) (**Figure 5C**). Immunofluorescence assay results using the mutants were compared to those of wide type UL46(3–18). All mutants, including NLS (3-4-6), NLS (3-6-9), NLS (3-6-18), NLS (6-9-18), and NLS (6-10-18), were present in the cytoplasm, and were absent from the nucleus (**Figure 5D**). Coincidently, among these mutants, the sixth amino acid had been changed from arginine to glycine. Therefore, we only mutated the sixth amino acid to glycine in UL46(3–18) to generate NLS (R6G). Confocal microscopy results revealed that NLS (R6G) localized in the cytoplasm (**Figure 5D**). Thus, UL46(3–18) peptide was

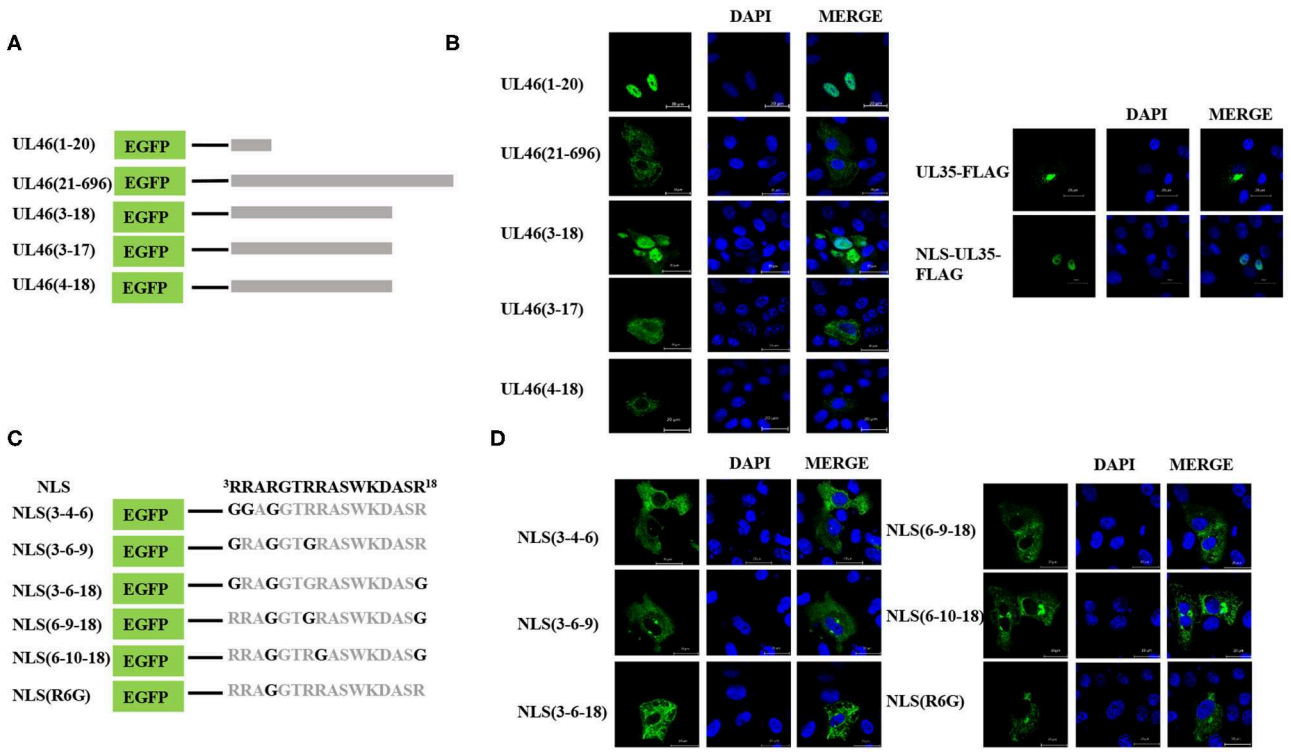

FIGURE 5 | Precise identification of the NLS of UL46. **(A)** A schematic representation of deletion mutants aa1–20, aa21–696, aa3–18, aa3–17, and aa4–18 fused with the C-terminus of EGFP. **(B)** Localization of aa1–20, aa21–696, aa3–18, aa3–17, and aa4–18 mutants; NLS-UL35-FLAG; and UL35-FLAG. All cell nuclei were stained with DAPI. Scale bars = 20 μm. **(C)** Schematic representations of point mutations in the NLS. **(D)** Subcellular localization of proteins harboring point mutations in their NLSs. Scale bars = 20 μm.

identified as the NLS of VP11/12 and the sixth N-terminal amino acid-arginine in UL46(3–18) was found to be the key element that determines the subcellular localization of VP11/12.

Binding of VP11/12 to α5 and α7 via NLS

The results described above indicate that VP11/12 contains a classical NLS, which may direct it to the nucleus. Thus, we considered the importin α/β pathway as a mediator of VP11/12 nuclear import. Seven different isoforms of importin have been characterized in mammalian cells (32, 33). To confirm our hypothesis, we constructed FLAG-tagged α1, α3, α4, α5, α6, α7, and α8 co-transfected with UL46-HA or ΔNLS-HA into 293T cells and performed IP assays, according to the standard protocol (34). After co-transfection, 293T cells were lysed by Pierce IP lysis buffer using protease inhibitors, and the lysates of the co-transfected cell were incubated with HA-tagged beads (Sigma, USA) overnight at 4°C. Thereafter, SDS-PAGE and western blotting were performed for the samples. IP assay results showed α5 and α7 to be co-immunoprecipitated with UL46-HA. The IP samples were immunoblotted with anti-HA and anti-FLAG MAb (Sigma). α1, α3, α4, α7, and α8 were detected only in the input samples (data not shown). UL46-HA was verified in both the input and IP samples, which confirmed that UL46 did not interact with the importins α1-, α3-, α4-, α7-, and α8-FLAG (**Figure 6** and data not shown). Furthermore, α5- and α7-FLAG were detected in both input and IP samples.

To verify that the NLS of VP11/12 is the interaction site between VP11/12 and α5 or α7, we constructed a plasmid, ΔNLS-UL46, in which the NLS of VP11/12 was truncated and contained the vector HA-tagged PCAGGS. The ΔNLS-UL46 was co-immunoprecipitated with α5- or α7-FLAG by HA-tagged beads. The results showed that α5 and α7 were detected in the input samples but not in the IP samples. These data revealed that α5 or α7 was possibly required for guiding VP11/12 to the nucleus and that deletion of NLS from VP11/12 abolished the VP11/12 binding to α5- or α7-FLAG. This further indicated that the α5 and α7 might meditate the nuclear import of VP11/12 (**Figure 6**).

Binding of VP11/12 to UL48 Through the NLS of VP11/12

UL48, encoding VP16, plays vital roles in promoting the assembly of a multicomponent complex with Oct-1 and HCF-1, to induce the expression of viral immediate–early genes (35) and secondary envelopment in both HSV-1 and PRV (36–39), and it can enter the nucleus in HSV-1 (40–42) and PRV (37). VP11/12 has been reported to interact with UL48 (11), although

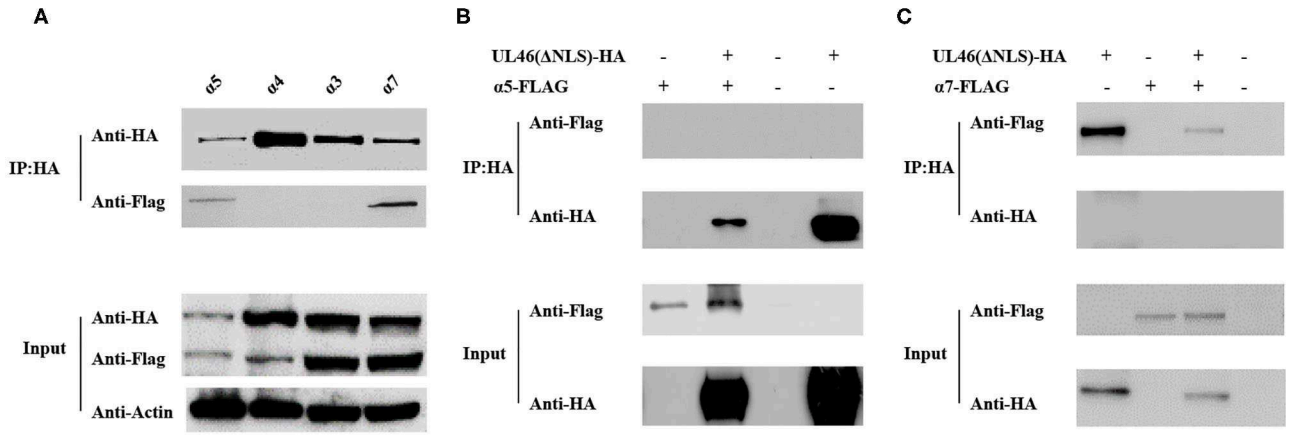

FIGURE 6 | UL46 binds to importins. **(A)** IP for 293T cells co-transfected with recombinant constructs encoding UL46-HA and FLAG-tagged α3, α4, α5, and α7. **(B)** IP for 293T cells co-transfected with recombinant constructs encoding UL46-ΔNLS-HA and α5. **(C)** IP for 293T cells co-transfected with recombinant constructs encoding UL46-ΔNLS-HA and α7.

the exact site has not yet been identified. To confirm whether the NLS of VP11/12 interacts with UL48, the plasmid UL48-FLAG was constructed, co-transfected with UL46-HA, and subjected to co-immunoprecipitation. The IP assay demonstrated that UL48-FLAG was detected in the input as well as IP samples. Alternatively, UL48-FLAG could not be tested when ΔNLS-UL46-HA (not UL46-HA) was in the proteins. Therefore, the NLS of VP11/12 was likely the same domain used to allow VP11/12 to interact with pUL48, thereby regulating the functions of pUL48 (**Figures 7A,B**). These results suggest that the NLS of VP11/12 is the domain by which VP11/12 regulates the functions of UL48.

Binding of VP11/12 to EP0 or STING Does Not Occur Through the NLS

EP0, the homolog of ICP0 in HSV-1, is a transactivating protein that can enhance the infectivity of PRV genomic DNA, couples with IE180 (43–45), and localizes to the nucleus in HSV-1 (42) and PRV (46). In HSV-1, the homolog of EP0, ICP0, interacts with VP11/12 (16, 17). To determine whether EP0 interacts with VP11/12 in PRV and whether the NLS of VP11/12 is the key element for VP11/12 to bind to EP0, we constructed the FLAG-tagged EP0 plasmid, EP0-FLAG. UL46-HA and ΔNLS-UL46 were co-transfected with EP0-FLAG, individually, in 293T cells, and the transfected cells were harvested after 30 hpt and subjected to co-immunoprecipitation. Results of SDS-PAGE and western blot analysis revealed that EP0-FLAG was expressed irrespective of co-transfection with UL46-HA or ΔNLS-UL46 (**Figures 7C,D**). Thus, the NLS of UL46 was not the key element.

HSV-1 VP11/12 has been reported to interact with STING via its 100 N-terminal amino acids (19). Therefore, we speculated that the N-terminus of PRV VP11/12 might also interact with STING. The IP assay in UL46-HA/STING-FLAG and ΔNLS-UL46/STING-FLAG showed that UL46-HA and ΔNLS-UL46 interacted with STING (**Figures 7E,F**). Therefore, the NLS was not the site contributing to their binding.

DISCUSSION

HSV-1 VP11/12 is a multifunctional tegument protein that interacts with many viral proteins and cellular proteins in immune signaling pathways, thereby contributing to several biological processes (17–19, 47–49). Moreover, HSV-1 VP11/12 and its homolog PRV VP11/12 both play roles in virus growth, most notably in the secondary envelopment (26, 27, 37). Previous studies on HSV-1 and PRV VP11/12 showed VP11/12 to be localized in the cytoplasm, rather than in the nucleus. Therefore, when nuclear localization of VP11/12 was observed, we considered determining its mechanism of nuclear localization, identifying the transport mechanisms, and investigating the significance of VP11/12 localization into the nucleus.

Nucleocytoplasmic shuttling proteins contain NLSs and NESs. Herein, we demonstrated that PRV VP11/12 shuttles between the nucleus and cytoplasm, which was the first report on nucleocytoplasmic shuttling of herpesvirus VP11/12. We also found that VP11/12 was to possibly localize in the nucleus and performed related experiments to identify the NLS. Furthermore, we confirmed that the nuclear export of VP11/12 occurred through its interaction with CRM1, because 20 ng/ml of LMB inhibited its nuclear export.

As schematically represented in **Figure 4**, a newly characterized NLS, containing basic clusters, was found to be responsible for the nuclear localization of VP11/12. After a series of mutation analyses and fluorescence microscopy, ^{3}RRARGTRRASWKDASR^{18} was identified as the functional NLS. VP11/12 appeared to have been phosphorylated heavily in at least 23 sites when HSV-1 infected, and phosphorylation played important roles in modulating VP11/12 abundance with

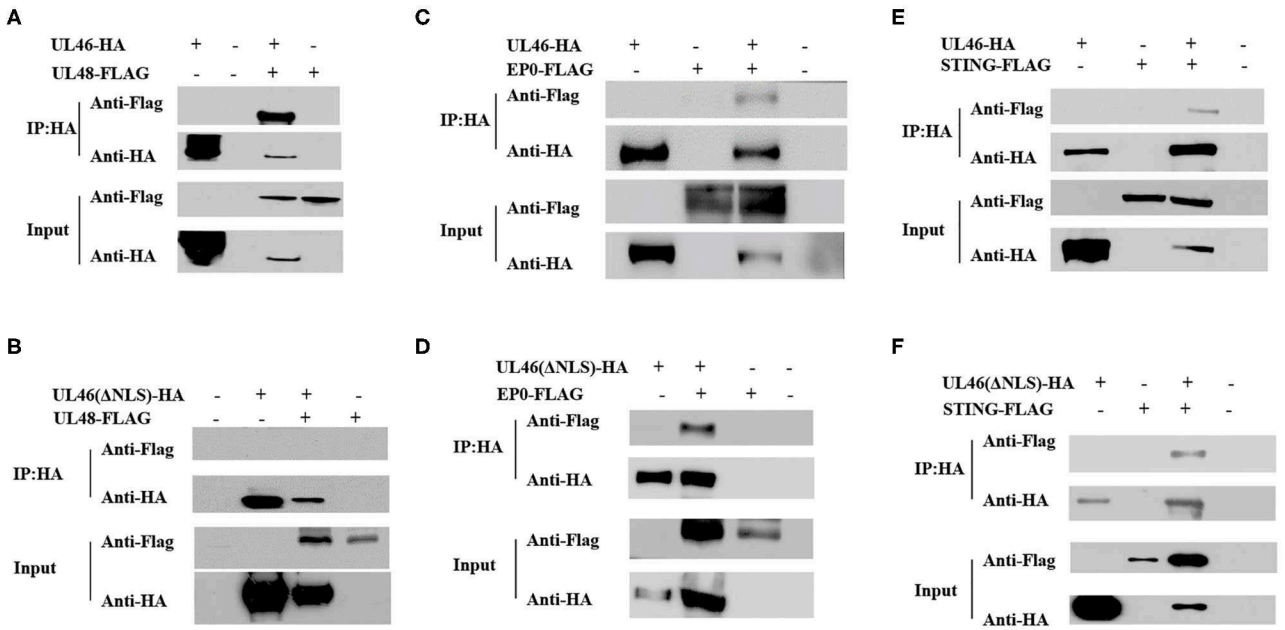

FIGURE 7 | The NLS of UL46 interacts with UL48. **(A)** IP for 293T cells co-transfected with recombinant constructs encoding UL46-HA and UL48-FLAG. **(B)** IP for 293T cells co-transfected with recombinant constructs encoding UL46-ΔNLS-HA and UL48-FLAG. **(C)** IP for 293T cells co-transfected with recombinant constructs encoding UL46-HA and EP0-FLAG. **(D)** IP for 293T cells co-transfected with recombinant constructs encoding UL46-ΔNLS-HA and EP0-FLAG. **(E)** IP for 293T cells co-transfected with recombinant constructs encoding UL46-HA and STING-FLAG. **(F)** IP for 293T cells co-transfected with recombinant constructs encoding UL46-ΔNLS-HA and STING-FLAG.

respect to ICP0 localization and interactions (16). According to the alignment of specific herpesvirus VP11/12 protein sequences, there was likely no phosphorylated site in the PRV NLS of VP11/12 (data not shown).

To identify the NLS of VP11/12, we truncated 48 amino acids from the N-terminus of VP11/12 and generated the plasmid UL46(1–48)-EGFP. Subsequent experiments demonstrated that UL46(1–48)-EGFP could be seen in both the nucleus and the cytoplasm (**Figure 4B**). Therefore, it was reasonably hypothesized that there is an NES in the N-terminal 48-amino-acid stretch. Considering that the NLS of VP11/12 is located in the N-terminal 3rd to 18th amino acids, coupled with previous studies, the export of leucine-rich NES-containing proteins may be inhibited by LMB (50); we predicted the NES to be between the 19th and 48th amino acids of VP11/12. To verify this hypothesis, we created point mutations containing leucine residues, generated the plasmid UL46(L30G-L31G-L38G-L45G)-EGFP, and observed it with a confocal microscope. Our result showed that UL46(L30G-L31G-L38G-L45G)-EGFP appeared in both the cytoplasm and nucleus (data not shown), thus indicating that the efficient NES is not the classical one that is located between the 19th and 48th residues. Therefore, we speculated that the NES in the N-terminus of VP11/12 may not be classical; and further experiments needs to be conducted to test for a more functional NES.

In a previous study, HSV-1 VP11/12 had been proven to interact with the host protein STING (19) and the viral protein ICP0, and HSV-1 and PRV VP11/12 interacted with UL48 (11); however, the interaction sites of VP11/12 were not all localized. Therefore, in this study, we proved for the first time that PRV VP11/12 interacted with the crucial antiviral protein STING, whereas ΔNLS-UL46 also interacted with STING, thus demonstrating that in PRV, VP11/12 could regulate the functions of STING in the cytoplasm and help PRV DNA to evade the host innate immunity (19). Furthermore, it is the first time to show that PRV VP11/12 interacts with PRV EP0, similar to that with STING and that ΔNLS-UL46 also interacts with EP0, thus possibly indicating that in PRV, EP0 helps to maintain the proper expression level of VP11/12. Considering that PRV EP0 and its homologous protein HSV-1 ICP0 can be transported between the cytoplasm and nucleus (46, 51) and that ICP0 influences numerous host nuclear proteins, such as cyclin D3, p53, ND10, p60, and the ubiquitin-specific protease USP7, in addition to regulating viral gene expression, stimulating lytic infection, and enhancing reactivation of latent infection (52–57), we reasonably assumed that VP11/12 might exhibit connections with the functions of EP0 in the nucleus.

The PRV VP11/12 interacted with PRV pUL48, and more importantly, the NLS of VP11/12 interacted with pUL48/VP16, the key activator of lytic infection by initiating the lytic program (37). A previous study revealed the translocation of pUL48 into the nucleus, depending on HCF (also referred to as C1, CFF, or VCAF) owing to the absence of NLS (58). In the late phase of HSV-2 infection, most VP11/12 co-localized with VP16, and VP11/12 could enhance α4 promoter-regulated gene expression when co-precipitating with VP16 (27). Thus, we hypothesized

that the NLS of PRV VP11/12 was conducive to the activation of PRV induced by pUL48, even though VP11/12 was not essential.

In summary, we verified the nucleocytoplasmic shuttling of VP11/12 and identified its NLS, ^{3}RRARGTRRASWKDASR^{18}. Furthermore, we identified interactions between PRV VP11/12 and EP0, PRV VP11/12 and pUL48, and PRV VP11/12 and the host protein, STING, which is critical for the growth of PRV. The significance of these interactions requires further investigation.

DATA AVAILABILITY STATEMENT

The raw data supporting the conclusions of this article will be made available by the authors, without undue reservation.

AUTHOR CONTRIBUTIONS

JX: experiment, writing, and design. FG: supervise and revise. JW: experiment and design. HZhe: supervise and design. XC, YL, HZhu, and XF: experiment. WT, YJ, LL, and NK: supervise. GL and GT: funding. All authors contributed to the article and approved the submitted version.

FUNDING

This work was supported by the National Key Research and Development Program of China (2016YFD0500100), the Shanghai Science and Technology Innovation Action Plan (17391901900), and the Shanghai Municipal Agriculture Science and Technology Key Project (2016, 4-2).

SUPPLEMENTARY MATERIAL

The Supplementary Material for this article can be found online at: https://www.frontiersin.org/articles/10.3389/fvets.2020.00484/full#supplementary-material

REFERENCES

1. An TQ, Peng JM, Tian ZJ, Zhao HY, Li N, Liu YM, et al. Pseudorabies virus variant in Bartha-K61-vaccinated pigs, China, 2012. *Emerg Infect Dis*. (2013) 19:1749–55. doi: 10.3201/eid1911.130177
2. Hu D, Zhang Z, Lv L, Xiao Y, Qu Y, Ma H, et al. Outbreak of variant pseudorabies virus in Bartha-K61-vaccinated piglets in central Shandong Province, China. *J Vet Diagn Invest*. (2015) 27:600–5. doi: 10.1177/1040638715593599
3. Tong W, Liu F, Zheng H, Liang C, Zhou YJ, Jiang YF, et al. Emergence of a Pseudorabies virus variant with increased virulence to piglets. *Vet Microbiol*. (2015) 181:236–40. doi: 10.1016/j.vetmic.2015.09.021
4. Pomeranz LE, Reynolds AE, Hengartner CJ. Molecular biology of pseudorabies virus: impact on neurovirology and veterinary medicine. *Microbiol Mol Biol Rev*. (2005) 69:462–500. doi: 10.1128/MMBR.69.3.462-500.2005
5. Grünewald K, Desai P, Winkler DC, Heymann JB, Belnap DM, Baumeister W, et al. Three-dimensional structure of herpes simplex virus from cryo-electron tomography. *Science*. (2003) 302:1396–8. doi: 10.1126/science.1090284
6. Schloegl C, Schmidt J, Boeckle M, Weiss BM, Kotrschal K. Grey parrots use inferential reasoning based on acoustic cues alone. *Proc R Soc Lond B Biol Sci*. (2012) 279:4135–42. doi: 10.1098/rspb.2012.1292
7. Heine JW, Honess RW, Cassai E, Roizman B. Proteins specified by herpes simplex virus. XII. The virion polypeptides of type 1 strains. *J Virol*. (1974) 14: 640–51. doi: 10.1128/JVI.14.3.640-651.1974
8. Lemaster S, Roizman B. Herpes simplex virus phosphoproteins. II Characterization of the virion protein kinase and of the polypeptides phosphorylated in the virion. *J Virol*. (1980) 35:798–811. doi: 10.1128/JVI.35.3.798-811.1980
9. Zhang Y, McKnight JL. Herpes simplex virus type 1 UL46 and UL47 deletion mutants lack VP11 and VP12 or VP13 and VP14, respectively, and exhibit altered viral thymidine kinase expression. *J Virol*. (1993) 67:1482–92. doi: 10.1128/JVI.67.3.1482-1492.1993
10. Kopp M, Klupp BG, Granzow H, Fuchs W, Mettenleiter TC. Identification and characterization of the pseudorabies virus tegument proteins UL46 and UL47: role for UL47 in virion morphogenesis in the cytoplasm. *J Virol*. (2002) 76:8820–33. doi: 10.1128/JVI.76.17.8820-8833.2002
11. Fuchs W, Granzow H, Mettenleiter TC. A pseudorabies virus recombinant simultaneously lacking the major tegument proteins encoded by the UL46, UL47, UL48, and UL49 genes is viable in cultured cells. *J Virol*. (2003) 77:12891–900. doi: 10.1128/JVI.77.23.12891-12900.2003
12. Klopfleisch R, Klupp BG, Fuchs W, Kopp M, Teifke JP, Mettenleiter TC. Influence of pseudorabies virus proteins on neuroinvasion and neurovirulence in mice. *J Virol*. (2006) 80:5571–6. doi: 10.1128/JVI.02589-05
13. Bras F, Dezelee S, Simonet B, Nguyen X, Vende P, Flamand A, et al. The left border of the genomic inversion of pseudorabies virus contains genes homologous to the UL46 and UL47 genes of herpes simplex virus type 1, but no UL45 gene. *Virus Res*. (1999) 60:29–40. doi: 10.1016/S0168-1702(98)00146-4
14. Klopfleisch R, Teifke JP, Fuchs W, Kopp M, Klupp BG, Mettenleiter TC. Influence of tegument proteins of pseudorabies virus on neuroinvasion and transneuronal spread in the nervous system of adult mice after intranasal inoculation. *J Virol*. (2004) 78:2956–66. doi: 10.1128/JVI.78.6.2956-2966.2004
15. Michael K, Klupp BG, Mettenleiter TC, Karger A. Composition of pseudorabies virus particles lacking tegument protein US3, UL47, or UL49 or envelope glycoprotein E. *J Virol*. (2006) 80:1332–9. doi: 10.1128/JVI.80.3.1332-1339.2006
16. Lin AE, Greco TM, Dohner K, Sodeik B, Cristea IM. A proteomic perspective of inbuilt viral protein regulation: pUL46 tegument protein is targeted for degradation by ICP0 during herpes simplex virus type 1 infection. *Mol Cell Proteom*. (2013) 12:3237–52. doi: 10.1074/mcp.M113.030866
17. Wagner MJ, Smiley JR. Herpes simplex virus requires VP11/12 to induce phosphorylation of the activation loop tyrosine. (Y394) of the Src family kinase Lck in T lymphocytes. *J Virol*. (2009) 83:12452–61. doi: 10.1128/JVI.01364-09
18. Wagner MJ, Smiley JR. Herpes simplex virus requires VP11/12 to activate Src family kinase-phosphoinositide 3-kinase-Akt signaling. *J Virol*. (2011) 85:2803–12. doi: 10.1128/JVI.01877-10
19. Deschamps T, Kalamvoki M. Evasion of the STING DNA sensing pathway by the VP11/12 of herpes simplex virus type 1. *J Virol*. (2017) 91:e00535–17. doi: 10.1128/JVI.00535-17
20. Kosugi S, Hasebe M, Entani T, Takayama S, Tomita M, Yanagawa H. Design of peptide inhibitors for the importin alpha/beta nuclear import pathway by activity-based profiling. *Chem Biol*. (2008) 15:940–9. doi: 10.1016/j.chembiol.2008.07.019
21. Kosugi S, Hasebe M, Tomita M, Yanagawa H. Systematic identification of cell cycle-dependent yeast nucleocytoplasmic shuttling proteins by prediction of composite motifs. *Proc Natl Acad Sci USA*. (2009) 106:10171–6. doi: 10.1073/pnas.0900604106
22. Nguyen Ba AN, Pogoutse A, Provart N, Moses AM. NLStradamus: a simple Hidden Markov Model for nuclear localization signal prediction. *BMC Bioinformatics*. (2009) 10:202. doi: 10.1186/1471-2105-10-202
23. la Cour T, Kiemer L, Molgaard A, Gupta R, Skriver K, Brunak S. Analysis and prediction of leucine-rich nuclear export signals. *Protein Eng Des*. (2004) 17:527–36. doi: 10.1093/protein/gzh062

24. Gorlich D, Mattaj IW. Nucleocytoplasmic transport. *Science*. (1996) 271:1513–8. doi: 10.1126/science.271.5255.1513
25. Donnelly M, Elliott G. Nuclear localization and shuttling of herpes simplex virus tegument protein VP13/14. *J Virol*. (2001) 75:2566–74. doi: 10.1128/JVI.75.6.2566-2574.2001
26. Murphy MA, Bucks MA, O'Regan KJ, Courtney RJ. The HSV-1 tegument protein pUL46 associates with cellular membranes and viral capsids. *Virology*. (2008) 376:279–89. doi: 10.1016/j.virol.2008.03.018
27. Kato K, Daikoku T, Goshima F, Kume H, Yamaki K, Nishiyama Y. Synthesis, subcellular localization and VP16 interaction of the herpes simplex virus type 2 UL46 gene product. *Arch Virol*. (2000) 145:2149–62. doi: 10.1007/s007050070045
28. Cardarelli F, Serresi M, Bizzarri R, Giacca M, Beltram F. *In vivo* study of HIV-1 Tat arginine-rich motif unveils its transport properties. *Mol Ther*. (2007) 15:1313–22. doi: 10.1038/sj.mt.6300172
29. Douglas MW, Diefenbach RJ, Homa FL, Miranda-Saksena M, Rixon FJ, Vittone V, et al. Herpes simplex virus type 1 capsid protein VP26 interacts with dynein light chains RP3 and Tctex1 and plays a role in retrograde cellular transport. *J Biol Chem*. (2004) 279:28522–30. doi: 10.1074/jbc.M311671200
30. Antinone SE, Shubeita GT, Coller KE, Lee JI, Haverlock-Moyns S, Gross SP, et al. The herpesvirus capsid surface protein, VP26, and the majority of the tegument proteins are dispensable for capsid transport toward the nucleus. *J Virol*. (2006) 80:5494–8. doi: 10.1128/JVI.00026-06
31. Palmeri D, Malim MH. (1999). Importin beta can mediate the nuclear import of an arginine-rich nuclear localization signal in the absence of importin alpha. *Mol Cell Biol*. 19, 1218–25. doi: 10.1128/mcb.19.2.1218
32. Tejomurtula J, Lee KB, Tripurani SK, Smith GW, Yao J. Role of importin alpha8, a new member of the importin alpha family of nuclear transport proteins, in early embryonic development in cattle. *Biol Reprod*. (2009) 81:333–42. doi: 10.1095/biolreprod.109.077396
33. Kelley JB, Talley AM, Spencer A, Gioeli D, Paschal BM. Karyopherin alpha7. (KPNA7), a divergent member of the importin alpha family of nuclear import receptors. *BMC Cell Biol*. (2010) 11:63. doi: 10.1186/1471-2121-11-63
34. Li L, Zhao K, Gao F, Jiang Y, Shan T, Tong W, et al. Restriction of porcine reproductive and respiratory syndrome virus replication by galectin-1. *Vet Microbiol*. (2019) 235:310–8. doi: 10.1016/j.vetmic.2019.07.024
35. Wilson AC, Cleary MA, Lai JS, LaMarco K, Peterson MG, Herr W. Combinatorial control of transcription: the herpes simplex virus VP16-induced complex. *Cold Spring Harb Symp Quant Biol*. (1993) 58:167–78. doi: 10.1101/SQB.1993.058.01.021
36. Mossman KL, Sherburne R, Lavery C, Duncan J, Smiley JR. Evidence that herpes simplex virus VP16 is required for viral egress downstream of the initial envelopment event. *J Virol*. (2000) 74:6287–99. doi: 10.1128/JVI.74.14.6287-6299.2000
37. Fuchs W, Granzow H, Klupp BG, Kopp M, Mettenleiter TC. The UL48 tegument protein of pseudorabies virus is critical for intracytoplasmic assembly of infectious virions. *J Virol*. (2002) 76:6729–42. doi: 10.1128/JVI.76.13.6729-6742.2002
38. Owen DJ, Crump CM, Graham SC. Tegument assembly and secondary envelopment of alphaherpesviruses. *Viruses-Basel*. (2015) 7:5084–114. doi: 10.3390/v7092861
39. Weinheimer SP, Boyd BA, Durham SK, Resnick JL, O'Boyle DR. II. Deletion of the VP16 open reading frame of herpes simplex virus type 1. *J Virol*. (1992) 66:258–69. doi: 10.1128/JVI.66.1.258-269.1992
40. Morrison EE, Stevenson AJ, Wang YF, Meredith DM. Differences in the intracellular localization and fate of herpes simplex virus tegument proteins early in the infection of Vero cells. *J General Virol*. (1998) 79:2517–28. doi: 10.1099/0022-1317-79-10-2517
41. Salsman J, Zimmerman N, Chen T, Domagala M, Frappier L. Genome-wide screen of three herpesviruses for protein subcellular localization and alteration of PML nuclear bodies. *PLoS Pathog*. (2008) 4:e1000100. doi: 10.1371/journal.ppat.1000100
42. Xing J, Wang S, Li Y, Guo H, Zhao L, Pan W, et al. Characterization of the subcellular localization of herpes simplex virus type 1 proteins in living cells. *Med Microbiol Immunol*. (2011) 200:61–8. doi: 10.1007/s00430-010-0175-9
43. Watanabe S, Ono E, Shimizu Y, Kida H. Pseudorabies virus early protein 0 transactivates the viral gene promoters. *J Gen Virol*. (1995) 76. (Pt 11):2881–5. doi: 10.1099/0022-1317-76-11-2881
44. Watanabe S, Ono E, Shimizu Y, Kida H. Mapping of transregulatory domains of pseudorabies virus early protein 0 and identification of its dominant-negative mutant. *Arch Virol*. (1996) 141:1001–9. doi: 10.1007/BF017 18604
45. Ono E, Watanabe S, Nikami H, Tasaki T, Kida H. Pseudorabies virus. (PRV) early protein 0 activates PRV gene transcription in combination with the immediate-early protein IE180 and enhances the infectivity of PRV genomic DNA. *Vet Microbiol*. (1998) 63:99–107. doi: 10.1016/S0378-1135(98)00 236-3
46. Cai M, Wang P, Wang Y, Chen T, Xu Z, Zou X, et al. Identification of the molecular determinants for nuclear import of PRV EP0. *Biol Chem*. (2019) 400:1385–94. doi: 10.1515/hsz-2019-0201
47. Zahariadis G, Wagner MJ, Doepker RC, Maciejko JM, Crider CM, Jerome KR, et al. Cell-type-specific tyrosine phosphorylation of the herpes simplex virus tegument protein VP11/12 encoded by gene UL46. *J Virol*. (2008) 82:6098–108. doi: 10.1128/JVI.02121-07
48. Strunk U, Saffran HA, Wu FW, Smiley JR. Role of herpes simplex virus VP11/12 tyrosine-based motifs in binding and activation of the Src family kinase Lck and recruitment of p85, Grb2, and Shc. *J Virol*. (2013) 87:11276–86. doi: 10.1128/JVI.01702-13
49. Schulz KS, Liu X, Klupp BG, Granzow H, Cohen JI, Mettenleiter TC. Pseudorabies virus pUL46 induces activation of ERK1/2 and regulates herpesvirus-induced nuclear envelope breakdown. *J Virol*. (2014) 88:6003–11. doi: 10.1128/JVI.00501-14
50. Fornerod M, Ohno M, Yoshida M, Mattaj IW. CRM1 is an export receptor for leucine-rich nuclear export signals. *Cell*. (1997) 90:1051–60. doi: 10.1016/S0092-8674(00)80371-2
51. Hutchinson I, Whiteley A, Browne H, Elliott G. Sequential localization of two herpes simplex virus tegument proteins to punctate nuclear dots adjacent to ICP0 domains. *J Virol*. (2002) 76:10365–73. doi: 10.1128/JVI.76.20.10365-10373.2002
52. Parkinson J, Everett RD. Alphaherpesvirus proteins related to herpes simplex virus type 1 ICP0 affect cellular structures and proteins. *J Virol*. (2000) 74:10006–17. doi: 10.1128/JVI.74.21.10006-10017.2000
53. Boutell C, Everett RD. The herpes simplex virus type 1. (HSV-1) regulatory protein ICP0 interacts with and Ubiquitinates p53. *J Biol Chem*. (2003) 278:36596–602. doi: 10.1074/jbc.M300776200
54. Hagglund R, Roizman B. Role of ICP0 in the strategy of conquest of the host cell by herpes simplex virus 1. *J Virol*. (2004) 78:2169–78. doi: 10.1128/JVI.78.5.2169-2178.2004
55. Antrobus R, Boutell C. Identification of a novel higher molecular weight isoform of USP7/HAUSP that interacts with the Herpes simplex virus type-1 immediate early protein ICP0. *Virus Res*. (2008) 137:64–71. doi: 10.1016/j.virusres.2008.05.017
56. Pfoh R, Lacdao IK, Georges AA, Capar A, Zheng H, Frappier L, et al. Crystal structure of USP7 ubiquitin-like domains with an ICP0 peptide reveals a novel mechanism used by viral and cellular proteins to target USP7. *PLoS Pathog*. (2015) 11:e1004950. doi: 10.1371/journal.ppat.1004950
57. Pozhidaeva AK, Mohni KN, Dhe-Paganon S, Arrowsmith CH, Weller SK, Korzhnev DM, et al. Structural characterization of interaction between human ubiquitin-specific protease 7 and immediate-early protein ICP0 of herpes simplex virus-1. *J Biol Chem*. (2015) 290:22907–18. doi: 10.1074/jbc.M115.664805
58. La Boissiere S, Hughes T, O'Hare P. HCF-dependent nuclear import of VP16. *EMBO J*. (1999) 18:480–9. doi: 10.1093/emboj/18.2.480

Conflict of Interest: The authors declare that the research was conducted in the absence of any commercial or financial relationships that could be construed as a potential conflict of interest.

frontiers in Veterinary Science

ORIGINAL RESEARCH
published: 05 November 2020
doi: 10.3389/fvets.2020.597843

Development of a Monoclonal Antibody Against Porcine CD163 SRCR5 Domain Which Partially Blocks Infection of PRRSV

Yujiao Zhang[1†], Kuan Zhang[1†], Hao Zheng[1,2], Changlong Liu[1], Yifeng Jiang[1], Nannan Du[3], Liwei Li[1], Guoxin Li[1], Lingxue Yu[1], Yanjun Zhou[1,2], Wu Tong[1,2], Kuan Zhao[1], Guangzhi Tong[1,2] and Fei Gao[1,2]*

[1] Department of Swine Infectious Diseases, Shanghai Veterinary Research Institute, Chinese Academy of Agricultural Sciences, Shanghai, China, [2] Jiangsu Co-innovation Center for the Prevention and Control of Important Animal Infectious Disease and Zoonosis, Yangzhou University, Yangzhou, China, [3] College of Animal Science, Fujian Agriculture and Forestry University, Fuzhou, China

OPEN ACCESS

Edited by:
Shao-Lun Zhai,
Guangdong Academy of Agricultural Sciences, China

Reviewed by:
Xiangdong Li,
Yangzhou University, China
Nicolas Bertho,
INRA Biologie, Épidémiologie et Analyse de Risque en santé animale (BIOEPAR), France

***Correspondence:**
Fei Gao
feigao@shvri.ac.cn

[†]These authors have contributed equally to this work

Specialty section:
This article was submitted to Veterinary Infectious Diseases, a section of the journal Frontiers in Veterinary Science

Received: 22 August 2020
Accepted: 13 October 2020
Published: 05 November 2020

Citation:
Zhang Y, Zhang K, Zheng H, Liu C, Jiang Y, Du N, Li L, Li G, Yu L, Zhou Y, Tong W, Zhao K, Tong G and Gao F (2020) Development of a Monoclonal Antibody Against Porcine CD163 SRCR5 Domain Which Partially Blocks Infection of PRRSV. Front. Vet. Sci. 7:597843. doi: 10.3389/fvets.2020.597843

Porcine reproductive and respiratory syndrome virus (PRRSV), which seriously endangers the world pig industry, invades host cells through receptor-mediated endocytosis involving clathrin. CD163 is an essential receptor for PRRSV during its infection of cells. The scavenger receptor cysteine-rich 5 (SRCR5) domain of the CD163 molecule is necessary for PRRSV infection, and interacts with glycoproteins GP2a and GP4 of PRRSV, allowing the virus to infect the host cells. In this study, a monoclonal antibody (mAb) against the SRCR5-6 region of porcine CD163 was developed, and the target epitope of the mAb was determined as ^{497}TWGTVCDSDF^{506}, which is directly adjacent to the ligand-binding pocket (LBP) domain (487-495aa) of CD163. Further study indicated that the mAb could partially block PRRSV infection of its target cells, pulmonary alveolar macrophages. The mAb developed in the study may provide a foundation of antiviral therapy for PRRSV.

Keywords: PRRSV, epitope, SRCR5, CD163, monoclonal antibody

INTRODUCTION

CD163 is a member of the scavenger receptor cysteine-rich (SRCR) family, and is mainly expressed on monocytes, macrophages (1), and specific subsets of dendritic cells (2). CD163, as a receptor that scavenges hemoglobin by mediating the endocytosis of haptoglobin-hemoglobin complexes during haemolysis (3) and also plays a role as an innate bacterial immune sensor, inducing pro-inflammatory cytokine production (4). Soluble CD163 is considered as a marker of macrophage activation and is strongly associated with Human immunodeficiency virus (HIV) and Hepatitis C virus infections (5). The abundance of CD163 is closely related to HIV infection, and the productivity of HIV infection was higher in CD163 abundant cells, whereas a significantly weaker HIV infection was observed in CD163-knocked-down macrophages (6).

The interaction between CD163 and the virus is particularly important, and has been extensively studied in relation to Porcine reproductive and respiratory syndrome virus (PRRSV) (7) and African swine fever virus (8), both of which have devastating impacts on the swine industry.

PRRSV is a major pathogen that seriously harms swine herds, causing immense economic losses to swine industry worldwide. Porcine reproductive and respiratory syndrome is characterized by late-term reproductive failure in sows and severe pneumonia in neonatal pigs. The PRRSV particle is enveloped and the viral genome is a single-stranded positive-sense RNA molecule. Alveolar macrophages (AMs) are the target cells of PRRSV, CD163 on porcine AM membranes has been revealed as an essential receptor mediating infection of PRRSV (9). CD163, occurs specifically on the surfaces of monocytes and macrophages and is a type I transmembrane protein. It has a molecular weight of about 130 kDa. It contains an extracellular region, transmembrane region, and intracellular region. Its extracellular domain contains nine cysteine-rich domains and two proline-serine-threonine-rich (PST) motifs (10). After the transient or stable expression of CD163 molecules, two PRRSV-impermissible cell lines supported both type I and type II PRRSV infections and produced progeny viral particles, indicating that CD163 plays a key role in promoting viral uncoating and the release of genomic RNA into the cytoplasm. During PRRSV infection, CD163 interacts with the glycosylated membrane proteins GP2a and GP4 of PRRSV to facilitate the replication of the virus (7). In the cell, CD163 co-locates with the N protein of PRRSV in early endosomes, but not in late endosomes (11). Further studies showed that the SRCR5 domain of the CD163 extracellular region plays a key role in PRRSV infection, and pig deleted SRCR5 of CD163 can fully resist the infection of PRRSV (12). Ma et al. (13) found that the R561 of CD163 SRCR5 has impact on PRRSV replication. In this study, the extracellular region of CD163 protein, SRCR5-SRCR6 was expressed and purified in a prokaryote and used to immunize BALB/c mice, to prepare a mouse anti-pig CD163 monoclonal antibody (mAb). The epitope ^{497}TWGTVCDSDF^{506} was identified, which is very adjacent to the LBP domain of CD163. The antibody can partly block the replication of PRRSV, confirming the important role of the LBP domain in PRRSV replication, which provides a future research direction for the treatment of PRRSV.

MATERIALS AND METHODS

Ethics Statement

All experimental protocols were conducted in accordance with the Guidelines for the Care and Use of Experimental Animals and approved by the Ethical Committee of the Shanghai Veterinary Research Institute, Chinese Academy of Agricultural Sciences (SHVRI-CAAS) (number SHVRI-SZ-20190602-02).

Cells and Virus

SP2/0 myeloma cells were cultured in Dulbecco's modified Eagle's medium (Gibco) containing 15% fetal bovine serum (FBS). AMs were prepared from the lung lavage fluid of 6-week-old healthy PRRSV-free piglets and cultured in RPMI 1,640 medium (Sigma) containing 10% heat-inactivated FBS at 37°C under 5% CO_2. Highly pathogenic PRRSV (HP-PRRSV) strain HuN4 labeled with EGFP, HuN4-EGFP, was stored in our laboratory, and the characteristics of HuN4-EGFP were consistent with HuN4 (GenBank accession no. EF635006) (14).

Expression and Purification of His-Fused CD163 SRCR5-6 Domain

Primers were designed according to the nucleotide sequence of porcine CD163 (GenBank accession no. EU016226). The SRCR5-6 domain of the CD163 was amplified with the primers and inserted into the vector pCold-I, and the positive plasmid was transformed into *Escherichia coli* BL21(DE)3. An aliquot (0.2 mL) of an overnight *E. coli* culture harboring the plasmid was diluted to 200 mL with Luria-Bertani (LB) broth and incubated until the mid-log phase (optical density [OD] ∼0.5) at 37°C. Protein expression was then induced with IPTG at a final concentration of 1 mM. After incubation at 16°C for 12 h, the cells were harvested by centrifugation and resuspended in 20 mL of lysis buffer (10 mM imidazole, 20 mM sodium phosphate, 0.5 M NaCl, pH 7.4). The cells were sonicated on ice and centrifuged for 10 min at 10,000 rpm/min. The precipitates and supernatants were separately electrophoresed with 12% SDS-PAGE and visualized with Coomassie Brilliant Blue staining. Then wash off the impure protein of the inclusion bodies with buffer I (2 M urea, 0.1% Triton 100, 50 mM NaCl, 0.2 mM EDTA, PBS, PH 7.4) and buffer II (2 M urea, 0.1% Triton100, PBS) for 10 min at 12,000 rpm/min successively, and dissolved the inclusion bodies with 1 mL Elution Buffer (8 M urea, 0.5 M NaCl, 20 mM NaHPO4, 20 mM NaH2PO4). An anti-His mAb was used to verify antigenic specificity of the purified protein by Western blotting.

Mouse Immunization Procedure

Five specific-pathogen-free mice were immunized subcutaneously with 100 ng of purified recombinant His-tagged CD163 SRCR5-6 protein emulsified in complete Freund's adjuvant. The mice were then given three further injections of the antigen mixed with incomplete Freund's adjuvant at 14-day intervals.

mAbs Screening

Splenocytes of an immunized mouse were isolated 2 weeks after the last immunization. The splenocytes were fused with the SP2/0 myeloma cells with polyethylene glycol 1450 (Sigma, USA). The fused cells were cultured in trophoderm-containing hypoxanthine-aminopterin-thymidine (HAT) medium and 15% FBS. The supernatants were collected for an indirect enzyme-linked immunosorbent assay (ELISA) to select positive mAb-producing hybridomas. The positive colonies were then sub-cloned more than three times with a limiting dilution assay. Female BALB/c mice were immunized with the positive clones by intra-peritoneal injection, which pre-injected with pristane to obtain ascites fluid.

Indirect ELISA

Ninety-six-well microplates were coated with 100 ng/well CD163 SRCR5-6 in carbonate coating buffer (pH 9.6) overnight at 4°C. The plates were then washed three times with PBST (1 × PBS, 0.1% Tween 20; 10 min per wash) and blocked with 5% skimmed milk at for 2 h at 37°C. After the plates were washed three times with PBST, 100 μL of the hybridoma supernatant, positive antiserum, or negative antiserum (blank control mouse serum)

was added to each well and incubated for 1 h at 37°C. After the plates were washed with PBST, a 1:10,000 dilution of HRP-conjugated goat anti-mouse IgG antibody in 5% skimmed milk was added to each well and the plates were incubated for 1 h at 37°C. After three washes, 50 μL of 3,3′,5,5′-tetramethylbenzidine (TMB) liquid (Amresco, Solon, Ohio, USA) was added to each well and the plates were incubated for 12 min at room temperature. The reaction was stopped by the addition of 50 μL of 2 M H_2SO_4. The OD values were measured immediately at a wavelength of 450 nm (OD_{450}).

Mapping the B-Cell Epitopes With Monoclonal Antibodies

The CD163 SRCR5 domain and SRCR6 domain are located between amino acids 477–482 of CD163. Sequences encoding CD163 amino acids 477–545, 535–614, and 604–682 were cloned into the pCold-TF vector after amplification with the primers shown in **Table 1**. Then transform these plasmids into BL21 (DE) 3 for expression.

To further map the epitope based on the first mapping results, a series of plasmids was constructed in pCold-TF with the primers shown in **Table 1**. *E. coli* BL21(DE3) cells were then transformed with these plasmids and the encoded peptides expressed. All the samples were separated electrophoretically with 12% SDS-PAGE and incubated with an anti-His antibody or the hybridoma supernatant.

To exactly map the epitope, several peptides were synthesized by Shanghai GL Peptide Ltd. ELISA plates were coated with the synthesized peptides (400 ng/well) in carbonate bicarbonate buffer (15 mM Na_2CO_3, 35 mM $NaHCO_3$, pH 9.6) and incubated overnight at 4°C. The plates were blocked with 5% skim milk in phosphate buffer containing 0.05% Tween 20 for 1 h at 37°C.

After the plates were washed three times, they were incubated at 37°C for 1 h with 100 μL of supernatant from the hybridoma cells or diluted antiserum. The plates were washed three times in PBST and incubated at 37°C for 1 h with HRP-conjugated goat anti-mouse IgG antibody (Proteintech Group, China) diluted 1:10,000 in PBST. The plates were then washed with PBST and incubated with 50 μL/well TMB liquid for 15 min at room temperature in the dark. After the reaction was stopped with 2 M H_2SO_4 (50 μL/well), the results were read as OD450 values (15).

Western Blotting

Cell lysates were prepared with RIPA buffer supplemented with protease inhibitors and phosphatase inhibitors. Equal amounts of cell lysates were fractionated with SDS-PAGE and then blotted onto nitrocellulose membranes. The membranes were blocked for 1 h at room temperature with 5% skim milk and then probed with mAb 1D7 supernatant for 2 h at room temperature. After the membranes were washed with TBST (10 min each), they were incubated with an HRP-conjugated goat anti-mouse antibody (1:6000; Proteintech) for 1 h at room temperature. After the membranes were washed three times, the signals were visualized with an ECL kit (Thermo Fisher) and detected with the Tanon 5200 Chemiluminescent Imaging System.

Identification of mAb Subtype

The supernatants of hybridoma cells were diluted 1:100, according to the introduction of the mouse monoclonal antibody subtype identification kit (Proteintech). The diluted supernatants of hybridoma cells were added to the plate(50 μL/well) and then mixed with 50 μL/well HRP-conjugated goat anti-mouse IgA+IgM+IgG antibodies. The plate was covered with sealing film and incubated for 1 h at room temperature. TMB (100 μL/well) was added to the plate, which was incubated for 10–20 min at room temperature in the dark. Stop solution (100 μL) was added to each well to stop the reaction. The OD_{450} values were then read and recorded.

Virus Blocking Test

Porcine AMs were cultured in a 24-well plate. Each group of cells included three repetitions, and the contents of three wells were mixed for RNA extraction. The AMs of different groups were pre-treated with or without different concentrations of 1D7 ascitic fluids for 2 h at 37°C. The cells were then infected with recombinant HP-PRRSV HuN4-EGFP at a multiplicity of infection (MOI) of 0.005, and incubated for 48 h at 37°C. The supernatants were cast off and the cells washed three times. The RNA was extracted from the cells with the Qiagen RNeasy® Mini Kit (Qiagen) and reverse transcribed into cDNA with TaKaRa PrimeScript RT Master Mix. Absolute quantitative real-time PCRs were performed in triplicate to determine the expression of ORF7 gene on transcription level. And TCID50 were also used to analysis the viral infection and replication.

Statistical Analysis

All results are representative of three independent experiments. Statistical analyses were performed with the GraphPad Prism 5.0 software (GraphPad). Significance was determined with Student's two-tailed *t*-test. Statistical significance: $^{*}p < 0.05$, $^{**}p < 0.01$, $^{***}p < 0.001$.

RESULTS

Preparation of Recombinant Proteins

Full-length CD163 and CD163 SRCR5-6 was amplified from cDNAs of total RNA of porcine AM (**Figure 1A**). However, the protein expression level of full-length CD163 was lower than that of CD163 SRCR5-6 (**Figure 1B**), not enough to generate sufficient antigen to induce a robust immune response. Because CD163 SRCR5 and SRCR6 are relatively conserved and are important for PRRSV infection, a recombinant His-fused CD163 SRCR5-6 protein was successfully expressed in *E. coli* BL21(DE3) cells (**Figure 1B**). The protein was expressed both in the cell supernatant and as inclusion bodies, but the His-fused CD163 SRCR5-6 protein was mainly present as inclusion bodies. The protein was then purified with urea gradient centrifugation. A western blotting analysis showed that the purified His-fused CD163 SRCR5-6 protein was identified by an anti-His mAb (**Figures 1C,D**).

TABLE 1 | Primer for plasmids construction.

Primer[a]	Sequence (5′-3′)[b]
pColdI-477-682aa-F	TCGGTACCCTCGAGGGAATGCCCAGGCTGGTTGGAGGGGAC
pColdI-477-682aa-R	AGCTTGAATTCGGATCTCATGAGCAGATTACAGAGGCCAC
pColdI-51-1116aa-F	CTCGAGGGATCCGAAATGCTGAGGCTAACGGGTGGTG
pColdI-51-1116aa-R	GTCGACAAGCTTGAATTTCATTGTACTTCAGAG
pCold-TF-477-545aa-F	AGGCATATGGAGCTCGGTACCCCCAGGCTGGTTGGAGGG
pCold-TF-477-545aa-R	TTCGGATCCCTCGAGGGTACCTCACTGGAATTCTTCAGCCCAGATC
pCold-TF-535-614aa-F	AGGCATATGGAGCTCGGTACCAGTGGACAGATCTGGGCTGAAG
pCold-TF-535-614aa-R	TTCGGATCCCTCGAGGGTACCTCATTCCATGTCCCAGTGAGAGTTGC
pCold-TF-604-682aa-F	AGGCATATGGAGCTCGGTACCTCCCTCTGCAACTCTCACTGGG
pCold-TF-604-682aa-R	TTCGGATCCCTCGAGGGTACCTCATGAGCAGATTACAGAGGCCACTT
pCold-TF-477-506aa-F	AGGCATATGGAGCTCGGTACCCCCAGGCTGGTTGGAGGG
pCold-TF-477-506aa-R	TTCGGATCCCTCGAGGGTACCTCAGAAGTCAGAATCACAGACGGTGC
pCold-TF-487-516aa-F	AGGCATATGGAGCTCGGTACCTCTGGTCGTGTTGAAGTACAACATG
pCold-TF-487-516aa-R	TTCGGATCCCTCGAGGGTACCTCACCTGCACAGCACGCTGGC
pCold-TF-497-526aa-F	AGGCATATGGAGCTCGGTACCACGTGGGGCACCGTCTGT
pCold-TF-497-526aa-R	TTCGGATCCCTCGAGGGTACCTCAGAGGGAAACCACAGTGCCG
pCold-TF-507-536-aa-F	AGGCATATGGAGCTCGGTACCTCTCTGGAGGCGGCCAGC
pCold-TF-507-536-aa-R	TTCGGATCCCTCGAGGGTACCTCAACTTCCTTCTCCAAAGTGAGCTCC

[a] *F denotes forward PCR primer; R denotes reverse PCR primer.*
[b] *Restriction sites, and homologous arm are underlined.*

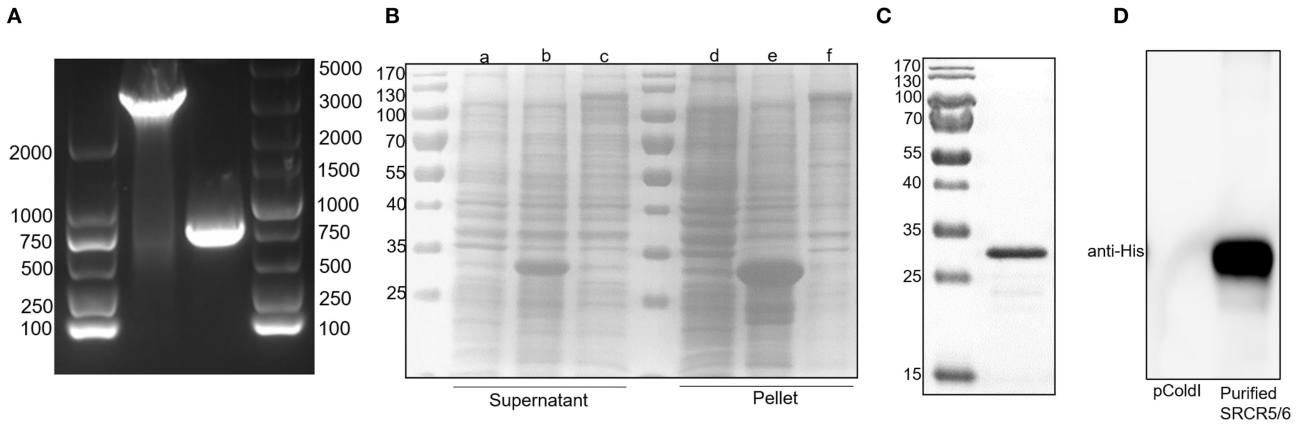

FIGURE 1 | Expression of His-tagged CD163 SRCR5-6 protein and its purification with SDS-PAGE. **(A)** Amplification of CD163 nucleotides 151-3348 and CD163 SRCR5-6. **(B)** Purification of pCold-I-SRCR5-6 with SDS-PAGE. Lanes a-c contain the supernatants of cells expressing pCold-I, pCold-I-SRCR5-6, and pCold-I-CD163, respectively, induced with IPTG, after ultrasonication. Lanes d-f contain the pellets of cells expressing pCold-I, pCold-I-SRCR5-6, and pCold-I-CD163, respectively, induced with IPTG, after ultrasonication. **(C)** Analysis of purified of His-tagged CD163 SRCR5-6 protein with SDS-PAGE. **(D)** Identification of purified His-tagged CD163 SRCR5-6 protein with western blotting.

Development of mAbs Against CD163 SRCR5-6

Five female BALB/c mice were separately immunized with the purified His-fused CD163 SRCR5-6 protein to generate hybridomas producing specific antibodies against CD163 SRCR5-6. A hybridoma clone (1D7) was identified by screening the supernatants with a CD163-SRCR5-6-specific indirect ELISA. CD163 is a molecular marker of macrophage maturation. The expression of CD163 in AMs is relatively high, whereas CD163 is completely absent from PK-15 cells. To verify the specificity of the mAb, the lysis of porcine AMs and PK-15 cells were used in Western Blotting (**Figure 2A**) and an immunofluorescence assay (**Figure 2B**). The results showed that 1D7 only reacted with the lysis of porcine AMs and could be used to detect endogenous CD163. The mAb subtype was then identified with a mouse monoclonal antibody subtypes detection kit (Proteintech). The heavy chain of 1D7 was IgG2a, whereas the light chain was a kappa chain (**Figure 2C**).

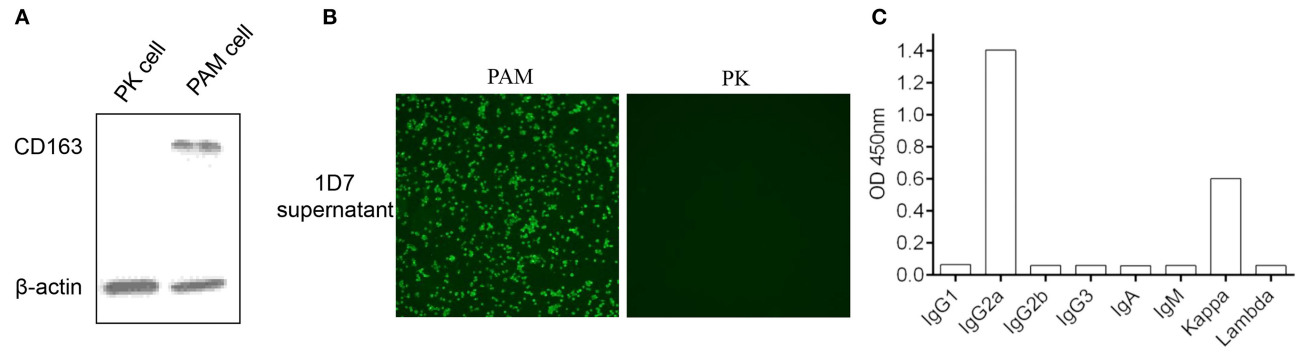

FIGURE 2 | Confirmation of the specificity of mAb 1D7. **(A)**. 1D7 was used for the analysis of endogenous CD163 expression of porcine AMs and PK cells with western blotting. **(B)** Immunofluorescence was used to analysis the specific of 1D7 mAb. **(C)**. Subtype identification of 1D7 with a mouse antibody subtype identification kit.

Epitope Identification of mAb 1D7

To identify the epitope recognized by the mAb, three overlapping fragments (F1, F2, F3) comprising partial length of CD163 SRCR5-6, were cloned into pCold-TF vector and the positive recombinant plasmids were transformed into *E. coli* BL21(DE)3 and induced by IPTG, and analyzed with Western blotting. The results showed that the epitope recognized by 1D7 was located between amino acids 477 and 535 (**Figure 3A**). Another four overlapping TF-tagged peptides (F4, F5, F6, F7) spanning amino acids 477–535 were then expressed. The epitope was within the region defined by amino acids 497–506 (**Figure 3A**). To confirm the minimal linear epitope recognized by 1D7, a series of peptides (P1–P7) spanning amino acids 497–506 of CD163 SRCR5-6 was synthesized by Shanghai GL Peptide Ltd. Based on the results of ELISA, we concluded that the minimal linear epitope recognized by 1D7 is ^{497}TWGTVCDSDF^{506} (**Figure 3B**).

mAb 1D7 Could Partially Block PRRSV Replication

To verify the neutralization activity of 1D7, the recombinant HuN4-EGFP was used. RT-qPCR, $TCID_{50}$ were used to detect the viral infection and replication. The number of ORF7 copies was lower in the infected cells pre-treated with both 1D7 supernatant and ascites fluid than those not treated with 1D7 (**Figures 4A–C**). At higher concentrations of 1D7, the expression of the viral replication was further reduced, indicating a dose-dependent relationship. The repeatability of the experiment was good. The mAb exerted some degree of viral blocking, but the effect was not very marked. We infer that the mAb is directed against the linear epitope ^{497}TWGTVCDSDF^{506}. Its blocking effect on viral infection was limited compared with the effects of polyclonal antibody with conformational epitopes (16).

DISCUSSION

PRRSV is characterized by high antigenic variability, so there is still no effective prevention or control measures for PRRSV infection. Studies of the PRRSV receptors may offer new avenues of research for its prevention and control. Many studies have confirmed that CD163 is an essential receptor for PRRSV on its host cells, and has been shown to interact with PRRSV proteins GP2a and GP4, facilitating the uncoating and release of the viral genome into the cytoplasm at the low pH within the early endosome (7). CD163-knockout pigs were fully resistant to HP-PRRSV (17), and pigs in which the SRCR5 domain of CD163 was deleted fully resisted PRRSV infection, further studies showed that pigs in which a 41-amino-acid fragment (amino acids 481–521) containing the LBP motif (amino acids 487–495) in the SRCR5 domain of CD163 deleted were fully resistant to PRRSV *in vivo* (18). Many researchers have focused on the CD163, indicating that SRCR5 deletion affects the uncoating of PRRSV rather than its entry, and overexpression of ADAM17 can downregulate the expression of CD163 on cell membranes following a reduction in PRRSV infection, while the inhibition of ADAM17 upregulates the membrane CD163 following a promotion in PRRSV infection, and TREM2 can facilitate PRRSV infection via increasing the expression of CD163 and decreases the cleavage of membrane CD163 mediated by ADAM17 (19, 20). However, many aspects of CD163 still require clarification before the role of CD163 in PRRSV replication can be determined.

At present, the mAb most frequently used in molecular research into pig CD163 is anti-CD163 mAb 2A10/11 which targets the SRCR1–3 (21), produced by Bio-Rad Laboratories. Because 2A10/11 can be used for flow cytometry, immunofluorescence, and immunoprecipitation, it has facilitated considerable research. However, clone 2A10/11 only recognizes porcine CD163 under non-reducing conditions when used for western blotting. This may be inconvenient for samples analyzed with western blotting, especially because such samples are so valuable.

In this study, we generated a mAb 1D7 against CD163 that recognizes porcine CD163 under reducing conditions for usage of western blotting. We also identified a new epitope in the CD163 SRCR5 domain (^{497}TWGTVCDSDF^{506}). Because the epitope is close to the LBP domain of CD163, there were fewer viral copies in AMs treated with 1D7 than in AMs treated with SP20 supernatant. Although the blocking effect

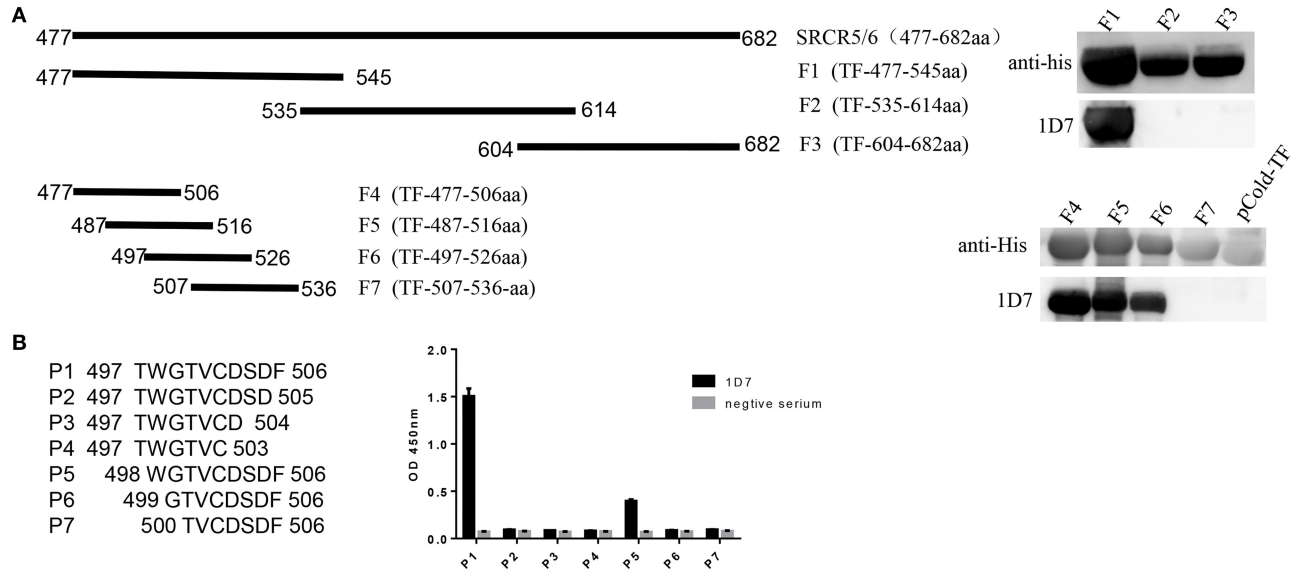

FIGURE 3 | Mapping the epitope of mAb 1D7. **(A)** A series of truncated SRCR5-6 were constructed to pCold-TF and was successfully expressed in *E. coli* BL21(DE3) cells. Protein expression was then induced with IPTG. After incubation at 16°C for 12 h, the cells were harvested for SDS-PAGE. Schematic diagram and western blotting results using 1D7 to probe truncated TF-SRCR5-6. **(B)** A battery of peptides corresponding to amino acids 497–506 were synthesized. Four hundred nano grams peptides were coated to the ELISA plates in order. Indirect ELISA was used to analysis the epitope of 1D7.

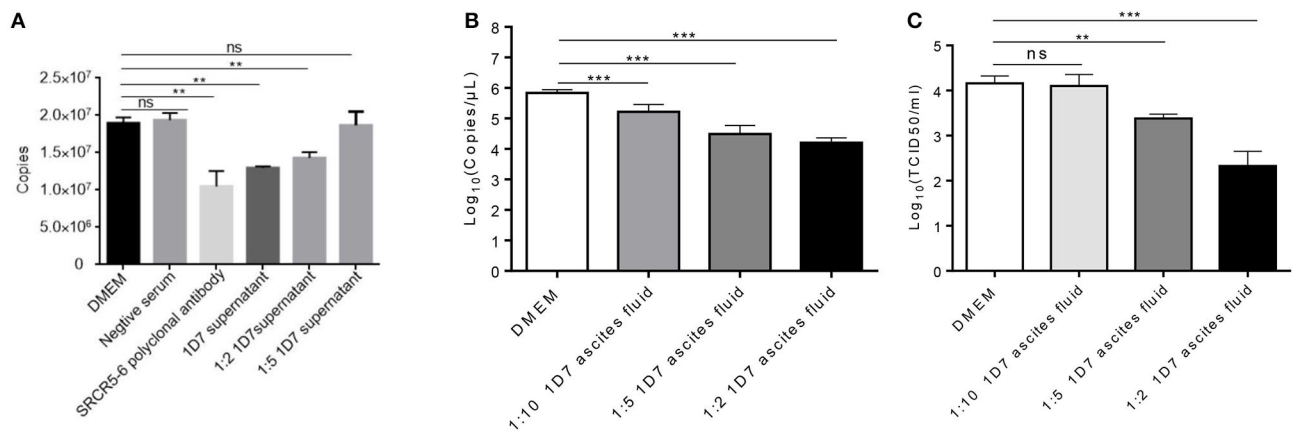

FIGURE 4 | Role of CD163 antibody 1D7 in blocking PRRSV infection. **(A)** Porcine AMs were pre-treated with different doses of 1D7 supernatant before PRRSV infection for 2 h at 37°C. The cells were then infected with HP-PRRSV HuN4, and incubated for 2 h at 37°C. The total RNA of AMs were extracted, and RT-qPCR was used to detect the transcription level of ORF7 mRNA. **(B)** Porcine AMs were pre-treated with different doses of 1D7 ascites fluid for 2 h at 37°C followed by HuN4-EGFP infection at a MOI of 0.005 for 48h at 37°C; the cell supernatants were then collected, and the total RNA of supernatants were extracted according to M&M. RT-qPCR was used to identify viral replication. **(C)** $TCID_{50}$ was also used to identify viral replication. Error bar: mean ± SEM; $^{**}p \leq 0.01$; $^{***}p \leq 0.001$.

of ascites fluid was better than 1D7 supernatant, it was still limited. In a word. 1D7, the anti-CD163 monoclonal antibody provides a foundation for the analysis of other biological functions of CD163, and the blocking effect of the mAb on PRRSV can provide a research idea and future research direction for the treatment of PRRSV. Therefore, the specific antibody directed against the CD163 SRCR5 domain generated in this study provides a tool for functional studies of CD163 and further investigation into the link between CD163 and viral infection.

DATA AVAILABILITY STATEMENT

The raw data supporting the conclusions of this article will be made available by the authors, without undue reservation.

ETHICS STATEMENT

The animal study was reviewed and approved by Laboratory Animal Welfare and Ethics Committee of the Shanghai Veterinary Research Institute-SHVRI-SZ-20190602-02.

AUTHOR CONTRIBUTIONS

FG and YZha: conceptualization, visualization and, wrote–original draft. YZha and KZhan: data curation and formal analysis. FG and GT: funding acquisition, project administration, resources, and supervision. YZha, KZhan, and CL: investigation. YZha, KZhan, HZ, ND, YZho, LY, GL, and WT: methodology. YZha, LL, and YJ: software. YZha, KZhan, WT, and KZhao: validation. YZha, FG, HZ, and KZhan: wrote–review and editing. All authors: have read and agreed to the published version of the manuscript.

FUNDING

We gratefully acknowledge support from the National Natural Science Foundation of China (31670158 and 31702240) and National Key Research and Development Program of China (2016YFE0112500 and 2017YFD0501104).

REFERENCES

1. Buechler C, Ritter M, Orso E, Langmann T, Klucken J, Schmitz G. Regulation of scavenger receptor CD163 expression in human monocytes and macrophages by pro- and antiinflammatory stimuli. *J Leukoc Biol.* (2000) 67:97–103. doi: 10.1002/jlb.67.1.97
2. Maniecki MB, Moller HJ, Moestrup SK, Moller BK. CD163 positive subsets of blood dendritic cells: the scavenging macrophage receptors CD163 and CD91 are coexpressed on human dendritic cells and monocytes. *Immunobiology.* (2006) 211:407–17. doi: 10.1016/j.imbio.2006.05.019
3. Kristiansen M, Graversen JH, Jacobsen C, Sonne O, Hoffman HJ, Law SK, et al. Identification of the haemoglobin scavenger receptor. *Nature.* (2001) 409:198–201. doi: 10.1038/35051594
4. Fabriek BO, van Bruggen R, Deng DM, Ligtenberg AJ, Nazmi K, Schornagel K, et al. The macrophage scavenger receptor CD163 functions as an innate immune sensor for bacteria. *Blood.* (2009) 113:887–92. doi: 10.1182/blood-2008-07-167064
5. Lidofsky A, Holmes JA, Feeney ER, Kruger AJ, Salloum S, Zheng H, et al. Macrophage activation marker soluble CD163 is a dynamic marker of liver fibrogenesis in human immunodeficiency virus/hepatitis C virus coinfection. *J Infect Dis.* (2018) 218:1394–403. doi: 10.1093/infdis/jiy331
6. Tuluc F, Meshki J, Spitsin S, Douglas SD. HIV infection of macrophages is enhanced in the presence of increased expression of CD163 induced by substance P. *J Leukoc Biol.* (2014) 96:143–50. doi: 10.1189/jlb.4AB0813-434RR
7. Das PB, Dinh PX, Ansari IH, de Lima M, Osorio FA, Pattnaik AK. The minor envelope glycoproteins GP2a and GP4 of porcine reproductive and respiratory syndrome virus interact with the receptor CD163. *J Virol.* (2010) 84:1731–40. doi: 10.1128/JVI.01774-09
8. Sanchez-Torres C, Gomez-Puertas P, Gomez-del-Moral M, Alonso F, Escribano JM, Ezquerra A, et al. Expression of porcine CD163 on monocytes/macrophages correlates with permissiveness to African swine fever infection. *Arch Virol.* (2003) 148:2307–23. doi: 10.1007/s00705-003-0188-4
9. Zhang QZ, Yoo DW. PRRS virus receptors and their role for pathogenesis. *Vet Microbiol.* (2015) 177:229–41. doi: 10.1016/j.vetmic.2015.04.002
10. Calvert JG, Slade DE, Shields SL, Jolie R, Mannan RM, Ankenbauer RG, et al. CD163 expression confers susceptibility to porcine reproductive and respiratory syndrome viruses. *J Virol.* (2007) 81:7371–9. doi: 10.1128/JVI.00513-07
11. Van Gorp H, Van Breedam W, Delputte PL, Nauwynck HJ. The porcine reproductive and respiratory syndrome virus requires trafficking through CD163-positive early endosomes, but not late endosomes, for productive infection. *Arch Virol.* (2009) 154:1939–43. doi: 10.1007/s00705-009-0527-1
12. Burkard C, Lillico SG, Reid E, Jackson B, Mileham AJ, Ait-Ali T, et al. Precision engineering for PRRSV resistance in pigs: Macrophages from genome edited pigs lacking CD163 SRCR5 domain are fully resistant to both PRRSV genotypes while maintaining biological function. *PLoS Pathog.* (2017) 13:e1006206. doi: 10.1371/journal.ppat.1006206
13. Ma H, Jiang L, Qiao S, Zhi Y, Chen XX, Yang Y, et al. The crystal structure of the fifth scavenger receptor cysteine-rich domain of porcine CD163 reveals an important residue involved in porcine reproductive and respiratory syndrome virus infection. *J Virol.* (2017) 91:e01897–16. doi: 10.1128/JVI.01897-16
14. Tong GZ, Zhou YJ, Hao XF, Tian ZJ, An TQ, Qiu HJ. Highly pathogenic porcine reproductive and respiratory syndrome, China. *Emerg Infect Dis.* (2007) 13:1434–6. doi: 10.3201/eid1309.070399
15. Kong N, Meng Q, Jiao Y, Wu Y, Zuo Y, Wang H, et al. Identification of a novel B-cell epitope in the spike protein of porcine epidemic diarrhea virus. *Virol J.* (2020) 17:46. doi: 10.1186/s12985-020-01305-1
16. Van Gorp H, Van Breedam W, Delputte PL, Nauwynck HJ. Sialoadhesin and CD163 join forces during entry of the porcine reproductive and respiratory syndrome virus. *J Gen Virol.* (2008) 89(Pt 12):2943–53. doi: 10.1099/vir.0.2008/005009-0
17. Yang H, Zhang J, Zhang X, Shi J, Pan Y, Zhou R, et al. CD163 knockout pigs are fully resistant to highly pathogenic porcine reproductive and respiratory syndrome virus. *Antiviral Res.* (2018) 151:63–70. doi: 10.1016/j.antiviral.2018.01.004
18. Guo C, Wang M, Zhu Z, He S, Liu H, Liu X, et al. Highly efficient generation of pigs harboring a partial deletion of the CD163 SRCR5 domain, which are fully resistant to porcine reproductive and respiratory syndrome virus 2 infection. *Front Immunol.* (2019) 10:1846. doi: 10.3389/fimmu.2019.01846
19. Guo L, Niu J, Yu H, Gu W, Li R, Luo X, et al. Modulation of CD163 expression by metalloprotease ADAM17 regulates porcine reproductive and respiratory syndrome virus entry. *J Virol.* (2014) 88:10448–58. doi: 10.1128/JVI.01117-14
20. Zhu Z, Zhang X, Dong W, Wang X, He S, Zhang H, et al. TREM2 suppresses the proinflammatory response to facilitate PRRSV infection via PI3K/NF-kappaB signaling. *PLoS Pathog.* (2020) 16:e1008543. doi: 10.1371/journal.ppat.1008543
21. Van Gorp H, Van Breedam W, Van Doorsselaere J, Delputte PL, Nauwynck HJ. Identification of the CD163 protein domains involved in infection of the porcine reproductive and respiratory syndrome virus. *J Virol.* (2010) 84:3101–5. doi: 10.1128/JVI.02093-09

Conflict of Interest: The authors declare that the research was conducted in the absence of any commercial or financial relationships that could be construed as a potential conflict of interest.

frontiers in Veterinary Science

REVIEW
published: 26 November 2020
doi: 10.3389/fvets.2020.572425

The Roles of Apoptosis in Swine Response to Viral Infection and Pathogenesis of Swine Enteropathogenic Coronaviruses

Zhichao Xu[1], *Yun Zhang*[1] *and Yongchang Cao*[1,2]*

[1] State Key Laboratory of Biocontrol, School of Life Science, Sun Yat-sen University, Guangzhou, China, [2] Higher Education Mega Center, School of Life Science, Sun Yat-sen University, Guangzhou, China

Apoptosis is a tightly regulated mechanism of cell death that plays important roles in various biological processes including biological evolution, multiple system development, anticancer, and viral infections. Swine enteropathogenic coronaviruses invade and damage villous epithelial cells of the small intestine causing severe diarrhea with high mortality rate in suckling piglets. *Transmissible gastroenteritis virus* (TGEV), *Porcine epidemic diarrhea virus* (PEDV), *Porcine deltacoronavirus* (PDCoV), and *Swine acute diarrhea syndrome coronavirus* (SADS-CoV) are on the top list of commonly-seen swine coronaviruses with a feature of diarrhea, resulting in significant economic losses to the swine industry worldwide. Apoptosis has been shown to be involved in the pathogenesis process of animal virus infectious diseases. Understanding the roles of apoptosis in host responses against swine enteropathogenic coronaviruses infection contribute to disease prevention and control. Here we summarize the recent findings that focus on the apoptosis during swine coronaviruses infection, in particular, TGEV, PEDV, PDCoV, and SADS-CoV.

Keywords: swine enteropathogenic coronaviruses, transmissible gastroenteritis virus, *porcine epidemic diarrhea virus*, *porcine deltacoronavirus*, swine acute diarrhea syndrome coronavirus, swine, apoptosis

OPEN ACCESS

Edited by:
Shao-Lun Zhai,
Guangdong Academy of Agricultural Sciences, China

Reviewed by:
Kwonil Jung,
The Ohio State University, United States
Francisco Rivera-Benítez,
Instituto Nacional de Investigaciones Forestales, Agrícolas y Pecuarias (INIFAP), Mexico

***Correspondence:**
Yongchang Cao
caoych@mail.sysu.edu.cn

Specialty section:
This article was submitted to Veterinary Infectious Diseases, a section of the journal Frontiers in Veterinary Science

Received: *14 June 2020*
Accepted: *28 October 2020*
Published: *26 November 2020*

Citation:
Xu Z, Zhang Y and Cao Y (2020) The Roles of Apoptosis in Swine Response to Viral Infection and Pathogenesis of Swine Enteropathogenic Coronaviruses. Front. Vet. Sci. 7:572425. doi: 10.3389/fvets.2020.572425

INTRODUCTION

Apoptosis, also known as programmed cell death, is a ubiquitous mode of cell death known to be responsible for clearance of unwanted, injured, or virus-infected cells (1, 2). Cells undergoing apoptosis are accompanied by characteristic morphological changes, including cell shrinkage and deformation, chromatin condensation, nuclear fragmentation, and plasma membrane blebbing, which forms the apoptotic body containing the fragments of nucleus or cytoplasm (3). Cell apoptosis is an active process, which involves a series of genes activation and expression, various proteins regulation. To date, it was reported that there are two main apoptotic pathways: the extrinsic/death receptor pathway (4) and the intrinsic/mitochondrial pathway (5). Death receptors belong to the tumor necrosis factor receptor (TNFR) superfamily (6). Members of the TNFR family are type I membrane surface receptors, which include the Fatty acid synthetase receptor (FasR), TNFR, Death receptor (DR)3, DR4, DR5, etc. (7–11). Their ligands belong to type II membrane proteins, which include Fatty acid synthetase ligand (FasL), TNF-α Apo3 ligand (Apo3L), Apo2 ligand (Apo2L), etc. (7–11). Upon death receptor-ligand binding, the adapter protein Fas-associated death domain (FADD) is recruited by death domain, then

associates with pro-cysteinyl aspartic acid protease (caspase)-8 *via* dimerization of the death effector domain and a death-inducing signaling complex (DISC) is formed to activate caspase-8, then caspase-8 results in the caspase-3 activation (12–14). Once caspase-3 is activated, the execution phase of apoptosis is triggered (12–14). The mitochondrial pathways involve some chemical or physical stimulus factors leading to change of the permeability of mitochondrial membrane, resulting in release of the cytochrome *c* (cyt *c*) or other apoptotic molecules into the cytoplasm cavity and activation of downstream caspases to initiate apoptosis (15, 16). In addition, T-cell mediated cytotoxicity involved with perforin-granzyme to kill target cells is known as another apoptotic pathway (17).

It is known that many viruses can evolve various sophisticated strategies to modulate apoptosis as a critical armament to complete their replication cycle (18), reflected in the relationship between viral infection and cell apoptosis is bidirectional. Viruses could hijack host's apoptotic pathway to delay apoptotic response, providing sufficient time for maximizing progeny virus production (19). On the other hand, viruses could induce apoptosis to enable the release and dissemination of viral progeny for further invasion to the neighboring cells at the late stages of viral infection (18).

Porcine coronaviruses (CoVs) are significant enteric and respiratory pathogens of swine. Six porcine CoVs have so far been identified: *transmissible gastroenteritis virus* (TGEV) (20), *porcine respiratory coronavirus* (PRCV) (21), *porcine epidemic diarrhea virus* (PEDV) (22), and *swine acute diarrhea syndrome coronavirus* (SADS-CoV) (23) in the *Alphacoronavirus* genus; porcine hemagglutinating encephalomyelitis virus (PHEV) (24) in the *Betacoronavirus* genus; *porcine deltacoronavirus* (PDCoV) (25) in the *Deltacoronavirus* genus. The clinical signs of swine enteropathogenic CoVs including TGEV, PEDV, PDCoV, and SADS-CoV are characterized by severe watery diarrhea with subsequent dehydration in pigs of all ages, and a high mortality rate in suckling piglets (26–29). The molecular surveillance studies indicated that swine enteropathogenic CoVs were common viral pathogen of pigs around the world (30–44) (**Figure 1**). In addition, co-infections of these diarrhea-associated viruses were commonly found in pig farms (45). For swine enteropathogenic CoVs infection prevention, the administration of vaccines and antiviral drugs are important tool. Currently a number of vaccines and antiviral drugs, such as killed, live-attenuated vaccine, shRNA expression vector are widely used to prevent swine enteropathogenic CoVs infection (46–49). However, it still can not stop the swine enteropathogenic CoVs outbreak, due to they are not optimal in terms of safety and efficacy, and large-scale infections still occur, resulting in the death of large numbers of piglets, causing huge economic losses to the pig industry (23, 50–52), indicating that a deeper understanding of the pathogenesis of swine enteropathogenic CoVs is needed to develop more effective prevention and control measures.

Although swine enteropathogenic CoVs might infect multiple organs in pigs, the intestinal tract is the major target organ, where virus replication is limited to intestinal villus epitheial cells (29,

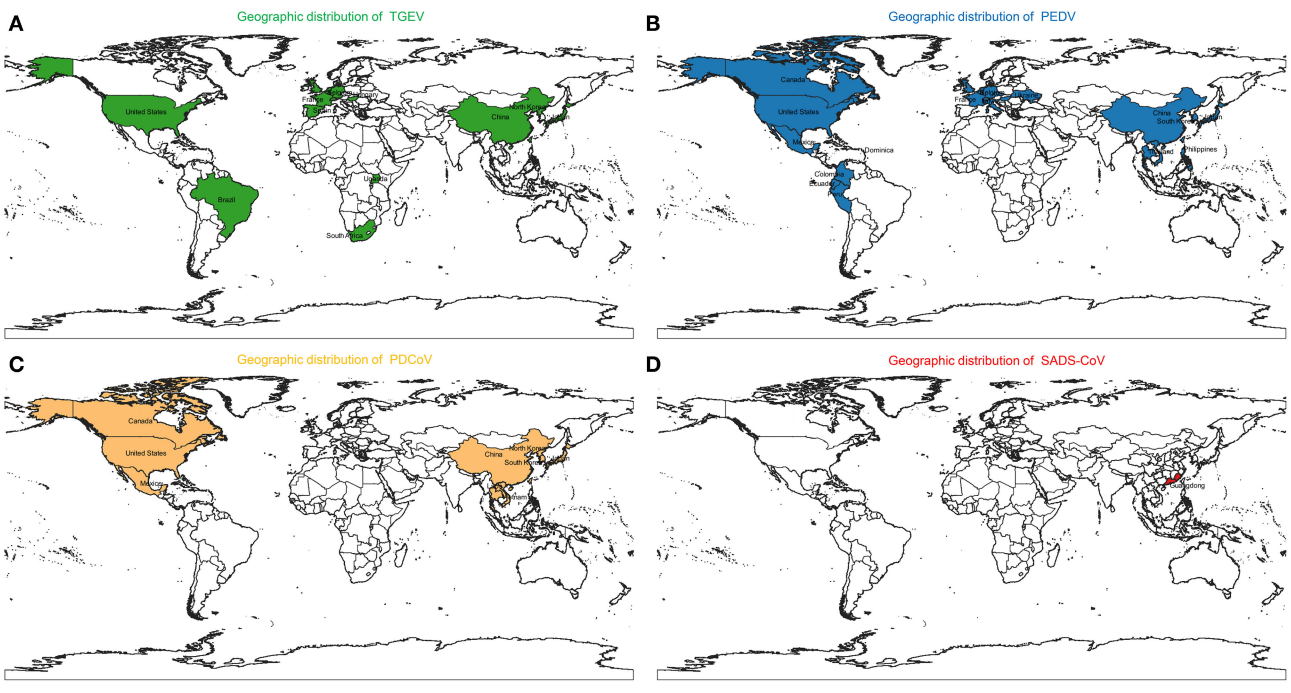

FIGURE 1 | Geographic distribution of **(A)** *Transmissible gastroenteritis virus* (TGEV), **(B)** *Porcine epidemic diarrhea virus* (PEDV), **(C)** *Porcine deltacoronavirus* (PDCoV), and **(D)** *Swine acute diarrhea syndrome coronavirus* (SADS-CoV).

TABLE 1 | Compare apoptotic cell death caused by the four swine enteropathogenic CoVs and the related mechanisms.

Virus	Genomic organization	Cell lines used in apoptotic studies	Virus-related apoptotic cell death occurs *in vitro* or *in vivo*	Apoptotic pathway	Apoptosis involved molecules	Contribution of apoptosis to virus replication	References
TGEV	5′ UTR-ORF1a/1b-S-3a-3b-E-M-N-7-3′ UTR	PK-15, IPEC-J2, HRT18, ST cells	*In vitro*	Extrinsic and intrinsic	miR-27b, RUNX1, Bax, Caspase 3/8/9, DJ-1, AIF, p53, ROS, FasL, Bax, PARP, p53, AIF	No effect	(54, 61, 74–82)
PEDV	5′ UTR-ORF1a/1b-ORF2-ORF3-ORF4-ORF5-ORF6-3′ UTR	IECs, Vero, Marc-145 cells	*In vitro* and *in vivo*	Extrinsic and intrinsic	Caspase 3/8, AIFM1, PARP, p53, ROS, AIF	Facilitate	(18, 53, 83–85)
PDCoV	5′ UTR-ORF1a/1b-S-E-M-ns6-N-ns7 3′ UTR	LLC-PK, ST cells	*In vitro*	Intrinsic	Bax, Caspase3/9, Cyt *c*, PARP	Facilitate	(86–89)
SADS-CoV	5′ UTR-ORF1a/1b-S-NS3-E-M-N-NS7a-3′ UTR	Vero, IPI-2I cells	*In vitro*	Extrinsic and intrinsic	Fas, Caspase3/8/9, Bax, Cyt *c*, PARP	Facilitate	(23, 90)

53). Diarrhea caused by pathogen infection associates with viral damage to intestinal epithelial cells, which plays an important role in the nutrition absorption (54), causes a breach of mucosal physical barriers and reduction of enzyme activities, leading to electrolyte imbalances, nutrient decomposition and absorption anomalies (53, 55). It has been reported that apoptosis, which occurs in the infection course of many CoVs (56, 57), is involved in viral pathogenesis and disease processes that promote cell death and tissue injury (58, 59). In this review, the roles of apoptosis in the pathogenesis and control of TGEV, PEDV, PDCoV, and SADS-CoV will be discussed, which may provide some clues to further understandings of pathogenesis of swine enteropathogenic CoVs.

APOPTOSIS ASSOCIATED WITH *TRANSMISSIBLE GASTROENTERITIS VIRUS* (TGEV)

Virus Characteristics of TGEV

TGEV is an enveloped, single-stranded, positive-sense RNA virus with a genome of appropriately 28 kb in length (20, 60). The full-length genome of TGEV is arranged in the order of: 5′ UTR-ORF1a/1b-S-3a-3b-E-M-N-7-3′ UTR, containing nine open reading frames (ORFs) encoding four structure proteins (S, M, N, E) and five non-structure proteins (61). The nsp1 protein of TGEV can efficiently suppress protein synthesis in mammalian (62). The nsp3 protein of TGEV can cleave a peptide mimicking the cognate nsp2|nsp3 cleavage site based on its papain-like protease 1 (PL1(pro)) domain (63). The N protein of TGEV belongs to a multifunctional phosphoprotein, which can package the RNA genome into a helical ribonucleoprotein, regulate viral RNA synthesis, and modulate of host cell metabolism (64). E protein promotes TGEV maturation in the secretory pathway (65). S1 and M proteins play a role in viral replication (66, 67). In addition, M protein can affect TGEV-induced IFN-α production (68).

The Role of Apoptosis in TGEV Infection

It was reported that TGEV invades and replicates in villous epithelial cells to provoke villous atrophy, causing severe diarrhea, and dehydration in piglets is the central event in the pathogenesis of TGEV infection (69, 70). Apoptosis plays a important role in the pathogenesis process of animal virus infectious diseases (71–73). Many studies shown that TGEV infection could induce apoptosis in PK-15 cells, swine testicular (ST) cells, swine kidney cells, MDCK-APN cells (canine kidney cell line expressing porcine APN) or human rectal tumor cells (HRT18, expressing porcine APN) (**Table 1**) (74–82, 91), which associates with intracellular molecules, such as p53, reactive oxygen species (ROS), mitochondrial apoptosis-inducing factor (AIF), poly (ADP-ribose) polymerase (PARP), and caspases (74, 82). Interestingly, TGEV may not induce apoptotic death of intestinal villous enterocytes *in vivo* (77). TGEV infection could decrease p300/CBP, down-regulate MDM2, and promote p53 phosphorylation at serine 15, 20, and 46, resulting in accumulation and activation of p53, then p53 induced ROS accumulation which leads to mitochondrial oxidative damage to release cyt *c* to the cytosol and thereby activate apoptosis in PK-15 cells (79, 91). In addition, TGEV infection up-regulated FasL to activate caspase-8 and cleaved Bid to tBid which was transferred to the mitochondria, resulting in release of cyt *c* into the cytoplasm to activate caspase-9 (78). Moreover, TGEV could down-regulate Bcl-2, increase the expression of Bax, and promote the transfer of Bax from cytoplasm

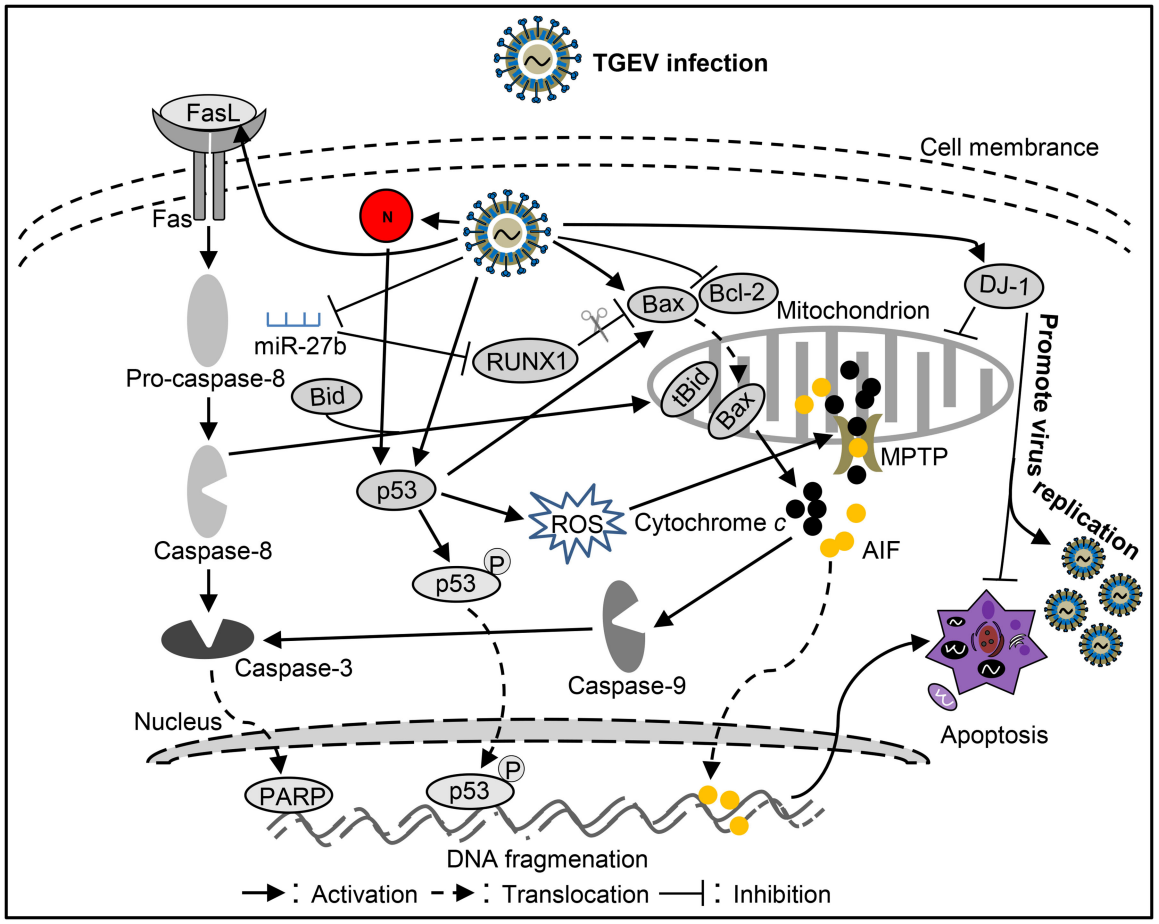

FIGURE 2 | Diagram of the roles of apoptosis in the pathogenesis of *Transmissible gastroenteritis virus* (TGEV) infection.

to mitochondria (78). Then, mitochondria released cyt *c* to activate caspase-9, and finally caspase-9 activates caspase-3 to induce cell apoptosis (78). microRNAs (miRNAs) play a key role in the regulation of virus-induced apoptosis (80). For instance, miR-27b can directly target the 3′ UTR of runt-related transcription factor 1 (RUNX1) mRNA to regulate the expression of RUNX1 in PK-15 cells (80). It has been found that TGEV infection can down-regulate the expression of miR-27b in host cells, thereby down-regulating the expression of RUNX1 and activating the Bax regulated expression of caspase-9/3 to induce cell apoptosis (80). These results suggest that TGEV can induce apoptosis through both extrinsic and intrinsic pathways (**Figure 2**) in PK-15 cells. Further analysis of the key viral proteins induced by TGEV showed that N protein could activate p53, p21 to eliminate cyclin B/cdc2, promote the transfer of Bax to mitochondria, lead to the release of cyt *c* from mitochondria, and activate caspase-9/3 to induce cell apoptosis (81) (**Figure 2**). Interestingly, N protein was cleaved at the position of VVPD359 by activated caspase-6/7 during TGEV-induced apoptosis (76) in human rectal tumor cell line, indicating that N protein plays a very important role in the interaction between virus and host during apoptotic process. It is well-known that viruses could manipulate apoptosis to complete their life cycle. It was reported that mitophagy induced by DJ-1 to counteract apoptosis could promote viral infection during TGEV infection (54) (**Figure 2**). The above studies confirmed that there may be a certain correlation between pathogenicity and apoptosis after TGEV infection. More research is needed on how apoptosis affects the proliferation and spread of TGEV during viral infection.

APOPTOSIS ASSOCIATED WITH *PORCINE EPIDEMIC DIARRHEA VIRUS* (PEDV)

Virus Characteristics of PEDV

PEDV is an enveloped, single-stranded, positive-sense RNA virus with a genome of appropriately 28 kb in length (22). The viral genome is sequentially composed of 5′ untranslated region (UTR), open reading frame 1a/1b (ORF1a/1b), ORF2-6, and 3′ UTR (84). The ORF 1a/1b cover the 5′-proximal two-thirds of the genome coding for replicase polyprotein (pp) la and

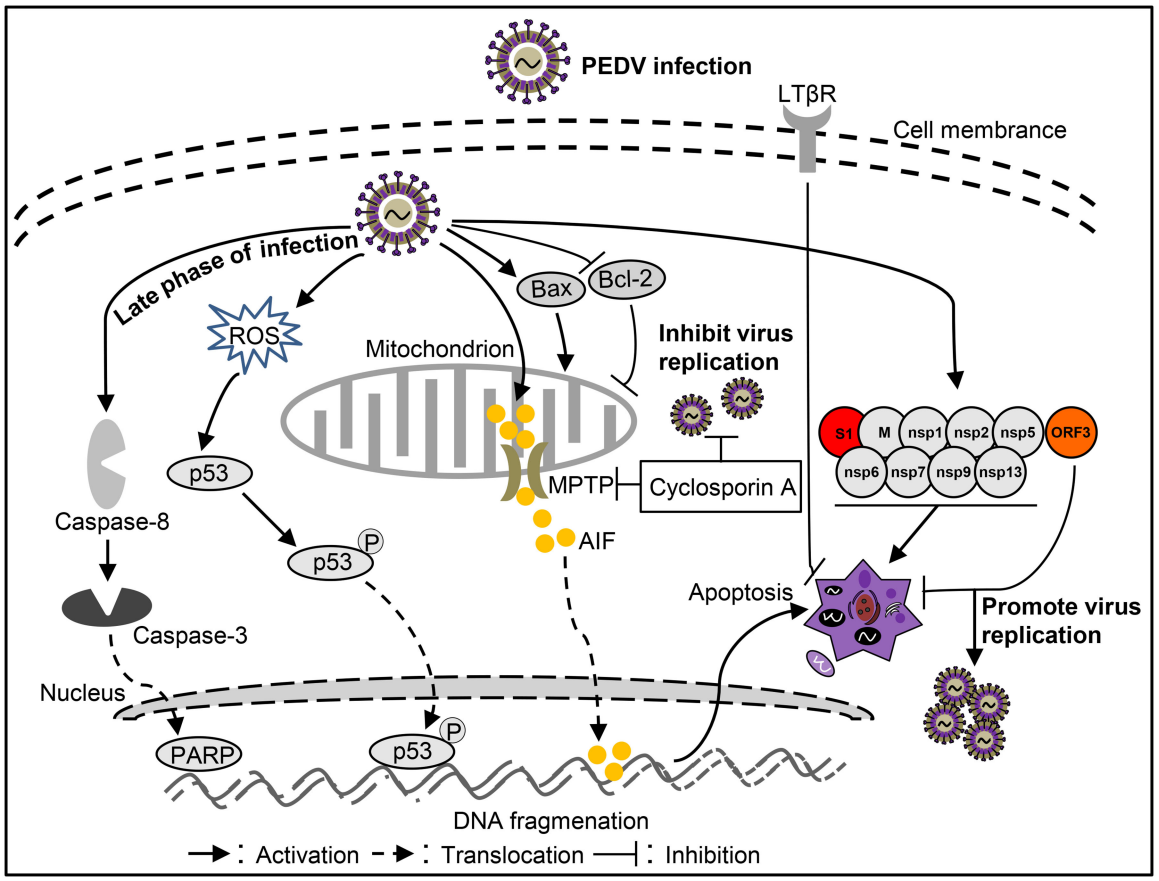

FIGURE 3 | Diagram of the roles of apoptosis in the pathogenesis of *Porcine epidemic diarrhea virus* (PEDV) infection.

pp1ab, respectively (84, 92). These pp1a and pp1ab polyproteins can be cleaved by internal proteases generating sixteen non-structural proteins, namely nsp1-16 (85). Moreover, the genome of PEDV encodes four structural proteins including the spike (S), envelope (E), membrane (M), and nucleocapsid (N) proteins, while ORF3 encodes an accessory protein (84). The functional form of the S protein is a trimer, which protrude from the viral membrane thus providing typical crown appearance of the CoVs (93). It functions during cell entry by binding to cellular receptors and causing fusion of the viral and host cell membranes (93). During maturation, the S protein is cleaved into a receptor-binding subunit S1 and a membrane-fusion subunit S2 (84). The E protein has ion channel activity and plays an important role in virion morphogenesis (93, 94). The M protein is the main component of the viral envelope and interacts with all structural components during viral particle assembly (93). The N protein packages the genomic RNA to form the helical nucleocapsid (RNP) (93). ORF3 protein was known to be related to PEDV pathogenicity (93). In addition, N and ORF3 are involved in viral replication (95, 96). Furthermore, the encoded N, M, E, ORF3, PLP2, nsp 1, nsp 3, nsp 5, nsp 7, nsp 14, nsp 15, nsp 16 proteins can antagonize Interferon-β production (97–100).

The Role of Apoptosis in PEDV Infection

PEDV infection can damages pig intestinal epithelial tissue and interfere with epithelial mucosal cell function, resulting in abnormal nutrient absorption and diarrhea (53). This phenomenon may be related to apoptosis caused by PEDV infection. Apoptosis of cells in the lamina propria or submucosa of PEDV-infected jejunum or ileum was increased (18, 101). However, PEDV may not induce apoptosis death of intestinal villous enterocytes *in vivo* (50), like TGEV and PDCoV. AIF could translocate to the nucleus to cause apoptosis after PEDV infection in Vero cells (18). Moreover, PEDV could promote p53 phosphorylation at serine 20 and subsequent translocation to the nucleus, leading to p53 activation and thereby apoptosis in Vero cells (83). During this process, ROS also accumulates to promote apoptosis (83). In addition, apoptosis was mediated by activation of caspase-8 and caspase-3 in the late stage of PEDV-infected Vero cells (102). Treatment with the inhibitor of pro-apoptotic molecule could significantly inhibit PEDV infection (18), indicating that apoptosis plays an important role in the PEDV pathogenicity. However, the host cells showed an anti-apoptotic effect through LTBR during PEDV infection (103). By analysis cell apoptosis induced by PEDV-related viral proteins, it was found that M, nsp1, nsp2, nsp5, nsp6, nsp7, nsp9, nsp13,

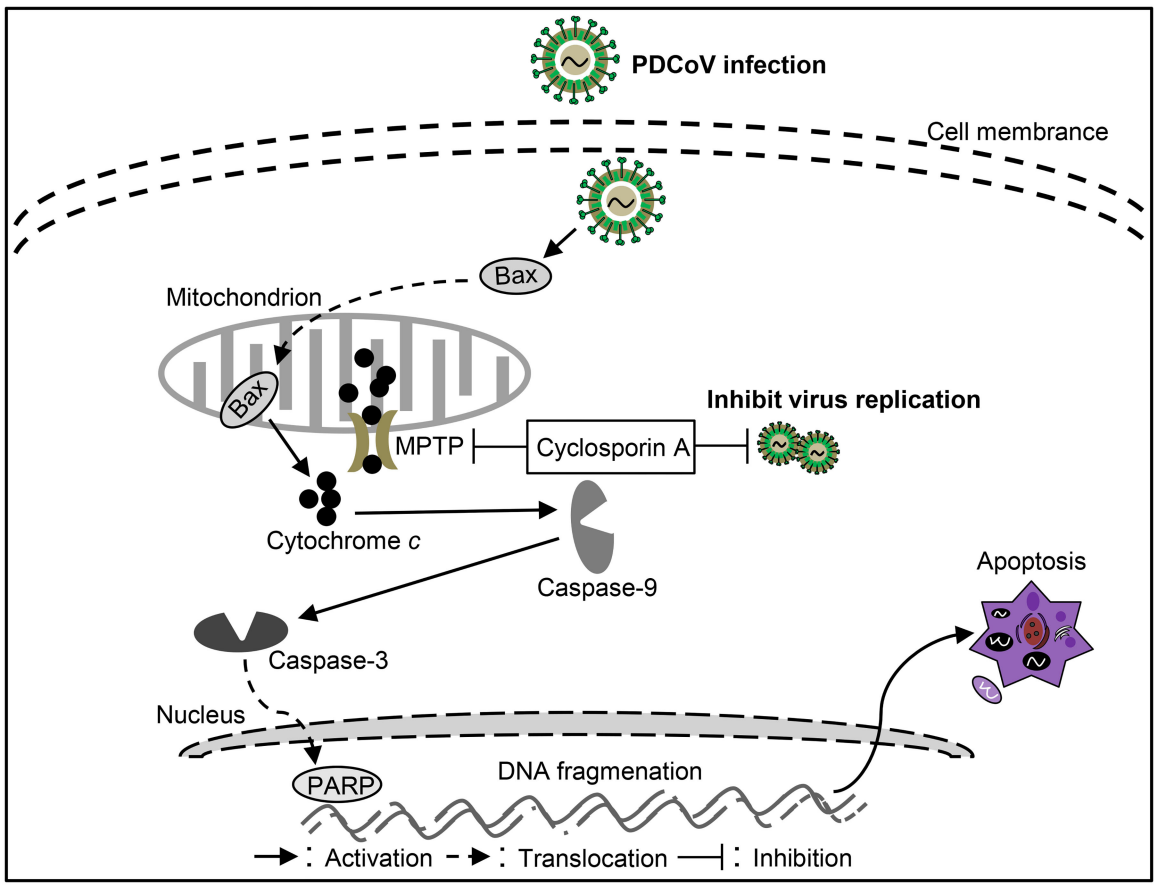

FIGURE 4 | Diagram of the roles of apoptosis in the pathogenesis of *Porcine deltacoronavirus* (PDCoV) infection.

and S1 proteins can induce apoptosis, among which S1 is the critical apoptotic-inducing protein in Vero cells, but the detailed molecular mechanism is still unclear (85). On the contrary, PEDV encoded ORF3 could inhibit cell apoptosis to promote virus proliferation (93), indicating that PEDV applies different strategies to regulate cell apoptosis in different stages of infection to complete viral proliferation. Although some studies have been conducted on the influence of PEDV on apoptosis (**Figure 3**), many questions remain unclear, such as how does S1 induce apoptosis? And what role does S1 portein induced-apoptosis play in virus-caused diarrhea? Clarifying these issues will help explain how PEDV causes diarrhea in pigs.

APOPTOSIS ASSOCIATED WITH *PORCINE DELTACORONAVIRUS* (PDCoV)

Virus Characteristics of PDCoV

PDCoV is an enveloped, single-stranded, positive-sense RNA virus with a genome of appropriately 25 kb in length (26). The genome organization of PDCoV are in the order of: 5′ untranslated region (UTR), open reading frame 1a/1b (ORF1a/1b), spike (S), envelope (E), membrane (M), non-structural protein 6 (ns6), nucleocapsid (N), non-structural protein 7 (ns7), and 3′ UTR (86, 87). The diverse dimerization forms of nsp9 protein could enhance their nucleic acid binding affinity (104). ns6 protein is an important virulence factor of PDCoV (105). It is known that N, nsp5, nsp15, ns6 contribute to inhibit interferon-β production (106–109).

The Role of Apoptosis in PDCoV Infection

PDCoV is a newly discovered virus that causes severe clinical diarrhea and intestinal pathological damage in piglets (88), but the pathogenesis of PDCoV infection is still largely unknown. Current studies showed that PDCoV infection could promote Bax translocation and mediate mitochondrial outer membrane permeabilization (MOMP), resulting in specific relocation of the mitochondrial cyt *c* into the cytoplasm, thus activating caspase-9/3 to initiate apoptosis in ST cells (88). These results indicate that PDCoV mediates cell apoptosis through a caspase-dependent endogenous apoptotic pathway (**Figure 4**). Moreover, apoptosis caused by PDCoV contributes to viral protein translation and the caspase-dependent intrinsic apoptosis pathway in PDCoV-infected ST cells is also used for facilitation of viral replication (88). Interestingly, PDCoV induces apoptosis in swine testicular and LLC porcine kidney cell lines *in vitro* but not in infected intestinal enterocytes *in vivo*. Another form of cell death,

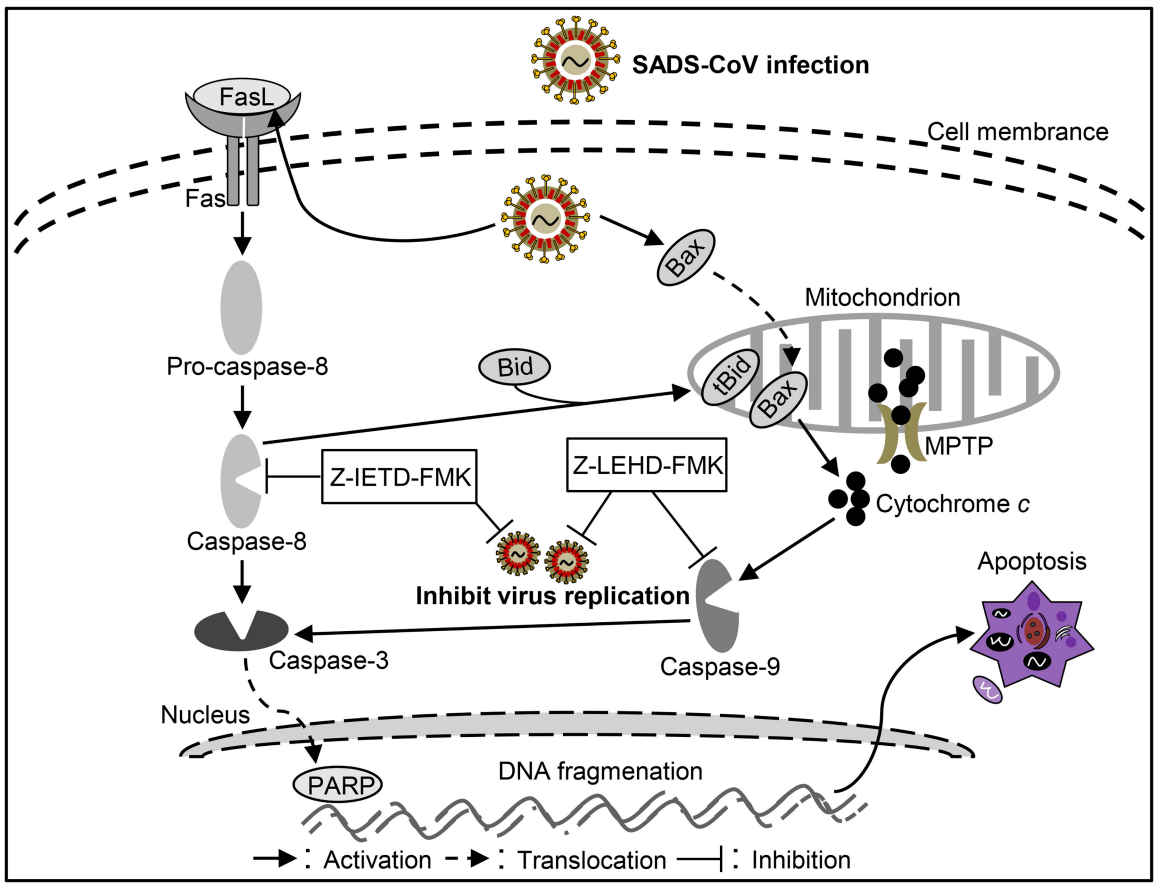

FIGURE 5 | Diagram of the roles of apoptosis in the pathogenesis of *Swine acute diarrhea syndrome coronavirus* (SADS-CoV) infection.

necrosis, has been found in PDCoV-infected swine intestinal enterocytes as well as in the porcine small intestinal epithelial cell line, IPEC-J2 *in vitro* (89). The above results indicate that a better model of cellular infection is needed to reflect the infection *in vivo*. In-depth study on the molecular mechanism of cell death caused by PDCoV infection will help to analyze the pathogenesis of PDCoV. In addition, the key proteins responsible for cell death caused by the virus still need to be further studied, which will help to identify virulence factors and provide guidance for prevention and control PDCoV infection.

APOPTOSIS ASSOCIATED WITH *SWINE ACUTE DIARRHEA SYNDROME CORONAVIRUS* (SADS-CoV)

Virus Characteristics of SADS-CoV

SADS-CoV, also named PEAV (110) and SeACoV (111), is an enveloped, single-stranded positive-sence RNA virus (110). The full-length genome of SADS-CoV is about 27 kb (110), arranged in the order of: 5′ UTR-ORF1a/1b-S-NS3-E-M-N-NS7a-3′ UTR (112). It is known that the S protein has many important characteristics in CoVs, such as virus attachment and entry, and induction of neutralizing antibodies *in vivo* (113). Of note, compare to other reported CoVs, SADS-CoV has the smallest S protein including 1,129 amino acids (110). To date, the papain-like protease 2 (PLP2) domain of nsp3 was shown to be able to cleave nsp1 proteins and also peptides mimicking the nsp2/nsp3 cleavage site and also have deubiquitinating and deISGynating activity (114). The function of other viral proteins of SADS-CoV remains to be further explored.

The Role of Apoptosis in SADS-CoV Infection

As another newly identified swine intestine CoV, detail information of the pathogenic mechanism of SADS-CoV remains unclear. It was reported that SADS-CoV infection could increased apoptosis in the small intestinal epithelial cell line IEC *in vitro* (90). SADS-CoV infection could up-regulate FasL, subsequentially activates caspase-8/3 to lead to apoptosis in Vero and IPI-2I cells (90). Moreover, activated caspase-8 could cleave Bid, then the cleaved Bid translocated to mitochondria participating in the destruction of mitochondria integrity and cyt *c* release to cytosol, which in turn facilitates caspase-9/3 activation thus result in apoptosis (90). In addition, SADS-CoV infection triggers Bax recruitment into the mitochondria, leading

to cyt *c* but not AIF release into cytoplasm to induce apoptosis through mitochondrial permeability transition pore (MPTP), which involve with cyclophilin D (CypD) in these processes (90). These results suggest SADS-CoV-induced apoptosis were mediated by both extrinsic and intrinsic pathways (**Figure 5**). The viral replication was affected with the inhibitors of caspase-8 or capases-9, indicating that SADS-CoV-induced apoptosis contributes to viral replication (90). Although it has been demonstrated well in SADS-CoV induced apoptosis, the function of viral protein in SADS-CoV-induced apoptosis and the exact mechanism underlying remains unclear. More efforts to elucidate the molecular mechanisms of SADS-CoV-induced apoptosis will help to explore the pathogenesis of SADS-CoV infection.

OTHER MECHANISMS ARE RELATED TO THE PATHOGENESIS OF SWINE ENTEROPATHOGENIC CoVs

Innate immunity is thought to be the first line of host defense against a wide variety of pathogenic infections (115). Of note, type I interferon (IFN-α/β), as important cytokines of innate immunity induced by virus invasion, could establish an anti-viral state in infected sites (116). In order to infect the organism and cause pathogenicity, the virus must break through the anti-viral state of the organism. It was reported that PEDV, PDCoV and SADS-CoV can inhibit the up-regulated expression of type I interferon through a variety of different mechanisms (100, 115, 117–120), thus leading to virus infection, indicating that the inhibition of type I interferon might relate to the pathogenesis of these viruses. In addition, inhibition of anti-viral status to promote viral infection might contribute to the occurrence of apoptosis (121). Interestingly, unlike PEDV, PDCoV, and SADS-CoV, TGEV infects the body can promote the up-regulated expression of IFN-β (122). IFN-β has been reported to induce apoptosis (123, 124). Whether the apoptosis induced by TGEV is related to the upregulation of IFN-β needs further study.

CONCLUSIONS

Lines of evidence indicate that apoptosis play critical roles in the pathogenesis of swine enteropathogenic CoVs. Most of the information is gleaned from the studies on the apoptosis of TGEV, PEDV, PDCoV, or SADS-CoV infections *in vitro* and *in vivo*. Viral proteins, such as N from TGEV, S1 from PEDV, are involved in regulation of virus-mediated apoptosis production, which might provide some clues to determine the virulence factors and serve as the targets of antiviral drugs. However, the roles of apoptosis in host response to swine enteropathogenic CoVs infection alone or co-infections are still far from elucidation and need to be further investigated. In addition, the apoptotic forms and mechanisms caused by these four swine enteropathogenic CoVs are different (**Table 1**), which whether involved with the differences of pathogenicity also needs further study. In brief, further investigation into the role of apoptosis in these swine enteropathogenic CoVs is conducive to elucidate of the pathogenesis of viral infections and develop an appropriate strategy for the prevention and control of swine diarrhea diseases.

AUTHOR CONTRIBUTIONS

ZX collected the data and wrote the paper. YZ revised the paper. YC checked and finalized the manuscript. All authors read and approved the final manuscript.

FUNDING

This work was supported by grants from the National Natural Science Foundation of China (#31902248), Doctoral Initiative Project of Natural Science Foundation of Guangdong Province (#2018A030310158) and Guangdong Basic and Applied Basic Research Foundation (#2019B1515210026).

REFERENCES

1. Bortner CD, Cidlowski JA. Cellular mechanism for the repression of apoptosis. *Annual Rev Pharmacol Toxicol.* (2002) 42:259–81. doi: 10.1146/annurev.pharmtox.42.083101.143836
2. Pandya NM, Jain SM, Santani DD. Apoptosis: a friend or foe? *Transplant Proc.* (2006) 33:2414–6. doi: 10.1016/S0041-1345(01)02057-7
3. Kroemer G, El-Deiry WS, Golstein P, Peter ME, Vaux D, Vandenabeele P, et al. Classification of cell death: recommendations of the nomenclature committee on cell death. *Cell Death Differ.* (2005) 12:1463–7. doi: 10.1038/sj.cdd.4401724
4. Schmitz I, Kirchhoff S, Krammer PH. Regulation of death receptor-mediated apoptosis pathways. *Int J Biochem Cell Biol.* (2000) 32:1123–36. doi: 10.1016/S1357-2725(00)00048-0
5. Gibson CJ, Davids MS. BCL-2 antagonism to target the intrinsic mitochondrial pathway of apoptosis. *Clin Cancer Res.* (2015) 21:5021–9. doi: 10.1158/1078-0432.CCR-15-0364
6. Jeong M, Lee EW, Seong D, Seo J, Kim JH, Grootjans S. USP8 suppresses death receptor-mediated apoptosis by enhancing FLIPL stability. *Oncogene*. (2017) 36:458–70. doi: 10.1038/onc.2016.215
7. Chicheportiche Y, Bourdon PR, Xu H, Hsu YM, Scott H, Hession C, et al. TWEAK, a new secreted ligand in the tumor necrosis factor family that weakly induces apoptosis. *J Biol Chem.* (1997) 272:32401–10. doi: 10.1074/jbc.272.51.32401
8. Ashkenazi A, Dixit VM. Death receptors: signaling and modulation. *Science.* (1998) 281:1305–8. doi: 10.1126/science.281.5381.1305
9. Peter ME, Krammer PH. Mechanisms of CD95 (APO-1/Fas)-mediated apoptosis. *Curr Opin Immunol.* (1998) 10:545–51. doi: 10.1016/S0952-7915(98)80222-7
10. Suliman ALA, Datta R, Srivastava RK. Intracellular mechanisms of TRAIL: apoptosis through mitochondrial-dependent and -independent pathways. *Oncogene.* (2001) 20:2122–33. doi: 10.1038/sj.onc.1204282
11. Rubio-Moscardo F, Blesa D, Mestre C, Siebert R, Balasas T, Benito A, et al. Characterization of 8p21.3 chromosomal deletions in B-cell lymphoma: TRAIL-R1 and TRAIL-R2 as candidate dosage-dependent tumor suppressor genes. *Blood.* (2005) 106:3214–22. doi: 10.1182/blood-2005-05-2013
12. Kischkel FC, Hellbardt S, Behrmann I, Germer M, Pawlita M, Krammer PH, et al. Cytotoxicity-dependent APO-1 (Fas/CD95)-associated proteins form a death-inducing signaling complex (DISC) with the receptor. *Embo J.* (1995) 14:5579–88. doi: 10.1002/j.1460-2075.1995.tb00245.x

13. Sprick MR, Weigand MA, Rieser E, Rauch CT, Juo P, Blenis J, et al. FADD/MORT1 and caspase-8 are recruited to TRAIL receptors 1 and 2 and are essential for apoptosis mediated by TRAIL receptor 2. *Immunity.* (2000) 12:599–609. doi: 10.1016/S1074-7613(00)80211-3
14. Kischkel FC, Lawrence DA, Tinel A, Leblanc H, Virmani A, Schow P, et al. Death receptor recruitment of endogenous caspase-10 and apoptosis initiation in the absence of caspase-8. *J Biol Chem.* (2001) 276:46639–46. doi: 10.1074/jbc.M105102200
15. Jiang S, Cai J, Wallace DC, Jones DP. Cytochrome c-mediated apoptosis in cells lacking mitochondrial DNA: signaling pathway involving release and caspase 3 activation is conserved. *J Biol Chem.* (1999) 274:29905–11. doi: 10.1074/jbc.274.42.29905
16. Li CY, Lee JS, Ko YG, Kim JI, Seo JS. Heat shock protein 70 inhibits apoptosis downstream of cytochrome c release and upstream of caspase-3 activation. *J Biol Chem.* (2000) 275:25665–71. doi: 10.1074/jbc.M906383199
17. Elmore S. Apoptosis: a review of programmed cell death. *Toxicol Pathol.* (2007) 35:495–516. doi: 10.1080/01926230701320337
18. Kim Y, Lee C. *Porcine epidemic diarrhea virus* induces caspase-independent apoptosis through activation of mitochondrial apoptosis-inducing factor. *Virology.* (2014) 460–1:180–93. doi: 10.1016/j.virol.2014.04.040
19. Roulston A, Marcellus RC, Branton PE. Viruses and apoptosis. *J Gen Virol.* (1999) 53:577–628. doi: 10.1146/annurev.micro.53.1.577
20. Doyle LP, Hutchings LM. A transmissible gastroenteritis in pigs. *J Am Vet Med Assoc.* (1946) 108:257–9.
21. Wesley RD, Woods RD, Hill HT, Biwer JD. Evidence for a porcine respiratory coronavirus, antigenically similar to transmissible gastroenteritis virus, in the United States. *J Vet Diagn Invest.* (1990) 2:312–7. doi: 10.1177/104063879000200411
22. Pensaert MB, Bouck PD. A new coronavirus-like particle associated with diarrhea in swine. *Arch Virol.* (1978) 58:243–7. doi: 10.1007/BF01317606
23. Peng Zhou HF, Tian L, Xing-Lou Y, Wei-Feng S, Wei Z, Yan Z, et al. Fatal swine acute diarrhoea syndrome caused by an HKU2-related coronavirus of bat origin. *Nature.* (2018) 556:255–8. doi: 10.1038/s41586-018-0010-9
24. Sasseville MJ, Boutin M, Gélinas AM, Dea S. Sequence of the 3'-terminal end (8.1 kb) of the genome of porcine haemagglutinating encephalomyelitis virus: comparison with other haemagglutinating coronaviruses. *J Gen Virol.* (2002) 83:2411. doi: 10.1099/0022-1317-83-10-2411
25. Woo PC, Lau SK, Lam CS, Lau CC, Tsang AK, Lau JH, et al. Discovery of seven novel Mammalian and avian coronaviruses in the genus deltacoronavirus supports bat coronaviruses as the gene source of alphacoronavirus and betacoronavirus and avian coronaviruses as the gene source of gammacoronavirus and deltacoronavirus. *J Virol.* (2012) 86:3995–4008. doi: 10.1128/JVI.06540-11
26. Zhang J. *Porcine deltacoronavirus*: overview of infection dynamics, diagnostic methods, prevalence and genetic evolution. *Virus Res.* (2016) 226:71–84. doi: 10.1016/j.virusres.2016.05.028
27. Lu X, Yang Y, Wang J, Jing Y, Qian Y. Impact of TGEV infection on the pig small intestine. *Virology J.* (2018) 15:102. doi: 10.1186/s12985-018-1012-9
28. Wen Z, Xu Z, Zhou Q, Li W, Wu Y, Du Y, et al. Oral administration of coated PEDV-loaded microspheres elicited PEDV-specific immunity in weaned piglets. *Vaccine.* (2018) 36:6803–9. doi: 10.1016/j.vaccine.2018.09.014
29. Xu Z, Zhang Y, Gong L, Huang L, Lin Y, Qin J, et al. Isolation and characterization of a highly pathogenic strain of Porcine enteric alphacoronavirus causing watery diarrhoea and high mortality in newborn piglets. *Transbound Emerg Dis.* (2019) 66:119–30. doi: 10.1111/tbed.12992
30. Bereiter M, Hasler J, Keller H. Transmissible gastroenteritis (TGE) in Switzerland: antibody persistence after infection and seroepidemiologic studies of the significance of the TGE virus as the cause of diarrhea. *Schwzer Archiv Für Tierhlkunde.* (1988) 130:237–48.
31. Song D, Park B. Porcine epidemic diarrhoea virus: a comprehensive review of molecular epidemiology, diagnosis, and vaccines. *Virus Genes.* (2012) 44:167–75. doi: 10.1007/s11262-012-0713-1
32. Carvajal A, Arguello H, Martinez-Lobo FJ, Costillas S, Miranda R, Pj GDN, et al. Porcine epidemic diarrhoea: new insights into an old disease. *Porcine Health Manag.* (2015) 1:12. doi: 10.1186/s40813-015-0007-9
33. Lin CM, Saif LJ, Marthaler D, Wang Q. Evolution, antigenicity and pathogenicity of global *porcine epidemic diarrhea virus* strains. *Virus Res.* (2016) 226:20–39. doi: 10.1016/j.virusres.2016.05.023
34. Sun D, Wang X, Wei S, Chen J, Feng L. Epidemiology and vaccine of *porcine epidemic diarrhea virus* in China: a mini-review. *J Vet Med Sci.* (2016) 78:355–63. doi: 10.1292/jvms.15-0446
35. Diep NV, Sueyoshi M, Izzati U, Fuke N, Teh APP, Lan NT, et al. Appearance of US-like porcine epidemic diarrhoea virus (PEDV) strains before US outbreaks and genetic heterogeneity of PEDVs collected in Northern Vietnam during 2012-2015. *Transbound Emerg Dis.* (2018) 65:e83–93. doi: 10.1111/tbed.12681
36. Hsu TH, Liu HP, Chin CY, Wang C, Zhu WZ, Wu BL, et al. Detection, sequence analysis, and antibody prevalence of *porcine deltacoronavirus* in Taiwan. *Arch Virol.* (2018) 163:3113–7. doi: 10.1007/s00705-018-3964-x
37. Jang G, Kim SH, Lee YJ, Kim S, Lee DS, Lee KK, et al. Isolation and characterization of Korean *porcine deltacoronavirus* strain KNU16-07. *J Vet Sci.* (2018) 19:577–81. doi: 10.4142/jvs.2018.19.4.577
38. Lara-Romero R, Gomez-Nunez L, Cerriteno-Sanchez JL, Marquez-Valdelamar L, Mendoza-Elvira S, Ramirez-Mendoza H, et al. Molecular characterization of the spike gene of the *porcine epidemic diarrhea virus* in Mexico, 2013-2016. *Virus Genes.* (2018) 54:215–24. doi: 10.1007/s11262-017-1528-x
39. Suzuki T, Shibahara T, Imai N, Yamamoto T, Ohashi S. Genetic characterization and pathogenicity of Japanese *porcine deltacoronavirus*. *Infect Genet Evol.* (2018) 61:176–82. doi: 10.1016/j.meegid.2018.03.030
40. Xu Z, Zhong H, Zhou Q, Du Y, Chen L, Zhang Y, et al. A highly pathogenic strain of *porcine deltacoronavirus* caused watery diarrhea in newborn piglets. *Virol Sin.* (2018) 33:131–41. doi: 10.1007/s12250-018-0003-8
41. Chen F, Knutson TP, Rossow S, Saif LJ, Marthaler DG. Decline of transmissible gastroenteritis virus and its complex evolutionary relationship with porcine respiratory coronavirus in the United States. *Sci Rep.* (2019) 9:3953. doi: 10.1038/s41598-019-40564-z
42. Perez-Rivera C, Ramirez-Mendoza H, Mendoza-Elvira S, Segura-Velazquez R, Sanchez-Betancourt JI. First report and phylogenetic analysis of *porcine deltacoronavirus* in Mexico. *Transbound Emerg Dis.* (2019) 66:1436–41. doi: 10.1111/tbed.13193
43. Yang YL, Yu JQ, Huang YW. Swine enteric alphacoronavirus (*swine acute diarrhea syndrome coronavirus*): An update three years after its discovery. *Virus Res.* (2020) 285:198024. doi: 10.1016/j.virusres.2020.198024
44. Lorincz M, Biksi I, Andersson S, Cságola A, Tuboly T. Sporadic re-emergence of enzootic porcine transmissible gastroenteritis in Hungary. *Acta Vet Hung.* (2014) 62:125–33. doi: 10.1556/avet.2013.043
45. Zhang F, Luo S, Gu J, Li Z, Li K, Yuan W, et al. Prevalence and phylogenetic analysis of porcine diarrhea associated viruses in southern China from 2012 to 2018. *BMC Vet Res.* (2019) 15:470. doi: 10.1186/s12917-019-2212-2
46. Gerdts V, Zakhartchouk A. Vaccines for *porcine epidemic diarrhea virus* and other swine coronaviruses. *Vet Microbiol.* (2017) 206:45–51. doi: 10.1016/j.vetmic.2016.11.029
47. Li K, Li H, Bi Z, Song D, Zhang F, Lei D, et al. Significant inhibition of re-emerged and emerging swine enteric coronavirus *in vitro* using the multiple shRNA expression vector. *Antiviral Res.* (2019) 166:11–8. doi: 10.1016/j.antiviral.2019.03.010
48. Gao X, Zhao D, Zhou P, Zhang L, Li M, Li W, et al. Characterization, pathogenicity and protective efficacy of a cell culture-derived *porcine deltacoronavirus*. *Virus Res.* (2020) 282:197955. doi: 10.1016/j.virusres.2020.197955
49. Xu Z, Liu Y, Peng P, Liu Y, Huang M, Ma Y, et al. Aloe extract inhibits *porcine epidemic diarrhea virus in vitro* and *in vivo*. *Vet Microbiol.* (2020) 249:108849. doi: 10.1016/j.vetmic.2020.108849
50. Jung K, Saif LJ. *Porcine epidemic diarrhea virus* infection: Etiology, epidemiology, pathogenesis and immunoprophylaxis. *Vet J.* (2015) 204:134–43. doi: 10.1016/j.tvjl.2015.02.017
51. Jung K, Hu H, Saif LJ. *Porcine deltacoronavirus* infection: etiology, cell culture for virus isolation and propagation, molecular epidemiology and pathogenesis. *Virus Res.* (2016) 226:50–9. doi: 10.1016/j.virusres.2016.04.009
52. Guo R, Fan B, Chang X, Zhou J, Zhao Y, Shi D, et al. Characterization and evaluation of the pathogenicity of a natural recombinant transmissible gastroenteritis virus in China. *Virology.* (2020) 545:24–32. doi: 10.1016/j.virol.2020.03.001

53. Wang XY, Zhao TQ, Xu DP, Zhang X, Ji CJ, Zhang DL. The influence of *porcine epidemic diarrhea virus* on pig small intestine mucosal epithelial cell function. *Arch Virol.* (2018) 164:83–90. doi: 10.1007/s00705-018-4061-x
54. Zhu L, Mou C, Xing Y, Jian L, Qian Y. Mitophagy in TGEV infection counteracts oxidative stress and apoptosis. *Oncotarget.* (2015) 7:27122–41. doi: 10.18632/oncotarget.8345
55. Rogers DG, Andersen AA. Intestinal lesions caused by two swine chlamydial isolates in gnotobiotic pigs. *J Vet Diagn Invest.* (1996) 8:433–40. doi: 10.1177/104063879600800405
56. Li FQ, Tam JP, Liu DX. Cell cycle arrest and apoptosis induced by the coronavirus infectious bronchitis virus in the absence of p53. *Virology.* (2007) 365:435–45. doi: 10.1016/j.virol.2007.04.015
57. Krähling V, Stein DA, Spiegel M, Weber F, Mühlberger E. Severe acute respiratory syndrome coronavirus triggers apoptosis via protein kinase R but is resistant to its antiviral activity. *J Virol.* (2009) 83:2298–309. doi: 10.1128/JVI.01245-08
58. Collins M. Potential roles of apoptosis in viral pathogenesis. *Am J Respir Crit Care Med.* (1995) 152:S20–24. doi: 10.1164/ajrccm/152.4_Pt_2.S20
59. Zhai Y, Ding N. MicroRNA-194 participates in endotoxemia induced myocardial injury via promoting apoptosis. *Eur Rev Med Pharmacol.* (2018) 22:2077–83. doi: 10.26355/eurrev_201804_14739
60. Curtis KM, Yount B, Baric RS. Heterologous gene expression from transmissible gastroenteritis virus replicon particles. *J Virol.* (2002) 76:1422–34. doi: 10.1128/JVI.76.3.1422-1434.2002
61. Enjuanes L, Dediego ML, lvarez E, Deming D, Sheahan T, Baric R. Vaccines to prevent severe acute respiratory syndrome coronavirus-induced disease. *Virus Res.* (2008) 133:45–62. doi: 10.1016/j.virusres.2007.01.021
62. Huang C, Lokugamage KG, Rozovics JM, Narayanan K, Semler BL, Makino S. Alphacoronavirus transmissible gastroenteritis virus nsp1 protein suppresses protein translation in mammalian cells and in cell-free HeLa cell extracts but not in rabbit reticulocyte lysate. *J Virol.* (2011) 85:638–43. doi: 10.1128/JVI.01806-10
63. Wojdyla JA, Manolaridis I, Van Kasteren PB, Kikkert M, Snijder EJ, Gorbalenya AE, et al. Papain-like protease 1 from transmissible gastroenteritis virus: crystal structure and enzymatic activity toward viral and cellular substrates. *J Virol.* (2010) 84:10063–73. doi: 10.1128/JVI.00898-10
64. Yount B, Curtis KM, Baric RS. Strategy for systematic assembly of large RNA and DNA genomes: transmissible gastroenteritis virus model. *J Virol.* (2000) 74:10600–11. doi: 10.1128/JVI.74.22.10600-10611.2000
65. Ortego J, Ceriani JE, Patino C, Plana J, Enjuanes L. Absence of E protein arrests transmissible gastroenteritis coronavirus maturation in the secretory pathway. *Virology.* (2007) 368:296–308. doi: 10.1016/j.virol.2007.05.032
66. Peng Y, Shilei H, Zhou Y, Luyi X, Wang K, Yang Y, et al. UBXN1 interacts with the S1 protein of transmissible gastroenteritis coronavirus and plays a role in viral replication. *Vet Res.* (2019) 50:28. doi: 10.1186/s13567-019-0648-9
67. Song Z, Yang Y, Wang L, Wang K, Ran L, Xie Y, et al. EIF4A2 interacts with the membrane protein of transmissible gastroenteritis coronavirus and plays a role in virus replication. *Res Vet Sci.* (2019) 123:39–46. doi: 10.1016/j.rvsc.2018.12.005
68. Laude H, Gelfi J, Lavenant L, Charley B. Single amino acid changes in the viral glycoprotein M affect induction of alpha interferon by the coronavirus transmissible gastroenteritis virus. *J Virol.* (1992) 66:743–9. doi: 10.1128/JVI.66.2.743-749.1992
69. Enjuanes L, van der Zeijst BAM. *Molecular Basis of Transmissible Gastroenteritis Virus Epidemiology.* Springer US (1995). doi: 10.1007/978-1-4899-1531-3_16
70. Gu JP, Yue XW, Xing R, Li CY, Yang ZB. Progress in genetically engineered vaccines for porcine transmissible gastroenteritis virus. *Rev Méd Vét.* (2012) 163:107–11.
71. Helen E, Grant M. Apoptosis: an innate immune response to virus infection. *Trends Microbiol.* (1999) 7:160–5. doi: 10.1016/S0966-842X(99)01487-0
72. Wen LS, Hsu HW, Liao MH, Long HL, Liu HJ. Avian reovirus σC protein induces apoptosis in cultured cells. *Virology.* (2004) 321:65–74. doi: 10.1016/j.virol.2003.12.004
73. Chen S, Cheng AC, Wang MS, Xi P. Detection of apoptosis induced by new type gosling viral enteritis virus *in vitro* through fluorescein annexin V-FITC/PI double labeling. *World J Gastroenterol.* (2008) 014:2174–8. doi: 10.3748/wjg.14.2174
74. Eleouet JF, Chilmonczyk S, Besnardeau L, Laude H. Transmissible gastroenteritis coronavirus induces programmed cell death in infected cells through a caspase-dependent pathway. *J Virol.* (1998) 72:4918–24. doi: 10.1128/JVI.72.6.4918-4924.1998
75. Sirinarumitr T, Kluge JP, Paul PS. *Transmissible gastroenteritis virus* induced apoptosis in swine testes cell cultures. *Arch Virol.* (1998) 143:2471–85. doi: 10.1007/s007050050477
76. Eléouët JF, Slee EA, Saurini F, Castagné N, Poncet D, Garrido C, et al. The viral nucleocapsid protein of transmissible gastroenteritis coronavirus (TGEV) is cleaved by caspase-6 and−7 during TGEV-induced apoptosis. *J Virol.* (2000) 74:3975–83. doi: 10.1128/JVI.74.9.3975-3983.2000
77. Kim B, Kim O, Tai JH, Chae C. *Transmissible gastroenteritis virus* induces apoptosis in swine testicular cell lines but not in intestinal enterocytes. *J Comp Pathol.* (2000) 123:64–6. doi: 10.1053/jcpa.2000.0386
78. Ding L, Xu X, Huang Y, Li Z, Zhang K, Chen G, et al. *Transmissible gastroenteritis virus* infection induces apoptosis through FasL- and mitochondria-mediated pathways. *Vet Microbiol.* (2012) 158:12–22. doi: 10.1016/j.vetmic.2012.01.017
79. Ding L, Zhao X, Huang Y, Du Q, Dong F, Zhang H, et al. Regulation of ROS in transmissible gastroenteritis virus-activated apoptotic signaling. *Biochem Biophys Res Commun.* (2013) 442:33–7. doi: 10.1016/j.bbrc.2013.10.164
80. Zhao X, Song X, Bai X, Fei N, Huang Y, Zhao Z, et al. miR-27b attenuates apoptosis induced by transmissible gastroenteritis virus (TGEV) infection via targeting runt-related transcription factor 1 (RUNX1). *Peer J.* (2016) 4:e1635. doi: 10.7717/peerj.1635
81. Ding L, Huang Y, Du Q, Dong F, Zhao X, Zhang W, et al. TGEV nucleocapsid protein induces cell cycle arrest and apoptosis through activation of p53 signaling. *Biochem Biophys Res Commun.* (2014) 445:497–503. doi: 10.1016/j.bbrc.2014.02.039
82. Hong M. p53- and ROS-mediated AIF pathway involved in TGEV-induced apoptosis. *J Vet Med Sci*. (2018) 80:1775–81. doi: 10.1292/jvms.18-0104
83. Xu X, Xu Y, Zhang Q, Yang F, Yin Z, Wang L, et al. *Porcine epidemic diarrhea virus* infections induce apoptosis in Vero cells via a reactive oxygen species (ROS)/p53, but not p38 MAPK and SAPK/JNK signalling pathways. *Vet Microbiol.* (2019) 232:1–12. doi: 10.1016/j.vetmic.2019.03.028
84. Kocherhans R, Bridgen A, Ackermann M, Tobler K. Completion of the porcine epidemic diarrhoea coronavirus (PEDV) genome sequence. *Virus Genes.* (2001) 23:137–44. doi: 10.1023/A:1011831902219
85. Chen Y, Zhang Z, Li J, Gao Y, Zhou L, Ge X, et al. *Porcine epidemic diarrhea virus* S1 protein is the critical inducer of apoptosis. *Virol J.* (2018) 15. doi: 10.1186/s12985-018-1078-4
86. Fangzhou C, Yinxing Z, Meizhou W, Xugang K, Yao L, He Q. *Full-Length Genome Characterization of Chinese Porcine Deltacoronavirus Strain CH/SXD1/2015*. Shanxi: Genome Announcements (2015).
87. Chen Q, Gauger P, Stafne M, Thomas J, Arruda P, Burrough E. Pathogenicity and pathogenesis of a United States *porcine deltacoronavirus* cell culture isolate in 5-day-old neonatal piglets. *Virology*. (2015) 482:51–9. doi: 10.1016/j.virol.2015.03.024
88. Lee Y, Lee C. *Porcine deltacoronavirus* induces caspase-dependent apoptosis through activation of the cytochrome c -mediated intrinsic mitochondrial pathway. *Virus Res.* (2018) 253:112–23. doi: 10.1016/j.virusres.2018.06.008
89. Jung K, Hu H, Saif LJ. *Porcine deltacoronavirus* induces apoptosis in swine testicular and LLC porcine kidney cell lines *in vitro* but not in infected intestinal enterocytes *in vivo*. *Vet Microbiol.* (2016) 182:57–63. doi: 10.1016/j.vetmic.2015.10.022
90. Zhang J, Han Y, Shi H, Chen J, Zhang X, Wang X, et al. *Swine acute diarrhea syndrome coronavirus*-induced apoptosis is caspase- and cyclophilin D- dependent. *Emerg Microbes Infect.* (2020) 9:439–56. doi: 10.1080/22221751.2020.1722758
91. Huang Y, Ding L, Li Z, Dai M, Zhao X, Li W, et al. *Transmissible gastroenteritis virus* infection induces cell apoptosis via activation of p53 signalling. *J Gen Virol.* (2013) 94:1807–17. doi: 10.1099/vir.0.051557-0
92. Lee C. *Porcine epidemic diarrhea virus*: An emerging and re-emerging epizootic swine virus. *Virology J.* (2016) 13:19. doi: 10.1186/s12985-016-0465-y
93. Si F, Hu X, Wang C, Chen B, Wang R, Dong S, et al. *Porcine epidemic diarrhea virus* (PEDV) ORF3 enhances viral proliferation by inhibiting

apoptosis of infected cells. *Viruses.* (2020) 12:214. doi: 10.3390/v12020214
94. Wang K, Xie S, Sun B. Viral proteins function as ion channels. *Biochim Biophys Acta.* (2011) 1808:510–5. doi: 10.1016/j.bbamem.2010.05.006
95. Shiyi Ye ZL, Fangzhou C, Wentao L, Xiaozhen G, Han H, Qigai H. *Porcine epidemic diarrhea virus* ORF3 gene prolongs S-phase, facilitates formation of vesicles and promotes the proliferation of attenuated PEDV. *Virus Genes.* (2015) 51:385–92. doi: 10.1007/s11262-015-1257-y
96. Shi D, Shi H, Sun D, Chen J, Zhang X, Wang X, et al. Nucleocapsid interacts with NPM1 and protects it from proteolytic cleavage, enhancing cell survival, and is involved in PEDV growth. *Sci Rep.* (2017) 7:39700. doi: 10.1038/srep39700
97. Xing Y, Chen J, Tu J, Zhang B, Chen X, Shi H, et al. The papain-like protease of *porcine epidemic diarrhea virus* negatively regulates type I interferon pathway by acting as a viral deubiquitinase. *J Gen Virol.* (2013) 94:1554. doi: 10.1099/vir.0.051169-0
98. Ding Z, Fang L, Jing H, Zeng S, Wang D, Liu L, et al. *Porcine epidemic diarrhea virus* nucleocapsid protein antagonizes beta interferon production by sequestering the interaction between IRF3 and TBK1. *J Virol.* (2014) 88:8936–45. doi: 10.1128/JVI.00700-14
99. Dang W, Liurong F, Yanling S, Huan Z, Gao L, Peng G, et al. *Porcine epidemic diarrhea virus* 3C-like protease regulates its interferon antagonism by cleaving NEMO. *J Virol.* (2015) 90:2090–101. doi: 10.1128/JVI.02514-15
100. Zhang Q, Shi K, Yoo D. Suppression of type I interferon production by *porcine epidemic diarrhea virus* and degradation of CREB-binding protein by nsp1. *Virology.* (2016) 489:252–68. doi: 10.1016/j.virol.2015.12.010
101. Curry SM, Schwartz KJ, Yoon KJ, Gabler NK, Burrough ER. Effects of *porcine epidemic diarrhea virus* infection on nursery pig intestinal function and barrier integrity. *Vet Microbiol.* (2017) 211:58–66. doi: 10.1016/j.vetmic.2017.09.021
102. Zhang X, Li P, Zheng Q, Hou J. Lactobacillus acidophilus S-layer protein-mediated inhibition of PEDV-induced apoptosis of Vero cells. *Vet Microbiol.* (2019) 229:159–67. doi: 10.1016/j.vetmic.2019.01.003
103. Altawaty T, Liu L, Zhang H, Tao C, Hou S, Li K, et al. Lack of LTβR increases susceptibility of IPEC-J2 cells to *porcine epidemic diarrhea virus*. *Cells.* (2018) 7:222. doi: 10.3390/cells7110222
104. Zeng Z, Feng D, Shi K, Ye G, Wang G, Fang L, et al. Dimerization of coronavirus Nsp9 with diverse modes enhances its nucleic acid binding affinity. *J Virol.* (2018) 92:e00692–18. doi: 10.1128/JVI.00692-18
105. Mengjia Z, Wan L, Peng Z, Dejian L, Rui L, Anan J, et al. Genetic manipulation of *porcine deltacoronavirus* reveals insights into NS6 and NS7 functions: a novel strategy for vaccine design. *Emerg Microbes Infect.* (2019) 20:20–31. doi: 10.1080/22221751.2019.1701391
106. Zhu X, Wang D, Zhou J, Pan T, Chen J, Yang Y, et al. *Porcine deltacoronavirus* Nsp5 antagonizes type i interferon signaling by cleaving STAT2. *J Virol.* (2017) 91:e00003–17. doi: 10.1128/JVI.00003-17
107. Fang P, Fang L, Ren J, Hong Y, Liu X, Zhao Y, et al. *Porcine deltacoronavirus* accessory protein NS6 antagonizes interferon beta production by interfering with the binding of RIG-I/MDA5 to double-stranded RNA. *J Virol.* (2018) 92:e00712–18. doi: 10.1128/JVI.00712-18
108. Ji L, Li S, Zhu W, Ma J, Yan Y. *Porcine deltacoronavirus* nucleocapsid protein suppressed IFN-β production by interfering porcine RIG-I dsRNA-binding and K63-linked polyubiquitination. *Front Immunol.* (2019) 10:24. doi: 10.3389/fimmu.2019.01024
109. Liu X, Fang P, Fang L, Hong Y, Zhu X, Wang D, et al. *Porcine deltacoronavirus* nsp15 antagonizes interferon-β production independently of its endoribonuclease activity. *Mol Immunol.* (2019) 114:100. doi: 10.1016/j.molimm.2019.07.003
110. Lang G, Jie L, Zhou Q, Xu Z, Li C, Yun Z, et al. A new bat-HKU2–like coronavirus in swine, China, 2017. *Emerg Infect Dis.* (2017) 23:1607–9. doi: 10.3201/eid2309.170915
111. Pan Y, Tian X, Qin P, Wang B, Zhao P, Yang YL, et al. Discovery of a novel swine enteric alphacoronavirus (SeACoV) in southern China. *Vet Microbiol.* (2017) 211:15–21. doi: 10.1016/j.vetmic.2017.09.020
112. Lau SKP, Woo PCY, Li KSM, Huang Y, Wang M, Lam CSF, et al. Complete genome sequence of bat coronavirus HKU2 from Chinese horseshoe bats revealed a much smaller spike gene with a different evolutionary lineage from the rest of the genome. *Virology.* (2007) 367:428–39. doi: 10.1016/j.virol.2007.06.009
113. Cruz DJM, Kim CJ, Shin HJ. The GPRLQPY motif located at the carboxy-terminal of the spike protein induces antibodies that neutralize *Porcine epidemic diarrhea virus*. *Virus Res.* (2008) 132:0–196. doi: 10.1016/j.virusres.2007.10.015
114. Wang L, Hu W, Fan C. Structural and biochemical characterization of SADS-CoV papain-like protease 2. *Protein Sci.* (2020) 29:1228–41. doi: 10.1002/pro.3857
115. Xu Z, Gong L, Peng P, Liu Y, Xue C, Cao Y. Porcine enteric alphacoronavirus Inhibits IFN-α, IFN-β, OAS, Mx1, and PKR mRNA expression in infected peyer's patches *in vivo*. *Front Vet Sci.* (2020) 7:449. doi: 10.3389/fvets.2020.00449
116. Xie S, Chen XX, Qiao S, Li R, Sun Y, Xia S, et al. Identification of the RNA Pseudoknot within the 3' end of the porcine reproductive and respiratory syndrome virus genome as a pathogen-associated molecular pattern to activate antiviral signaling via RIG-I and toll-like receptor 3. *J Virol.* (2018) 92:18. doi: 10.1128/JVI.00097-18
117. Luo J, Fang L, Dong N, Fang P, Ding Z, Wang D, et al. *Porcine deltacoronavirus* (PDCoV) infection suppresses RIG-I-mediated interferon-β production. *Virology.* (2016) 495:10–7. doi: 10.1016/j.virol.2016.04.025
118. Shi P, Su Y, Li R, Liang Z, Dong S, Huang J. PEDV nsp16 negatively regulates innate immunity to promote viral proliferation. *Virus Res.* (2019) 265:57–66. doi: 10.1016/j.virusres.2019.03.005
119. Ji L, Wang N, Ma J, Cheng Y, Wang H, Sun J, et al. *Porcine deltacoronavirus* nucleocapsid protein species-specifically suppressed IRF7-induced type I interferon production via ubiquitin-proteasomal degradation pathway. *Vet Microbiol.* (2020) 250:108853. doi: 10.1016/j.vetmic.2020.108853
120. Zhou Z, Sun Y, Yan X, Tang X, Li Q, Tan Y, et al. *Swine acute diarrhea syndrome coronavirus* (SADS-CoV) antagonizes interferon-beta production via blocking IPS-1 and RIG-I. *Virus Res.* (2020) 278:197843. doi: 10.1016/j.virusres.2019.197843
121. Fletcher NF, Wilson GK, Murray J, Hu K, Lewis A, Reynolds GM, et al. Hepatitis C virus infects the endothelial cells of the blood-brain barrier. *Gastroenterology.* (2012) 142:634–43.e6. doi: 10.1053/j.gastro.2011.11.028
122. Zhou Y, Wu W, Xie L, Wang D, Ke Q, Hou Z, et al. Cellular RNA helicase DDX1 is involved in transmissible gastroenteritis virus Nsp14-induced interferon-beta production. *Front Immunol.* (2017) 8:940. doi: 10.3389/fimmu.2017.00940
123. Yen JH, Ganea D. Interferon beta induces mature dendritic cell apoptosis through caspase-11/caspase-3 activation. *Blood.* (2009) 114:1344–54. doi: 10.1182/blood-2008-12-196592
124. Hogner K, Wolff T, Pleschka S, Plog S, Gruber AD, Kalinke U, et al. Macrophage-expressed IFN-β contributes to apoptotic alveolar epithelial cell injury in severe influenza virus pneumonia. *PLoS Pathog.* (2013) 9:e1003188. doi: 10.1371/journal.ppat.1003188

Conflict of Interest: The authors declare that the research was conducted in the absence of any commercial or financial relationships that could be construed as a potential conflict of interest.

frontiers in Veterinary Science

ORIGINAL RESEARCH
published: 07 January 2021
doi: 10.3389/fvets.2020.539444

Investigation of Genetic Relatedness of *Brucella* Strains in Countries Along the Silk Road

Zhiguo Liu[1], Chengling Wang[1], Kongjiao Wei[1], Zhongzhi Zhao[2], Miao Wang[3], Dan Li[1], Heng Wang[4], Qiang Wei[5] and Zhenjun Li[1]**

[1] National Institute for Communicable Disease Control and Prevention, Beijing, China, [2] Qinghai Institute for Endemic Diseases Prevention and Control, Xining, China, [3] Ulanqab Center for Endemic Disease Control and Prevention, Ulanqab, China, [4] Hangzhou Center for Disease Control and Prevention, Hangzhou, China, [5] Chinese Center for Disease Control and Prevention, Beijing, China

In this study, MLVA (multiple-locus variable-number tandem repeat analysis) genotype data of *Brucella* strains from 11 countries along the Silk Road were downloaded from the MLVAbank. MLVA data of strains were applied to the constructed Minimum Spanning Tree to explore the species/biovars distribution, geographic origins, and genetic relationships of the strains analyzed. Moreover, whole-genome sequencing–single-nucleotide polymorphism (WGS-SNP) phylogenetic analysis of the genome of *Brucella melitensis* strains from GenBank was performed to discriminate the relatedness of strains further and investigate the transmission pattern of *B. melitensis* brucellosis. A total of 1,503 *Brucella* strains were analyzed in this study: 431 *Brucella abortus* strains (29.8%), 1,009 *B. melitensis* strains (65.7%), and 63 *Brucella suis* strains (4.5%). *B. melitensis* biovar 3 was the dominant species and was shown to be widespread in all of the examined regions, suggesting that the prevention and surveillance of the *B. melitensis* population are a main challenge in these countries. A wide host spectrum was observed for this *Brucella* population; many animal reservoirs are a potential reason for the continuous brucellosis circulation in these countries. Although the *B. abortus* strains from the examined regions had common geographic origins, only a few shared genotypes were observed in different countries. These data revealed that the majority *of B. abortus* strains were spreading within the national borders. However, the *B. melitensis* strains from Italy originated from a Western Mediterranean lineage; strains from the other 10 countries originated from Eastern Mediterranean lineage, and this lineage was shared by strains from three to nine different countries, suggesting that the introduction and reintroduction of the disease in the 10 countries might have occurred in the past. Furthermore, the most shared MLVA-16 genotypes were formed in the *B. melitensis* strains from China, Kazakhstan, and Turkey, suggesting that the introduction and trade in sheep and goats have occurred frequently in these countries. WGS-SNP analysis showed that the *B. melitensis* in this study originated from the Malta (Italy) region. According to their territorial affiliation between four clade strains from these countries in genotype B, the absence of a clear differentiation suggests that strains continuously expand and spread in countries along with Silk Road. Active exchange and trade of animals (sheep and goats) among these countries are reasonable

OPEN ACCESS

Edited by:
Shao-Lun Zhai,
Guangdong Academy of Agricultural Sciences, China

Reviewed by:
Jo Stevens,
University of Edinburgh, United Kingdom
Zhai Qi,
Guangdong Academy of Agricultural Sciences, China

***Correspondence:**
Qiang Wei
weiqiang@chinacdc.cn
Zhenjun Li
lizhenjun@icdc.cn

Specialty section:
This article was submitted to Veterinary Infectious Diseases, a section of the journal Frontiers in Veterinary Science

Received: *01 March 2020*
Accepted: *17 November 2020*
Published: *07 January 2021*

Citation:
Liu Z, Wang C, Wei K, Zhao Z, Wang M, Li D, Wang H, Wei Q and Li Z (2021) Investigation of Genetic Relatedness of Brucella Strains in Countries Along the Silk Road. Front. Vet. Sci. 7:539444. doi: 10.3389/fvets.2020.539444

explanations. *B. suis* strains from different nations showed unique geographic origins and epidemiological characteristics. Therefore, there is an urgent need for the control of transfer and trade of infected sheep (goats) in countries along the Silk Road, namely, the strengthening of the entry–exit quarantine of sheep and goats and improvements in the diagnosis of animal brucellosis.

Keywords: *Brucella spp.*, silk road, species/biovar, host lineages, geographic origin, genetic relatedness

INTRODUCTION

Brucellosis is a zoonotic infectious disease caused by members of the genus *Brucellae*, circulating in more than 170 countries, especially in the Mediterranean, Asia, and Central and South America (1). The disease is primarily contracted through direct or indirect contact with infected animals and their contaminants, although the consumption of contaminated animal products can also cause infection. Low fever, sweating, fatigue, and joint pain are the most common clinical manifestations of patients (2). Chronic brucellosis is challenging to cure, which affects the quality of life of patients and causes great family and socioeconomic burdens (3). In females, abortion and stillbirth are the main manifestations, whereas orchitis and sterility are common in males (4). Therefore, brucellosis not only has a significant impact on the husbandry and health of the human population, but is also closely related to many fields such as public safety, food hygiene, and foreign trade (5).

Although human brucellosis (HB) is one of the most common bacterial zoonotic diseases, its occurrence greatly differs between geographic areas. The highest annual incidences of HB per million of the population are observed in Syria and Mongolia (1); for instance, 39,838 human cases were reported in Syria in 2007. Mongolia has a high incidence of brucellosis in humans and animals due to livestock husbandry; livestock seroprevalence ranged from 0.5 to 1.8% in 2011 (6). Moreover, a total of 684,380 HB cases were reported in mainland China during 1950–2018, and the incidence of HB peaked in 2014 (4.32/100,000) (7). Kazakhstan is a hyperendemic area, considering the very high incidence rates in the human population and farm animals (1). From 1999 to 2016, 38,557 new cases of HB were recorded, with annual counts of cases ranging from 1,443 (2014) to 3,596 (2004) (8). In Pakistan, the high age-wise prevalence was recorded as 32.25% (98/304) by enzyme-linked immunosorbent assay (ELISA) ($P < 0.05$) in 21- to 30-year-old females (9). In India, the seroprevalence of brucellosis among cattle and goats was estimated to be 1.1 and 11.2%, respectively (10). Brucellosis is still reported from all types of farms and domestic livestock in Russia; between 1999 and 2009, the number of infected sites increased, ranging from 54 in 2001 to 112 in 2009 (11). The incidence of HB in Turkey is 26 per 100,000 (12), and 18,264 new brucellosis cases were reported in 2004 (13); moreover, pediatric brucellosis may constitute 20% to 30% of all brucellosis cases in the world (14). Previous research reported that 22 (5.1%) tested by Rose Bengal Test (RBT) and 58 (13.5%) tested using the blocking ELISA assay were positive for *Brucella* in wild boar hunted in the Campania region of Italy during 2016–2017 (15). Each year a relatively small number of cases are reported in Germany, but within the last 2 years, an increase of cases was observed (16). Many comprehensive brucellosis controls have been developed in the majority of countries, including testing-slaughter, restricted infected animal transfer, and vaccination of livestock. However, brucellosis is still an endemic zoonosis in these nations (17).

The Silk Road Economic Belt has had a profound effect on economic prosperity, cultural diversity, foreign trades, and many other characteristics of nations along the road; therefore, it might also provide opportunities for the spread of zoonotic diseases (18). Indeed, zoonotic diseases such as plague and anthrax are associated with commercial activities related to the Silk Road (19, 20), especially in countries along the line of the road. Indeed, these countries have high amounts of husbandry, and brucellosis circulates between humans and animals in Italy, Germany, Turkey, Iran, and Kazakhstan (21–25). Accordingly, there is the potential for transmission of brucellosis during processing of animals and trade of animal products. Currently, MLVA-16 genotyping of *Brucella* strains can be used for trace-back and trace-forward investigations, as well as the identification of the spreading route (26), and MLVA-11 is often used to trace back the geographic origin of strains (27). Moreover, whole-genome sequencing–single-nucleotide polymorphism (WGS-SNP) is likely to be a suitable tool for trace-back analysis of *Brucella melitensis*, as it is capable of suggesting the potential geographic origin of a given strain (16). Therefore, this study was conducted to better understand the epidemiological characteristics of brucellosis in countries along the Silk Road, provide valuable information for strengthening trade cooperation, and launch a corresponding strategy of prevention and control of brucellosis.

MATERIALS AND METHODS

Data Source

Data pertaining to MLVA-16 of 1,503 *Brucella* from 11 related countries including China, Kazakhstan, Turkey, Germany, Italy, Iran, Israel, Lebanon, Mongolia, Syria, and India were obtained from the international MLVAbank database (http://microbesgenotyping.i2bc.paris-saclay.fr/databases) (2016–2018·V1.4.0), including the strain number (Named by the database), species/biovars, host types, isolated region, Panel 1 genotype, MLVA-11 genotype, and the number of tandem repeats at MLVA-16 loci. Moreover, strains from Kyrgyzstan and Tajikistan were not found in the international MLVAbank database.

TABLE 1 | Species distribution characteristics of *Brucella* strains in countries along the Silk Road.

Species-biovars	China	Kazakhstan	Turkey	Germany	Italy	Iran	Israel	Lebanon	Mongolia	Syria	India	Total
B. abortus†	—	98	—	—	—	—	—	—	—	—	—	98
B. abortus bv.1	5	36	—	2	7	—	—	—	—	—	13	63
B. abortus bv.3	65	1	1	3	116	—	—	—	—	—	—	188
B. abortus bv.6	—	78	—	—	—	—	—	—		1	—	79
B. abortus bv.7	—	—	1	—	—	—	—	—	3	—	—	4
B. abortus Rough	—	—	—	—	—	—	—	—	—	—	1	1
B. melitensis†	119	107	32	—	2	7	—	27	—	16	2	313
B. melitensis bv.1	52	14	7	4	4	—	10	—	5	—	3	99
B. melitensis bv.2	12	1	18	7	3	—	1	1	—	3	4	50
B. melitensis bv.3	123	3	175	8	217	2	2	—	—	—	4	534
B. melitensis Rough	—	—	—	—	—	—	1	—	4	—	—	5
B. melitensis atypical	—	—	—	—	—	—	—	—	—	—	9	9
B. suis bv.1	18	—	—	—	—	—	—	—	—	—	—	18
B. suis bv.2	—	—	—	34	10	—	—	—	—	—	—	44
B. suis bv.3	—	—	—	—	—	—	—	—	—	—	1	1
Total	394	338	234	58	359	9	14	28	12	20	37	1,503

†*unknown in biotypes; —, no data.*

Strain Isolation and Identification

A total of 1,503 *Brucella* strains were collected from samples of patients and animals from 11 different countries. According to standard bacteriology approaches, all of the strains were isolated and identified (28). Conventional identification methods were used to assign the strains to biotypes. All of the strains were gram-negative, agglutinated with polyvalent brucellosis serum, had oxidase and catalase activity, synthesized urease, and were capable of growing in atmospheric conditions. Subsequently, BCSP-31 polymerase chain reaction (PCR) (29), AMOS-PCR (30), and/or *Brucella* ladder PCR (31) were applied to verify the results from the biotyping assays.

DNA Preparation and Genotyping

A fresh single *Brucella* strain clone was picked up from a solid agar medium surface and then heat-inactivated at 80°C for 20 min. Subsequently, DNA was isolated using a phenol/chloroform extraction method and/or the QIAamp DNA Mini Kit (Qiagen, United States) according to the manufacturer's instructions. The MLVA-16 assay was performed as previously described (32, 33). Briefly, 16 loci were divided into three panels: Panel 1 (also called MLVA-8), Panel 2A, and Panel 2B. The combination of panels MLVA-8 and 2A was called MLVA-11, whereas the combination of all three panels (16 loci) was designated MLVA-16. The MLVA-11 panel allows for tracing the geographic origin of the strains analyzed, whereas the Panel 2B loci are highly discriminatory, and their combination with MLVA-11 was used for molecular epidemiology investigation. PCR was used to determine the number of repeats from each sample, and its products were purified and directly sequenced using an ABI Prism Big Dye Terminator. Size analysis of VNTR repeats was performed using GeneMapper 4.1 (Applied Biosystems).

Data Processing and Analysis

A total of 1,503 *Brucella* strains were downloaded from the MLVAbank database, including 394 in China, 359 in Italy, 338 in Kazakhstan, 234 in Turkey, 58 in Germany, 37 in India, 28 in Lebanon, 20 in Syria, 14 in Israel, 12 in Mongolia, and 9 in Iran (**Supplementary Table 1**). The downloaded data were processed according to the species/biovars and genotypes of all *Brucella* strains using Excel 2016 software (Microsoft Corporation, Redmond, WA, USA). At the same time, the species/biovars and distribution regions of the strains were analyzed to investigate the epidemiological correlation of *Brucella* in the above countries. Subsequently, the Minimum Spanning Tree (MST) of *Brucella abortus* strains, *B. melitensis* strains, and *Brucella suis* strains were constructed using the BioNumerics 7.6 software based on the MLVA-11 data, and the genotype distribution and geographical origin of the strains were analyzed. The BioNumerics 7.6 software (Applied Maths, Sint-Martens-Latem, Belgium) based on unweighted pair group method using arithmetic averages was applied to construct the MST of *B. abortus* strains, *B. melitensis* strains, and *B. suis* strains based on MLVA-16 data and to explore their genetic relatedness. Moreover, the WGS-SNP phylogenetic analysis (34) was performed in 39 *B. melitensis* from 14 countries along the Silk Road (**Supplementary Table 2**) to explore further the genetic relatedness of strains and the transmission pattern of brucellosis in these nations.

RESULTS

Species/Biovar Distribution Characteristics of *Brucella* Strains

Among the 1,503 strains of *Brucella*, 431 (28.7%) were *B. abortus*, 1,009 (67.1%) were *B. melitensis*, and 63 (4.2%) were *B. suis* (**Table 1**). *B. abortus* strains included four biovars: 63 in biovar

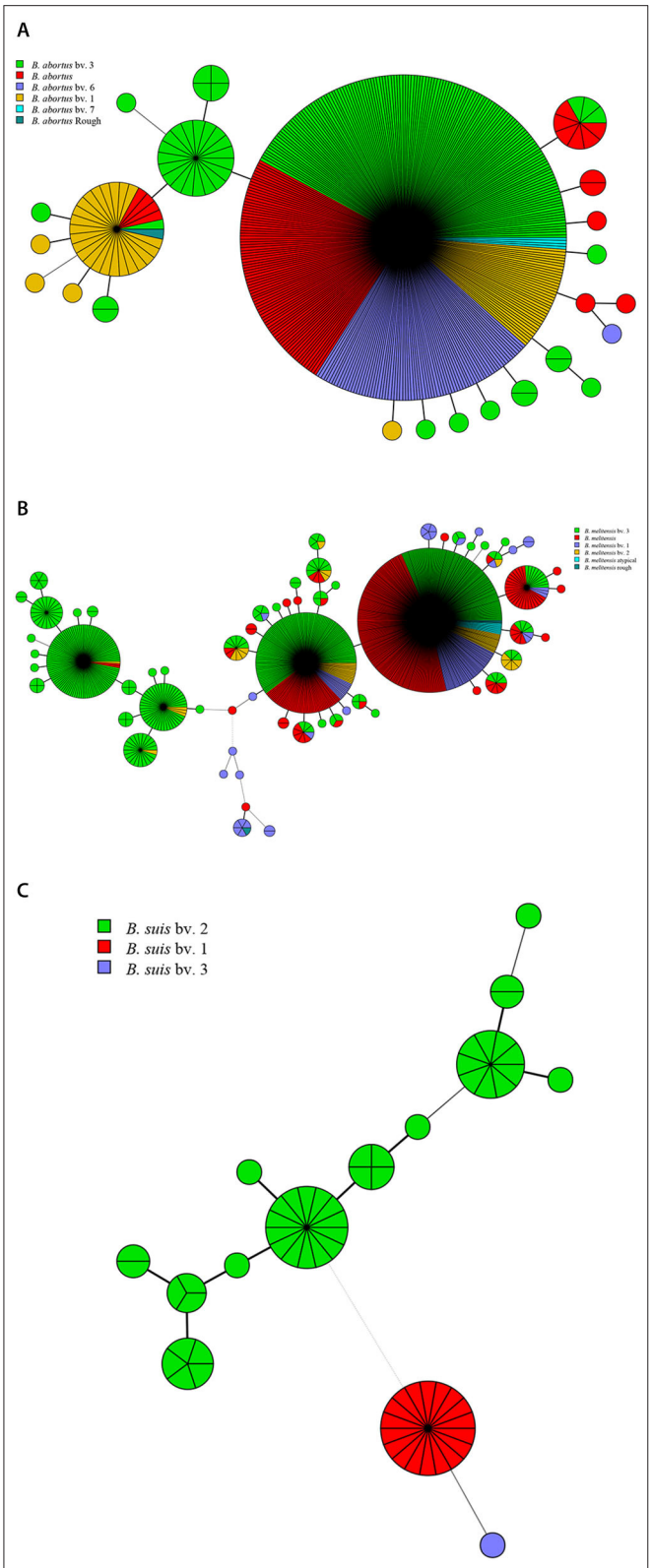

FIGURE 1 | Species/biovars distributed characteristics of *B. abortus* **(A)**, *B. melitensis* **(B)**, and *B. suis* **(C)**. Color coding according to species/biovar; circle size depicts the number of strains.

1, 188 in biovar 3, 79 in biovar 6, four in biovar 7, one in rough strain, and another 98 strains have not been identified (**Figure 1A**). Among the *B. melitensis* strains, 99 strains in biovar 1, 50 strains in biovar 2, 532 strains in biovar 3, five strains in rough, and nine strains were atypical, and 313 strains of unknown biovars were observed (**Figure 1B**). Among the 63 *B. suis* strains, 18 were in biovar 1, 44 in biovar 2, and one in biovar 3 (**Figure 1C**). All three *Brucella* species were observed in China, Germany, and Italy (**Table 1**). Both *B. abortus* and *B. melitensis* were circulating in the remaining seven countries. Five different biotypes were found in *B. melitensis* species; five biotypes were observed in *B. abortus* species, whereas three biotypes were recorded in *B. suis* species. *B. melitensis* was the dominant population in all countries examined, and *B. abortus* biovar 3 and *B. melitensis* biovar 3 were the dominant species in countries along the Silk Road (**Table 1**). *B. suis* biovar 1 was found exclusively in Chinese strains, and *B. suis* biovar 2 was observed in Germany and Italy (**Table 1**).

Host Lineages Profiles of *Brucella* Strains

In this study, a total of 13 kinds of hosts were observed in all of the countries analyzed, including humans, cattle, sheep, camels, buffalo, goats, bharals, dogs, deer, swine, boars, hares, and wild swine, of which 583 strains were found in humans, 448 in cattle, and 363 in sheep (**Table 2**). The hosts of *B. abortus* strains included cattle, sheep, camels, buffalo, and humans, of which 92.0% of strains were collected from cattle (**Figure 2A**). The hosts of *B. melitensis* strains included goats, sheep, cattle, deer, bharals, camels, humans, and dogs. Remarkably, approximately 56.8% (573/1,009) of strains were from humans, and this host was distributed widely in all of the countries; moreover, 35.3% (353/1,009) of the strains were obtained from sheep (**Figure 2B**, **Table 2**). Deer, humans, sheep, swine, boars, hares, and wild swine were common hosts from isolated *B. suis* strains, and 55.6% (35/63) of the strains from Germany and Italy were found in wild swine (**Figure 2C**). However, humans, cattle, and sheep were the main hosts of the *B. suis* strains in China (**Table 2**). The most extensive hosts of *Brucella* in this study were observed in China, followed by Italy, Kazakhstan, and India (**Table 2**).

Geographic Origin and Genetic Relatedness of *B. abortus* Strains

There were 24 MLVA-11 genotypes among *B. abortus* strains (72, 82, 201, and 70 were the most common genotypes). Of these, genotype 72 was overwhelming, accounting for 80.5% (347/431) (**Figure 3A**). Genotype 72 was shared by strains from Kazakhstan, China, Italy, Mongolia, and Turkey. Genotype 210 was shared by Italian and Chinese strains, whereas genotype 82 was shared by strains from Kazakhstan, German, Italy, China, and India (**Figure 3B**). MST analysis of *B. abortus* strains revealed that some MLVA-16 shared genotypes were found in strains from Kazakhstan, Italy, and China. Moreover, in Kazakhstan and China, Kazakhstan and Italy, and Kazakhstan, Italy, and China, a limited number of strains consisted of shared

TABLE 2 | Host profiles of *Brucella* strains in countries along the Silk Road.

Host	China	Kazakhstan	Turkey	Germany	Italy	Iran	Israel	Lebanon	Mongolia	Syria	India
B. abortus	Cattle, humans, ovines	Cattle, camels	Humans	Cattle	Buffalo, cattle, ovines	—	—	—	Cattle	Cattle	Buffalo, human, cattle
B. melitensis	Humans, ovines, deer, bharals, camels, caprines, cattle	Cattle, dogs, humans, ovine	Humans	Humans	Caprines, cattle, humans, ovines	Humans	Ovine, human, cattle	Human	Human	Human, ovine	Ovine, human, caprine
B. suis	Deer, humans, ovines, swine	—	—	Boars, hares, swine	Wild boars	—	—	—	—	—	Human

—, *no data.*

genotypes. In contrast, no shared genotype was found in other countries (**Figure 3C**).

Geographic Origins and Genetic Relatedness of *B. melitensis* Strains

There were 62 MLVA-11 genotypes in 1,009 strains of *B. melitensis*, of which 116, 125, 87, 96, 111, and 91 were the most common genotypes (**Figure 4A**). Among these, genotype 116 was overwhelmingly dominant, accounting for 40.9% (413/1,009), whereas genotypes 125, 87, 96, 111, and 91 accounted for 20.0% (202/1,009), 10.6% (107/1,009), 4.6% (45/1,009), 3.8% (38/1,009), and 2.2% (22/1,009), respectively. Based on the geographic origin, *B. melitensis* genotypes 116, 125, and 111 belong to an Eastern Mediterranean lineage, whereas genotypes 87, 96, 91, and 162 belong to the Western Mediterranean lineage. Genotypes 116, 125, and 111 were shared by strains from 10 countries, except Italy (**Figure 4B**). Genotype 116 was shared by strains from China, Germany, India, Iran, Kazakhstan, Lebanon, Mongolia, Syria, and Turkey, whereas type 125 was shared by strains from nine countries, namely, China, Germany, Iran, Israel, Italy, Kazakhstan, Lebanon, Syria, and Turkey. Otherwise, genotype 111 was observed in China, Kazakhstan, and Turkey. However, genotypes 87, 96, 91, and 162 were found almost exclusively in the Italian strains, and only two strains from Germany were represented in genotype 96 (**Figure 4B**). MST analysis based on MLVA-16 data of *B. melitensis* strains indicated that 1,009 strains of *B. melitensis* were clustered into two groups (A and B). The strains in Italy have formed an independent group A, whereas the other 10 countries' strains were clustered into group B (**Figure 4C**). Multiple shared genotypes in group B were observed in different countries, including China, Kazakhstan, and Turkey; China, Turkey, and Syria; China, Kazakhstan, and Mongolia; China and India; Turkey, Lebanon, and Syria; Turkey and Lebanon; Turkey and Syria; Turkey and India; and Turkey and Iran. The most shared genotypes were observed among the Chinese and Kazakhstan strains (**Figure 4C**).

WGS-SNP Analysis of 39 *B. melitensis* Strains From 14 Countries Along the Silk Road

Phylogenetic analysis based on WGS-SNPs revealed the geographic clustering profile of *B. melitensis* strains from these countries; 39 *B. melitensis* strains were divided into two groups (A and B). Group A included the strains from the Western Mediterranean Region (Italy and Malta) and located at the base of the tree. Group B included the strains from regions of Asia, covering a broad geographic area that could be subdivided into four clades: (I) Middle East (Iran, Iraq, Turkey, Syria), China, and Bulgaria; (II) Turkey, Russia, China, Georgia, and India; (III) China-Russia; (IV) Turkmenistan, Afghanistan, Iran, and Pakistan (**Figure 5**).

Geographical Origin and Genetic Relatedness of *B. suis* Strains

There were 14 MLVA-11 genotypes in 63 strains of *B. suis*, and MLVA-11 genotypes 33, 57, and 44 were predominant, accounting for 28.6% (18/63), 22.2% (14/63), and 7.0% (9/63), respectively; the remaining 11 genotypes contained one to five strains from the respective country (**Figure 6A**). Genotypes 33, 31, 57, and 44 were unique to Chinese, India, German, and Italian strains, respectively (**Figure 6B**). MST analysis based on MLVA-16 data revealed that 63 strains of *B. suis* from Germany, Italy, China, and India formed three independent branches (A–C). The majority of strains from Germany clustered in branch A, and all Italy strains and a few German strains clustered in branch B. Strains from China and India ($n = 1$) were grouped in branch C. No shared MLVA-16 genotypes were found in strains from different countries (**Figure 6C**).

DISCUSSION

Brucellosis is prevalent in Italy, Germany, Turkey, Iran, Kazakhstan, China, and other countries, along with the Silk Road. Moreover, a considerable number of *Brucella* strains

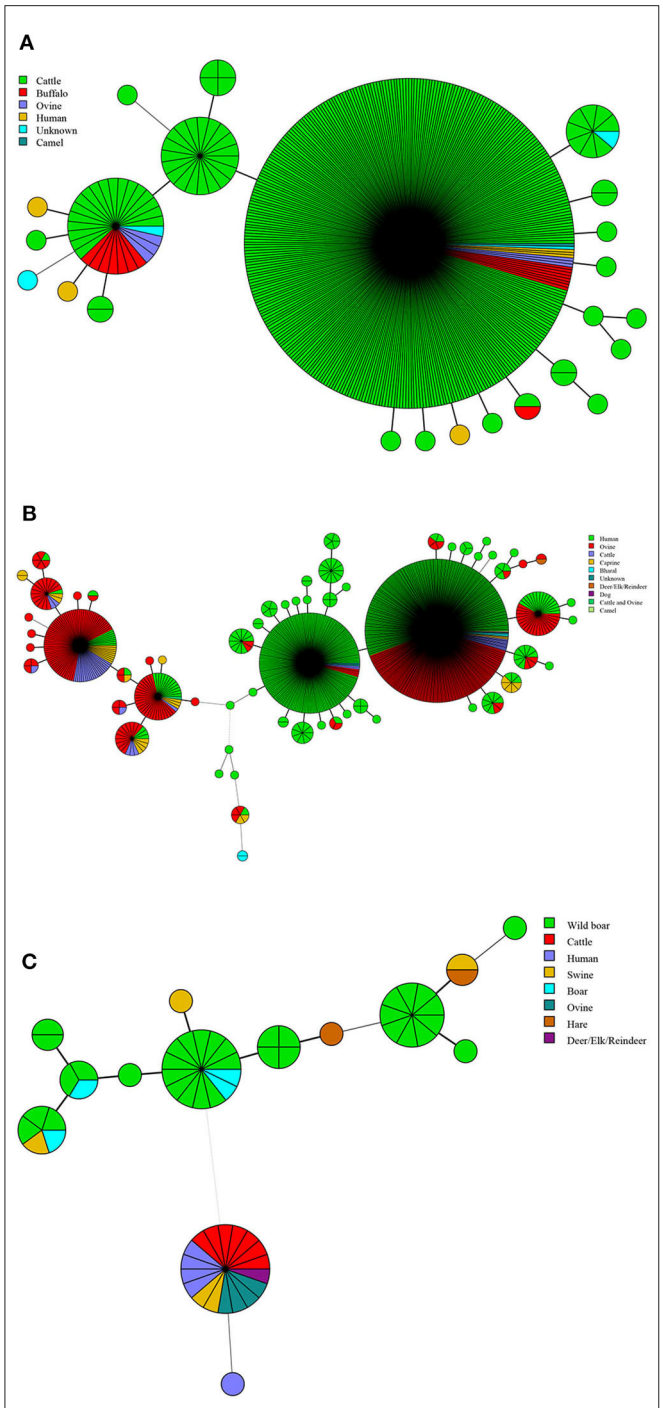

FIGURE 2 | Host lineages profile of *B. abortus* **(A)**, *B. melitensis* **(B)**, and *B. suis* strains **(C)**. Color-coding according to hosts types; circle size depicts the number of strains.

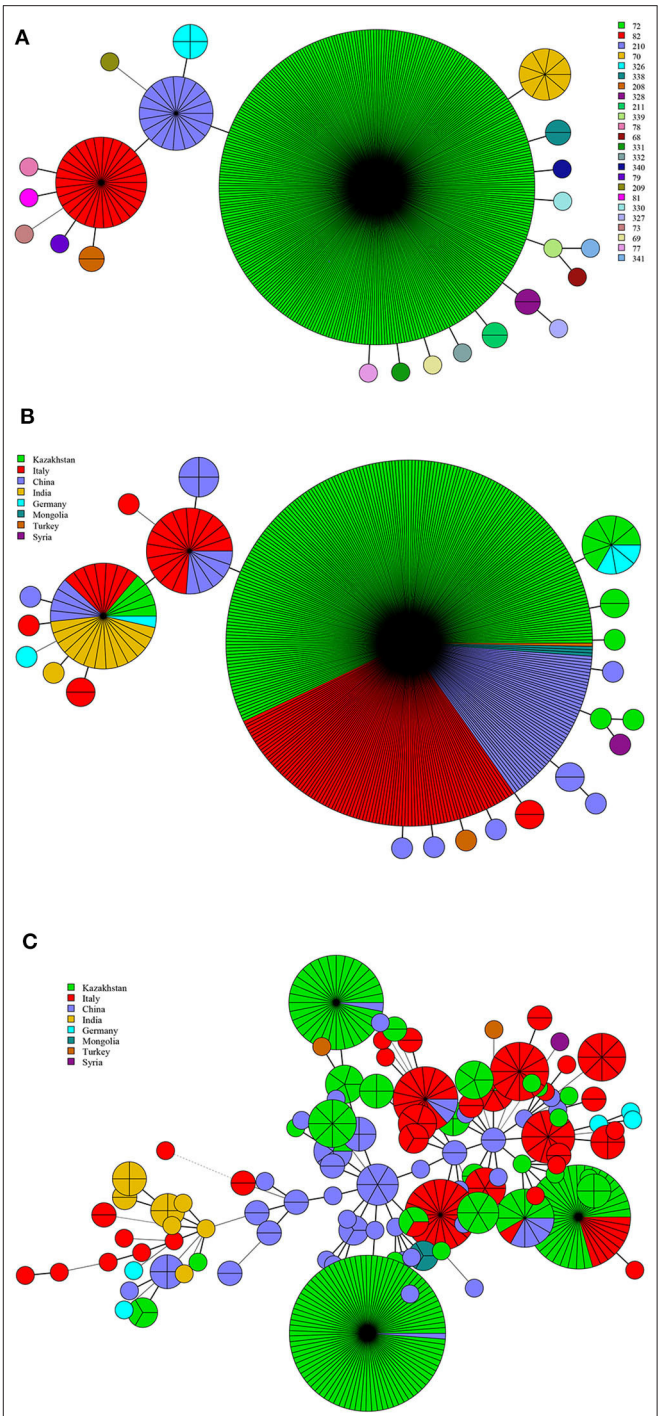

FIGURE 3 | MLVA-11 genotype **(A)**, geographic origin **(B)**, and genetic relatedness characteristics **(C)** of *B. abortus* strains. (Color-coding according to MLVA-11 genotypes **(A,B)** and MLVA-16 genotypes (countries, **C**); circle size depicts the number of strains).

have been isolated, providing a basis for investigation of the genetic correlation characteristics among strains. In this study, *B. abortus*, *B. melitensis* strains, and *B. suis* strains accounted for 28.7% (431/1,503), 67.1% (1,009/1,503), and 4.2% (63/1,503) of the total, respectively. Moreover, *B. melitensis* biovar 3 accounted for 52.9% (534/1,009) of the total. The distribution characteristic of pathogenic bacteria population and *Brucella* biovars was similar to the previous study; *B. melitensis* is the most important zoonotic agent, followed by *B. abortus* and *B. suis* (35, 36). This correlates with the fact that the worldwide control of bovine brucellosis (due to *B. abortus*)

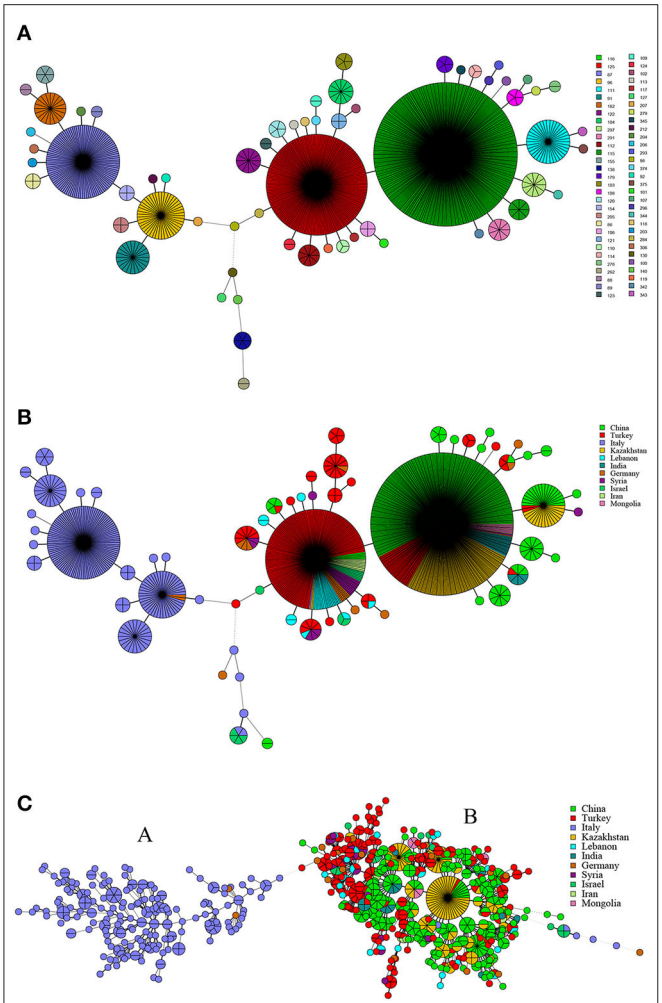

FIGURE 4 | MLVA-11 genotype **(A)**, geographic origin **(B)**, and genetic relatedness characteristics **(C)** of *B. melitensis* strains. (Color-coding according to MLVA-11 genotypes **(A,B)** and MLVA-16 genotypes (countries, **C**); circle size depicts the number of strains).

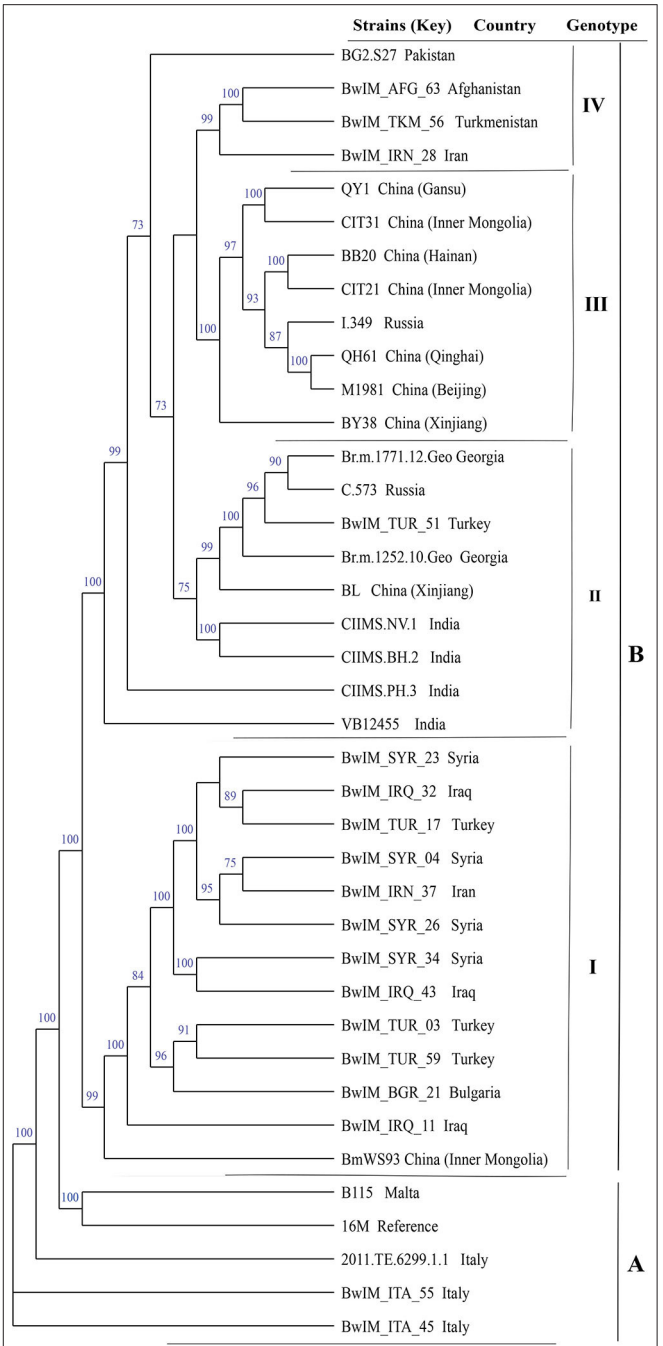

FIGURE 5 | Whole-genome sequencing–single-nucleotide polymorphism phylogenetic analysis of 39 *B. melitensis* strains from 14 countries along the Silk Road.

has been achieved to a greater extent than the control of sheep and goat brucellosis (due to *B. melitensis*), these latter species being the most important domestic animals in many developing countries (17). *B. melitensis* strains were distributed widely in all of the countries examined; 56.8% (573/1,009) strains were obtained from humans, and 35.3% (353/1,009) were from sheep. These data indicated that *B. melitensis* strains are the predominant pathogen responsible for human and animal brucellosis in these countries. These findings suggest that identical or similar epidemiological characteristics of brucellosis might be found in countries along the Silk Road (37). Globally, despite the remarkable results achieved by the majority of industrialized countries, where bovine brucellosis has been eradicated or controlled, small ruminant brucellosis remains a problem in some of these countries (38). Our current study confirmed that *B. melitensis* is a latent "travel bacterium" that continuously spreads and expands from Northern China to Southern China (39). From 1970 to 2015, *B. melitensis* has been the pathogen isolated most frequently in human cases, accounting for more than 99% of *Brucella* spp. isolated from humans in Italy (40). Similarly, the species that causes the most frequent brucellosis and produces the most severe disease picture is *B. melitensis* in Turkey (13). Although 28.7% of total strains were of *B. abortus*, most of them were obtained from cattle, and its pathogenicity to humans was significantly lower than *B. melitensis* strains (17). Moreover, *B. suis* biovar 2 strains in this study were from a wild animal; *B. suis* biovar 1 and biovar 3 from humans and *B. suis* strains were observed in limited

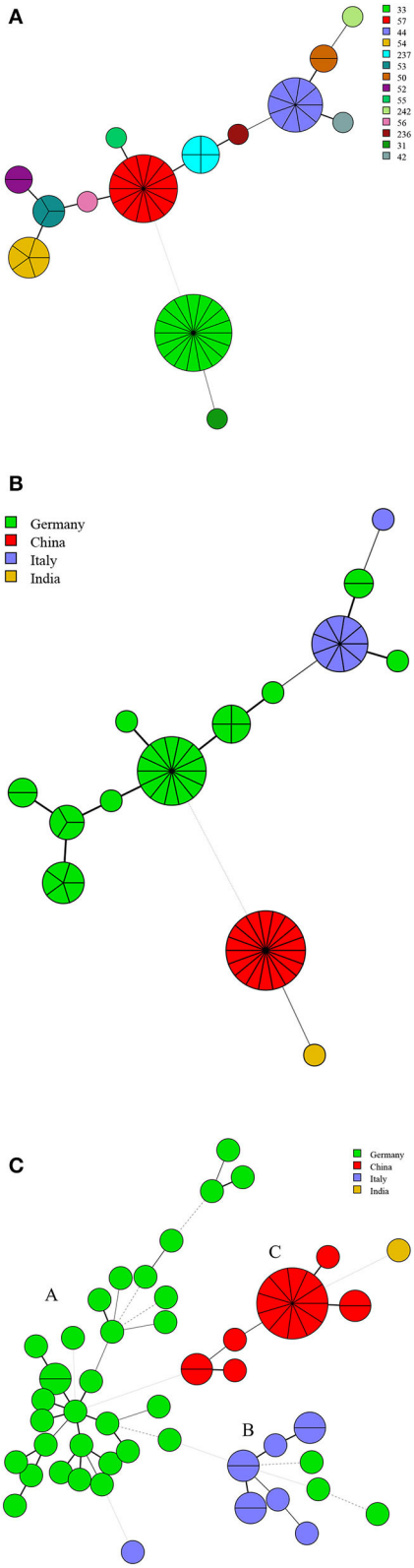

FIGURE 6 | MLVA-11 genotype **(A)**, geographic origin **(B)**, and genetic relatedness characteristics **(C)** of *B. suis* strains. (Color-coding according to MLVA-11 genotypes **(A,B)** and MLVA-16 genotypes (countries, **C**); circle size depicts the number of strains).

countries; fewer strains were isolated from humans, and the *B. suis* biovar 2 is not an essential pathogen for humans in contrast to *B. suis* biovars 1, 3, and 4 (17). Therefore, to solve the brucellosis problem in countries along the Silk Road, we should focus more on the *B. melitensis* strains than *B. abortus* and *B. suis* populations, and it is urgent to strengthen the detection and management of the infected sheep and goats in these countries.

In the present study, *B. abortus* strains and *B. melitensis* strains had a wide host spectrum, including many livestock and wild animals. Some shared genotypes were observed in different hosts among each species, indicating that these wild animals might become a source for reintroducing *Brucella* strains in domestic ruminants and humans (41). *B. abortus* and *B. melitensis* are the most regularly transmitted species between wild and domestic ungulates. They are most frequently associated with the conflicting needs of wildlife and agriculture and the risk of human disease (42). This confirmed the widespread existence and natural epidemic origin of brucellosis in countries along the Silk Road (43, 44), which poses severe challenges to the prevention and surveillance of brucellosis in these countries.

Based on the MLVA-11 analysis of *B. abortus* strains, genotypes 72, 201, 82, and 70 were more common; each of them was shared by strains from two to five countries, especially 72 being the predominant genotype and shared by strains from Kazakhstan, China, Italy, Mongolia, and Turkey. These findings demonstrate that the *B. abortus* strains from these countries have high homogeneity and common geographic origins (45, 46). MST analysis of *B. abortus* strains revealed that there were bovine brucellosis outbreaks in Kazakhstan, Italy, and China, but the number of cases of cross-infection among countries was limited (47). This was not only closely related to the reduction in virulence of *B. abortus* strains, but also restricted by factors such as larger size in cattle, higher transportation costs, and trade policies.

Among the 1,009 *B. melitensis* population, genotypes 116, 125, and 111 originated from the Eastern Mediterranean lineage, and genotypes 87, 96, and 91 originated from Western Mediterranean lineage. These findings demonstrate that the *B. melitensis* strains from countries along the Silk Road have two different geographical origins. The strains from Italy originated from a Western Mediterranean lineage, and strains from the other 10 countries originated from an Eastern Mediterranean lineage. Moreover, genotypes 116, 125, and 111 were shared by strains from nine, nine, and three countries, respectively, indicating that the strains from these countries had the same geographical origin. This suggests that the introduction and reintroduction of the disease among the 10 countries might have occurred in the past (48, 49). Based on MST analysis revealed that *B. melitensis* strains clustered into two groups, with strains in Italy forming a relatively independent group A, whereas strains in the remaining 10 countries clustered into group B. In addition, there were at least 10 shared MLVA-16 genotypes in strains from group B. The most shared genotypes were formed in strains from China, Kazakhstan, and Turkey. It was previously suggested that *B. melitensis* strains in China, Turkey, and Kazakhstan were epidemiologically correlated, and the prevalence of *B. melitensis* brucellosis in these countries resulted from a common infectious source (16, 50, 51). The breeding and trade of small ruminants

were the main economic source and industrial pillar of the vast agricultural and pastoral areas in Turkey, Kazakhstan, and China, and animal introduction and trade were extremely frequent in these countries. The results were consistent with those of previous studies that showed the majority of *B. melitensis* strains in Kazakhstan were genetically related to strains transmitted in China and were closely related to the long-term trading partnership between the two countries (52). Therefore, WGS-SNP analysis indicated that *B. melitensis* were originated from Malta (Italy) regions, strains from group B forming the four subclades, but do not have a clear differentiation according to their territorial affiliation, indicating the frequent penetration of the *B. melitensis* strains from one country to another (53). Active exchange and trade of animals (sheep and goats) among these countries could promote pathogen dissemination, and there was continuous expansion and spread in countries along with Silk Road. Recently, many infectious diseases have emerged, and most of their pathogens originated from zoonosis; some of the diseases spread worldwide by the international flow of goods, people, and animals (54). We suggest that implementing a larger scale of vaccine coverage of small ruminants would significantly reduce infection in livestock and humans. Moreover, restricting movement in positive sheep and goats among different countries and the regular disinfection of the farm environments could effectively reverse the trend of increasing brucellosis in countries along the Silk Road.

B. suis strains in Germany, China, Italy, and India represent a unique predominated genotype, respectively, suggesting that each of these strains had an exclusive geographic origin. MST analysis revealed that MLVA-16 shared genotypes were not found in different countries' strains, demonstrating that *B. suis* strains were only prevalent in their respective countries. This was possibly related to environmental adaptability and economic and social factors influencing hosts of *B. suis* strains. *B. suis* biovar 2 is largely restricted to continental Europe and is maintained in wild animal (*Suidae* and hares) populations (40). We suggest that enhanced surveillance regulation for wild animals in Europe is essential for the prevention of strain spill over into the livestock. Moreover, further genome comparison analysis of more *B. suis* strains from all over the world will increase our understanding of *B. suis* brucellosis epidemiology.

Our research has some limitations. Most of the data were derived from highly concentrated time and location, rather than from continuous time points and wide coverage areas, so they may only partly reflect the truth situation of brucellosis in the regions examined. Second, data on animals' epidemiology and movements in these countries were not available. A focus on risk analysis or statistical analysis of hosts from the spatiotemporal or species-location perspective is essential.

CONCLUSION

In this study, the species distribution, host lineage profiles, geographical origin, and genetic relatedness and the epidemiological correlation of *Brucella* species in countries along the Silk Road were discussed. *B. abortus* was found to share the same geographic origin, but the transmission area was limited to their respective countries. However, *B. melitensis* strains were the dominant population in these countries and had two main geographic origins, and strains from the same geographic origin showed extensive gene sharing. *B. suis* strains from respective countries showed unique geographic origins and epidemiological characteristics. The surveillance and control of *B. melitensis* strains were identified as major problems among *Brucella* species in countries along the Silk Road. The control of its main host (sheep and goat) should be strengthened. Effective vaccination limits *Brucella* infection, restricts shedding, hampers transmission from animal to animal, and diminishes zoonosis risk (55). The corresponding regulations should be strictly implemented when introducing animals to prevent the spread of this species. Moreover, improving scientific research to achieve early diagnosis and implement joint prevention and control is recommended.

DATA AVAILABILITY STATEMENT

All of the data generated or analyzed during this study are included in this published article, and the supplementary information files will be freely available to any scientist wishing to use them for non-commercial purposes upon request via e-mail with the corresponding author.

AUTHOR CONTRIBUTIONS

ZhiL performed strain download, MLVA typing and cluster analysis. CW drafted the manuscript. KW, HW, MW, ZZ and DL conducted data processing. ZheL and ZhiL participated in design of the study and critically reviewed the manuscript and ZheL managed the project. QW revised the manuscript critically. All authors have read and approved the final manuscript.

FUNDING

This study was supported by the National Key R&D Program of China (Grant Numbers 2018ZX10734404, 2018ZX10734401, and 2017ZX10303401), the Nature Science Fund of Inner Mongolia Autonomous Region (Grant Number 2018MS08004), and the National Science and Technology Major Project on Important Infectious Diseases Prevention and Control (Grant Number 2018ZX10734404). The funders played no role in study design, data collection, analysis, decision to publish, or manuscript preparation.

ACKNOWLEDGMENTS

The authors thank all the staff of MLVAbank for the data collected and standardized during *Brucella* genotyping. The authors also thank Accdon (www.accdon.com) for linguistic assistance during the preparation of this manuscript.

SUPPLEMENTARY MATERIAL

The Supplementary Material for this article can be found online at: https://www.frontiersin.org/articles/10.3389/fvets.2020.539444/full#supplementary-material

REFERENCES

1. Pappas G, Papadimitriou P, Akritidis N, Christou L, Tsianos EV. The new global map of human brucellosis. *Lancet Infect Dis.* (2006) 6:91–9. doi: 10.1016/S1473-3099(06)70382-6
2. Esmaeilnejad-Ganji SM, Esmaeilnejad-Ganji SMR. Osteoarticular manifestations of human brucellosis: a review. *World J Orthop.* (2019) 10:54–62. doi: 10.5312/wjo.v10.i2.54
3. Ahmed W, Zheng K, Liu ZF. Establishment of chronic infection: brucella's stealth strategy. *Front Cell Infect Microbiol.* (2016) 6:30. doi: 10.3389/fcimb.2016.00030
4. Mcelwain TF, Thumbi SM. Animal pathogens and their impact on animal health, the economy, food security, food safety and public health. *Rev Sci Tech.* (2017) 36:423–433. doi: 10.20506/rst.36.2.2663
5. Al Dahouk S, Nöckler K. Implications of laboratory diagnosis on brucellosis therapy. *Expert Rev Anti Infect Ther.* (2011) 9:833–45. doi: 10.1586/eri.11.55
6. Kang SI, Her M, Erdenebaatar J, Vanaabaatar B, Cho H, Sung SR, et al. Molecular epidemiological investigation of *Brucella melitensis* circulating in Mongolia by MLVA16. *Comp Immunol Microbiol Infect Dis.* (2017) 50:16–22. doi: 10.1016/j.cimid.2016.11.003
7. Yang H, Zhang S, Wang T, Zhao C, Zhang X, Hu J, et al. Epidemiological characteristics and spatiotemporal trend analysis of human brucellosis in China, 1950-2018. *Int J Environ Res. Public Health.* (2020) 17:82. doi: 10.3390/ijerph17072382
8. Shevtsova E, Vergnaud G, Shevtsov A, Shustov A, Berdimuratova K, Mukanov K, et al. Genetic diversity of *Brucella melitensis* in Kazakhstan in relation to world-wide diversity. *Front Microbiol.* (2019) 10:1897. doi: 10.3389/fmicb.2019.01897
9. Niaz S, Raqeeb A, Khan A, Nasreen, A.mir S, Zhu L, et al. Status of human brucellosis in district Malakand, Khyber Pakhtunkhwa, Pakistan. *J Infect Public Health.* (2020) doi: 10.1016/j.jiph.2019.12.013
10. Behera SK, Das D, Balasubramani K, Chellappan S, Rajaram K, Kumar Mohanta H, et al. P. Seroprevalence and risk factors of brucellosis in livestock in the wildlife and livestock interface area of Similipal Biosphere Reserve, India. *Vet World.* (2020) 13:465–70. doi: 10.14202/vetworld.2020.465-470
11. Denisov AA, Sclyarov OD, Salmakov KM, Shumilov KV. The Russian experience in brucellosis veterinary public health. *Rev Off Int Epizoot.* (2013) 32:229–37. doi: 10.20506/rst.32.1.2199
12. Kutlu M, Ergonul O, Sayin-Kutlu S, Guven T, Ustun C, Alp-Cavus S, et al. Risk factors for occupational brucellosis among veterinary personnel in Turkey. *Prev Vet Med.* (2014) 117:52–8. doi: 10.1016/j.prevetmed.2014.07.010
13. Denk A, Demirdag K, Kalkan A, Ozden M, Cetinkaya B, Kilic SS. In vitro activity of Brucella melitensis isolates to various antimicrobials in Turkey. *Infect Dis.* (2015) 47:364–9. doi: 10.3109/00365548.2014.988748
14. Gül S, Satilmi,ş OK, Ozturk B, Gökçe MI, Kuscu F. Seroprevalence of brucellosis among children in the Middle Anatolia Region of Turkey. *J Health Popul Nutr.* (2014) 32:577–9.
15. Montagnaro S, D'ambrosi F, Petruccelli A, Ferrara G, D'alessio N, Iovane V, et al. A serological survey of brucellosis in eurasian wild boar (Sus scrofa) in campania Region, Italy. *J Wildl Dis.* (2020) 56:424–8. doi: 10.7589/2019-04-095
16. Georgi E, Walter MC, Pfalzgraf MT, Northoff BH, Holdt LM, Scholz HC, et al. Whole genome sequencing of *Brucella melitensis* isolated from 57 patients in Germany reveals high diversity in strains from Middle East. *PLoS ONE.* (2017) 12:e0175425. doi: 10.1371/journal.pone.0175425
17. Godfroid J, Cloeckaert A, Liautard JP, Kohler S, Fretin D, Walravens K, et al. From the discovery of the Malta fever's agent to the discovery of a marine mammal reservoir, brucellosis has continuously been a re-emerging zoonosis. *Vet. Res.* (2005) 36:313–326. doi: 10.1051/vetres:2005003
18. Acharya KP. Brucellosis in Nepal - a potential threat to public health professionals. *Curr Health Sci J.* (2016) 42:396–407. doi: 10.12865/CHSJ.42.04.10
19. Simonson TS, Okinaka RT, Wang B, Easterday WR, Huynh L, U'ren JM, et al. Bacillus anthracis in China and its relationship to worldwide lineages. *BMC Microbiol.* (2009) 9:71. doi: 10.1186/1471-2180-9-71
20. Cui Y, Yu C, Yan Y, Li D, Li Y, Jombart T, et al. Historical variations in mutation rate in an epidemic pathogen, Yersinia pestis. *Proc Natl Acad Sci USA.* (2013) 110:577–582. doi: 10.1073/pnas.1205750110
21. Al Dahouk S, Neubauer H, Hensel A, Schoneberg I, Nockler K, Alpers K, et al. Changing epidemiology of human brucellosis, Germany, 1962-2005. *Emerg Infect Dis.* (2007) 13:1895–900. doi: 10.3201/eid1312.070527
22. Yumuk Z, O'callaghan D. Brucellosis in Turkey – an overview. *Int J Infect Dis.* (2012) 16:e228–35. doi: 10.1016/j.ijid.2011.12.011
23. Beauvais W, Coker R, Nurtazina G, Guitian J. Policies and livestock systems driving brucellosis re-emergence in Kazakhstan. *Ecohealth.* (2017) 14:399–407. doi: 10.1007/s10393-015-1030-7
24. Garofolo G, Di Giannatale E, Platone I, Zilli K, Sacchini L, Abass A, et al. Origins and global context of *Brucella abortus* in Italy. *BMC Microbiol.* (2017) 17:28. doi: 10.1186/s12866-017-0939-0
25. Golshani M, Buozari S. A review of brucellosis in Iran: epidemiology, risk factors, diagnosis, control, and prevention. *Iran Biomed J.* (2017) 21:349–59. doi: 10.18869/acadpub.ibj.21.6.349
26. Wareth G, El-Diasty M, Melzer F, Schmoock G, Moustafa SA, El-Beskawy M, et al. MLVA-16 genotyping of *Brucella abortus* and *Brucella melitensis* isolates from different animal species in Egypt: geographical relatedness and the mediterranean lineage. *Pathogens.* (2020) 9:498. doi: 10.3390/pathogens9060498
27. Liu ZG, Wang LJ, Piao DR, Wang M, Liu RH, Zhao HY, et al. Molecular investigation of the transmission pattern of *Brucella suis* 3 from inner Mongolia, China. *Front Vet Sci.* (2018) 5:271. doi: 10.3389/fvets.2018.00271
28. Alton GG, Jones LM, Angus RD, Verger JM. *Techniques for the Brucellosis Laboratory*. (1988).
29. Baily GG, Krahn JB, Drasar BS, Stoker NG. Detection of *Brucella melitensis* and *Brucella abortus* by DNA amplification. *J Trop Med Hyg.* (1992) 95:271.
30. Bricker BJ, Halling SM. Differentiation of *Brucella abortus* bv. 1, 2, and 4, *Brucella melitensis*, *Brucella ovis*, and *Brucella suis* bv. 1 by PCR. *J Clin Microbiol.* (1994) 32:2660–6. doi: 10.1128/JCM.32.11.2660-2666.1994
31. Ledwaba MB, Gomo C, Lekota KE, Le Flèche P, Hassim A, Vergnaud G, et al. H. Molecular characterization of *Brucella species* from Zimbabwe. *PLoS Negl Trop Dis.* (2019) 13:e0007311. doi: 10.1371/journal.pntd.0007311
32. Le Flèche P, Jacques I, Grayon M, Al Dahouk S, Bouchon P, Denoeud F, et al. Evaluation and selection of tandem repeat loci for a Brucella MLVA typing assay. *BMC Microbiol.* (2006) 6:9. doi: 10.1186/1471-2180-6-9
33. Liu ZG, Di DD, Wang M, Liu RH, Zhao HY, Piao DR, et al. (2017) MLVA genotyping characteristics of human *Brucella melitensis* isolated from Ulanqab of inner mongolia China. *Front Microbiol.* 8:6. doi: 10.3389/fmicb.2017.00006
34. Li Z, Wang XM, Zhu X, Wang M, Cheng H, Li D, et al. Molecular characteristics of brucella isolates collected from humans in Hainan Province, China. *Front Microbiol.* (2020) 11:452. doi: 10.3389/fmicb.2020.00452
35. Deqiu S, Donglou X, Jiming Y. Epidemiology and control of brucellosis in China. *Vet Microbiol.* (2002) 90:165–182. doi: 10.1016/S0378-1135(02)00252-3
36. Lim JS, Min KD, Ryu S, Hwang SS, Cho SI. Spatial analysis to assess the relationship between human and bovine brucellosis in South Korea, 2005-2010. *Sci Rep.* (2019) 9:6657. doi: 10.1038/s41598-019-43043-7
37. Tan KK, Tan YC, Chang LY, Lee KW, Nore SS, Yee WY, et al. Full genome SNP-based phylogenetic analysis reveals the origin and global spread of Brucella melitensis. *BMC Genom.* (2015) 16:93. doi: 10.1186/s12864-015-1294-x
38. Madut NA, Muwonge A, Nasinyama GW, Muma JB, Godfroid J, Jubara AS, et al. The sero-prevalence of brucellosis in cattle and their herders in Bahr el Ghazal region, South Sudan. *PLoS Negl Trop Dis.* (2018) 12:e0006456. doi: 10.1371/journal.pntd.0006456
39. Zhu X, Zhao Z, Ma S, Guo Z, Wang M, Li Z, et al. Brucella melitensis, a latent "travel bacterium," continual spread and expansion from Northern to Southern China and its relationship to worldwide lineages. *Emerg Microbes Infect.* (2020) 9:1618–27. doi: 10.1080/22221751.2020.1788995
40. De Massis F, Zilli K, Di Donato G, Nuvoloni R, Pelini S, Sacchini L, et al. Distribution of Brucella field strains isolated from livestock, wildlife populations, and humans in Italy from 2007 to 2015. *PLoS ONE.* (2019) 14:e0213689. doi: 10.1371/journal.pone.0213689

41. Mailles A, Rautureau S, Le Horgne JM, Poignet-Leroux B, D'arnoux C, Dennetière G, et al. Re-emergence of brucellosis in cattle in France and risk for human health. *Euro Surveill.* (2012) 17:20227.
42. Bengis RG, Leighton FA, Fischer JR, Artois M, Mörner T, Tate CM. The role of wildlife in emerging and re-emerging zoonoses. *Rev Sci Tech.* (2004) 23:497–511. doi: 10.20506/rst.23.2.1498
43. Freeman BA, Pearson GR, Hines WD. Host-parasite relationships in brucellosis. 3. behavior of avirulent Brucella in tissue culture monocytes. *J Infect Dis.* (1964) 114:441–9. doi: 10.1093/infdis/114.5.441
44. Vered O, Simon-Tuval T, Yagupsky P, Malul M, Cicurel A, Davidovitch N. The price of a neglected zoonosis: case-control study to estimate healthcare utilization costs of human brucellosis. *PLoS ONE.* (2015) 10:e0145086. doi: 10.1371/journal.pone.0145086
45. Shevtsova E, Shevtsov A, Mukanov K, Filipenko M, Kamalova D, Sytnik I, et al. Epidemiology of Brucellosis and Genetic Diversity of Brucella abortus in Kazakhstan. *PLoS ONE.* (2016) 11:e0167496. doi: 10.1371/journal.pone.0167496
46. Sun MJ, Di DD, Li Y, Zhang ZC, Yan H, Tian LL, et al. Genotyping of *Brucella melitensis* and *Brucella abortus* strains currently circulating in Xinjiang, China. *Infect Genet Evol.* (2016) 44:522–529. doi: 10.1016/j.meegid.2016.07.025
47. Ma SY, Liu ZG, Zhu X, Zhao ZZ, Guo ZW, Wang M, et al. Molecular epidemiology of *Brucella abortus* strains from cattle in Inner Mongolia, China. *Prev Vet Med.* (2020) 183:105080. doi: 10.1016/j.prevetmed.2020.105080
48. Garofolo G, Sacchini F, Ancora M, Travaglini D, Tittarelli M. Multiple-locus variable-number tandem repeat analysis (MLVA) of *Brucella melitensis* strains isolated in Italy, Greece and Israel. In: *International Research Conference Including the 67th Annual Brucellosis Research Meeting*, Berlin (2014).
49. Vergnaud G, Hauck Y, Christiany D, Daoud B, Pourcel C, Jacques I, et al. Genotypic expansion within the population structure of classical brucella species revealed by MLVA16 typing of 1404 brucella isolates from different animal and geographic origins, 1974-2006. *Front Microbiol.* (2018) 9:1545. doi: 10.3389/fmicb.2018.01545
50. Tappe D, Melzer F, Schmoock G, Elschner M, Lam TT, Abele-Horn M, et al. Isolation of *Brucella melitensis* biotype 3 from epidural empyema in a Bosnian immigrant in Germany. *J Med Microbiol.* (2012) 61:1335–7. doi: 10.1099/jmm.0.038612-0
51. Shevtsov A, Ramanculov E, Shevtsova E, Kairzhanova A, Tarlykov P, Filipenko M, et al. Genetic diversity of *Brucella abortus* and *Brucella melitensis* in Kazakhstan using MLVA-16. *Infect Genet Evol.* (2015) 34:173–80. doi: 10.1016/j.meegid.2015.07.008
52. Daugaliyeva Capital A, C., Sultanov A, Usserbayev B, Baramova S, Modesto P, et al. Genotyping of *Brucella melitensis* and *Brucella abortus* strains in Kazakhstan using MLVA-15. *Infect Genet Evol.* (2018) 58:135–44. doi: 10.1016/j.meegid.2017.12.022
53. Pisarenko SV, Kovalev DA, Volynkina AS, Ponomarenko DG, Rusanova DV, Zharinova NV, et al. Global evolution and phylogeography of *Brucella melitensis* strains. *BMC Genomics.* (2018) 19:353. doi: 10.1186/s12864-018-4762-2
54. Maeda K. Globalization and zoonosis. *Nihon Rinsho.* (2016) 74:1948–1955.
55. Moreno E. Retrospective and prospective perspectives on zoonotic brucellosis. *Front Microbiol.* (2014) 5:213. doi: 10.3389/fmicb.2014.00213

Conflict of Interest: The authors declare that the research was conducted in the absence of any commercial or financial relationships that could be construed as a potential conflict of interest.

frontiers in Veterinary Science

ORIGINAL RESEARCH
published: 16 February 2021
doi: 10.3389/fvets.2021.639141

Comparison of Host Cytokine Response in Piglets Infected With Toxigenic and Non-toxigenic *Staphylococcus hyicus*

Yan Li[1,2,3,4], *Hongchao Gou*[1,2,3,4], *Pinpin Chu*[1,2,3,4], *Kunli Zhang*[1,2,3,4], *Zhiyong Jiang*[1,2,3,4], *Rujian Cai*[1,2,3,4], *Shuai Song*[1,2,3,4], *Zhibiao Bian*[1,2,3,4] *and Chunling Li*[1,2,3,4]*

[1] *Institute of Animal Health, Guangdong Academy of Agricultural Sciences, Guangzhou, China,* [2] *Guangdong Provincial Key Laboratory of Livestock Disease Prevention, Guangzhou, China,* [3] *Guangdong Open Laboratory of Veterinary Public Health, Guangzhou, China,* [4] *Scientific Observation and Experiment Station of Veterinary Drugs and Diagnostic Techniques of Guangdong Province, Guangzhou, China*

OPEN ACCESS

Edited by:
Feng Li,
South Dakota State University, United States

Reviewed by:
Jinping Chen,
Guangdong Academy of Science (CAS), China
Mohanned Naif Alhussien,
National Dairy Research Institute (ICAR), India

***Correspondence:**
Chunling Li
lclcare@163.com

Specialty section:
This article was submitted to Veterinary Infectious Diseases, a section of the journal Frontiers in Veterinary Science

Received: *08 December 2020*
Accepted: *26 January 2021*
Published: *16 February 2021*

Citation:
Li Y, Gou H, Chu P, Zhang K, Jiang Z, Cai R, Song S, Bian Z and Li C (2021) Comparison of Host Cytokine Response in Piglets Infected With Toxigenic and Non-toxigenic Staphylococcus hyicus. Front. Vet. Sci. 8:639141. doi: 10.3389/fvets.2021.639141

Staphylococcus hyicus is the most common causative agent of exudative epidermitis (EE) in piglets. *Staphylococcus hyicus* can be grouped into toxigenic and non-toxigenic strains based on its ability to cause EE in pigs. However, the inflammatory response of piglets infected with toxigenic and non-toxigenic *S. hyicus* has not been elucidated. In this study, we evaluated the serum cytokine profile in piglets inoculated with toxigenic and non-toxigenic *S. hyicus* strains and recorded the clinical signs in piglets. Fifteen piglets were divided into three groups ($n = 5$) and inoculated with a toxigenic strain (ZC-4), a non-toxigenic strain (CF-1), and PBS (control), respectively. The changes in serum levels of cytokines (interleukin [IL]-1β, IL-4, IL-6, IL-8, IL-10, IL-12, granulocyte-macrophage colony-stimulating factor, interferon-γ, transforming growth factor-β1, and tumor necrosis factor-α) were evaluated using a cytokine array at 6, 24, 48, and 72 h post inoculation. The results showed that piglets infected with the toxigenic strain exhibited more severe clinical signs and higher mortality than those infected with the non-toxigenic strain. The serum levels of pro-inflammatory cytokine IL-1β were significantly increased in toxigenic-and non-toxigenic-strain-infected piglets compared to those in the control group ($p < 0.05$), while the anti-inflammatory cytokine IL-10 was significantly up-regulated only in toxigenic group than in control group ($p < 0.05$). These results indicated that piglets infected with toxigenic and non-toxigenic *S. hyicus* showed differential infection status and inflammatory responses. Both toxigenic- and non-toxigenic- *S. hyicus* infection could induce a pro-inflammatory reaction in piglets. In addition, the toxigenic strain induced a strong anti-inflammatory response in piglets as indicated by the increased serum level of IL-10, which may be associated with the severe clinical signs and increased mortality and may be the key cytokine response responsible for pathogenic mechanisms of *S. hyicus*.

Keywords: *Staphylococcus hyicus*, toxigenic and atoxigenic, cytokine response, interleukin-10, pathogenicity

INTRODUCTION

Staphylococcus hyicus, a gram-positive bacterium, is one of the major opportunistic and zoonotic pathogens causing exudative epidermitis (EE) in pigs, primarily suckling and newly weaned piglets (1, 2). Exudative epidermitis is characterized by exfoliation of the skin; a thick, greasy, brown greasy exudate (3); suppurative pneumonia; and sepsis (4), which may lead to dehydration and subsequent death (5). Remarkably, a strain of *S. hyicus* was isolated from the blood culture and bone from a man suffering from debilitating subacute lumbar pain (6). Previous studies indicate that exfoliative toxin is the main virulence factor that induces the disease (7, 8). According to its ability to induce EE and to produce exfoliative toxin, *S. hyicus* has been divided into toxigenic and non-toxigenic strains (8, 9). At least five exfoliative toxins, named SHETB (10), ExhA, ExhB, ExhC, and ExhD (11) have been described. The exfoliative toxins selectively digested porcine desmoglein 1 directly in the porcine epidermis, causing separation of cells in the stratum spinosum and rapid intraepidermal spread of organisms (12).

Cytokines are a group of small, secretory proteins that mediate a variety of immunomodulatory and inflammatory responses (13, 14). It is well-known that inflammatory cytokines, including pro-inflammatory cytokines [e.g., interleukin (IL)-1β, IL-6, IL-8, tumor necrosis factor alpha (TNF-α), chemokine, interferons] and anti-inflammatory cytokines (e.g., IL-4, IL-6, IL-10, and IL-13) play significant roles in the inflammatory responses to infections. Many studies have demonstrated the key role of cytokines in the occurrence, development, and prevalence of infectious diseases (15–17).

The study of cytokine expression characteristics in *S. hyicus* infection is significant for understanding the inflammatory response and the pathogenic mechanism of *S. hyicus* and may facilitate efficient treatment in *S. hyicus* infection. To date, there are no reports on the cytokine response in piglets infected with *S. hyicus*. Thus, in the present study, we investigated the expression of 10 serum cytokines [IL-1β, IL-4, IL-6, IL-8, IL-10, IL-12, granulocyte-macrophage colony-stimulating factor (GM-CSF), interferon (IFN)-γ, transforming growth factor (TGF)-β1, and TNF-α] in piglets infected with toxigenic and non-toxigenic *S. hyicus*.

MATERIALS AND METHODS

Bacteria

A toxigenic *S. hyicus* strain, ZC-4 (GenBank no. JQ728535), carrying exfoliative toxin ExhA was isolated in Guangdong Province, China, in 2010. A non-toxigenic *S. hyicus* strain, CF-1 (GenBank no. JQ728492), carrying no exfoliative toxin was isolated in Guangdong Province, China, in 2011.

Animals and Experimental Design

Fifteen, 25-day-old, *S. hyicus*-free piglets were obtained from a farm in Guangzhou and randomly divided into three groups with five piglets per group. The piglets in the toxigenic and non-toxigenic groups were intramuscularly injected in the neck with *S. hyicus* ZC-4 and CF-1, respectively, at a dose of 9.0×10^9 CFU per piglet. The piglets in the control group were intramuscularly injected with 2 mL of phosphate buffered saline (PBS). The animals were kept in separate rooms.

All animal procedures were approved by the Ethics Committee of Institute of Animal Health, Guangdong Academy of Agricultural Sciences according to Guangdong Province Laboratory Animal Management Regulations. The license number was SYXK (Yue) 2016-0165.

Clinical and Pathological Examination

The piglets were monitored at 6, 24, 48, and 72 h and 1 week post inoculation for clinical signs, including rectal temperature, and any clinical signs were scored. At 6, 24, 48, and 72 h after inoculation, blood and serum samples were collected for cytokine analysis. For histological examination, samples of lung, lymph nodes, spleen, kidney, liver, and skin were collected at 72 h post inoculation, fixed in 10% formalin solution, routinely processed, and embedded in paraffin wax; tissue sections were stained with hematoxylin and eosin (HE) as previously described. Moreover, heart and lung samples of the inoculated piglets were collected for the examination of bacterial presence using gram staining, biochemical properties and PCR amplification of the 16S rRNA gene in the toxigenic and non-toxigenic groups and *ExhA* gene in the toxigenic group.

Bacterial Isolation, Morphology, and Biochemical Characteristics

Heart and lung samples of the infected piglets were collected aseptically for bacterial isolation and cultured on LB agar plates containing 5 % sheep red blood cells at 37°C for 18 h. Gram staining was performed using the following protocol: a single colony was placed in a drop of physiological saline on a glass slide, and the specimen was fixed carefully by passing the slide through a flame. Then, the slide was flooded with ammonium oxalate crystal violet for 1 min and then washed with water. The slide was flooded with iodine solution for 1 min followed by flooding with ethanol for 30 s. The slide was treated with sand yellow solution for 1 min, washed with water, and then air-dried. Finally, the slide was observed under the light microscope. Biochemical properties were characterized using the commercial kit from Hangzhou Microbiological Reagents Limited Company (Hangzhou, China) following the manufacturer's instructions.

PCR Amplification of 16S rRNA and Exfoliative Toxin Gene

Bacterial DNA was extracted from pure culture of the heart and lung of piglets infected and identified as *S. hyicus* using QIAGEN DNeasy Blood and Tissue Kit (Qiagen, Basel, CH) according to the manufacturer's protocol. PCR amplification of 16S rRNA and exfoliative toxin gene was performed using the following primers: 16S rRNA-F (5′-AGAGTTTGATCCTGG CTTAG-3′); 16S rRNA-R (5′-TGACGGGCGGTGTGTACAA-3′). ExhA-F (5′-ATAGAGGAGAAATCAACATG-3′); ExhA-R (5′-CTATAGTTACTTGACCTCTA -3′).

In brief, the reaction mixture (final volume 20 μL) contained 10 μL of 2×Taq Master Mix, 0.5 μM of forward and reverse

primer, and 1 μL of template DNA. The thermal cycling consisted of an initial denaturation step at 94°C for 5 min; followed by 35 cycles at 94°C for 1 min, 56°C for 1 min, and 72°C for 90 s; and a final extension step at 72°C for 10 min.

Cytokine Analysis

Serum levels of GM-CSF, IL-1β, IL-6, IL-10, TGF-β1, IFNγ, IL-4, IL-8, IL-12p40, and TNF-α in piglets were measured using the RayBiotech porcine cytokine array Q1 (QAP-CYT-1-1, RayBiotech, Norcross, GA, USA) according to the manufacturer's instructions.

ELISA Analysis

ELISA was used to determine the serum concentration of IL-1β, IL-8, IL-10, and IL-12 in inoculated piglets. IL-1β (#ELP-IL1b-1) and IL-8 (#ELP-IL8-1) were quantified using RayBio® ELISA kit (RayBiotech, Inc., Norcross, GA, USA), and IL-10 (#P1000) and IL-12 (P1240) were quantified by R&D ELISA kit (R&D Systems, USA).

Statistical Analysis

All data were presented as means ± standard deviation (SD). The statistical analysis was conducted by using the unpaired Student's *t*-test in GraphPad Prism 5 software. Differences with a value of $p < 0.05$ were considered statistically significant.

RESULTS

Clinical Signs and Gross Lesions

Piglets in the toxigenic and non-toxigenic groups showed increased rectal temperature (between 40.5 and 41°C) at 6 h post infection, but decreased rectal temperature (<40.5°C) at 24 h, 48 h, and 72 h post infection. Notably, the rectal temperature of piglets in the toxigenic group was higher than those in the non-toxigenic group at all time points (**Figure 1**). Piglets in the toxigenic group exhibited a range of clinical signs, such as listlessness, red body surface, trembling body, gathering, swollen eyes, and exfoliation of small areas of skin on the ears, belly, hind legs, and tails at 24 h post infection. At 48 h post infection, serious clinical signs appeared, exfoliation of large areas of skin with fluid exudation; then scabs began to form in the areas that had shed skin. Moreover, one of five piglets infected with ZC-4 died at 1 week post inoculation. In the non-toxigenic group, inoculated piglets only showed mild listlessness at 24 h post infection. Neither clinical signs (**Table 1**) nor significant increases in body temperature (**Figure 1**) were observed in control animals throughout the study. The analysis of anatomical lesions showed that, in the toxigenic group, the mandibular lymph nodes showed the most prominent gross lesions with diffused hemorrhage, whereas no significant changes were observed in lung and liver. There were no obvious pathological changes in the organs in piglets in the non-toxigenic group.

Pathological Examination

The skin and kidneys showed the most obvious lesions. Histological examination showed that the skin lesions in piglets in the toxigenic group were characterized by cuticular exfoliation, incomplete and excessive hyperkeratosis, and inflammatory cell hyperplasia of the epidermis, whereas piglets in the non-toxigenic group exhibited hyperkeratosis and inflammatory cell hyperplasia of the epidermis; the control piglets showed no pathological changes in the skin tissues. Degeneration of the uriniferous tubule epithelium was evident in the toxigenic and

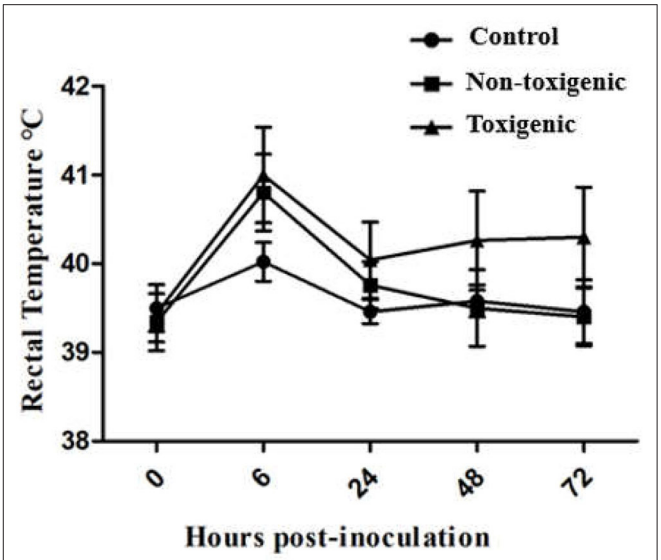

FIGURE 1 | Changes in rectal temperature of piglets at 0, 6, 24, 48, and 72 h post in toxigenic group, non-toxigenic group, and control group. Each data point represents the mean ± standard deviation (SD) generated from five pigs in each group.

TABLE 1 | Outcomes of inoculation of piglets in toxigenic and non-toxigenic groups with *Staphylococcus hyicus* infection.

Hours post infection	Group	Clinical signs[a]	Morbidity[b]	Mortality[c]
6 h	Control	–	0/5	0/5
	Non-toxigenic	–	0/5	0/5
	Toxigenic	–	0/5	0/5
24 h	Control	–	0/5	0/5
	Non-toxigenic	+	0/5	0/5
	Toxigenic	++	5/5	0/5
48 h	Control	–	0/5	0/5
	Non-toxigenic	–	0/5	0/5
	Toxigenic	+++	5/5	0/5
72 h	Control	–	0/5	0/5
	Non-toxigenic	–	0/5	0/5
	Toxigenic	+++	5/5	0/5
1 W	Control	–	0/4	0/4
	Non-toxigenic	–	0/4	0/4
	Toxigenic	+++	4/4	1/4

[a] *Clinical sign: + depressed; ++ exfoliation of a small area; +++ exfoliation of a large area; –no clinical symptom.*
[b] *Morbidity = Number of sick pigs/total experimental piglets per group.*
[c] *Mortality = Number of dead pigs/total experimental piglets per group.*

non-toxigenic groups, whereas no pathological changes were observed in the control group (**Figure 2**). The liver, lung, spleen, and lymph nodes showed no visible lesions.

Isolation and Identification of *Staphylococcus hyicus*

Staphylococcus was isolated in pure culture from the heart and lung of piglets and identified as *S. hyicus* by morphological examination and biochemical identification. Gram staining showed that the isolated bacteria were clustered, grape-like cocci (*Staphylococcus*) with gram-positive staining. The results of morphological tests were confirmed by the detection of a specific fragment (1,359 bp) of 16S rRNA gene in piglets in the toxigenic and non-toxigenic groups; the fragment was not detected in the control group piglets. In addition, a specific fragment (865 bp) of the *ExhA* gene was detected in piglets in the toxigenic group but not in piglets in the non-toxigenic and control groups.

Serum Cytokine Levels

At 6, 24, 48, and 72 h post infection, blood samples were collected, and the serum levels of 10 cytokines (GM-CSF, IL-1β, IL-6, IL-10, TGF-β1, IFNγ, IL-4, IL-8, IL-12p40, and TNF-α) were assessed. Significant differences between *S. hyicus* (CF-1 and ZC-4)-infected and control piglets and between ZC-4-infected and CF-1 infected piglets are shown in **Table 2**.

Serum levels of four cytokines (IL-1β, IL-8, IL-10, and IL-12) differed significantly between the infected and control piglets ($p < 0.05$). Among these cytokines, IL-1β levels in the toxigenic and non-toxigenic groups rapidly increased at 6 h post infection, but no significant change was observed at the following sampling time point (**Figures 3A,B**, **4A,B**). Serum concentration of IL-8 decreased at 6 and 24 h post infection in ZC-4-infected piglets and at 24 h post infection in CF-1-infected piglets (**Figures 3B**, **4B**). In ZC-4-infected piglets, IL-10 levels were elevated at 48 h post infection but not at other time points; in piglets in the non-toxigenic group, IL-10 levels were not elevated at any time points (**Figures 3C**, **4C**). IL-12 levels decreased at 72 h after infection in ZC-4-infected piglets, whereas no decrease was observed in the CF-1 group (**Figures 3D**, **4D**). Levels of three cytokines were significantly different between the toxigenic and non-toxigenic groups; IL-8 and IL-12 levels were lower in ZC-4-infected piglets at 24 and 72 h post infection, respectively, whereas IL-10 levels were higher in ZC-4-infected piglets at 48 h post infection.

Validation of Cytokine Levels With the ELISA Assay

To confirm our observations from the cytokine antibody array, ELISA assay was used to quantitatively measure the expression levels of IL-8, IL-1β, IL-10, and IL-12. As shown in **Figure 5A**, IL-8 expression in the toxigenic and non-toxigenic groups was significantly lower ($p < 0.05$) than that in the control group at 6 and 24 h after infection. In the toxigenic and non-toxigenic groups, IL-1β levels were significantly higher ($p < 0.05$) than those in the control group (**Figure 5B**). Notably, 48 h post infection, IL-10 levels in the toxigenic group were significantly higher ($p < 0.05$) than those in the non-toxigenic and control groups; IL-10 levels in the non-toxigenic group and control

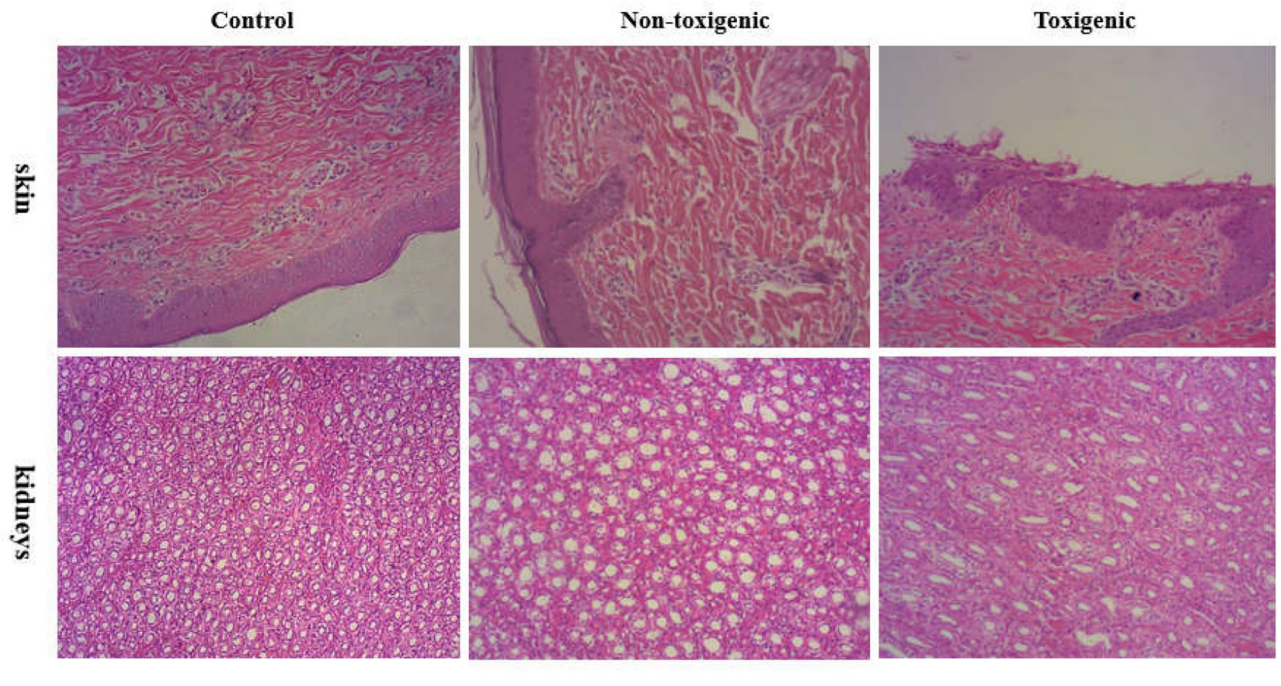

FIGURE 2 | Histophathological changes in the skin and kidneys of piglets from toxigenic group, non-toxigenic group, and control group at 72 h post infection. The tissues were stained with hematoxylin and eosin (magnification 100×).

TABLE 2 | Serum levels of cytokines in piglets over the course of *Staphylococcus hyicus* infection.

Cytokine	Non-toxigenic/Control				Toxigenic/Control				Toxigenic/Non-toxigenic			
	6 h	24 h	48 h	72 h	6 h	24 h	48 h	72 h	6 h	24 h	48 h	72 h
IL-1β	**<0.05**	ns	ns	ns	**<0.05**	ns	ns	ns	ns	ns	ns	ns
IL-4	ns	ns	ns	ns	ns	ns	ns	ns	ns	ns	ns	ns
IL-6	ns	ns	ns	ns	ns	ns	ns	ns	ns	ns	ns	ns
IL-8	ns	**<0.05**	ns	ns	**<0.05**	**<0.0001**	ns	ns	ns	**<0.05**	ns	ns
IL-10	ns	ns	ns	ns	ns	ns	**<0.05**	ns	ns	ns	**<0.05**	ns
IL-12	ns	ns	ns	ns	ns	ns	ns	**<0.05**	ns	ns	ns	**<0.01**
GM-CSF	ns	ns	ns	ns	ns	ns	ns	ns	ns	ns	ns	ns
IFNγ	ns	ns	ns	ns	ns	ns	ns	ns	ns	ns	ns	ns
TGF-β1	ns	ns	ns	ns	ns	ns	ns	ns	ns	ns	ns	ns
TNF-α	ns	ns	ns	ns	ns	ns	ns	ns	ns	ns	ns	ns

The p-value was conducted by using the unpaired Student's t-test in GraphPad Prism 5 software. ns, not significant, differences with a value of $p < 0.05$, $p < 0.01$, and $p < 0.0001$ were considered statistically significant.

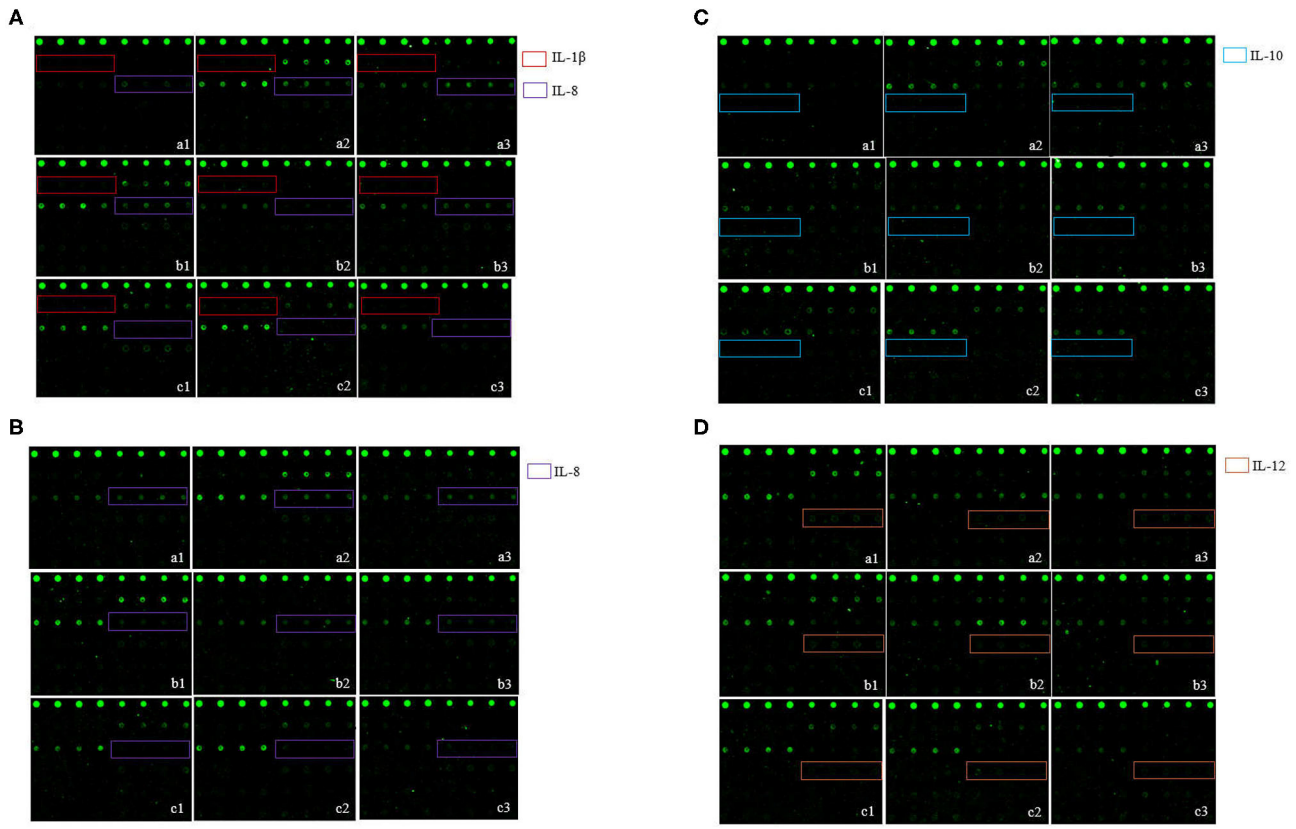

FIGURE 3 | The *S. hyicus* infection associated serum cytokine profiles in piglets at 6 h **(A)**, 24 h **(B)**, 48 h **(C)**, and 72 h **(D)** post-inoculation. In the profiles of antibody arrays, the levels of cytokines are proportional to their flurescence intensity. In these arrays, each antibody was printed in four duplicates, and the locations of the serum cytokines are noted in colored boxes. a1, a2, and a3 represent the results of three different piglets in control group, b1, b2, and b3 represent the results of three different piglets in non-toxigenic group, c1, c2, and c3 represent the results of three different piglets in toxigenic group.

groups did not differ significantly (**Figure 5C**). IL-12 levels in the toxigenic group were significantly lower than those in the non-toxigenic and control groups; there was no significant difference in the IL-12 levels between the non-toxigenic and control groups (**Figure 5D**).

DISCUSSION

The cytokine network plays a critical role in modulating the inflammatory response to bacterial infection (18, 19). The host immune response is a significant predictor of both persistence

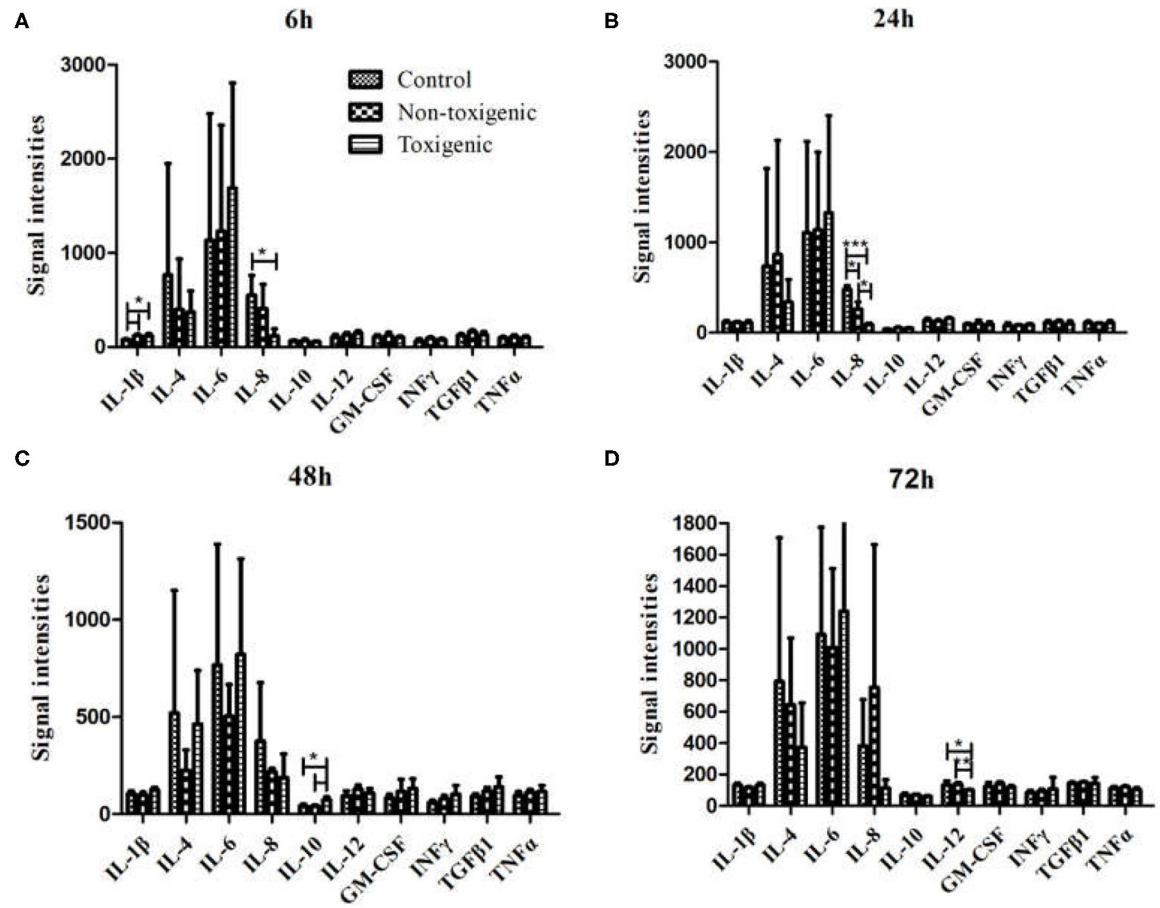

FIGURE 4 | Serum cytokine levels in *Staphylococcus hyicus*-infected piglets at 6 h **(A)**, 24 h **(B)**, 48 h **(C)**, and 72 h **(D)** post inoculation. The significance of value were tested by Graphpad Software. ***$p < 0.0001$, **$p < 0.01$, *$p < 0.05$.

of infection and outcomes (20–22). To date, the host immune response, especially cytokine response, induced by *S. hyicus* remains poorly understood; therefore, more research is required to better characterize it. In the present study, we evaluated the inflammatory response in piglets infected with toxigenic and non-toxigenic strains of *S. hyicus* by measuring the serum levels of cytokines, including pro-inflammatory cytokines (IL-1β, IL-6, IL-8, TNF-α, and IFNγ) and anti-inflammatory cytokines (IL-4, IL-10, and TGF-β1).

The results demonstrated that piglets infected with toxigenic and non-toxigenic *S. hyicus* strains exhibited differential clinical signs and outcomes; the morbidity and mortality rates were higher in the toxigenic group than in the non-toxigenic group and control group, indicating the stronger virulence of the toxigenic strain ZC-4 than that of non-toxigenic strain CF-1. These results are consistent with previous reports that the exfoliative toxin is the most important determinant of *S. hyicus* virulence and may cause dehydration and subsequent death in piglets (8–10). Infection with the toxigenic strain of *S. hyicus* induced both an inflammatory reaction and an anti-inflammatory response as indicated by the cytokine assay results—a significant increase in the levels of a pro-inflammatory cytokine (IL-1β) and an anti-inflammatory cytokine (IL-10). In the non-toxigenic group, only an inflammatory reaction was induced as suggested the increased serum level of IL-1β. These results demonstrated that the toxigenic and non-toxigenic strains of *S. hyicus* induce different inflammatory reactions and that the exfoliative toxin plays an important role in the inflammatory response of piglets to *S. hyicus* infection.

Pro-inflammatory cytokines such as IL-1β, IL-6, IL-8, and TNF-α mediate the early inflammatory response and amplify the inflammatory response (23, 24). In the present study, infection with *S. hyicus* (toxigenic strain and non-toxigenic strain) induced a robust IL-1β response, as indicated by the elevated serum IL-1β levels 6 h post infection in both toxigenic-strain-infected piglets and non-toxigenic-strain-infected piglets. IL-1β is a typical primary pro-inflammatory cytokine that initiates an inflammatory response in the immune system (25). Elevated levels of circulating IL-1β have been reported to cause acute inflammatory response in bacterial infection. Our findings of increased IL-1β levels were consistent with those observed in infections caused by *S. aureus and S. epidermidis* (26, 27). The

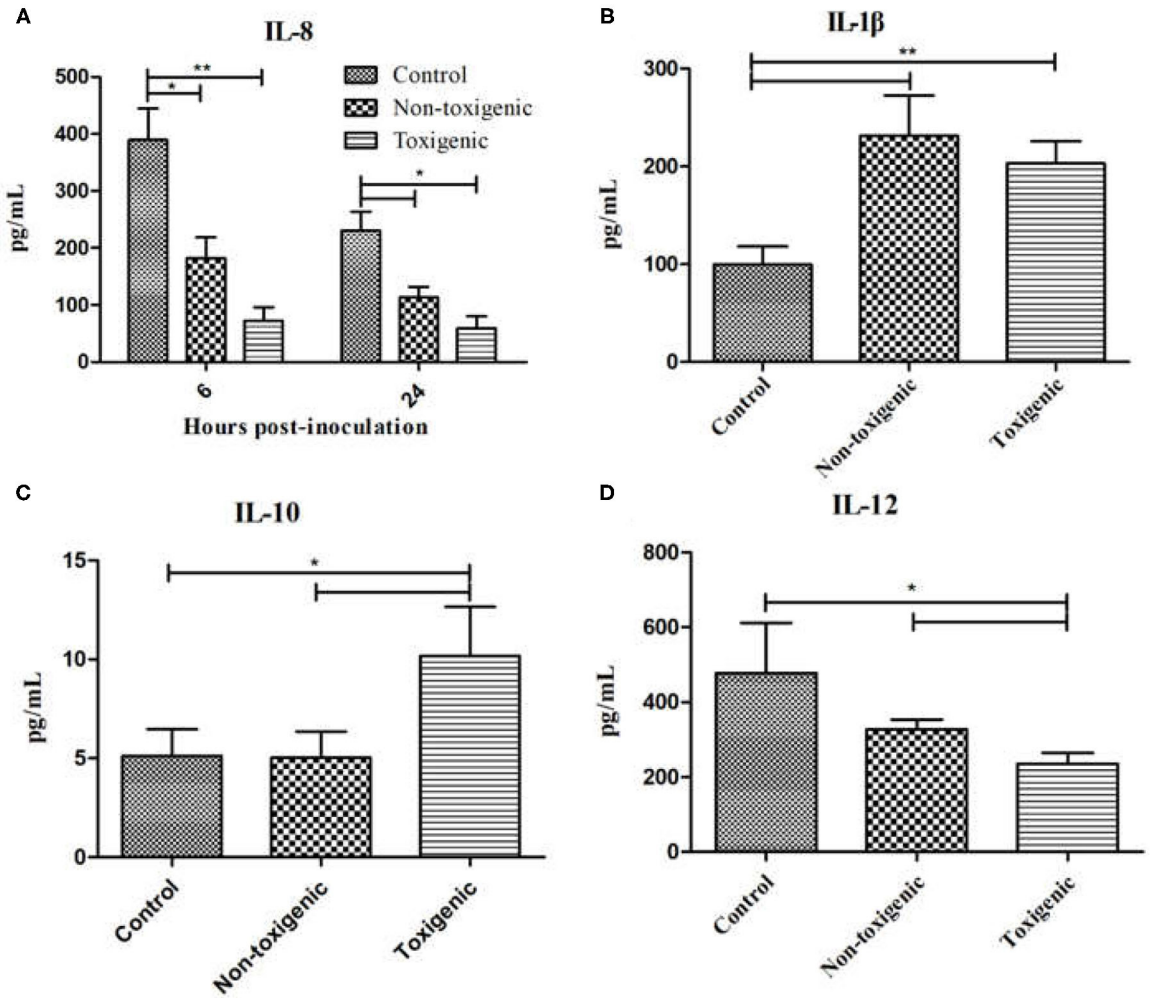

FIGURE 5 | Serum interleukin (IL)-8, IL-1β, IL-10, and IL-12 levels in *Staphylococcus hyicus*-infected piglets using ELISA. Data are expressed as mean (± SD) protein concentration (pg/mL). $^{**}p < 0.01$; $^{*}p < 0.05$. IL-8 expression at 6 and 24 h post inoculation **(A)**, IL-1β expression at 6 h post inoculation **(B)**, IL-10 expression at 48 h post inoculation **(C)**, IL-12 expression at 72 h post inoculation **(D)**.

serum levels of IL-8 in piglets infected with *S. hyicus* were also examined in the present study. IL-8 is another important inflammatory cytokine playing a key role in initiating the inflammatory responses against bacterial pathogens (28, 29). However, in the present study, the expression level of the inflammatory factor IL-8 was sharply decreased in both toxigenic group and non-toxigenic group at 6 and 24 h post infection, which is inconsistent with the levels induced by *S. aureus* infection (30).

IL-12 is necessary for survival in respiratory infection with methicillin-resistant *S. aureus* and increased pulmonary clearance of methicillin-resistant *S. aureus* (31). The expression level of IL-12 significantly reduced in toxigenic-strain-infected piglets 72 h post infection, consistent with our previous findings of reduced IL-12 levels in toxigenic-strain–infected mice (32) and findings of another study which also reported a lack of inflammatory IL-12 in *S. epidermidis* infection (33). IL-12 plays a key role in the development and augmentation of Th1 responses during infection and inflammation (34) and has been identified as a critical cytokine in the pathogenesis of several inflammatory diseases such as rheumatoid arthritis (35), inflammatory bowel disease (36), and *S. aureus* infection (37, 38). Notably, the IL-12 serum concentration in piglets infected with the non-toxigenic strain was not only reduced but elevated. The severe clinical signs and the reduced IL-12 levels in toxigenic-strain-infected piglets suggest that IL-12 is an important predictive factor of the infection status of piglets infected with *S. hyicus*.

Anti-inflammatory cytokines, including IL-4, IL-10, and TGF-β, regulate the inflammatory response. In addition to the pro-inflammatory response described above, a robust anti-inflammatory response was induced by the toxigenic strain of *S. hyicus*, as indicated by the increased levels of IL-10. IL-10 is a major immunomodulatory cytokine that is

able to inhibit the synthesis and release of other cytokines, thereby inhibiting cell-mediated immunity and extending the duration of viremia during the early stage of infection (39, 40). Remarkably, in the present study, 48 h post infection, IL-10 levels significantly increased in the toxigenic-strain-infected piglets but not in the non-toxigenic-strain-infected piglets. Overexpression of anti-inflammatory mediators results in immunosuppression, which hinders the host's ability to clear the primary infection, and leads to the development of secondary infection (20). Induction of IL-10 production by *S. aureus* may also facilitate immune evasion, which under certain circumstances is a form of immunomodulation (41). The IL-10 data above indicates that the toxigenic strain of *S. hyicus* induces an immunosuppression response in piglets and IL-10 release is a part of the pathogenic mechanism of *S. hyicus*. The present findings of upregulated IL-10 levels are consistent with a previous report that elevated IL-10 concentration was associated with a predominantly anti-inflammatory response and worse outcome (20, 40, 42). An initial elevation of IL-10 was also found to be associated with poor outcomes in other infections, such as Bartonella Quintana bacteremia (43) and candidemia (44). In the present study, elevated serum IL-10 also predicted worse outcome, as indicated by the severe clinical signs and high mortality in the toxigenic-strain-infected piglets and the absence of clinical signs and mortality in the non-toxigenic-strain-infected piglets, which did not exhibit elevated IL-10. Previous studies have reported that *S. epidermidis* infection enhanced IL-10 expression and improved the anti-inflammatory effects (33). The present study demonstrated that exposure to *S. hyicus* increased serum IL-10 levels in piglets, suggesting that IL-10 participates in the anti-inflammatory response during *S. hyicus* infection. In the present study, increased serum levels of IL-10 and decreased serum levels of IL-12 were both observed in the toxigenic-strain-infected piglets, which was consistent with the findings in *S. epidermidis* infection (33).

A previous study indicated that *S. aureus* exotoxins contribute to evading the host immune response and destroying host tissue, thus increasing the severity of infection (45). In the present study, the *S. hyicus* strain ZC-4 with exfoliative toxin ExhA induced a strong anti-inflammatory response and increased the severity of infection; thus, we speculated that the exfoliative toxin of *S. hyicus* is a potential key factor contributing to the anti-inflammatory response. Several studies have characterized the host inflammatory responses induced by *S. aureus* and *S. epidermidis* (46, 47), but to date, no research on the inflammatory response induced by *S. hyicus* has been reported. This study is the first to evaluate the host cytokine response to *S. hyicus* infection in piglets, contributing to the knowledge on pathogenesis of *S. hyicus* and providing basic information for treating exudative epidermitis (EE) in pigs.

This is a preliminary study about the host cytokine response induced by *S. hyicus*, and there are several limitations to our study. Because only one toxigenic strain and one non-toxigenic strain were used to study the cytokine response, data obtained are insufficient to comprehensively analyze the inflammatory response induced by *S. hyicus*. More toxigenic strains should be used to investigate the levels of anti-inflammatory cytokines to verify the findings on the anti-inflammatory response and cytokines critical for the pathogenicity of a toxigenic strain of *S. hyicus*.

CONCLUSIONS

In conclusion, the present study found that the pro-inflammatory cytokine IL-1β was upregulated in piglets infected with a toxigenic strain and a non-toxigenic strain of *S. hyicus*, and levels of the anti-inflammatory cytokine IL-10 increased only in piglets infected with the toxigenic strain; thus, the two *S. hyicus* strains induce different cytokine responses in infected piglets. The upregulated IL-1β level indicated a significant pro-inflammatory response in *S. hyicus* infection. IL-10 expression levels were also significantly upregulated, indicating that the anti-inflammatory response was induced by infection with the toxigenic strain. Our findings suggest that elevated IL-10 level maybe associated with severe *S. hyicus* infection, and IL-10 may be the key cytokine responsible for the pathogenic mechanisms of *S. hyicus*.

Presently, our knowledge of the ability of *S. hyicus* to induce an inflammatory response during infection is limited. Future research should include an in-depth analysis of the inflammatory response in *S. hyicus* infection using more *S. hyicus* strains and the factors, such as toxins, that contribute to inflammation and immune priming.

DATA AVAILABILITY STATEMENT

The original contributions presented in the study are included in the article/**Supplementary Material**, further inquiries can be directed to the corresponding author/s.

ETHICS STATEMENT

The animal study was reviewed and approved by the Animal Experimental Ethics Committee of the Institute of Animal Health, Guangdong Academy of Agricultural Sciences.

AUTHOR CONTRIBUTIONS

YL performed the experiments and drafted the manuscript. SS, ZB, and RC prepared materials for the experiments. PC and ZJ participated in the experiments. KZ and HG contributed to the data analysis. CL conceived the study. All authors read and approved the final manuscript.

FUNDING

This study was supported by the National key R&D projects (2016YFD0500709), the Natural Science Foundation

Program of Guangdong Province (2020A1515010475), the Natural Science Foundation of China (31772776) and the Innovation Team Project of Modern Agricultural Industrial Technology System of Guangdong Province (2019KJ119).

SUPPLEMENTARY MATERIAL

The Supplementary Material for this article can be found online at: https://www.frontiersin.org/articles/10.3389/fvets.2021.639141/full#supplementary-material

REFERENCES

1. Foster AP. Staphylococcal skin disease in livestock. *Vet Dermatol.* (2012) 23:342–51. doi: 10.1111/j.1365-3164.2012.01093.x
2. Wang L, Wu ZW, Li Y, Dong JG, Zhang LY, Liang PS, et al. Profiling and identification of novel immunogenic proteins of *staphylococcus hyicus* ZC-4 by immunoproteomic assay. *PLoS ONE.* (2016) 11:e0167686. doi: 10.1371/journal.pone.0167686
3. Jones LD. Observation of exudative epidermitis. *Vet Med.* (1961) 14:1028–33.
4. Wang MY, Hu JY, Zhu LS, Guo CG, Lu HB, Guo CM, et al. A fatal suppurative pneumonia in piglets caused by a pathogenic coagulase-positive strain of *Staphylococcus hyicus*. *Vet Res Commun.* (2017) 41:139–46. doi: 10.1007/s11259-017-9682-0
5. L'Ecuyer C, Jericho K. Exudative epidermitis in pigs: etiological studies pathology. *Can J Comp Med Vet Sci.* (1966) 30:94.
6. Foissac M, Lekaditi M, Loutfi B, Ehrhart A, Dauchy FA. Spondylodiscitis and bacteremia due to *staphylococcus hyicus* in an immunocompetent man. *Germs.* (2016) 6:106–10. doi: 10.11599/germs.2016.1097
7. Andresen LO, Bille-Hansen V, Wegener HC. *Staphylococcus hyicus* exfoliative toxin:purification and demonstration of antigenic diversity among toxins from virulent strains. *Microb Pathog.* (1997) 22:113–22. doi: 10.1006/mpat.1996.0097
8. Wegener HC, Andresen LO, Bille-hansen V. *Staphylococcus hyicus* virulence in relation to exudative epidermitis in pigs. *Can J Vet Res.* (1993) 57:119–25.
9. Tanabe T, Sato H, Sato H, Watanabe K, Hirano M, Hirose K, et al. Correlation between occurrence of exudative epidernitis and exfoliative toxin-producing ability of *Staphylococcus hyicus*. *Vet Microbiol.* (1996) 48:9–17. doi: 10.1016/0378-1135(95)00144-1
10. Sato H, Watanabe T, Higuchi K, Teruya K, Ohtake A, Murata Y, et al. Chromosomal and extrachromosomal synthesis of exfoliative toxin from *Staphylococcus hyicus*. *J Bacteriol.* (2000) 182:4096–100. doi: 10.1128/jb.182.14.4096-4100.2000
11. Andresen LO, Ahrens P. A multiplex PCR for detection of genes encoding exfoliative toxins form *staphylococcus hyicus*. *J Appl Microbiol.* (2004) 96:1265–70. doi: 10.1111/j.1365-2672.2004.02258.x
12. Fudaba Y, Nishifuji K, Andresen LO. *Staphylococcus hyicus* exfoliative toxins selectively digest porcine desmoglein 1. *Microb Pathog.* (2005) 39:171–6. doi: 10.1016/j.micpath.2005.08.003
13. Rathinam VA, Fitzgerald KA. Inflammasome complexes: emerging mechanisms and effector funtions. *Cell.* (2016) 165:792–800. doi: 10.1016/j.cell.2016.03.046
14. Hotamisligil GS. Inflammation, metaflammation and immunometabolic disorders. *Nature.* (2017) 542:177–85. doi: 10.1038/nature21363
15. Baxt LA, Garza-Mayers AC, Goldberg MB. Bacterial subversion of host innate immune pathways. *Science.* (2013) 340:697–701. doi: 10.1126/science.1235771
16. Van Belleghem JD, Clement F, Merabishvili M, Lavigne R, Vaneechoutte M. Pro- and anti-inflammatory response of peripheral blood mononuclear cells induced by *Staphylococcus aureus* and *Pseudomonas aeruginosa* phages. *Sci Rep*. (2017) 7:8004. doi: 10.1038/s41598-017-08336-9
17. Yu LH, He J, Wang LL, Yi HX. Inflammatory profiles revealed the dysregulation of cytokines in adult patients of HFMD. *Int J Infect Dis.* (2019) 79:12–20. doi: 10.1016/j.ijid.2018.11.001
18. Gouwy M, Struyf S, Proost, P, Damme JV. Synergy in cytokine and chemokine networks amplifies the inflammatory response. *Cytokine Growth R.* (2005) 16:561–80. doi: 10.1016/j.cytogfr.2005.03.005
19. Pinheiro-Torres AP, Ferreia-Duarte AP, Takeshita WM, Gushiken VO, Roncalho-Buck IA, et al. Airways exposure of bacterial superantigen SEB enhances bone marrow eosinophil poputation and facilates its egress to blood and lung tissue. *Life Sci.* (2021) 264:118685. doi: 10.1016/j.lfs.2020.118685
20. Emi M, Joyce B, Rosemary CS. A dysregulated balance of proinflammatory and anti-inflammatory host cytokine response early during therapy predicts persistence and mortality in *Staphylococcus aureus* bacteremia. *Crit Care Med.* (2016) 44:671–9. doi: 10.1097/CCM.0000000000001465
21. Rose WE, Eickhoff JC, Shukla SK. Elevated serum interleukin-10 at time of hospital admission is predictive of mortality in patients with *Staphylococcus aureus* bacteremia. *J Infect Dis.* (2012) 206:1604–11. doi: 10.1093/infdis/jis552
22. Krutz JR, Goggins JA, McLachlan JB. Salmonella infection: interplay between the bacteria and host immune system. *Immunol Lett*. (2017) 190:42–50. doi: 10.1016/j.imlet.2017.07.006
23. Duque GA, Descoteaux A. Macrophage cytokines: involvement in immunity and infectious diseases. *Front Immunol.* (2014) 5:491. doi: 10.3389/fimmu.2014.00491
24. Srinivas L, Vellichirammal NN, Alex AM, Nair C, Nair IV, Banerjee M. Pro-inflammatory cytokines and their epistatic interactions in genetic susceptibility to schizophrenia. *J Neuroinflammation.* (2016) 13:105–17. doi: 10.1186/s12974-016-0569-8
25. Wooff Y, Man SM, Aggio-Bruce R. IL-1 family members mediate cell death, inflammation and angiogenesis in retinal degenerative diseases. *Front Immunol*. (2019) 10:1618. doi: 10.3389/fimmu.2019.01618
26. Suresh S, Sankar P, Telang AG, Kesavan M, Sarkar SN, et al. Nanocurcumin ameliorates *Staphylococcus aureus*-induce mastitis in mouse by suppressing NF-κB signaling and inflammation. Int. *Immunopharmacol.* (2018) 65:408–12. doi: 10.1016/j.intimp.2018.10.034
27. Petropoulos IK, Vantzou CV, Lamari FN, Karamanos NK, Anastassiou ED, Pharmakakis NM. Expression of TNF-α, IL-1β, and IFN-γin Staphylococcus epidermidis slime-positive experimental endophthalmitis is closely related to clinical inflammatory scores. *Graefe's Arch Clin Exp Ophthalmol*. (2006) 244:1322–8. doi: 10.1007/s00417-006-0261-2
28. Eucker TP, Samuelson DR, Hunzicker-Dunn M, Konkel ME. The focal complex of epithelial cells provides a signaling platform for interleukin-8 induction in response to bacterial pathogens. *Cell Microbiol.* (2014) 16:1441–55. doi: 10.1111/cmi.12305
29. Liu L, Li Q, Han P, Li X, Zeng H, Zhu Y, et al. Evaluation of interleukin-8 in expression prostatic secretion as a reliable marker of inflammation in benign prostatic hyperplasia. *Urology.* (2009) 74:340–4. doi: 10.1016/j.urology.2009.02.064
30. Kang SS, Noh SY, Park OJ. *Staphylococcus aureus* induces IL-8 expression through its lipoproteins in the human intestinal epithelial cell, Caco-2. *Cytokine.* (2015) 75:174–80. doi: 10.1016/j.cyto.2015.04.017
31. Nguyen QT, Furuya YC, Robert S. Role of interleukin-12 in protection agaist pulmonary infection with methicillin-resistant *Staphylococcus aureus*. *Antimicrob Agents CH.* 5(2015) 9:6308–16. doi: 10.1128/AAC.00968-15
32. Li Y, Wang L, Zhang LY, Liu YL, Jiang ZY, Cai RJ, et al. Serum cytokine modulation after *Staphylococcus hyicus* infection on BALB/c mice. *Genet Mol Res.* (2015) 14:16682–93. doi: 10.4238/2015.December.11.16
33. Gutierrez-Murgas YM, Skar G, Ramirez D, Beaver M, Snowden JN. IL-10 plays an important role in the control of inflammation but not in the bacterial burden in *S epidermidis* CNS catheter infection. *J Neuroinflammation.* (2016) 13:271. doi: 10.1186/s12974-016-0741-1
34. Chyuan IT, Lai JH. New insights into the IL-12 and IL-23: from a molecular basis to clinical application in immune-mediated inflammation and cancers. *Biochem Pharmacol.* (2020) 175:113928. doi: 10.1016/j.bcp.2020.113928
35. Rope RM, Shahrara S. Possible roles of IL-12-family cytokines in rheumatoid arthritis. *Nat Rev Rheumatol.* (2012) 9:252–6. doi: 10.1038/nrrheum.2012.170

36. Jostins L, Ripke S, Weersma RK, Duerr RH, McGovern DP, Hui KY. Host-microbe interactions have shaped the genetic architecture of inflammatory bowel disease. *Nature.* (2012) 491:119–24. doi: 10.1038/nature11582
37. Miller LS, Cho JS. Immunity agaist *Staphylococcus aureus* cutaneous infections. *Nat Rev Immunol.* (2011) 11:505–18. doi: 10.1038/nri3010
38. Held J, Preube C, Doser A, Richter L, Heppner F, Stenzel W, et al. Enhanced acute immune response in IL-12p35$^{-/-}$mice is followed by accelerated distinct repair mechanisms in *Staphylococcus aureus*-induced murine brain abscess. *J Infect Dis.* (2013) 208:749–60. doi: 10.1093/infdis/jit126
39. Levan TD, Romberger DJ, Siahpush M, Grimm BL, Ramos AK, Johansson PL, et al. Relationship of systemic IL-10 levels with proinflammatory cytokine responsiveness and lung function in agriculture workers. *Resp Res.* (2018) 19:166. doi: 10.1186/s12931-018-0875-z
40. Rose WE, Shukla SK, Berti AD. Increased endovascular *Staphylococcus aureus* inoculum is the link between elevated serum interlerkin 10 concentrations and mortality in patients with bacteremia. *Clin Infect Dis.* (2017) 64:1406–12. doi: 10.1093/cid/cix157
41. Li ZG, Peters AG, Damian AC, Madrenas J. Immunomodulation and disease tolerance to *Staphylococcus aureus*. *Pathogens.* (2015) 4:793–815. doi: 10.3390/pathogens4040793
42. Zhao S, Wu D, Wu P, Wang Z, Huang J. Serum IL-10 predicts worse outcome in cancer patients: a meta-analysis. *PLoS ONE.* (2015) 10:e0139598. doi: 10.1371/journal.pone.0139598
43. Capo C, Amirayan-Chevillard N, Brouqui P, Raoult D, Merge J, et al. Bartonella Quintana bacteremia and overproduction of interleukin-10: model of bacterial persistence in homeless people. *J Infect Dis.* (2003) 187:837–44. doi: 10.1086/368384
44. Johnson MD, Plantinga TS, van de Vosse E. Cytokine gene polymorphisms and the outcome of invasion candidiasis: A prospective cohort study. *Clin Infect Dis.* (2012) 54:502–10. doi: 10.1093/cid/cir827
45. Adhikari RP, Ajao AO, Aman MJ, Karuzam H, Sarwar J, Lydecker AD, et al. Lower antibody levels to *Staphylococcus aureus* exotoxins are associated with sepsis in hospitalized adults with invasive S.aureus infection. *J Infect Dis.* (2012) 206:915–23. doi: 10.1093/infdis/jis462
46. Dong Y, Glaser K, Schlegel N, Claus H, Speer CP. An underestimated pathogen: *Staphylococcus epidermidis* induces pro-inflammatory responses in human alveolar epithelial cells. *Cytokine.* (2019) 123:154761. doi: 10.1016/j.cyto.2019.154761
47. Troger B, Heidemann M, Osthues I, Knaack D, Gopel W, Herting E. Modulation of *S epidermidis*-induced innate immune responses in neonatal whole blood. *J Microbiol Immunol.* (2020) 53:240–9. doi: 10.1016/j.jmii.2018.04.008

Conflict of Interest: The authors declare that the research was conducted in the absence of any commercial or financial relationships that could be construed as a potential conflict of interest.

frontiers in Veterinary Science

ORIGINAL RESEARCH
published: 05 July 2021
doi: 10.3389/fvets.2021.697839

The New Porcine Epidemic Diarrhea Virus Outbreak May Mean That Existing Commercial Vaccines Are Not Enough to Fully Protect Against the Epidemic Strains

Qi Gao [1], Zezhong Zheng [1,2], Heng Wang [1,3,4], Songqiang Yi [5], Guihong Zhang [1,2,3,4] and Lang Gong [1,4]**

[1] College of Veterinary Medicine, South China Agricultural University, Guangzhou, China, [2] Guangdong Laboratory for Lingnan Modern Agriculture, Guangzhou, China, [3] Key Laboratory of Zoonosis Prevention and Control of Guangdong Province, South China Agricultural University, Guangzhou, China, [4] National Engineering Research Center for Breeding Swine Industry, South China Agricultural University, Guangzhou, China, [5] Agricultural Technology Extension Center of Jiangxi Province, Nanchang, China

OPEN ACCESS

Edited by:
Shao-Lun Zhai,
Guangdong Academy of Agricultural Sciences, China

Reviewed by:
Yifeng Jiang,
Chinese Academy of Agricultural Sciences (CAAS), China
Lei Zhou,
China Agricultural University, China

***Correspondence:**
Lang Gong
gonglang@scau.edu.cn
Guihong Zhang
guihongzh@scau.edu.cn

Specialty section:
This article was submitted to Veterinary Infectious Diseases, a section of the journal Frontiers in Veterinary Science

Received: 20 April 2021
Accepted: 26 May 2021
Published: 05 July 2021

Citation:
Gao Q, Zheng Z, Wang H, Yi S, Zhang G and Gong L (2021) The New Porcine Epidemic Diarrhea Virus Outbreak May Mean That Existing Commercial Vaccines Are Not Enough to Fully Protect Against the Epidemic Strains. Front. Vet. Sci. 8:697839. doi: 10.3389/fvets.2021.697839

Background: On October 30, 2020, piglets and sows in the farrowing house of a pig farm in Jiangxi showed clinical symptoms such as anorexia, watery diarrhea, and vomiting. Epidemiological test, clinical necropsy, and RT-PCR test were carried out on the pig farm for diagnosis. After comprehensive considerations, the disease was judged as porcine epidemic diarrhea virus infection.

Results: Thereafter, a series of comprehensive prevention and control measures such as emergency vaccination with autogenous vaccines were adopted. Half a month after inoculation with autogenous vaccines for the farm, the mortality rate of newborn piglets in the farrowing house began to decline, and production gradually returned to being stable. The second-generation sequencing analysis and phylogenetic analysis showed that the porcine epidemic diarrhea virus (PEDV) sequence obtained from the stool and small intestine samples of the diseased pigs on the farm was 97.8% homologous to the vaccine strain. At the same time, antibody testing found that the vaccinated pigs on the pig farm had satisfactory immune response.

Conclusion: This case indicated that the PEDV outbreak on the pig farm might aggravate owing to the strain being mutated and could escape the immune protection of the existing vaccine. This case has accumulated technical data for the clinical prevention and control of porcine epidemic diarrhea.

Keywords: cross protection, phylogenetic analysis, porcine epidemic diarrhea virus, strain variation, PEDV

INTRODUCTION

Porcine epidemic diarrhea is an acute and highly contagious intestinal infectious disease caused by porcine epidemic diarrhea virus infection. The disease is prevalent in the cold season and is transmitted through fecal–oral transmission. Its clinical symptoms include elevated body temperature, anorexia, vomiting, diarrhea, dehydration, etc., (1). Porcine epidemic diarrhea virus

(PEDV) is a single-stranded RNA virus belonging to the genus *Coronavirus*, family *Coronaviridae*, with a genome length of 28 kb (2). The disease was first discovered in England and Belgium in 1971 (3) and successively discovered in China in the early 1980's (4). Since October 2010, a new variant strain of porcine epidemic diarrhea has appeared, which has been widespread in China and other major pig-raising countries in the world, and its prevalence in East Asia and North America is severe, causing large economic losses to the farms (5, 6). PEDV infection has become one of the main reasons for the high mortality of suckling piglets.

Vaccination is an important way to control infectious diseases. In 1994, Ma et al. (7) used the attenuated CV777 strain to prepare an inactivated vaccine with aluminum gel adjuvant. After immunizing piglets, the active and passive protection efficiency exceeded 85%. In 1995, the study team successfully developed a commercial transmissible gastroenteritis virus (TGEV) + PEDV bivalent vaccine. In 1998, Tong et al. confirmed that the CV777 strain obtained by continuous *in vitro* passage for 90 generations is suitable for the preparation of attenuated vaccines. In 1999, they successfully developed a PEDV + TGEV bivalent vaccine. The ratio of virion counts of TGEV to PEDV was 1:1. After immunization, the active and passive protection rates against PEDV were as high as 97.7 and 98%, respectively (8, 9). The PEDV vaccine strains in these two commercial vaccines were both classic CV777 strains. Before 2010, these two bivalent vaccines were widely used in China, effectively controlling the spread of PEDV and TGEV.

After the outbreak of PED in the United States in 2013, Collin et al. prepared an inactivated vaccine of the American isolate (G2 genotype) and proved that inactivated PEDV can induce sufficient humoral immunity level in immunized 4-week-old piglets (10). The PEDV strain used in the PEDV–TGEV and PoRV trivalent attenuated live vaccine produced by the Harbin Veterinary Research Institute subordinated to the Chinese Academy of Agricultural Sciences in early 2015 was still CV777. The PEDV strain in the bivalent vaccine marketed in November of the same year was ZJ08, which belongs to the G1b subtype (11). In December 2017, the PEDV bivalent inactivated vaccine and attenuated vaccine prepared by Prof. Xiao of Huazhong Agricultural University were successfully marketed. The vaccine strain was AJ1102, which was isolated in 2011, and belongs to the G2b type (12).

In the winter of 2020, a new wave of PEDV epidemic swept across China. The question is, why was there a large-scale outbreak of PEDV under the conditions that biosafety control was so strict under a non-plague background, and whether new strains have emerged. Here, we report a clinical case of PEDV in Jiangxi, which indicates that China's existing PED variant vaccines may not fully protect against the PEDV epidemic strain.

CASE PRESENTATION

Case Farm Characteristics

Recently, a case of PEDV infection occurred in a pig farm in Jiangxi. There were 8,082 sows on hand in the mating house of the pig farm, which were divided into 10 groups, with 800 pigs in each group. There were 902 sows in the farrowing house, with 80 farrowing beds as a unit and five units constituting a building. Before the onset of the disease, the farm recorded 25 weaned piglets per sow per year, and the loss of farrowing house was 8%. Loss from conservation and fattening was <6%. The pig farm regularly tested for enteric pathogens, and TGEV/PDCOV and PEDV had not occurred in the last 2 years. There had often been sporadic cases of porcine reproductive and respiratory syndrome (PRRS) on the pig farm.

Routinely used immunization regimens include vaccination of sows with live PRRS vaccine, swine fever vaccine, live pseudorabies vaccine, foot-and-mouth disease O+A vaccine, Japanese encephalitis vaccine, and parvovirus vaccine. Sows were immunized with a live PED vaccine and an inactivated vaccine at 30 days before delivery and 14 days before delivery, respectively.

Clinical Presentation and Interventions

On October 28, 2020, at first, 80% of the sows in a farrowing unit developed depression, fatigue, and anorexia. Three days later, they developed mushy persistent diarrhea. The body temperature was normal or slightly higher, and they showed anorexia and had fully recovered about 7 days after onset. Piglets presented with epidemic diseases with watery diarrhea and vomiting as the main clinical symptoms. Vomiting usually occurred after eating or feeding on breast milk. The severity of symptoms varied with age. The younger the age, the more severe the symptoms. In a period of 1–3 days after newborn piglets within 7 days of age developed diarrhea, they were severely dehydrated and died, with a mortality rate of 90 to 100%. Diarrhea occurred successively in sows in other units 5 days later. After on-site anatomy and laboratory testing of feces and tissues, PEDV was determined to be the pathogen underlying this epidemic. Therefore, on October 31, the staff closed the pigsty where diarrhea occurred, treated the sows and piglets with amoxicillin- or lincomycin-containing drinking water for healthcare, and disinfected the pigsty with Denaishuang dry powder and kept it dry on November 7; intramuscular injection of autogenous vaccine was administered on November 11. The main ingredients of Denaishuang dry powder are essential oils, plant extracts, yucca products, seaweed products, and kaolin. Denaishuang dry powder plays a role in disinfecting the pig house and keeping it dry. The farrowing house was disinfected, the pigsty was dried and decontaminated with hot water at 60°C, the sick pigs were given salt solution for replenishment, and the farrowing house was cleaned, disinfected, and dried; on November 13, weaned piglets with secondary infection were treated with antibiotics. On November 16th, the sow swinery of the mating house was restored, the personnel were released from lockdown, and the empty swinery units were cleaned and disinfected. After adopting a series of comprehensive prevention and control measures such as emergency vaccination with autogenous vaccine, the mortality rate of newborn piglets on the farrowing room of this farm dropped significantly at half a month after vaccination, and production gradually returned to stable (**Figure 1**).

In general, there were four units with the most severe clinical symptoms of PED on this farm, and the mortality rate of suckling piglets was 40%. On this farm, a total of 85 sows died and 187 litters had abortion, with an incidence rate of 30%, and a total of

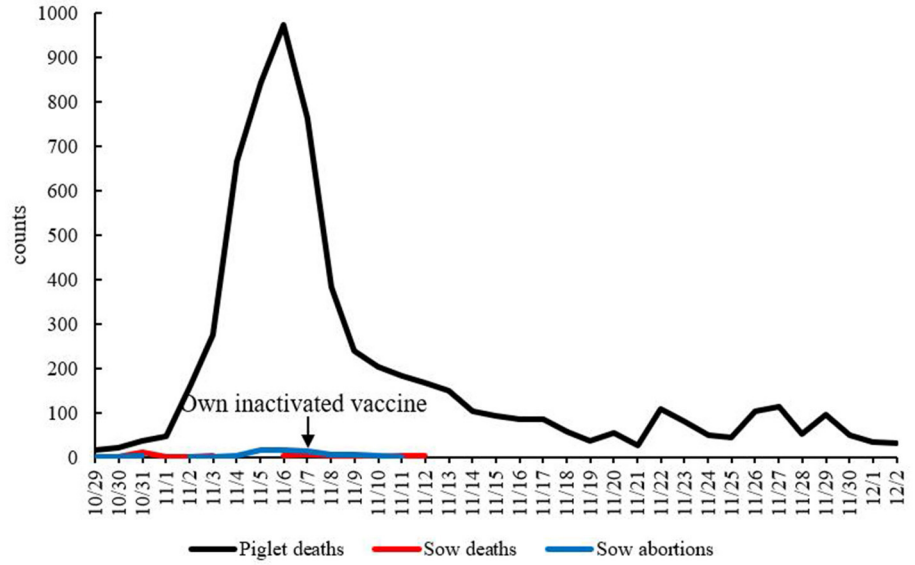

FIGURE 1 | Time–mortality dynamic curve. The *x*-axis shows time, and the *y*-axis shows the number of died pigs. The arrow is the time for the farm to inject its own inactivated vaccine.

6,455 piglets died, with an incidence rate of 70%. At the current price, the net profit per pig was 300 US dollars, and the direct loss was nearly two million US dollars. Some weaned piglets also experienced diarrhea, weight loss, and growth retardation. The total loss from piglet feeding was 12%. In the fattening house, there was no sign of PED.

Epidemiological investigations revealed that at half a month before the outbreak of PED, PEDV broke out in another pig farm 800 m away from the farm.

Laboratory Findings

After preliminary confirmation of the PEDV pathogen by the pig farm laboratory, fecal samples, milk, and serum of 20 sows, as well as the feces and intestines of three infected piglets, were sent to South China Agriculture University for sequence analysis and serological testing. In order to reveal the molecular characteristics of the virus and determine the relationship among the current epidemic strains in China and other subtype strains, the bootstrap method of MEGA6.0 software was used to analyze the evolutionary tree of domestic isolates and reference strains from different sources at different times, which indicated that the strain formed a new and unique branch in the PEDV genotype II (**Figure 2**), which had the closest genetic distance to the genotype I strain. The base sequence of the S1 gene has been uploaded to NCBI, and the GenBank number is MW646416. The S1 gene homology comparative analysis of this strain showed that it had 98.1–100% homology with 59 epidemic strains uploaded by NCBI in the past year, 91.8% homology with the CV777 strain, 97.8% homology with the AJ1102 vaccine strain, and 97.3–98.1% homology with the 89 strains prevalent in 2014–2015 measured by our laboratory (**Table 1**), indicating that the PEDV of the current outbreak had mutated. Please see **Supplementary Figure 1** for specific similarities. The similarity with the 2020 strain was also poorer by 1–2% compared with the 2014–2015 strain, indicating that PEDV had continuously mutated.

To evaluate the immunizing effect of the PED vaccine in this farm, 20 diseased sows in farrowing season were randomly selected before the immunization with autogenous inactivated vaccines and numbered 1–20. Colostrum, feces, and serum were collected, respectively to test the levels of PED antigen and IgA antibody in the colostrum, as well as the levels of PED antigen in feces and specific IgG antibody in serum. The results showed that the pigs had a good immune response after immunization with the PED vaccine, with high levels of IgA and IgG antibodies. However, for the three sows numbered 8, 11, and 20, despite the high levels of IgA in milk and serum IgG antibodies, there were still detectable PED antigens (**Table 2**). PED antigens were detected in the feces of more sows, indicating that the antibody levels produced by the existing commercial vaccines cannot completely neutralize the new epidemic strain of PEDV.

To evaluate the fecal virus shedding of sows during the disease course, we conducted a 2-week monitoring of virus shedding on seven diseased sows. The results showed that the affected sows had intermittent virus shedding within 2 weeks after delivery. Some of the sows shed a great load of virus due to individual differences (**Table 3**).

DISCUSSION AND CONCLUSIONS

In recent years, PEDV has repeatedly broken out in China and has become one of the deadliest pathogens infecting pig herds. Existing measures such as immunization, biosafety, and feeding

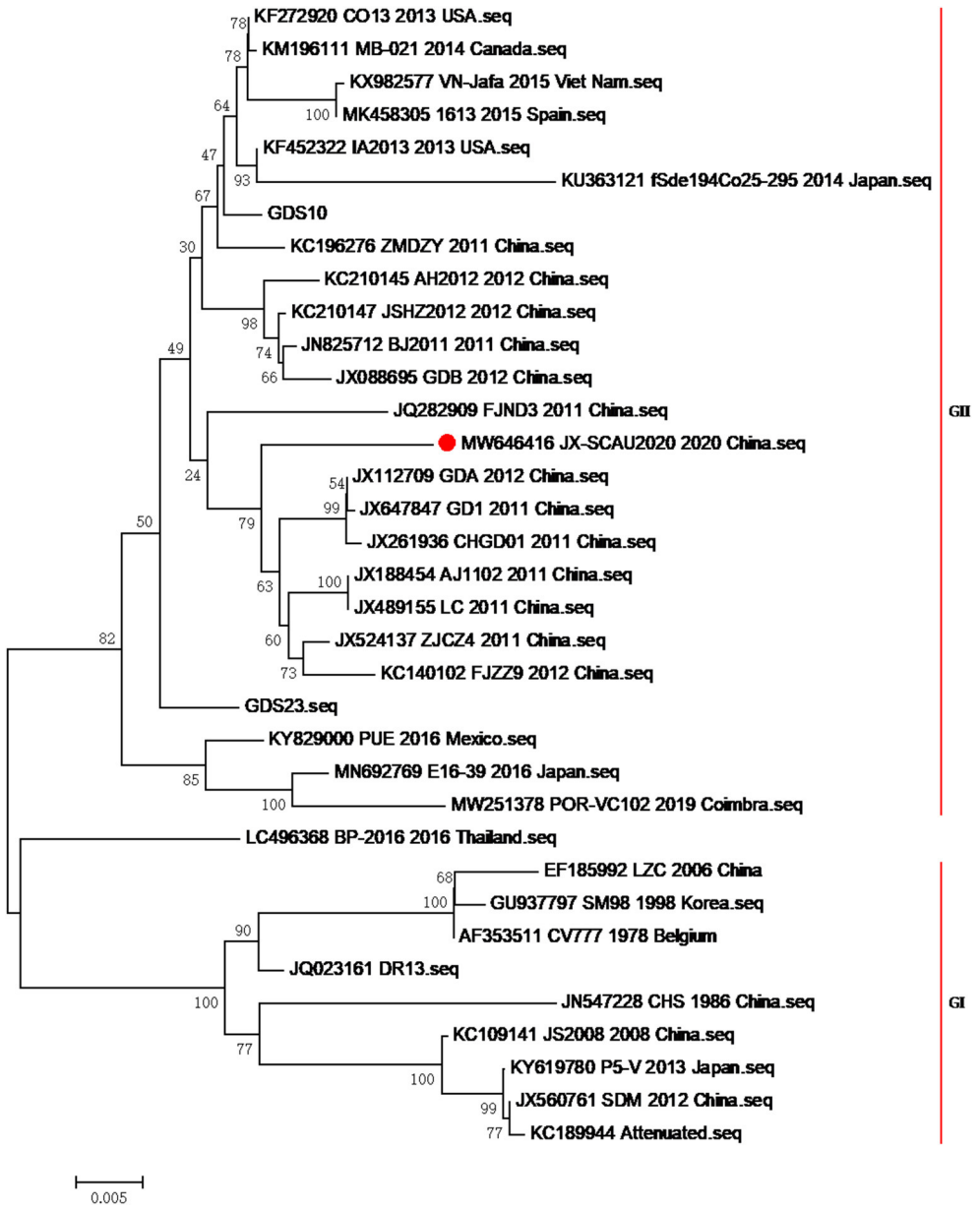

FIGURE 2 | Phylogenetic trees of isolates and a representative virus based on the S gene sequence. The tree was performed by neighbor-joining method using MEGA with 1,000 bootstrap replicates. The GenBank accession numbers, strains, years, and places of isolation are shown on the right in order, and the genogroups of the virus are shown on the right of strains.

TABLE 1 | Comparison of S1 gene homology between PEDV epidemic strain and vaccine strain in 2020.

Strain comparison	S1 homology
59 epidemic strains in 2020	98.1–100%
CV777 strain	90.3–92.1%
AJ1102 vaccine strain	96.8–97.9%
89 strains from 2014 to 2015	97.3–98.1%

with tissues from diseased animals cannot prevent its spread (13, 14). Although, vaccines prepared with G1a subtype strains have been developed and promoted for decades, it is precisely because of long-term use that its shortcomings are exposed. The amino acid mutation rate of the immunogen S gene of epidemic strains and vaccine strains has reached as high as 10% (15). The rapid development and promotion of new vaccines based on G2b subtype antigens have effectively prevented the spread of PEDV in China in the past 10 years. At present, all the genotypes of PEDV exist in China.

Owing to the pressure of herd immunity, the S gene of the coronavirus has frequently mutated, and changes in some amino acids have caused antigenic drift and escape from the

TABLE 2 | Analysis of antibody and virus shedding of infected sows.

No.	Antigen		Antibody	
	Colostrum	Feces	Milk IgA	Serum IgG
1		36.77	1.225	1.532
2		–	2.013	1.428
3		–	1.934	1.62
4		33.8	0.463	1.219
5		34.71	0.488	0.893
6		–	0.887	1.117
7		34.27	0.382	0.681
8	37.11	–	0.585	0.788
9		–	1.542	0.889
10		34.5	1.368	1.213
11	34.49	–	0.906	0.982
12		35.65	0.627	0.4136
13		–	1.327	1.348
14		–	2.323	1.787
15		–	0.185	0.685
16		–	2.086	1.782
17		–	0.041	0.182
18		32.12	0.862	0.464
19		–	0.808	0.686
20	38.21	35.32	0.332	0.514

TABLE 3 | Monitoring results of continuous virus shedding of diseased sows.

No.	11.3	11.4	11.5	11.6	11.7	11.8	11.9	11.10	11.11	11.12	11.13
1	–	–	37.74	–	36.26	36.44	–	36.12	–	38.34	38.06
2	–	35.97	–	34.49	36.03	–	36.17	37.37	**30.66**	35.58	–
3	–	36.99	–	–	–	33.78	–	39.64	36.41	36.94	–
4	–	–	–	–	–	39.16	35.03	34.37	36.68	–	–
5	–	35.24	36.72	–	–	–	36.93	33.49	33.8	–	–
6	–	36.13	35.71	**30.21**	36.03	–	–	32.08	–	–	–
7	–	–	–	**29.87**	–	–	–	37.43	37.1	38.25	–

Bold values indicate the copies of PEDV is the highest and the amount of pigs excreted is the most.

protection of existing vaccines (16). Therefore, a periodic update of coronavirus vaccine strains becomes urgent. However, even the latest PED variant vaccine strain was isolated in 2011. For example, the antigenic difference has been confirmed in the virus neutralization experiment between the epidemic strain and vaccine strain of bovine coronavirus (17). Neutralization of the virus with hyperimmune serum showed that there is only one serotype of PEDV. However, an increasing number of field surveys show that a mismatch between virus sequence analysis and serum neutralization test indicates a big difference between the antigenicity of PEDV epidemic strain and the vaccine strain. To date, the attenuated vaccine of the mutant strain continues to play a partial protective role (18). However, an increasing number of pig farms, which have undergone normal immunization procedures, continue to have outbreaks of PEDV, and the isolated strains have confirmed it to be a highly pathogenic epidemic strain.

Following the occurrence of PED in the pig farm, the outbreak has spread fast and has incurred huge losses; thus, a vaccine strain that matches that of the epidemic in the pig farm must be selected for the immunization program. At present, there are only few PED vaccine strains available in China, and pig farms will most probably use autogenous inactivated vaccines for emergency immunization. Inactivated vaccines mainly act through humoral immunity and can produce a large amount of IgA. IgA antibodies are considered the most important protective antibodies in pig colostrum and provide a protective effect for piglets (19). Our research results show that although the vaccine could produce high titers of IgA antibody, some pigs still shed virus in the milk. This shows that the existing vaccine may not completely neutralize the PEDV epidemic strain. PEDV is mainly transmitted through feces and mouth, and the viral load carried in feces is very high. Data show that 1 g of feces dissolved in 100 L of water

is highly infectious to pigs (20). Our continuous monitoring of the fecal virus shedding of diseased sows found that they could intermittently shed virus for more than 2 weeks; thus, it is particularly important to strengthen disinfection and adopt biosafety measures. From the perspective of the hazards of PEDV, before 2015, PEDV caused fulminant epidemics nationwide. Since 2016, as China has gradually gained a clear understanding of the prevention and control of PED, acute fulminant epidemics have decreased significantly. It is worth noting that the pathogenicity of highly pathogenic strains has not decreased.

To summarize, PEDV outbreaks on large-scale pig farms occurred regularly in the second half of 2020. The protective effects of inactivated and attenuated live PEDV vaccines available on the market are not satisfactory. The disease may develop despite elevated antibody titers following immunization with vaccines, which indicates that the existing vaccines may not provide adequate immune protection against epidemic strains. This may be related to the overall health of the pig herd and weak cross-protection between strains. The farm described in this report, where the infection occurred, could finally control the epidemic through immunization with autogenous inactivated vaccines, biosafety measures, and strict cleaning and disinfection. Therefore, the prevention and control of porcine epidemic diarrhea warrant comprehensive prevention and control measures. By appropriate selection of a suitable vaccine and effective management measures, ideal prevention and control may be achieved.

DATA AVAILABILITY STATEMENT

The datasets presented in this study can be found in online repositories. The names of the repository/repositories and accession number(s) can be found below: NCBI GenBank; accession no. MW646416.

AUTHOR CONTRIBUTIONS

LG analyzed the data and drafted the manuscript. QG and ZZ carried out most of the experiments. HW and SY participated in the study design. GZ conceived the study. All authors read and approved the final manuscript.

FUNDING

This research was funded by the Natural Science Foundation of Guangdong Province (2020A1515110315), Science and Technology Project of Guangdong Pig Industrial Park (GDSCYY2020-024), and the Industry Technology System of Modern Agriculture Construction Fund (CARS-35).

SUPPLEMENTARY MATERIAL

The Supplementary Material for this article can be found online at: https://www.frontiersin.org/articles/10.3389/fvets.2021.697839/full#supplementary-material

Supplementary Figure 1 | Percentages of nucleotide identity among 26 PEDV isolates based on S gene sequence.

REFERENCES

1. Lee C. Porcine epidemic diarrhea virus: an emerging and re-emerging epizootic swine virus. *Virol J*. (2015) 12:193. doi: 10.1186/s12985-015-0421-2
2. Jung K, Saif LJ. Porcine epidemic diarrhea virus infection: etiology, epidemiology, pathogenesis, and immunoprophylaxis. *Vet J*. (2015) 204:134–43. doi: 10.1016/j.tvjl.2015.02.017
3. Debouck P, Pensaert M. Experimental infection of pigs with a new porcine enteric coronavirus, CV 777. *Am J Vet Res*. (1980) 41:219–23.
4. Hua X, Dekun X, Dianying W, Weizheng Z, Fengyu Z, Huaijun G. Study on the cultivation of porcine epidemic diarrhea virus using porcine fetal intestinal monolayer cells. *J Vet Univ*. (1984) 4:202–8.
5. Liang W, Zhou D, Geng C, Yang K, Duan Z, Guo R, et al. Isolation and evolutionary analyses of porcine epidemic diarrhea virus in Asia. *PeerJ*. (2020) 8:e10114. doi: 10.7717/peerj.10114
6. Huang YW, Dickerman AW, Piñeyro P, Li L, Fang L, Kiehne R, et al. Origin, evolution, and genotyping of emergent porcine epidemic diarrhea virus strains in the United States. *mBio*. (2013) 4:e00737–13. doi: 10.1128/mBio.00737-13
7. Siqi M, Ming M, Li ZJF. Porcine epidemic diarrhea virus adapts to Vero cell culture and prepares the immune efficacy test of inactivated aluminum hydroxide vaccine by passage cytotoxicity (In Chinese). *Chin Livestock Poult Infect Dis*. (1994) 15–19.
8. Youen T, Li F, Weijie L, Yuanmao Z, Ming W, Siqi M. Study on the attenuated vaccine of transmissible gastroenteritis and epidemic diarrhea in pigs (In Chinese). *Chin J Prevent Vet Med*. (1999) 21:406–10.
9. Youen T, Li F, Weijie L, Ming W, Siqi M. Cultivation of attenuated strains of swine epidemic diarrhea (In Chinese). *Chin Livestock Poult Infect Dis*. (1998) 20:10–3.
10. Collin EA, Anbalagan S, Okda F, Batman R, Nelson E, Hause BM. An inactivated vaccine made from a U.S. field isolate of porcine epidemic disease virus is immunogenic in pigs as demonstrated by a dose-titration. *BMC Vet Res*. (2015) 11:62. doi: 10.1186/s12917-015-0357-1
11. Liu H, Han Y, Lu Y. Emergency vaccination of porcine transmissible gastroenteritis porcine epidemic diarrhea combined live vaccine (HB08+ZJ08 strain) in parturient sows on the protective effect of newborn piglets (In Chinese). *Pig*. (2018) 2018:101–3. doi: 10.13257/j.cnki.21-1104/s.2018.03.040
12. Bi J, Zeng S, Xiao S, Chen H, Fang L. Complete genome sequence of porcine epidemic diarrhea virus strain AJ1102 isolated from a suckling piglet with acute diarrhea in China. *J Virol*. (2012) 86:10910–1. doi: 10.1128/JVI.01919-12
13. Lowe J, Gauger P, Harmon K, Zhang J, Connor J, Yeske P, et al. Role of transportation in spread of porcine epidemic diarrhea virus infection, United States. *Emerg Infect Dis*. (2014) 20:872–4. doi: 10.3201/eid2005.131628
14. Olanratmanee EO, Kunavongkrit A, Tummaruk P. Impact of porcine epidemic diarrhea virus infection at different periods of pregnancy on subsequent reproductive performance in gilts and sows. *Anim Reprod Sci*. (2010) 122:42–51. doi: 10.1016/j.anireprosci.2010.07.004
15. Kim SH, Lee JM, Jung J, Kim IJ, Hyun BH, Kim HI, et al. Genetic characterization of porcine epidemic diarrhea virus in Korea from 1998 to 2013. *Arch Virol*. (2015) 160:1055–64. doi: 10.1007/s00705-015-2353-y
16. Lin CM, Saif LJ, Marthaler D, Wang Q. Evolution, antigenicity, and pathogenicity of global porcine epidemic diarrhea virus strains. *Virus Res*. (2016) 226:20–39. doi: 10.1016/j.virusres.2016.05.023
17. Kanno T, Ishihara R, Hatama S, Uchida I. Antigenic variation among recent Japanese isolates of bovine coronaviruses belonging to phylogenetically distinct genetic groups. *Arch Virol*. (2013). 158:1047–53. doi: 10.1007/s00705-012-1587-1

18. Sun D, Wang X, Wei S, Chen J, Feng L. Epidemiology and vaccine of porcine epidemic diarrhea virus in China: a mini-review. *J Vet Med Sci*. (2016) 78:355–63. doi: 10.1292/jvms.15-0446
19. Zhang E, Wang J, Li Y, Huang L, Wang Y, Yang Q. Comparison of oral and nasal immunization with inactivated porcine epidemic diarrhea virus on intestinal immunity in piglets. *Exp Ther Med*. (2020) 20:1596–606. doi: 10.3892/etm.2020.8828
20. Tianzhi L, Xinyou Y, Ying Z. The prevalence and prevention and control measures of swine epidemic diarrhea (In Chinese). *Chin J Prevent Vet Med*. (2018) 35:98–99.

Conflict of Interest: The authors declare that the research was conducted in the absence of any commercial or financial relationships that could be construed as a potential conflict of interest.

frontiers in Veterinary Science

ORIGINAL RESEARCH
published: 03 September 2021
doi: 10.3389/fvets.2021.726723

Single Multiple Cross Displacement Amplification for Rapid and Real-Time Detection of Porcine Circovirus 3

Zhibiao Bian[1,2,3,4], *Rujian Cai*[1,2,3,4], *Zhiyong Jiang*[1,2,3,4], *Shuai Song*[1,2,3,4], *Yan Li*[1,2,3,4], *Pinpin Chu*[1,2,3,4], *Kunli Zhang*[1,2,3,4], *Dongxia Yang*[1,2,3,4], *Hongchao Gou*[1,2,3,4]* and *Chunling Li*[1,2,3,4]*

[1] Institute of Animal Health, Guangdong Academy of Agricultural Sciences, Guangzhou, China, [2] Guangdong Provincial Key Laboratory of Livestock Disease Prevention, Guangzhou, China, [3] Maoming Branch, Guangdong Laboratory for Lingnan Modern Agriculture, Maoming, China, [4] Scientific Observation and Experiment Station of Veterinary Drugs and Diagnostic Techniques of Guangdong Province, Guangzhou, China

OPEN ACCESS

Edited by:
Feng Li,
South Dakota State University, United States

Reviewed by:
Yijun Du,
Shandong Academy of Agricultural Sciences, China
Shaohui Wang,
Shanghai Veterinary Research Institute, Chinese Academy of Agricultural Sciences (CAAS), China

***Correspondence:**
Hongchao Gou
gouhc@hotmail.com
Chunling Li
lclcare@163.com

Specialty section:
This article was submitted to Veterinary Infectious Diseases, a section of the journal Frontiers in Veterinary Science

Received: *17 June 2021*
Accepted: *04 August 2021*
Published: *03 September 2021*

Citation:
Bian Z, Cai R, Jiang Z, Song S, Li Y, Chu P, Zhang K, Yang D, Gou H and Li C (2021) Single Multiple Cross Displacement Amplification for Rapid and Real-Time Detection of Porcine Circovirus 3. Front. Vet. Sci. 8:726723. doi: 10.3389/fvets.2021.726723

Since 2016, a novel porcine circovirus, PCV3, has been infecting pigs, causing significant economic losses to the pig industry. In recent years, the infection rate of PCV3 has been increasing, and thus rapid and accurate detection methods for PCV3 are essential. In this study, we established a novel probe-based single multiple cross displacement amplification (P-S-MCDA) method for PCV3. The method was termed as P-S-MCDA. The P-S-MCDA uses seven primers to amplify the capsid gene, and the assay can be performed at 60°C for 30 min, greatly shortening the reaction time. The results of P-S-MCDA can not only be monitored in real time through fluorescence signals but also be determined by observing the fluorescence of the reaction tubes using a smartphone-based cassette. This method demonstrated good specificity and the same sensitivity as qPCR, with a minimum detection limit of 10 copies. In 139 clinical samples, the coincidence rate with qPCR was 100%. The P-S-MCDA can be widely applied in PCV3 detection in laboratories or in rural areas.

Keywords: PCV3, single multiple cross displacement amplification, detection, probe, quantitative

INTRODUCTION

Porcine circovirus (PCV), one of the smallest known animal viruses, belongs to the family *Circovirus*. Two members of PCV are well-known, namely, PCV1 and PCV2 (1). In 2016, a novel PCV, PCV3, was identified in the USA. Many other countries have also reported the presence of PCV3 in piglets, for example, the UK (2), Germany (3), China (4), Japan (5), Brazil (6), and Russia (7). PCV3 causes a variety of pathological symptoms in piglets and sows such as porcine dermatitis and nephrotic syndrome (PDNS)-like clinical signs, reproductive failure, cardiac pathology, and multi-system inflammation (8). Virus genome detection from the tissues of infected animals has shown that the degree of PCV3 infection in animals gradually increases, eventually infecting almost all tissues and organs (9). Moreover, the virus has spread rapidly among pigs and wild boars. Strikingly, PCV3 was recently found to be epidemic in cattle, mice, deer, and ticks. The ability of PCV3 to undergo cross-species transmission and circulation among a broad range of animals

suggests that it may pose a severe threat to other animals (10). This complicates the control measures for PCV3. To date, the virus has caused huge economic losses in the global pig industry (11). Therefore, it is necessary to develop a rapid and accurate detection method to describe and control the epidemiological characteristics of PCV3.

The common diagnostic methods for PCV3 include virus isolation, indirect immunofluorescence testing, ELISA, and nucleic acid detection. Although virus isolation and indirect immunofluorescence testing are standard detection methods, they are complicated and need to be conducted in laboratories with suitable conditions. Hence, nucleic acid detection methods, including PCR, qPCR, and isothermal amplification, are more widely used in PCV3 detection. Previous nucleic acid detection methods for PCV3 include PCR (12), SYBR Green-based qPCR (13), TaqMan-based qPCR (14), loop-mediated isothermal amplification (LAMP) (15), and recombinase polymerase amplification (RPA) (16). Characteristics of qPCR-based methods are high sensitivity and specificity, but the expensive thermal cycler instruments limit their wide application. In contrast, isothermal amplification assays are usually easy to operate, but their less specific properties limit their use in accurate detection.

Recently, a novel isothermal amplification strategy named single multiple cross displacement amplification (S-MCDA) has been developed that not only is more sensitive than LAMP but also can significantly shorten the reaction time (17). To realize the aim of rapid and accurate detection of PCV3, we established a novel probe based on the S-MCDA method, termed as P-S-MCDA, in this study. The P-S-MCDA is not only capable of quantitative analysis of PCV3 in real time but also specific, sensitive, and easy to operate. Moreover, the P-S-MCDA assay results can be visually determined using a small handheld device. When the method was compared with qPCR in analyzing clinical samples, an equal consistency ratio was obtained. Therefore, our P-S-MCDA assay may provide a priority choice for the rapid diagnosis of PCV3.

MATERIALS AND METHODS

Ethics Statement

All animal experiments were reviewed and approved by the ethical and ethics commission (Institute of Animal Health, Guangdong Academy of Agricultural Sciences, China) under license number SYXK (Yue) 2011-0116. Moreover, sample collection in this study was performed in accordance with national and local laws or guidelines.

Virus, Bacteria, and Cells

As previously described, PCV2 isolate HN6 (GenBank no: KM035762.1), PCV1, pseudorabies virus (PRV) GD-WH strain (GenBank no: KT936468.1), *Haemophilus parasuis* (HPS) serotype 5, *Streptococcus suis* (SS) serotype 2, and *Actinobacillus pleuropneumoniae* (APP) Serovar 1 were preserved in our laboratory. They were first used to extract nucleic acids and then to evaluate the specificity of the P-S-MCDA.

Animals and Clinical Samples

In 2020–2021, a total of 139 clinical samples from pig farms in Guangdong Province were collected and sent to our laboratory for detection. These clinical samples included blood, lung, kidney, brain, spleen, lymph node, and tonsil. In addition, 15 blood samples were collected from specific-pathogen-free (SPF) pigs (5 months old) that were purchased from the Laboratory Animal Center of Southern Medical University Guangzhou (4). All samples were stored at −80°C until DNA extraction.

DNA Extraction

All viral DNA for the study was extracted by using a HiPure Viral RNA/DNA Kit (Magen, China) according to the manufacturer's instructions. Bacterial DNA was extracted using the TaKaRa MiniBEST Bacteria Genomic DNA Extraction Kit Ver. 3.0 (Takara, China) according to the manufacturer's protocol. All of the final DNA was stored at −80°C.

Plasmid Construction

The construction of plasmids was done exactly as previously described (18). The capsid gene used to construct the plasmid was amplified from nucleic acid positive for PCV3, and the products were purified using the Cycle Pure Kit according to the manufacturer's instructions (Omega, USA). The pMDTM19-T Vector (TaKaRa Biotechnology, China) and the obtained target gene were ligated overnight at 16°C using T4 DNA Ligase (TaKaRa Biotechnology, China). After the pMD19T-capsid plasmid was transformed into DH5α competent cells, the plasmid DNA was extracted using a Plasmid Mini Kit I (Omega, USA).

P-S-MCDA Primers and Probes Design

The conserved region of the capsid gene was determined by alignment of PCV3 strains indexed in the GenBank (accession nos: MF589105.1, MF589107.1, MF769811.1, MF769807.1, MF084994.1, KX778720.1, KX898030.1, MG310152.1, MF079254.1, and MG250187.1). According to the principle of S-MCDA, capsid gene sequences of PCV3-US/MO2015 strain (accession no: KX778720.1) were input for P-S-MCDA primer design by using the software Primer Premier 5.0 (17). Among multiple sets of primers, the primers targeting the conserved regions of the capsid gene were selected for subsequent analysis. P-S-MCDA primers used in this study are listed in **Table 1**. In addition, a probe and its complementary quencher oligonucleotides were included.

P-S-MCDA Assay

To establish the P-S-MCDA, the reaction mixture containing 1× Isothermal Amplification Buffer (New England Biolabs, USA), 6 mM $MgSO_4$ (New England Bio-labs, USA), 1.6 mM High Pure dNTPs (TransGen Biotech, China), and 8U Bst WarmStart DNA Polymerase (New England Biolabs, USA) was prepared. To perform the P-S-MCDA reaction, the concentration of primers was optimized and determined as 1.6 μM CP1/CP2, 0.2 μM F1/F2, 0.8 μM C1/D1, 0.24 μM R1, and 0.32 μM quencher. Then, the reaction tube was incubated in a real-time PCR detection system (Roche Light Cycler 480 II, Switzerland). The reaction

TABLE 1 | Primers of the P-S-MCDA assay for PCV3.

Primer name	Sequences 5′→3′	Genome position[a]
CP1 (C1+P1)	CTCACCCAGGACAAAGCCTCTT-CATTGAACGGTGGGGTCAT	C1: 1,497–1,518 P1: 1,443–1,461
CP2 (C2+P2)	TGGTTTCGGGGTGAAGTAACGG-AGACGACCCTTATGCGGAA	C2: 1,541–1,562 P2: 1,604–1,622
F1	CCGGGACATAAATGCTCCAA	1,411–1,430
F2	CCACAAACACTTGGCTCCA	1623–1,641
C1	CTCACCCAGGACAAAGCCTCTT	1,497–1,518
D1	CCCACCCCATGGCTCAACA	1,465–1,483
R1	FAM-[b]*CGGGTTTGCGCTCAGCCATCCGTTCAGTCCGTCAGGTCAG*-ATTCTGGCGGGAACTACC	1,523–1,540
Quencher	[b]*CTGACCTGACGGACTGAACGGATGGCTGAGCGCAAACCCG*-Dabcyl	None

[a]*The genome of PCV3-US/MO2015 strain (accession no: KX778720.1).*
[b]*Italic font indicates complementary oligonucleotides flanked at 5′ of R1 primer.*

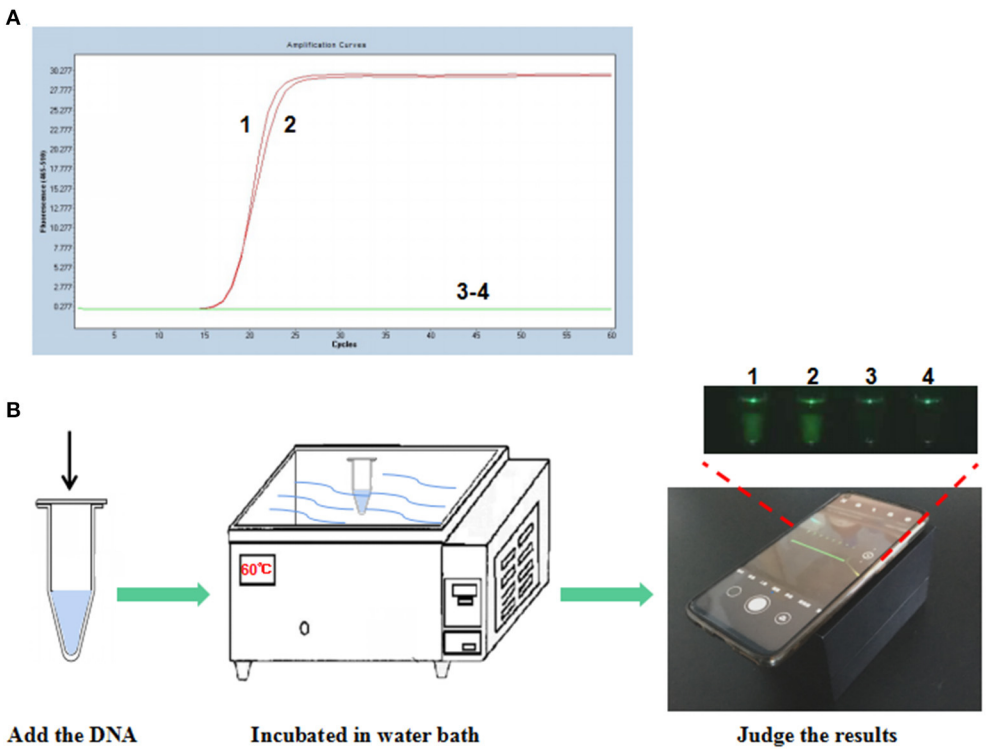

FIGURE 1 | Establishment of the P-S-MCDA assay for PCV3. **(A)** P-S-MCDA method assay by the Roche Light Cycler 480 II. **(B)** Flowchart of the P-S-MCDA method combined with smartphone-based cassette. Lanes or Tubes 1–2, 10^5 copies of pMD19T-capsid plasmid DNA. Lanes or Tubes 3–4, ddH_2O.

program was set as follows: 30 cycles at 60°C for 1 min. FAM fluorescence signals were obtained at the end of each cycle step. The results could be directly judged by color changes or *via* the cycle threshold (Ct) value. A Ct value ≤ 30 indicated positive results, while a Ct value > 30 indicated negative results.

P-S-MCDA Assay in the Smartphone-Based Cassette

P-S-MCDA is conducted at a constant temperature of 60°C in a water bath for 30 min (YIHENG Technical, China). Then, the reaction tube is placed into a smartphone-based cassette (19), and the photos are obtained using a Nova5z smartphone (Huawei, China). The result of each reaction tube can be determined *via* color judgment by eye. A positive reaction fluoresces green, while a negative reaction has no color.

TaqMan-Based qPCR

TaqMan-based qPCR of PCV3 was conducted in accordance with the previous report (14). The 25-μL reaction mixture contained 0.4 μM of each primer and probe, 1× qPCR Probe Master

Mix (Vazyme, China), and 2 μL template DNA. The reaction program was set as follows: 95°C for 3 min followed by 40 cycles at 95°C for 10 s and 60°C for 60 s. FAM fluorescence signals were obtained at the end of each annealing step by the real-time PCR detection system (Roche Light Cycler 480 II, Switzerland). Results with a Ct value of <40 were considered positive, while results with no Ct value within 40 cycles were considered negative.

Specificity Analysis

DNA extracted from PCV1, PCV2, PRV GD-WH strain, HPS, SS, and APP were used as DNA templates for evaluating the specificity of the method. P-S-MCDA and qPCR were conducted in a real-time PCR detection system (Roche Light Cycler 480 II, Switzerland).

Sensitivity Analysis

The pMD19T-capsid plasmid was diluted to 10^5, 10^4, 10^3, 10^2, 10^1, 10^0, and 10^{-1} copies as standard DNA to assess the sensitivity of P-S-MCDA. The negative control (ddH_20) was also tested. The detection limit of the P-S-MCDA was compared with qPCR in parallel.

Evaluation of Clinical Application

A total of 139 suspected clinical samples and 15 blood samples from SPF pigs were used for DNA extraction and P-S-MCDA detection. Meanwhile, the results were verified by TaqMan-based qPCR.

RESULTS

Establishment of the P-S-MCDA

To establish the P-S-MCDA method, seven primers were used to amplify the target gene. One of the amplified primers, R1, was linked with an extra oligonucleotide and modified at the 5′ end with FAM fluorescence. In the initial reaction system, R1 can be combined by its complementary quencher primer, and the fluorescence signal is dampened. In the process of incubation at 60°C for 30 min, P-S-MCDA primers initiate the circular reaction after binding to the PCV3 capsid gene, and the quencher primer is displaced by the reverse elongation complementary with R1 primer. At this point, a fluorescence signal will be released and monitored. The negative control has no fluorescence curve because no circular reaction exists in the tube. Therefore, the positive result of the P-S-MCDA will be calculated as the Ct value by the real-time PCR detection system or judged by using the smartphone-based cassette (**Figures 1A,B**).

Specificity of the P-S-MCDA

To evaluate the specificity of the P-S-MCDA method, DNA samples extracted from PCV2, PCV1, PRV GD-WH strain, HPS, SS, and APP were analyzed in parallel with the PCV3 capsid gene. The results showed that only the PCV3 capsid gene could initiate

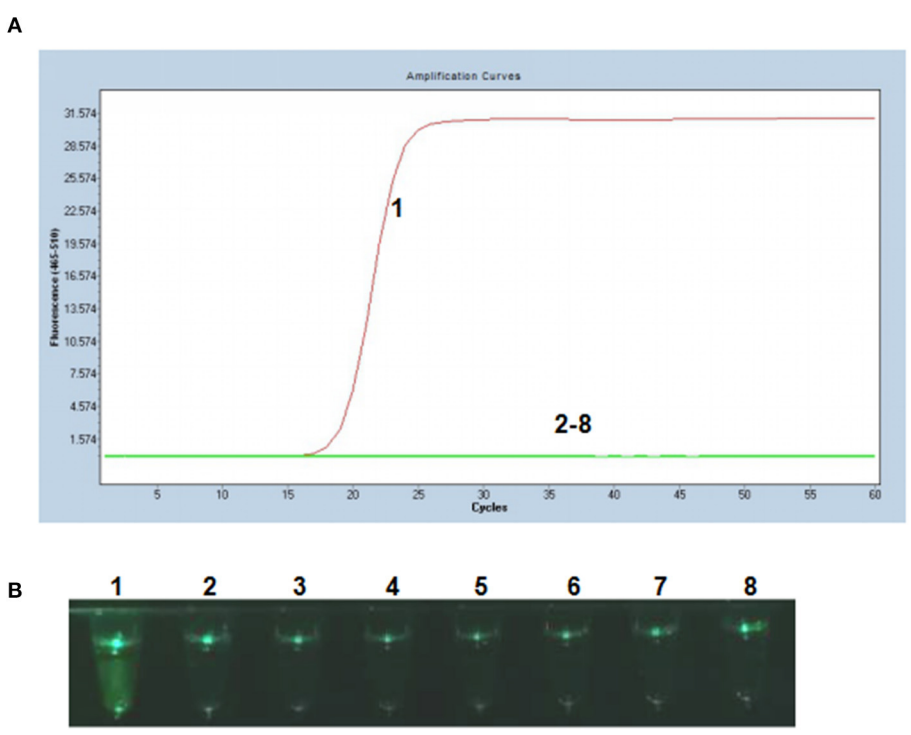

FIGURE 2 | Specificity of the P-S-MCDA assay for PCV3. **(A)** Specificity of P-S-MCDA by the Roche Light Cycler 480 II. **(B)** Specificity of P-S-MCDA by the smartphone-based cassette. Lane or Tube 1, 10^5 copies of pMD19T-capsid plasmid DNA. Lanes or Tubes 2–8, ddH_2O, PCV2, PCV1, PRV GD-WH strain, HPS, SS, and APP, respectively.

the P-S-MCDA reaction with a fluorescence curve (**Figure 2A**) or a fluoresces green tube (**Figure 2B**). This demonstrated the specificity of the P-S-MCDA.

Sensitivity of the P-S-MCDA

Tenfold serial dilutions of PCV3 capsid gene DNA (10^5, 10^4, 10^3, 10^2, 10^1, 10^0, and 10^{-1} copies) were used as DNA templates to compare the detection limits of the P-S-MCDA with qPCR. In this study, P-S-MCDA displayed a minimum detection limit of 10 copies in 30 min (**Figure 3A**). Moreover, we found that the fluorescence signal was strong enough to be observed in a smartphone-based cassette (**Figure 3B**). When the serially diluted samples were analyzed by qPCR, the 10 copies detection limit was also observed (**Figure 3C**).

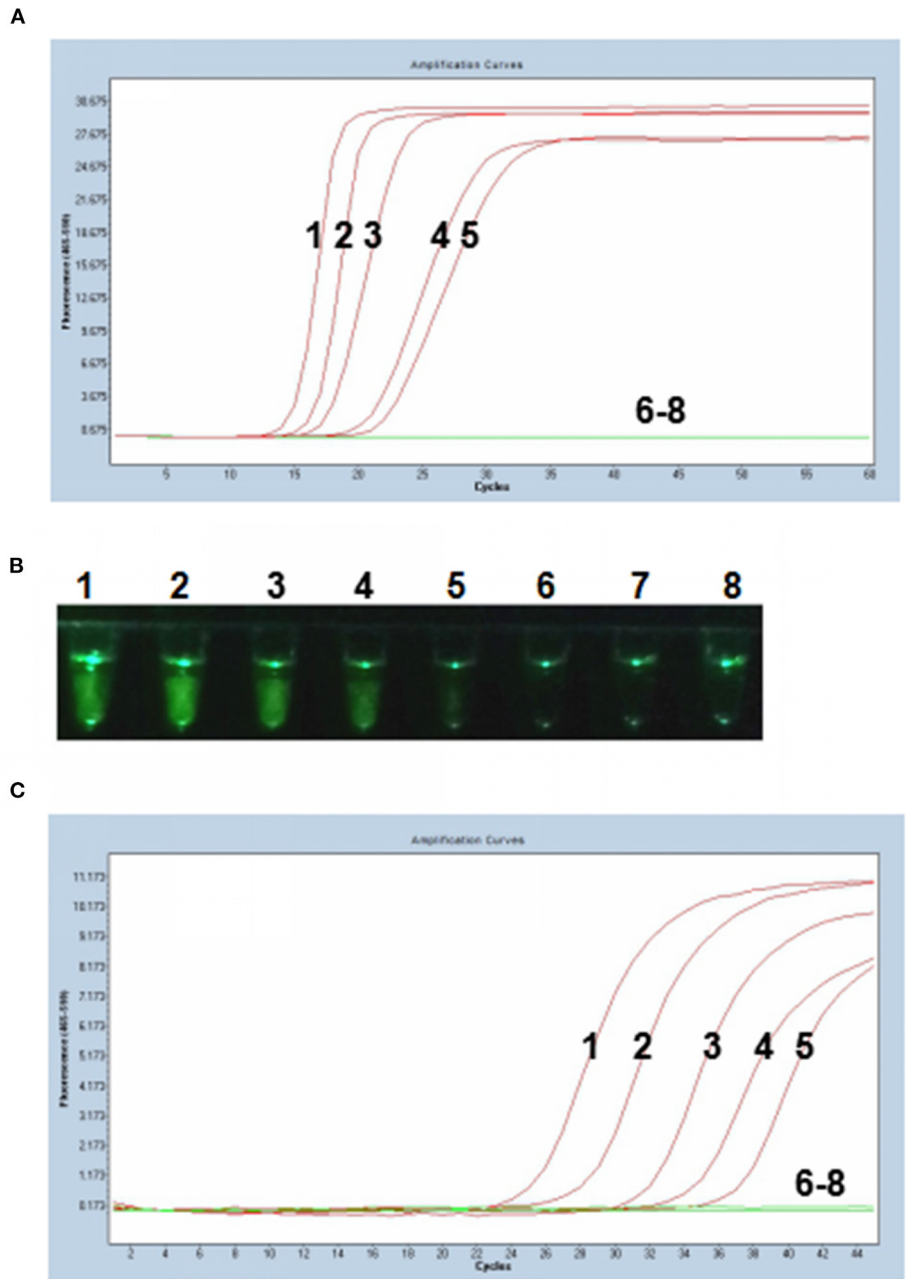

FIGURE 3 | Comparison of sensitivity of the P-S-MCDA and qPCR. **(A)** Sensitivity of P-S-MCDA by the Roche Light Cycler 480 II. **(B)** Sensitivity of P-S-MCDA using a smartphone-based cassette. **(C)** Sensitivity of qPCR by the Roche Light Cycler 480 II. Lanes or Tubes 1–7, DNA of pMD19T-capsid plasmid (10^5, 10^4, 10^3, 10^2, 10^1, 10^0, and 10^{-1} copies). Lane or Tube 8, ddH_2O.

TABLE 2 | Detection of PCV3 in clinical samples by the P-S-MCDA and qPCR.

Method	No. of positive samples	No. of negative samples	Detection rate[a]
P-S-MCDA	40	99	28.78%
qPCR	40	99	28.78%

[a] *Detection rate was defined by no. of positive samples/no. of total samples(%).*

Evaluation of Clinical Application

Among 139 clinical samples, 40 positive results were detected by the qPCR method. The positive rate was 28.78% (40/139). Additionally, the P-S-MCDA assay showed a consistent positive rate with TaqMan-based qPCR (**Table 2**). Furthermore, 15 blood tissues sampled from SPF pigs were analyzed by using both P-S-MCDA and qPCR to test the accuracy of P-S-MCDA for diagnosis of negative animals. Negative results were obtained using both methods.

DISCUSSION

Since PCV3 was identified in 2016, further studies have uncovered its pathological features in piglets and cross-species transmission possibility. Therefore, it is necessary to establish a highly efficient and sensitive detection method to perform further molecular epidemiological investigations and facilitate timely control. In this study, we established a novel PCV3 P-S-MCDA detection method.

The P-S-MCDA combines the advantages of qPCR and isothermal strand-displacement polymerization reaction in that the method not only ensures the high sensitivity of qPCR but also can amplify target genes under constant temperature. Compared with qPCR, the reaction without complex thermal deformation steps only needs to be in a constant temperature environment of 60°C, so it can be easily performed. Compared with colorimetric isothermal amplification, P-S-MCDA is a probe-based real-time fluorescence detection method, avoiding the possible non-specific reactions and the uncertainty of results caused by visual errors. Moreover, the reaction system can be carried out at a constant temperature of 60°C and completed within 30 min, and the results can be visually judged by the real-time detection system or using a smartphone-based cassette (19). The test can save 20 min compared with novel polymerase spiral reaction (20), 40 min compared with real-time loop-mediated isothermal amplification (15), and at least 60 min compared with qPCR or PCR (13, 14).

The PCV3 ORF2 gene is associated with host-range specificity and virus independence as it encodes the capsid protein of PCV3. The gene has a strongly conserved sequence. Therefore, it is advisable to use ORF2 as a target fragment for nucleic acid detection (21, 22). In our study, seven primers of the P-S-MCDA spanning eight distinct regions of the target gene were designed using the software Primer Premier 5.0. The primer design procedure is easier to perform than LAMP. The analysis showed that this method had good specificity, with no cross false reaction with other porcine viral pathogens. Most isothermal amplification techniques use color change (4, 20) or turbidity (17) to interpret the results, but P-S-MCDA monitors the amplification of the target gene in real time quantitatively by the real-time PCR detection system. Therefore, the P-S-MCDA not only avoids the error of visual interpretation of the results but also is capable of quantitative analysis of target gene sequences. The detection limit of the P-S-MCDA is as low as 10 copies, consistent with qPCR and 10 times more sensitive than previously reported PCR results (18, 23–25). Moreover, a practical pathogen detection method not only needs to be rapid, specific, sensitive, and simple but also to be economical. Compared to many testing methods, P-S-MCDA has desirable economical features such as lower reagent cost compared to RAA (26) and less equipment requirements than droplet digital PCR (27).

In analyzing clinical samples, P-S-MCDA showed a consistent accuracy rate compared with qPCR methods. What is noticeable is that some laboratories on the clinical frontier may have limit advanced equipment, such as the expensive real-time PCR detection system. Moreover, another advance of the P-S-MCDA method is that it can be combined with a smartphone-based cassette, and thus only a simple box can be used to determine the results by eye. Therefore, the P-S-MCDA can be used to real-time quantitative monitor of target genes by the real-time PCR detection system and can also be applied in rural areas with limited facilities.

In summary, the P-S-MCDA assay was demonstrated to be a simple, rapid, sensitive, specific, and economical detection method for PCV3. It is valuable for PCV3 real-time detection in laboratories or at point of care testing in rural areas.

DATA AVAILABILITY STATEMENT

The raw data supporting the conclusions of this article will be made available by the authors, without undue reservation.

ETHICS STATEMENT

The animal study was reviewed and approved by Institute of Animal Health, Guangdong Academy of Agricultural Sciences, China. The license number was SYXK (Yue) 2011-0116.

AUTHOR CONTRIBUTIONS

ZB performed the experiments and drafted the manuscript. HG conceived the experiments and revised the manuscript. PC, KZ, and DY prepared materials for the experiments. SS, ZJ, and YL participated in the analysis of the data. CL and RC supervised the study. All authors read and approved the final manuscript.

FUNDING

This work was supported by grants from the Key Areas of Research and Development Program of Guangdong, China (No. 2019B020217002), the Natural Science Foundation of China (No. 31902273), the Natural Science Foundation of Guangdong,

China (Nos. 2019A1515010757 and 2020A1515010475), the Science and Technology Program of Guangzhou, China (No. 201906040005), and the Special Fund for Scientific Innovation Strategy-Construction of High Level Academy of Agriculture Science (Nos. R2017YJ-YB2005 and R2018QD-094).

ACKNOWLEDGMENTS

We thank Dr. Jianmin Zhang (College of Veterinary Medicine, South China Agricultural University) for kindly providing the device named smartphone-based cassette.

REFERENCES

1. Han L, Yuan GF, Chen SJ, Dai F, Hou LS, Fan JH, et al. Porcine circovirus type 2 (PCV2) infection in Hebei Province from 2016 to 2019: a retrospective study. *Arch Virol*. (2021) 166:2159–2171. doi: 10.1007/s00705-021-05085-z
2. Collins PJ, McKillen J, Allan G. Porcine circovirus type 3 in the UK. *Vet Rec*. (2017) 181:599. doi: 10.1136/vr.j5505
3. Fux R, Söckler C, Link EK, Renken C, Krejci R, Sutter G, et al. Full genome characterization of porcine circovirus type 3 isolates reveals the existence of two distinct groups of virus strains. *Virol J*. (2018) 15:25. doi: 10.1186/s12985-018-0929-3
4. Gou H, Bian Z, Cai R, Jiang Z, Song S, Li Y, et al. The colorimetric isothermal multiple-self-matching-initiated amplification using cresol red for rapid and sensitive detection of porcine circovirus 3. *Front Vet Sci*. (2020) 7:407. doi: 10.3389/fvets.2020.00407
5. Hayashi S, Ohshima Y, Furuya Y, Nagao A, Oroku K, Tsutsumi N, et al. First detection of porcine circovirus type 3 in Japan. *J Vet Med Sci*. (2018) 80:1468–72. doi: 10.1292/jvms.18-0079
6. Tochetto C, Lima DA, Varela APM, Loiko MR, Paim WP, Scheffer CM, et al. Full-genome sequence of porcine circovirus type 3 recovered from serum of sows with stillbirths in Brazil. *Transbound Emerg Dis*. (2018) 65:5–9. doi: 10.1111/tbed.12735
7. Yuzhakov AG, Raev SA, Alekseev KP, Grebennikova TV, Verkhovsky OA, Zaberezhny AD, et al. First detection and full genome sequence of porcine circovirus type 3 in Russia. *Virus Genes*. (2018) 54:608–11. doi: 10.1007/s11262-018-1582-z
8. Jiang H, Wang D, Wang J, Zhu S, She R, Ren X, et al. Induction of porcine dermatitis and nephropathy syndrome in piglets by infection with porcine circovirus type 3. *J Virol*. (2019) 93:e02045-18. doi: 10.1128/jvi.02045-18
9. Ouyang T, Niu G, Liu X, Zhang X, Zhang Y, Ren L. Recent progress on porcine circovirus type 3. *Infect Genet Evol*. (2019) 73:227–33. doi: 10.1016/j.meegid.2019.05.009
10. Jiang H, Wei L, Wang D, Wang J, Zhu S, She R, et al. ITRAQ-based quantitative proteomics reveals the first proteome profiles of piglets infected with porcine circovirus type 3. *J Proteomics*. (2020) 212:103598. doi: 10.1016/j.jprot.2019.103598
11. Liu Y, Meng H, Shi L, Li L. Sensitive detection of porcine circovirus 3 by droplet digital PCR. *J Vet Diagn Invest*. (2019) 31:604–7. doi: 10.1177/1040638719847686
12. Nguyen NH, Do Tien D, Nguyen TQ, Nguyen TT, Nguyen MN. Identification and whole-genome characterization of a novel Porcine Circovirus 3 subtype b strain from swine populations in Vietnam. *Virus Genes*. (2021) 57:385–389. doi: 10.1007/s11262-021-01844-x
13. Hou CY, Xu T, Zhang LH, Cui JT, Zhang YH, Li XS, et al. Simultaneous detection and differentiation of porcine circovirus 3 and 4 using a SYBR Green ı-based duplex quantitative PCR assay. *J Virol Methods*. (2021) 293:114152. doi: 10.1016/j.jviromet.2021.114152
14. Palinski R, Piñeyro P, Shang P, Yuan F, Guo R, Fang Y, et al. A novel porcine circovirus distantly related to known circoviruses is associated with porcine dermatitis and nephropathy syndrome and reproductive failure. *J Virol*. (2017) 91:e01879-16. doi: 10.1128/jvi.01879-16
15. Wang H, Liu X, Zeng F, Zhang T, Lian Y, Wu M, et al. Development of a real-time loop-mediated isothermal amplification assay for detection of porcine circovirus 3. *BMC Vet Res*. (2019) 15:305. doi: 10.1186/s12917-019-2037-z
16. Wang J, Zhang Y, Zhang R, Han Q, Wang J, Liu L, et al. Recombinase polymerase amplification assay for rapid detection of porcine circovirus 3. *Mol Cell Probes*. (2017) 36:58–61. doi: 10.1016/j.mcp.2017.09.001
17. Wang Y, Wang Y, Ma AJ, Li DX, Luo LJ, Liu DX, et al. Rapid and sensitive isothermal detection of nucleic-acid sequence by multiple cross displacement amplification. *Sci Rep*. (2015) 5:11902. doi: 10.1038/srep11902
18. Ku X, Chen F, Li P, Wang Y, Yu X, Fan S, et al. Identification and genetic characterization of porcine circovirus type 3 in China. *Transbound Emerg Dis*. (2017) 64:703–8. doi: 10.1111/tbed.12638
19. Wen J, Gou H, Wang S, Lin Q, Chen K, Wu Y, et al. Competitive activation cross amplification combined with smartphone-based quantification for point-of-care detection of single nucleotide polymorphism. *Biosens Bioelectron*. (2021) 183:113200. doi: 10.1016/j.bios.2021.113200
20. Ji J, Xu X, Wang X, Zuo K, Li Z, Leng C, et al. Novel polymerase spiral reaction assay for the visible molecular detection of porcine circovirus type 3. *BMC Vet Res*. (2019) 15:322. doi: 10.1186/s12917-019-2072-9
21. Oh T, Chae C. First isolation and genetic characterization of porcine circovirus type 3 using primary porcine kidney cells. *Vet Microbiol*. (2020) 241:108576. doi: 10.1016/j.vetmic.2020.108576
22. Chung HC, Nguyen VG, Park YH, Park BK. Genotyping of PCV3 based on reassembled viral gene sequences. *Vet Med Sci*. (2021) 7:474–82. doi: 10.1002/vms3.374
23. Wang J, Zhang Y, Wang J, Liu L, Pang X, Yuan W. Development of a TaqMan-based real-time PCR assay for the specific detection of porcine circovirus 3. *J Virol Methods*. (2017) 248:177–80. doi: 10.1016/j.jviromet.2017.07.007
24. Yang K, Jiao Z, Zhou D, Guo R, Duan Z, Tian Y. Development of a multiplex PCR to detect and discriminate porcine circoviruses in clinical specimens. *BMC Infect Dis*. (2019) 19:778. doi: 10.1186/s12879-019-4398-0
25. Yuan L, Liu Y, Chen Y, Gu X, Dong H, Zhang S, et al. Optimized real-time fluorescence PCR assay for the detection of porcine Circovirus type 3 (PCV3). *BMC Vet Res*. (2020) 16:249. doi: 10.1186/s12917-020-02435-y
26. Li Y, Yu Z, Jiao S, Liu Y, Ni H, Wang Y. Development of a recombinase-aided amplification assay for rapid and sensitive detection of porcine circovirus 3. *J Virol Methods*. (2020) 282:113904. doi: 10.1016/j.jviromet.2020.113904
27. Zhang Y, Zhang Z, Wang Z, Wang Z, Wang C, Feng C, et al. Development of a droplet digital PCR assay for sensitive detection of porcine circovirus 3. *Mol Cell Probes*. (2019) 43:50–7. doi: 10.1016/j.mcp.2018.11.005

Conflict of Interest: The authors declare that the research was conducted in the absence of any commercial or financial relationships that could be construed as a potential conflict of interest.

Publisher's Note: All claims expressed in this article are solely those of the authors and do not necessarily represent those of their affiliated organizations, or those of the publisher, the editors and the reviewers. Any product that may be evaluated in this article, or claim that may be made by its manufacturer, is not guaranteed or endorsed by the publisher.

frontiers in Veterinary Science

ORIGINAL RESEARCH
published: 25 October 2021
doi: 10.3389/fvets.2021.730701

Buffalo-Origin Seneca Valley Virus in China: First Report, Isolation, Genome Characterization, and Evolution Analysis

Xia Zhou[1,2,3†], Wei-Fang Liang[1†], Guang-Bin Si[1], Jin-Hui Li[1], Zhi-Fei Chen[1], Wei-You Cai[1], Dian-Hong Lv[2,3], Xiao-Hui Wen[2,3], Qi Zhai[2,3], Shao-Lun Zhai[2,3], Ming Liao[2,3*] and Dong-Sheng He[1*]*

[1] College of Veterinary Medicine, South China Agricultural University, Guangzhou, China, [2] Institute of Animal Health, Guangdong Academy of Agricultural Sciences, Scientific Observation and Experiment Station of Veterinary Drugs and Diagnostic Techniques of Guangdong Province, Ministry of Agriculture of Rural Affairs, Guangzhou, China, [3] Key Laboratory of Animal Disease Prevention of Guangdong Province, Guangzhou, China

OPEN ACCESS

Edited by:
Min Yue,
Zhejiang University, China

Reviewed by:
Laura Nicoleta Burga,
University of Otago, New Zealand
Alexey V. Rakov,
Somov Institute of Epidemiology and Microbiology, Russia

***Correspondence:**
Shao-Lun Zhai
zhaishaolun@163.com
orcid.org/0000-0003-3217-2256
Ming Liao
mliao@scau.edu.cn
Dong-Sheng He
dhe@scau.edu.cn

[†] These authors have contributed equally to this work

Specialty section:
This article was submitted to Veterinary Infectious Diseases, a section of the journal Frontiers in Veterinary Science

Received: 25 June 2021
Accepted: 20 September 2021
Published: 25 October 2021

Citation:
Zhou X, Liang W-F, Si G-B, Li J-H, Chen Z-F, Cai W-Y, Lv D-H, Wen X-H, Zhai Q, Zhai S-L, Liao M and He D-S (2021) Buffalo-Origin Seneca Valley Virus in China: First Report, Isolation, Genome Characterization, and Evolution Analysis. Front. Vet. Sci. 8:730701. doi: 10.3389/fvets.2021.730701

Pigs are the main host of Seneca Valley virus (SVV), previously known as Senecavirus A (SVA). Pigs affected by SVV have vesicles in the nose, hooves, and limp and may cause death in some severe cases. Occasionally, SVV has also been detected in mice, houseflies, environmental equipment, and corridors in pig farms. Moreover, it was successfully isolated from mouse tissue samples. In this study, an SVV strain (SVA/GD/China/2018) was isolated from a buffalo with mouth ulcers in the Guangdong province of China using seven mammalian cell lines (including BHK-21, NA, PK-15, ST, Vero, Marc-145, and MDBK). The genome of SVA/GD/China/2018 consists of 7,276 nucleotides. Multiple-sequence alignment showed that SVA/GD/China/2018 shared the highest nucleotide similarity (99.1%) with one wild boar-origin SVV strain (Sichuan HS-01) from the Sichuan province of China. Genetic analysis revealed that SVA/GD/China/2018 clustered with those porcine-origin SVV strains. To the best of our knowledge, this is the first report of SVV infection in buffalo, which might expand the host range of the virus. Surveillance should be expanded, and clinical significance of SVV needs to be further evaluated in cattle.

Keywords: Seneca Valley virus, porcine, buffalo, first report, cell lines, host diversity

INTRODUCTION

Seneca Valley virus (SVV), previously named Senecavirus A (SVA), is the only member of the *Senecavirus* genus in the *Picornaviridae* family. A typical SVV genome structure is L-VP4-VP2-VP3-VP1-2A-2B-2C-3A-3B-3C-3D. Both the 5′ and 3′ ends are untranslated regions (UTRs) (1). Pigs infected with SVV primarily present with vesicular rash on the nose and coronary band vesicles (2). In severe cases, limping and death occur due to acute myocarditis, heart degeneration, transient fever, and neurological pathology (3). Although SVV was detected in samples as early as 1988 (4), it did not cause any obvious clinical symptoms in pigs before 2008. Sporadic outbreaks of obviously pathogenic SVV occurred between 2008 and 2014. Since 2015, large-scale outbreaks have appeared in the United States, Canada, Brazil, China, Thailand, and Vietnam (2–5). SVV has been detected in mice, houseflies, environmental equipment, and corridors in pig farms and was successfully

isolated from mouse tissue samples (6). However, there are no reports of SVV in buffalo. In this study, one SVV strain was first isolated from a buffalo farm in Guangdong, China. The virus was successfully cultured in BHK-21 and NA cells (mouse-origin), PK-15 and ST cells (pig-origin), Vero and Marc-145 cells (monkey-origin), and MDBK cells (bovine-origin). In addition, the viral genome was sequenced and characterized.

MATERIALS AND METHODS

Sample Information

In October 2018, foot and mouth disease (FMD)-like clinical signs, including fever, hoof decay, and limping, were observed in three buffaloes from a buffalo farm ($n = 80$) in Guangdong, China. Three oral swabs were collected by the farm owner and transported to the Animal Disease Diagnostic Center, Institute of Animal Health, Guangdong Academy of Agricultural Sciences, using an insulated container with an ice pack.

Detection of Potential Pathogens

The viral DNA/RNAs were extracted from the oral swab fluids with the AxyPrep Body Fluid Viral DNA/RNA Miniprep Kit (Corning Life Sciences Co., Ltd., Wujiang, China) and used for reverse transcription PCR to detect foot-and-mouth disease virus (FMDV) (Shenzhen Aodong Inspection and Testing Technology Co., Ltd., Shenzhen, China), vesicular stomatitis virus (VSV) (Guangzhou Vipotion Biotechnology Co., Ltd., Guangzhou, China), bovine viral diarrhea virus (BVDV), bluetongue virus (BTV), and bovine alpha herpesvirus 1 (BoHV-1) according to the reference protocols (7). SVV was also detected using primers SVV-JCF (5′-ATGGTTGGTTTAGCCTGCACAAG-3′) and SVV-JCR (5′-AAGCACGGATGAGACAGAGTTCCAA-3′). One-step RT-PCR (TaKaRa One Step PrimeScript™ RT-PCR Kit, Otsu, Shiga, Japan) was performed with a final reaction volume of 25 μl, containing 12.5 μl 2 × 1 step buffer (Takara, Inc., Shiga, Japan), 0.5 μl PrimeScript One-Step Enzyme Mix (including reverse transcriptase and DNA polymerase), 3 μl viral RNA, 0.5 μl of each primer (10 μmol/l), and 8 μl RNase-free ddH_2O. PCR conditions were as follows: 50°C for 30 min, 94°C for 5 min followed by 35 cycles of 94°C for 30 s, 59°C for 30 s, and 72°C for 30 s, then the final extension step was 72°C for 5 min. The PCR products were purified with an agarose gel DNA extraction kit (Takara Biomedical Technology, Beijing, Co., Ltd.). The gene cloning experiments were conducted with TaKaRa pMD19-T Vector Cloning Kit (Otsu, Shiga, Japan) and *E. coli* DH5α competent cells (Otsu, Shiga, Japan). In addition, the positive recombinant plasmids were obtained using AxyPrep Plasmid Miniprep Kit (Corning Life Sciences Co., Ltd., Wujiang, China) and sequenced by the Sanger sequencing method (Sangon Biotech Co., Ltd. Shanghai, China).

The Isolation and Propagation of SVV

Eight cell lines from four different origins were used for virus isolation, which were stored at College of Veterinary Medicine, South China Agricultural University, and Institute of Animal Health, Guangdong Academy of Agricultural Sciences. We used eight cell types of four different origins to isolate the virus. BHK-21 cells, PK-15 cells, ST cells, Vero cells, Marc-145 cells, MDCK cells, and MDBK cells were cultured and passaged in the following growth medium: Dulbecco's modified Eagle's medium (DMEM) (4.5 g/l D glucose, Gibco™, Grand Island, NY, USA). The NA cells were cultured using 1640 medium (RPMI, Gibco™, USA) supplemented with 10% (v/v) fetal bovine serum (FBS, Gibco™, South American). Before the virus inoculation, cell monolayers were washed three times with phosphate-buffered saline without Mg_{2+} and Ca_{2+} [$PBS^{(-/-)}$] to remove FBS and cell metabolites. The virus was added to the cells and incubated at 37°C with a 5% CO_2 incubator for 1 h. After virus attachment, the virus inoculum was removed and the $PBS^{(-/-)}$ was also used to wash the cell monolayers three times again. Then, the maintenance medium (NA cells: 1640, RPMI, Gibco™, USA, other seven cells: DMEM, 4.5 g/l D glucose, Gibco™,

TABLE 1 | Primers used for genome amplification of SVV.

Primer	Nucleotide sequence (5′-3′)	Denaturation temperature	Annealing temperature	Extension temperature	Extension time	Product length (bp)
SVV 1-F	TTTGAAATGGGGGGCTGGGC	95°C	62°C	72°C	30 s	482 bp
SVV 1-R	GTACTCATGGTGGTAGCAGTCACGTGG					
SVV 2-F	ATCACTGAACTGGAGCTCGA	98°C	57°C	68°C	90 s	1,443 bp
SVV 2-R	AGGAGTTCTGTGTCTCTGAGGA					
SVV 3-F	AGTCTCTTGGCACATACTATCGG	98°C	58°C	68°C	100 s	1,614 bp
SVV 3-R	AAGCACGGATGAGACAGAGTTC					
SVV 4-F	TTAAGGTACTGGAGAAGGACGC	98°C	57°C	68°C	90 s	1,385 bp
SVV 4-R	TGGCATTGATCATAGTGGTGAG					
SVV 5-F	TTGGCTCATGATGCCTTCAT	98°C	56°C	68°C	90 s	1,437 bp
SVV 5-R	GTCCAAACTTGTCTAGATTGTTAGGG					
SVV 6-F	CAACAGACCTTCTGGACTTACAC	98°C	57°C	68°C	90 s	1,505 bp
SVV 6-R	AGAGCAGTCCTGATGATCACA					
SVV 7-F	CTCCTTCGAGGCTCTCATCT	98°C	58°C	68°C	35 s	707 bp
SVV 7-R	TCTGTTCCGACTGAGTTCTCC					

USA) supplemented with 2% (v/v) FBS was added to cells for propagation and passage. The cytopathic effects (CPE) were monitored daily until >90% of the cells showed CPE. The cells were frozen and thawed for three times between −80°C and room temperature, and the virus was filtered with a 0.22-μm filter to remove cell debris and stored at −80°C until further study. Then, the harvested virus solution was identified by RT-PCR and subcultured. SVV was then purified by the virus plaque assay (8). The appropriate plaques were collected and diluted with an appropriate amount of phosphate-buffered saline (PBS, Gibco™). Plaques identified as positive by RT-PCR were inoculated into PK-15 cells and BHK-21 cells, and then passaged and recorded.

Genome Amplification of SVV

The SVV genome was amplified using seven pairs of primers (**Table 1**) from one of two positive oral swabs. The target fragments were amplified by the one-step TaKaRa kit (TaKaRa), and the reaction system was 50 μl, including 1 μl PrimeScript One-Step Enzyme Mix, 25 μl 2 × one-step buffer, 1 μl forward primer (10 μmol/l), 1 μl reverse primer (10 μmol/l), 5 μl RNA template, and 17 μl RNase-free ddH_2O. Cycling conditions were as follows: 50°C for 30 min, pre-denaturation temperature for 5 min followed by 40 cycles of denaturation temperature for 30 s, annealing temperature for 30 s or 15 s, and extension temperature for 30–100 s, separately. A final extension condition was 10 min at 68 or 72°C (**Table 1**). The target fragments were purified and recovered by an agarose gel DNA extraction kit (TaKaRa). Then each of the seven amplicons of SVV was cloned into pMD19-T. The ligated vector pMD19-T (TaKaRa) was introduced into *E. coli* competent cell DH5α (TaKaRa) for cloning. The extracted plasmids were sent to Sangon Biotech Co., Ltd. (Guangzhou Branch), for sequencing.

Sequence Analysis of SVV

We constructed a genetic evolutionary tree based on the SVV polyprotein gene with 1,000 bootstrap replicates using MEGA 6.06 software (neighbor-joining method). Full-length nucleotide and amino acid sequence alignments between SVA/GD/China/2018 and other 35 SVV strains published from

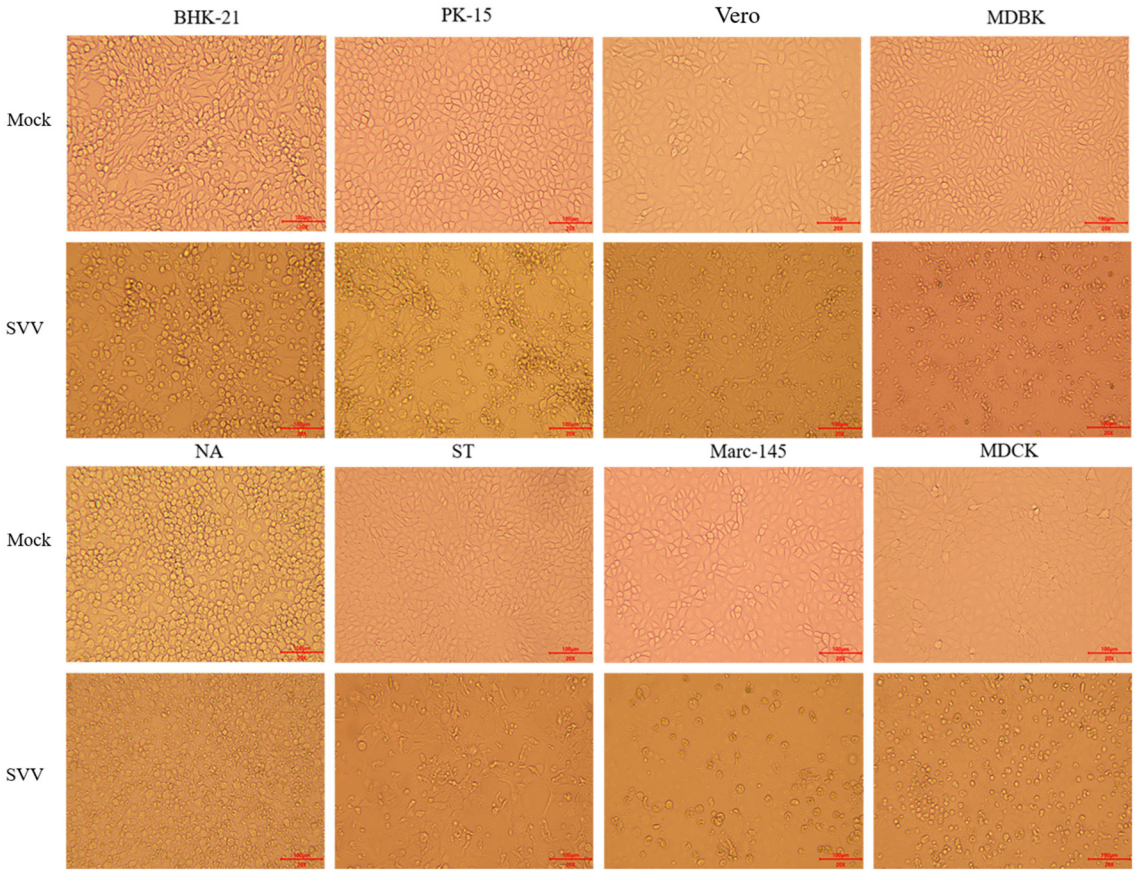

FIGURE 1 | Image of virus isolation with eight different types of cells. The virus was cultured in eight different types of cells, BHK-21 and NA cells, PK-15 and ST cells, Vero and Marc-145 cells, MDBK cells, and MDCK cells. The obvious cytopathic effect, CPE (20×), produced cellular rounding, refraction, cell death, shedding, and floating with BHK-21, PK-15, ST, and Vero cells after 36 h. However, the similar phenomena were not occurred until 96 h in NA cells, Marc-145 cells, and MDBK cells. The virus cannot be cultured for more than four passages with MDCK cells. "Mock" means the negative control cells, and "SVV" means positive control cells that virus propagated.

TABLE 2 | Partial nucleotide and amino acid percentage identities of the SVA/GD/China/2018 strain compared with other SVV strains.

Country	Area	Strain	GenBank number	Nucleotide similarity	Polyprotein similarity
China	Guangdong	CH-GDYD-2017	MG428683	97.3%	98.8%
	Guangdong	CH-GDLZ02-2017	MG428681	97.4%	98.8%
	Guangdong	GD06/2017	MH316117	97.6%	99.1%
	Guangdong	CH-01-2015	KT321458	96%	98.8%
	Guangxi	SVA/GX/CH/2018	MK039162	96.9%	98.6%
	Heilongjiang	SVA/HLJ/CHA/2016	KY419132	97.9%	99.1%
	Sichuan	Sichuan HS-01	MH588717	99.1%*	99.3%
	Sichuan	SVV-SC-01	MH716015	96.4%	98.5%
	Fujian	CH-FJ-2017	KY747510	98.6%	99.1%
	Fujian	SVA CH/FuJ/2017	MH490944	97.6%	99.0%
	Henan	CH-HNSL-2017	KY747512	98.6%	99.0%
	Henan	HN01-2017	MH064433	97.5%	98.8%
	Anhui	AH01-CH-2016	MF460448	97.8%	99.3%
	Hebei	HB01-2017	MF967574	97.6%	98.9%
	Hebei	HB-CH-2016	KX377924	96%	98.7%
USA	Kansas	KS15-01	KX019804	98.5%	99.4%*
	Iowa	USA/IA44662/2015 P1	KU954089	98.4%	99.4%*

Indicates maximum.

China and other countries were performed by MegAlign software (DNAStar Lasergene.v7.1) using Clustal W.

RESULTS

SVV Detection, Isolation, and Propagation

SVV was detected in two of three samples using RT-PCR, and one of two positive oral swabs was used for genome amplification and sequencing. The buffalo-origin SVV was named SVA/GD/China/2018 (GenBank Accession No. MN615881). The virus was purified and propagated stably to 30 passages in BHK-21 cells, NA cells, PK-15 cells, ST cells, Vero cells, Marc-145 cells, and MDBK cells, but it was propagated only to four passages in MDCK cells in which the SVV cannot be detected after four passages (**Figure 1**).

Characterization and Sequence Analysis of Buffalo-Origin SVV

The genome of SVA/GD/China/2018 consists of 7,276 nucleotides. The sequence analysis showed that the genome similarity of SVA/GD/China/2018 was 93.4–99.1% and the polyprotein similarity was 97.5–99.4% compared with the other 35 known SVV strains (**Table 2**). Interestingly, SVA/GD/China/2018 shared the highest nucleotide similarity (99.1%) with the wild boar strain (Sichuan HS-01) and the highest polyprotein similarity (99.4%) with the KS15-01 strain. Genetic evolutionary analysis revealed that SVA/GD/China/2018 clustered in the same branch with Sichuan HS-01 from Sichuan, China (**Figure 2**).

Compared with the published SVV sequences (**Figure 3**), SVA/GD/China/2018 was found to have seven unique amino acid substitutions (**Figure 2**) as follows: 440A (alanine)—V (valine), 497E (glutamic acid)—K (lysine), and 511A (alanine)—V (valine) at the VP3 protein; 1119V (valine)—I (isoleucine) at the 2C protein; 1430A (alanine)—V (valine) at the 3A protein; 1710H (histidine)—Y (tyrosine) at the 3C protein; and 1854V (valine)—I (isoleucine) at the 3D protein.

DISCUSSION

Viruses such as FMDV (9) and BTV (10), causing symptoms such as ulcers in the mouth and hoof nails, are prevalent in cattle. The results showed that FMDV, BVDV, BTV, VSV, and BoHV-1 were negative, but SVV was detected. This finding was not predicted. Thus, surveillance of SVV in cattle is urgently needed along with animal regression tests.

In order to study the host tropism nature of the virus at the cellular level, eight types of cell lines from four different origins were used to isolate virus from the one of two positive oral swabs. The virus was then successfully purified and cultured to over 30 generations stably in BHK-21 and NA cells of mouse origin, PK-15 and ST cells of pig origin, Vero and

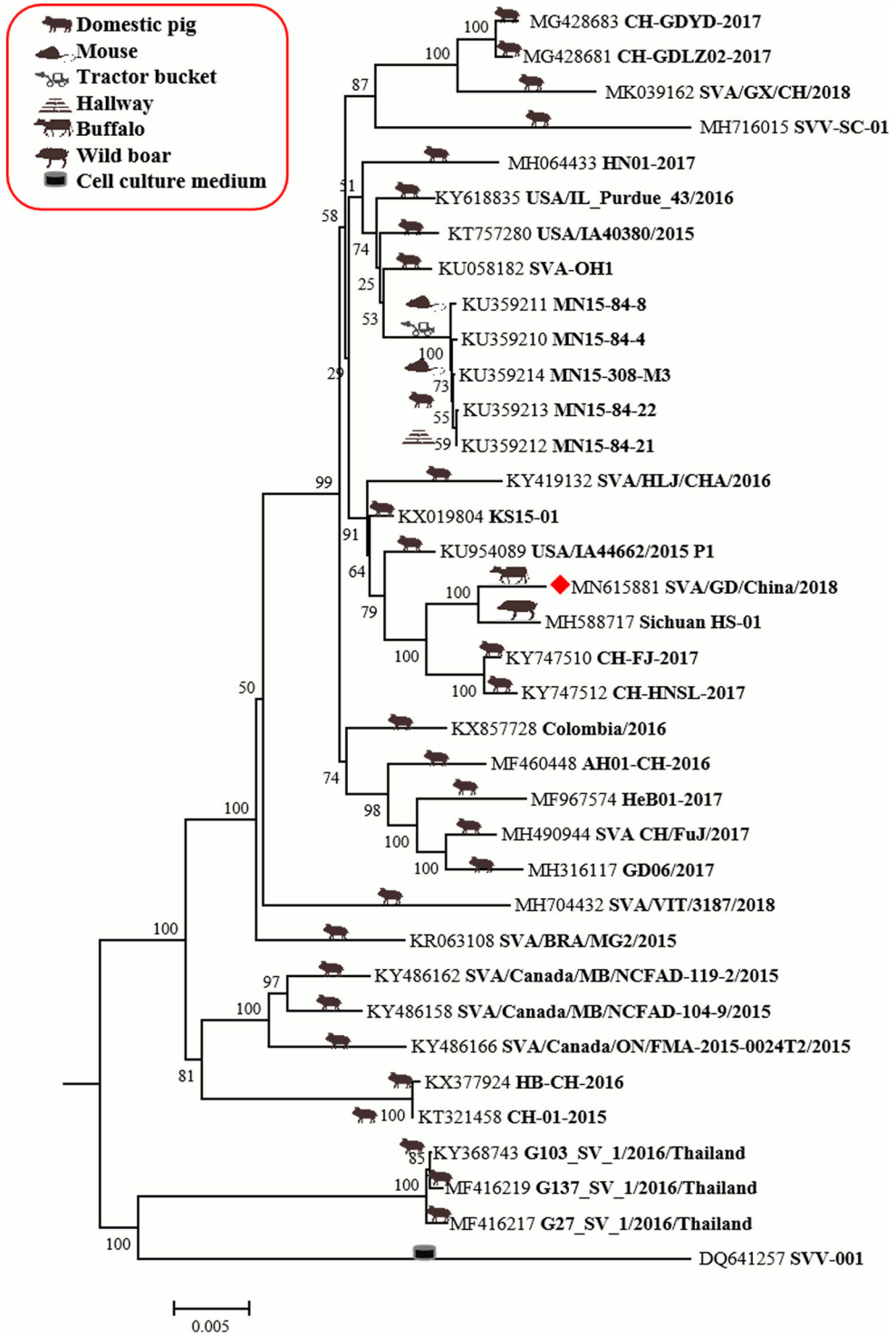

FIGURE 2 | The phylogenetic analysis of SVV based on polyprotein nucleotides. Neighbor-joining tree generated with 1,000 bootstrap samplings (MEGA 6.06). The diamond shape represents the strain in this study. The icon before the accession number indicates the host source of the sequence. At present, only SVA/GD/China/2018 has been derived from diseased buffalo and is in the same branch and closely related to the wild boar-origin strain, Sichuan HS-01.

Marc-145 cells of monkey origin, and MDBK cells of bovine origin. However, it could be cultured to only four generations in MDCK cells of dog origin, which indicated that MDCK was not the sensitive cell line for SVV. Alternatively, some special measures are needed such as adding trypsin (11). The typical cytopathic effect (CPE), including rounding of cells, refraction,

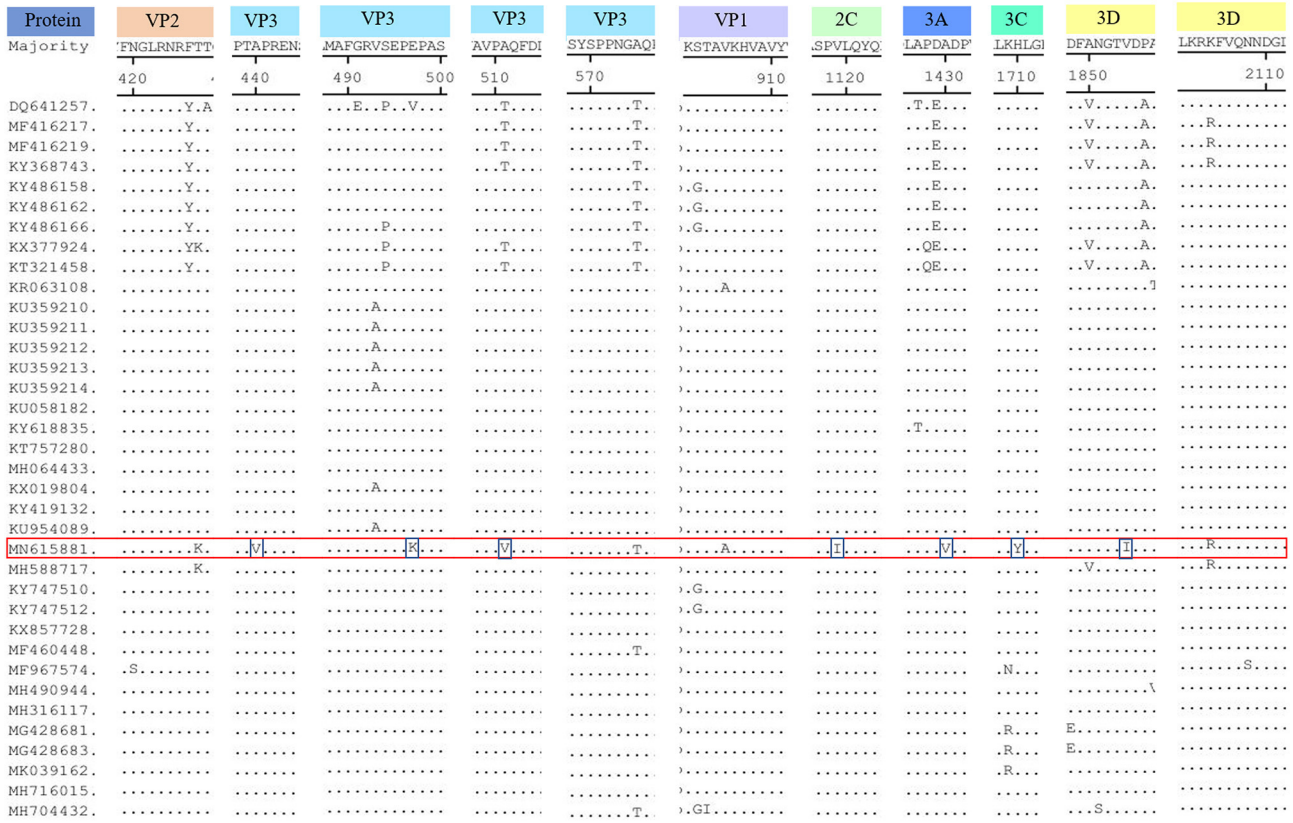

FIGURE 3 | Amino acid sequence alignment of the polyproteins. The SVA/GD/China/2018 strain had seven different amino acids, including 440A (alanine)—V (valine), 497E (glutamic acid)—K (lysine), 511A (alanine)—V (valine) at the VP3 protein; 1119V (valine)—I (isoleucine) at the 2C protein; 1430A (alanine)—V (valine) at the 3A protein; 1710H (histidine)—Y (tyrosine) at the 3C protein, 1854V (valine)—I (Isoleucine) at the 3D protein. For mutations pertaining to amino acids at position 427K (lysine, VP2 protein), 2104R (arginine, 3D protein) was the same as the first wild boar strain, Sichuan HS-01, in China. The "red frame" indicates the buffalo-origin Seneca Valley virus sequence we isolated, and the "blue frame" indicates the different amino acids compared with other sequences.

cell death, shedding, and floating, were observed on BHK-21, PK-15, ST, and Vero cells after 36 h, but there was no CPE on another four cells until 96 h (**Figure 1**). These phenomena indicated that rats, cattle, and monkeys might also be the host of SVV (8), but not dogs. According to previous studies, SVV is pathogenic and causes clinical symptoms in pigs, but it is unclear whether SVV infection could result in visible clinical symptoms in cattle (12). Whether the species supporting replication of SVV in their related cell lines are competent hosts for the virus still needs further confirmation. More studies on related primary cell lines need to be done, such as swine acute diarrhea syndrome coronavirus (SADS-CoV), avian influenza virus, and severe acute respiratory syndrome coronavirus 2 (SARS-CoV-2) (13–15).

The genome of SVA/GD/China/2018 shared lower nucleotide similarity (96–97.6%) and polyprotein similarity (98.8–99.1%) compared with those strains from Guangdong and near Guangdong (**Table 2**). Interestingly, it shared the highest nucleotide similarity with a wild boar-origin strain (Sichuan HS-01) and the highest polyprotein similarity with the KS15-01 strain, which indicated that SVA/GD/China/2018 was a mutant strain (16). To date, the majority of studies on the genetic relationship analysis of SVV were based on its nucleotide sequence (17–19), while some studies were based on amino acid sequence (20) or on the nucleotide sequence and amino acid sequence simultaneously (21). Because this is the first time to report SVV in buffalo, it is particularly important to investigate and analyze the origin and variation of the virus strain in detail. Therefore, we used both nucleotide sequence and amino acid sequence data of SVV for genetic evolution analysis. Our results showed that the constructed genetic evolutionary tree based on the nucleotide sequence and amino acid sequence of the virus showed a completely consistent trend: SVA/GD/China/2018 is located in the same branch as Sichuan HS-01 from Sichuan, China, indicating that the potential buffalo-derived strain originated from swine. However, the distance between Guangdong and Sichuan is more than 2,000 km long; therefore,

further analysis and investigation about how it was transmitted are required.

Interestingly, excluding the possibility of the primers used for amplification to introduce changes in the amplicons, SVA/GD/China/2018 shared the same different amino acids at both 427K (lysine, VP2 protein) and 2104R (arginine, 3D protein) positions, as the first wild boar strain, Sichuan HS-01 (GenBank Accession No. MH588717), in China. In contrast to other porcine strains, they have only one or two mutations. This finding reveals that the virus may have undergone adaptive changes in different hosts (20); however, further investigation is required to elucidate the role of these two residues. VP1 contains a hypervariable region with at least two antigenic sites located at both amino acid 140–160 and amino acid 200–213 sites (22). It has been reported that 228K in VP1, 141–143LDV, and 143–148DGK in VP2 are the primary antigenic sites of FMDV (23). None of these three motifs and antigenic sites of the SVA/GD/China/2018 strain have changed, indicating similar antigenicity and biological characteristics of this strain compared to others (24). The majority of the characteristics are unique, because the different amino acids were located in the VP3 protein. However, further study is required to investigate the effect of these changes.

In summary, we isolated a buffalo-origin SVV strain for the first time and cultured the virus in seven cell lines of different animal origins, and genetic evolution studies revealed the possibility of cross-species transmission of SVV (25).

DATA AVAILABILITY STATEMENT

The datasets presented in this study can be found in online repositories. The names of the repository/repositories and accession number(s) can be found below: https://www.ncbi.nlm.nih.gov/genbank/, MN615881.

ETHICS STATEMENT

Ethical review and approval were not required for the study because the samples used in the present study were taken from field animals by veterinarians. The samples were taken and submitted to Institute of Animal Health, Guangdong Academy of Agricultural Sciences.

AUTHOR CONTRIBUTIONS

XZ and W-FL carried out conceptual and experimental work and wrote the first draft of the manuscript. G-BS, J-HL, Z-FC, and W-YC contributed to the writing and review of the manuscript. D-HL, X-HW, QZ, S-LZ, ML, and D-SH supervised. All authors have approved this manuscript for publication.

FUNDING

This study was mostly supported by a grant (Grant No. 2019B020217002) from the Guangdong Provincial Department of Science and Technology, and two grants (Disciplinary Team Construction Program, Grant No. 202122TD and Jinying's Star Talent Program, Grant No. R2018PY-JX003) from Guangdong Academy of Agricultural Sciences, a grant (Grant No. 201906040005) from Guangzhou Science and Technology Bureau, and two grants (Grant Nos. 2021KJ114 and 2021KJ119) from Guangdong Provincial Department of Agriculture and Rural Affairs. Moreover, this study was also partly supported by the Maoming Branch and Zhaoqing Branch, Guangdong Laboratory for Lingnan Modern Agriculture, and Scientific Observation and Experiment Station of Veterinary Drugs and Diagnostic Techniques of Guangdong Province, Ministry of Agriculture of Rural Affairs, and Key Laboratory of Animal Disease Prevention of Guangdong Province.

REFERENCES

1. Venkataraman S, Reddy SP, Loo J, Idamakanti N, Hallenbeck PL, Reddy VS. Structure of Seneca Valley Virus-001, an oncolytic picornavirus representing a new genus. *Structure*. (2008) 16:1555–61. doi: 10.1016/j.str.2008.07.013
2. Leme RA, Oliveira TES, Alcântara BK, Headley SA, Alfieri AF, Yang M, et al. Clinical manifestations of senecavirus a infection in neonatal pigs, Brazil, 2015. *Emerg Infect Dis*. (2016) 22:1238–41. doi: 10.3201/eid2207.151583
3. Vannucci FA, Linhares DCL, Barcellos DESN, Lam HC, Collins J, Marthaler D. Identification and complete genome of Seneca Valley Virus in vesicular fluid and sera of pigs affected with idiopathic vesicular disease, Brazil. *Transbound Emerg Dis*. (2015) 62:589–93. doi: 10.1111/tbed.12410
4. Wang L, Prarat M, Hayes J, Zhang Y. Detection and genomic characterization of Senecavirus A, Ohio, USA, 2015. *Emerg Infect Dis*. (2016) 22:1321–3. doi: 10.3201/eid2207.151897
5. Liu J, Zha Y, Li H, Sun Y, Wang F, Lu R, et al. Novel recombinant Seneca Valley Virus isolated from slaughtered pigs in Guangdong Province. *Virol Sin*. (2019) 34:722–4. doi: 10.1007/s12250-019-00139-8
6. Joshi LR, Mohr KA, Clement T, Hain KS, Myers B, Yaros J, et al. Detection of the emerging Picornavirus Senecavirus A in pigs, mice, and houseflies. *J Clin Microbiol*. (2016) 54:1536–45. doi: 10.1128/JCM.03390-15
7. Claus MP, Alfieri AF, Folgueras-Flatschart ÁV, Wosiacki SR, Médici KC, Alfieri AA. Rapid detection and differentiation of bovine herpesvirus 1 and 5 glycoprotein C gene in clinical specimens by multiplex-PCR. *J Virol Methods*. (2005) 128:183–8. doi: 10.1016/j.jviromet.2005.05.001
8. Chen L, Zhang J, Wang M, Pan S, Mou C, Chen Z. Pathogenicity of two Chinese Seneca Valley virus. (SVV) strains in mice and pigs. *Microb Pathog*. (2019) 136:103695. doi: 10.1016/j.micpath.2019.103695
9. Peng J, Yi J, Yang W, Ren J, Wen Y, Zheng H, et al. Advances in foot-and-mouth disease virus proteins regulating host innate immunity. *Front Microbiol*. (2020) 11:2046. doi: 10.3389/fmicb.2020.02046
10. Haegeman A, Vandaele L, De Leeuw I, Oliveira AP, Nauwynck H, Van Soom A, et al. Failure to remove Bluetongue Serotype 8 Virus. (BTV-8) from *in vitro* produced and *in vivo* derived bovine embryos and subsequent transmission of BTV-8 to recipient cows after embryo transfer. *Front Vet Sci*. (2019) 6:432. doi: 10.3389/fvets.2019.00432
11. Kong F, Niu X, Liu M, Wang Q. Bile acids LCA and CDCA inhibited porcine deltacoronavirus replication *in vitro*. *Vet Microbiol*. (2021) 257:109097. doi: 10.1016/j.vetmic.2021.109097
12. Zhang S, Cao Y, Yang Q. Transferrin receptor 1 levels at the cell surface influence the susceptibility of newborn piglets to PEDV infection. *PLoS Pathog*. (2020) 16:e1008682. doi: 10.1371/journal.ppat.1008682
13. Edwards CE, Yount BL, Graham RL, Leist SR, Hou YJ, Dinnon KH, et al. Swine acute diarrhea syndrome coronavirus replication in primary human cells reveals potential susceptibility to infection. *Proc Natl Acad Sci USA*. (2020) 117:26915–25. doi: 10.1073/pnas.2001046117

14. Ruiz-Hernandez R, Mwangi W, Peroval M, Sadeyen JR, Ascough S, Balkissoon D, et al. Host genetics determine susceptibility to avian influenza infection and transmission dynamics. *Sci Rep*. (2016) 6:26787. doi: 10.1038/srep26787
15. Zhu Y, Feng F, Hu G, Wang Y, Yu Y, Zhu Y, et al. A genome-wide CRISPR screen identifies host factors that regulate SARS-CoV-2 entry. *Nat Commun*. (2021) 12:961. doi: 10.1038/s41467-021-21213-4
16. Wang M, Chen L, Pan S, Mou C, Shi K, Chen Z. Molecular evolution and characterization of novel Seneca Valley virus. (SVV) strains in South China. *Infect Genet Evol*. (2019) 69:1–7. doi: 10.1016/j.meegid.2019.01.004
17. Wang H, Niu C, Nong Z, Quan D, Chen Y, Kang O, et al. Emergence and phylogenetic analysis of a novel Seneca Valley virus strain in the Guangxi Province of China. *Res Vet Sci*. (2020) 130:207–11. doi: 10.1016/j.rvsc.2020.03.020
18. Leme RA, Zotti E, Alcântara BK, Oliveira MV, Freitas LA, Alfieri AF, et al. Senecavirus A: an emerging vesicular infection in Brazilian pig herds. *Transbound Emerg Dis*. (2015) 62:603–11. doi: 10.1111/tbed.12430
19. Saeng-chuto K, Stott CJ, Wegner M, Kaewprommal P, Piriyapongsa J, Nilubol D. The full-length genome characterization, genetic diversity and evolutionary analyses of Senecavirus A isolated in Thailand in 2016. *Infect Genet Evol*. (2018) 64:32–45. doi: 10.1016/j.meegid.2018.06.011
20. Xu W, Hole K, Goolia M, Pickering B, Salo T, Lung O, et al. Genome wide analysis of the evolution of Senecavirus A from swine clinical material and assembly yard environmental samples. *PLoS ONE*. (2017) 12:e0176964. doi: 10.1371/journal.pone.0176964
21. Qian S, Fan W, Qian P, Chen H, Li X. Isolation and full-genome sequencing of Seneca Valley virus in piglets from China, 2016. *Virol J*. (2016) 13:173. doi: 10.1186/s12985-016-0631-2
22. Saeng-chuto K, Rodtian P, Temeeyasen G, Wegner M, Nilubol D. The first detection of Senecavirus A in pigs in Thailand, 2016. *Transbound Emerg Dis*. (2018) 65:285–8. doi: 10.1111/tbed.12654
23. Bai X, Bao H, Li P, Wei W, Zhang M, Sun P, et al. Effects of two amino acid substitutions in the capsid proteins on the interaction of two cell-adapted PanAsia-1 strains of foot-and-mouth disease virus serotype O with heparan sulfate receptor. *Virol J*. (2014) 11:132. doi: 10.1186/1743-422X-11-132
24. Chen Y, Xu Q, Tan C, Li X, Chi X, Cai B, et al. Genomic analysis of codon usage shows influence of mutation pressure, natural selection, and host features on Senecavirus A evolution. *Microb Pathog*. (2017) 112:313–9. doi: 10.1016/j.micpath.2017.09.040
25. Cui J, Li F, Shi ZL. Origin and evolution of pathogenic coronaviruses. *Nat Rev Microbiol*. (2019) 17:181–92. doi: 10.1038/s41579-018-0118-9

Conflict of Interest: The authors declare that the research was conducted in the absence of any commercial or financial relationships that could be construed as a potential conflict of interest.

Publisher's Note: All claims expressed in this article are solely those of the authors and do not necessarily represent those of their affiliated organizations, or those of the publisher, the editors and the reviewers. Any product that may be evaluated in this article, or claim that may be made by its manufacturer, is not guaranteed or endorsed by the publisher.

Advantages of publishing in Frontiers

OPEN ACCESS
Articles are free to read for greatest visibility and readership

FAST PUBLICATION
Around 90 days from submission to decision

HIGH QUALITY PEER-REVIEW
Rigorous, collaborative, and constructive peer-review

TRANSPARENT PEER-REVIEW
Editors and reviewers acknowledged by name on published articles

Frontiers
Avenue du Tribunal-Fédéral 34
1005 Lausanne | Switzerland

Visit us: www.frontiersin.org
Contact us: frontiersin.org/about/contact

REPRODUCIBILITY OF RESEARCH
Support open data and methods to enhance research reproducibility

DIGITAL PUBLISHING
Articles designed for optimal readership across devices

FOLLOW US
@frontiersin

IMPACT METRICS
Advanced article metrics track visibility across digital media

EXTENSIVE PROMOTION
Marketing and promotion of impactful research

LOOP RESEARCH NETWORK
Our network increases your article's readership